Phagocytic and Inflammatory Properties of NOD Macrophages.

Kristian Anthony Niels Houlberg

Thesis presented for the degree of Ph.D
The University of Edinburgh
2008

Abstract

The morbidity associated with diabetes mellitus is increasing worldwide; within the UK alone it now affects approximately 1.3 million people. It is a leading cause of cardiovascular mortality, the leading cause of blindness and the single largest cause of end-stage renal failure. The non-obese diabetic (NOD) mouse has become the best characterised animal model for autoimmune diabetes which accounts for approximately 15% of all human cases. In recent years there has been an increased interest in the importance of macrophages (Mφ) in the pathogenesis of diabetes in NOD mice as well as the complications of diabetes. Recent studies of NOD Mφ have indicated impaired phagocytosis of apoptotic cells (AC) whilst there is conflicting data regarding the inflammatory phenotype of NOD Mφ *in vitro*.

This study set out to examine the phagocytic capacity of NOD Mφ *in vitro* and *in vivo* and identify the molecular nature of the defect involved in the previously reported impaired uptake of AC. In addition, the inflammatory nature of different populations of NOD-derived Mφ was determined *in vitro* and their responses to inflammatory stimuli *in vivo* comprehensively assessed.

Robust *in vitro* phagocytosis assays, using either microscopy or flow cytometry were developed and adapted to evaluate phagocytosis of a wide range of particles including AC, latex beads and pneumococci. NOD derived Mφ exhibited a marked *in vitro* phagocytic defect for AC and latex beads but not pneumococci opsonised with IgG. A peritoneal phagocytosis assay was then used to examine phagocytosis of AC and latex beads *in vivo*. Mathematical modelling of AC and peritoneal Mφ (PMφ) numbers indicated that PMφ from NOD mice took twice as long to ingest an AC *in vivo* compared to control C57BL/6 PMφ. Study of peritoneal AC clearance in various NOD congenic strains strongly suggested that the gene(s) responsible for the phagocytic defect were located on idd 18 on chromosome 3. This locus contains the exciting candidate gene *Vav3* that is involved in the intracellular regulation of Mφ phagocytosis.

The inflammatory phenotypes of bone marrow derived macrophages (BMDMφ), PMφ and pleural Mφ (PLMφ) were then compared. *In vitro* studies indicated that BMDMφ were hyper-inflammatory whilst resident Mφ were hypo-responsive to the same stimuli compared to control C57BL/6 Mφ. Mφ dependent and independent models of inflammation were employed to examine the behaviour of NOD Mφ *in vivo*. NOD mice recruited fewer leukocytes in both thioglycollate

peritonitis and carrageenan pleurisy but no differences in chemokine levels were evident. In contrast to the diminished leukocyte recruitment evident in Mφ dependent models of inflammation, NOD mice were able to mount an extremely vigorous immune response associated with prominent leukocyte infiltration in delayed-type hypersensitivity pleurisy. Thus, although it is relatively straightforward to examine Mφ function *in vitro*, the analysis of the role of Mφ as co-ordinators of inflammatory response *in vivo* is much more complex and the mechanisms underlying the diminished leukocyte response of NOD mice in Mφ dependent models of inflammation remain unclear.

This study examined the phagocytic defect of NOD Mφ with congenic studies suggesting the involvement of the *Vav3* gene in idd 18. BMDMφ and resident Mφ of NOD mice exhibit opposite responses to inflammatory stimuli *in vitro*. In addition, NOD mice exhibit diminished responses *in vivo* in Mφ dependent models of inflammation. The underlying mechanisms for this remain unclear

Dedicated to Sue, Jake, Harry, Eden and Oliver.

Acknowledgements

Declaration

I, Kristian Anthony Niels Houlberg, declare that this thesis was composed myself and the work contained herein is my own and was done by myself with the technical help of people I have acknowledged in the appropriate section, and this work has not been submitted for any other degree or professional qualification except as specified.

_____

Kristian A.N. Houlberg

Table of Contents

Index of Figures

Index of Tables

Abbreviations

%	:	percentage
°C	:	degrees Celsius
7-AAD	:	7 aminoactinomycin
AC	:	apoptotic cell
AGE	:	advanced glycation end-products
AIF	:	apoptosis inducing factor
ANOVA	:	analysis of variance
Apaf-1	:	apoptosis protease activating factor 1
APC	:	allophycocyanin
BB	:	bio-breeding
BMDMφ	:	bone marrow derived macrophage
CBA	:	cytometric bead array
CD40L	:	CD40 ligand
CG	:	carrageenan
CO_2	:	carbon dioxide
CR	:	complement receptor
CSF-1	:	colony stimulating factor 1
ctla-4	:	cytotoxic T lymphocyte-associated antigen 4
DC	:	dendritic cell
DIABLO	:	direct inhibitor of apoptosis binding protein with a low isoelectric point
DMEM/F12	:	dulbecco's modified eagle medium with F12
DTH	:	delayed type hypersensitivity
ELISA	:	enzyme linked immuno sorbant assay
FACS	:	fluorescence-activated cell sorter
FasL	:	fas ligand
FBS	:	foetal bovine serum
FcR	:	Fc receptor
FITC	:	fluorescein isothiocyanate
GAD	:	glutamic acid decarboxylase
GEF	:	guanidine exchange factors
H_2O_2	:	hydrogen peroxide
HBSS	:	hanks balanced salt solution
HSP-60	:	heat shock protein 60
ip	:	intraperitoneally
ipl	:	intrapleurally
IA-2	:	insulinoma associated protein 2
IAP	:	inhibitor of apoptosis protein
idd	:	insulin dependent diabetes
IFNγ	:	interferon gamma
Ig	:	immunoglobulin
IGIF	:	IFNγ inducing factor
IL	:	interleukin

iNOS	:	inducible nitric oxide synthase
ITAM	:	immunoreceptor tyrosine-based activation motif
KC	:	keratinocyte chemoattractant
KO	:	knockout
LPS	:	lipopolysaccharide
MCP-1	:	monocyte chemoattractant protein l
MEGF	:	multiple epidermal growth factor-like domains
MDR	:	Mφ disappearance reaction
Mφ	:	macrophage
MHC	:	major histocompatibility complex
MIP-1α	:	Mφ-inflammatory protein 1 alpha
MIP-2	:	Mφ-inflammatory protein 2
MODY	:	maturity onset diabetes of the young
NHS	:	National Health Service
NK	:	natural killer
NO	:	nitric oxide
NOD	:	non-obese diabetic
NON	:	non-obese non-diabetic
O2-	:	superoxide anion
PBS	:	phosphate buffered saline without calcium and magnesium
pdcd-1	:	programmed cell death 1
PE	:	phycoerythrin
PLMφ	:	pleural Mφ
PMN	:	polymorphonuclear cell (or neutrophil)
PMφ	:	peritoneal Mφ
PS	:	phosphatidylserine
RAGE	:	AGE receptor
RANTES	:	regulated upon activation normal T cell expressed and secreted
rbc	:	red blood cells
RPMI	:	Roswell Park Memorial Institute 1640 media
SLE	:	systemic lupus erythematosis
smac	:	second mitochondria-derived activator of caspase
SRA	:	scavenger receptor A
SREC	:	scavenger receptor expressed by endothelial cells
T1DM	:	type 1 diabetes mellitus
T2DM	:	type 2 diabetes mellitus
Tc	:	cytotoxic T cell
TCR	:	T cell receptor
TG	:	thioglycollate
TGF-β	:	transforming growth factor beta
T_h	:	T helper cells
TLR	:	toll like receptor
TNFα	:	tumour necrosis factor alpha
TNFR	:	tumour necrosis factor receptor
Treg	:	regulatory T cells
TSP	:	thrombospondin

WHO   : World Health Organisation

Chapter 1. Introduction

1.1 DIABETES MELLITUS

Diabetes mellitus is a complex metabolic disease characterised by elevated blood glucose levels. It continues to be defined by the World Health Organisation (WHO) as a fasting plasma glucose level greater than 7.0mmol/l or plasma glucose of greater than 11.0mmol/l, 2 hours after a glucose load (WHO, 2006). Type 1 diabetes mellitus (T1DM) results from autoimmune destruction of the insulin producing β cells in the islets of Langerhan within the pancreas and invariably requires treatment with daily injections of insulin. Type 2 diabetes mellitus (T2DM) is a syndrome resulting from a variable combination of increased peripheral insulin resistance (primarily in the liver, muscle and adipose tissue) and a relative lack of insulin secretion. T2DM is usually managed by a combination of diet, oral hypoglycaemic agents and sometimes insulin. Together T1DM and T2DM account for the vast majority of cases of diabetes mellitus although additional, rarer classifications exist such as gestational diabetes when hormones produced during pregnancy reduce a woman's sensitivity to insulin or Maturity Onset Diabetes of the Young (MODY) used to describe dominantly inherited, monogenic defects of insulin secretion, excluding T2DM, occurring at any age, (Fajans et al., 2001) .

Around 1.3 million people in England are known to have diabetes, of which T1DM accounts for approximately 15% (DoH, 2001); while T2DM accounts for most of the remaining 85% of diabetic patients. The incidence of diabetes mellitus is increasing globally with projections suggesting that 366 million people will be affected by 2030 compared with 171 million in the year 2000 (Wild et al., 2004); Indeed it is estimated that 3 million people will be affected by the year 2010 within the UK (Amos et al., 1997). The current estimated prevalence of T1DM in the UK is one per 700 to 1,000 children, yielding a total population with T1DM aged under 25 years in the UK of approximately 25,000 (DoH, 2007). Whilst increased obesity and decreased physical activity can explain the increased incidence of T2DM, the factors underlying the 3 to 4% increased incidence in T1DM witnessed across Europe (Eurodiab, 2000), including the UK (Gardner et al., 1997) and especially in young children, are poorly understood.

Diabetes mellitus carries an enormous cost: morbidity to the patient and financial to the Nation Health Service (NHS). The risks to diabetics from coronary heart disease and stroke are up to 5 and 3 times higher than in the general population respectively.

It is the leading cause of blindness in people under the age of 60 and the largest single cause of end stage renal failure. Excluding accidents, diabetes is the biggest cause of lower limb amputation. The life expectancy of UK patients with T1DM is reduced by 20 years compared to the general population whilst those with T2DM suffer a 10 year reduction in life expectancy. It is estimated that the treatment of people with diabetes mellitus accounts at least 5% of the total NHS budget and 10% of hospital in-patient resources. In addition, 1 in 20 diabetic patients require care from the social services because of disability (DoH, 2001).

Although the management and treatment of T1DM has improved immeasurably in the last 100 years, from a rapidly fatal condition to a treatable disease, clearly the burden on patients and the health service remains tremendous. Unsurprisingly therefore, research into diabetes was the subject of a major review by the Department of Health in October 2002 to focus future areas of research. It was understood that "genetic and immunological contributions have been identified in part" but further work on the factors underlying the aetiology of diabetes was warranted, in particular "characterisation of the genes involved, environmental triggers and immunological events" (DoH, 2002).

1.2 THE NON-OBESE-DIABETIC MOUSE

It is generally recognised that T1DM is an autoimmune disease with a protracted and unpredictable onset. Whilst the appearance of autoantibodies carries a high prognostic value, they can predate the onset of symptoms by several years and do not exactly predict whether or when disease will occur. The pancreas is a difficult organ to study in humans, as it is difficult to image and not amenable to biopsy. Experimental animal models are tools that enable researchers to study the aetiology and pathogenesis of complex diseases and interventions *in vivo* and *in vitro*, in ways not possible in humans. They do however remain an approximation of the human disease and insights gained from animal models ultimately have to be tested against the human condition.

The Non-Obese Diabetic (NOD) mouse is one model of spontaneous autoimmune diabetes whilst another model in common usage is the BioBreeding (BB) rat (Nakhooda et al., 1978). Since its introduction the NOD mouse has become the pre-eminent model due to its better defined genome, increased availability of monoclonal

reagents and lower maintenance costs (Atkinson and Leiter, 1999). Streptozotocin has been used for over 30 years to induce diabetes in rodents (Katsilambros et al., 1970). Although Streptozotocin provides useful insights into the effects of diabetes and is not limited to specific genetic backgrounds, Streptozotocin induced diabetes has limited value to those studying the aetiology of T1DM. Lastly Zucker rats (Stern et al., 1972) and db db mice (Hummel et al., 1966) have been used extensively as spontaneous models for T2DM.

1.2.1 Background to the NOD mouse strain

Makino and colleagues were developing a strain of cataract-prone mice from the outbred Jcl:ICR line when they recognised an individual female mouse developed classic signs of diabetes mellitus (Makino et al., 1980). Breeding pairs were formed from her offspring and selection performed on the basis of spontaneous diabetes and reproductive ability. The NOD and non-obese non-diabetic (NON) strains were formed 6 generations later.

From the outset a strong sex bias in the incidence of diabetes was reported: 80 per cent in females and less than 20% in males (Makino et al., 1980). The reported incidence subsequently has varied greatly between institutions, from 60 to 80% in females and 20 to 30 % in males (Kikutani and Makino, 1992). Castration of mice up to the age of 7 weeks increases the incidence of diabetes among male mice and decreases the incidence seen among female mice (Lampeter et al., 1989). Perhaps unsurprisingly, the incidence is highest when mice are kept in the strictest germ-free conditions (Bach, 2005).

Because of extensive in-breeding there is an assumption that all NOD mice, in various colonies around the world, are genetically identical. In must be remembered however that NOD mice were taken out of Japan at different time points in the 1980s (relatively early in the evolution of the strain) and used to establish individual colonies with little (or no) subsequent inter-breeding between them. The NOD mice colonies held by Merck (USA) and Charles River (France) separated with approximately 30 back-cross generations between them in the 1980s and it is likely that subtle differences exist between various NOD colonies (personal communication, Linda Wicker).

From as young as 3 weeks old, both male and female NOD mice start to develop mononuclear immune cell infiltrates around the islets of Langerhans in the pancreas (peri-insulitis). In both sexes, these infiltrates expand and start to invade the islets (insulitis) such that by 10 weeks of age severe insulitis is almost a universal finding of NOD mice with diabetes typically developing after 12 weeks of age if it is to occur (Anderson and Bluestone, 2005). It has therefore been argued (Andre et al., 1996) that autoimmune diabetes in the NOD mouse requires the breakdown of at least 2 checkpoints against autoimmunity. The first checkpoint is the initiation of insulitis which is seen in virtually all NOD mice (completely penetrant) and the second is the progression to overt diabetes which does not occur in the majority of male mice (incompletely penetrant).

The nature of the inflammatory cell infiltrate comprising the insulitis has been extensively investigated for over 25 years. Early reports and descriptions concentrated on the lymphocytic component (Miyazaki et al., 1985) and although CD4$^+$ T cells comprise the majority of the leukocytes, CD8$^+$ T cells, NK cells, B cells, dendritic cells (DC) and macrophages (Mφ) are also clearly apparent (Anderson and Bluestone, 2005).

In addition to the organ-specific autoimmune disease of diabetes mellitus, NOD mice are also prone to a range of other autoimmune diseases (table 1.1), suggesting a genetic background that is generally 'autoimmune-permissive'.

Autoimmune Disease	Comment	Reference
Coombes-positive Haemolytic Anaemia	Spontaneous Mice > 200 days Diabetic > non-diabetic	(Baxter et al., 1991)
Thyroiditis similar to Hashimoto's thyroiditis	Experimentally induced Mice > 4 months	(Many et al., 1996)
Sialitis similar to Sjogren's Syndrome	Spontaneous Mice > 4 months old	(Hu et al., 1992)
Peripheral polyneuropathy similar to CIPD*	Spontaneous Mice > 20 weeks old	(Salomon et al., 2001)
Autoimmune Prostatitis	Experimentally induced: particularly aggressive Young male mice	(Rivero et al., 1998)
Systemic Lupus Erythematosis-like disease	Experimentally induced by iv BCG (Prevents autoimmune diabetes in young mice)	(Silveira and Baxter, 2001)

Table 1- 1   Autoimmune conditions to which NOD mice are prone
* Chronic Inflammatory Demyelinating Polyneuropathy

1.2.2 Diabetes susceptibility loci in NOD mice

Although insulitis is almost universal amongst NOD mice, as mentioned above, autoimmune diabetes is not. The relevant parts of the NOD genome that contribute to diabetes susceptibility or protection have been the focus of research groups for almost 30 years. Genetic linkage studies have identified 21 different chromosomal loci contributing to disease susceptibility (insulin dependent diabetes [idd] loci 1 through to 21) to date.

Congenic NOD strains have been formed whereby genetic material from non-autoimmune-prone strains has been substituted for the various idd loci. These substitute genes are frequently derived from either C57BL/6 or C57BL/10 mice. As techniques have become increasingly refined, it has become possible to generate congenic NOD strains with ever smaller chromosomal segments replaced, thus tightening the resolution of the various idd loci to fewer and fewer candidate genes. Consequently, what was originally considered a single idd locus has often been subdivided into 2 or 3 distinct regions, each containing a few putative susceptibility genes. For example idd 5 has been split into idd 5.1 and idd 5.2.

Although several loci have had the putative gene(s) narrowed down to a select few, in only one or 2 instances have the genes responsible for particular loci been positively identified. The few examples include idd 1, the Major Histocompatibility Complex (MHC) Class II haplotype, idd 5.1 which has been confirmed as the T cell regulatory gene, Cytotoxic T Lymphocyte-associated Antigen 4 (ctla-4) and idd 3 which has been identified as the interleukin (IL) 2 gene. Table 1.2 summarises the current understanding regarding the different idd loci, however the list is under constant revision.

idd Locus	Chromosome	Putative genes or phenotype	References
1	17	MHC class II haplotype (H2^{g7}) essential for the development of diabetes	(Wicker et al., 1995)
2	9	Interferon-γ Inducing Factor (IGIF)	(Rothe et al., 1997)
3	3	Interleukin 2 (IL-2)	(Podolin et al., 2000)
4	11	Interleukin 12 (IL-12) subunit p40	(Simpson et al., 2003)
4	11	Psmb6 (involved in peptide formation for class I expression in response to IFNγ) Pld2 (regulates phagocytosis) Cxcl16, Alox15, Alox12e,	(Ivakine et al., 2006)
4.3	11	csf2 (GM-CSF gene)	(Litherland et al., 2005)
5.1	1	Cytotoxic T Lymphocyte-associated Antigen 4 (ctla-4)	(Vijayakrishnan et al., 2004)
5.2	1	Nramp1 (an endosomal ion transporter)	(Kissler et al., 2006; Wicker et al., 2004)

Table 1- 2   idd loci (1 to 5) and candidate genes

idd Locus	Chromosome	Putative genes or phenotype		References
6	6	Toll-Like Receptor (TLR) 1		(Vallois et al., 2007)
		Thymocyte resistance to apoptosis		(Bergman et al., 2003)
7	7	None reported		(McAleer et al., 1995)
8	14	None reported		(McAleer et al., 1995)
9.1	4	8 candidate genes identified, none immunologically active		(Eaves et al., 2002)
9.2	4	TNFR2 CD30	Members of the TNF Receptor Family	(Lyons et al., 2000)
9.3	4	CD137		(Lyons et al., 2000)
10	3	CD101		(Penha-Goncalves et al., 2003)
11	4	Uncertain. (May control B cell Marginal Zone enlargement)		(Brodnicki et al., 2000; Rolf et al., 2005)
12	Unclear	None reported		

Table 1- 2   idd loci (6 to 12) and candidate genes

idd Locus	Chromosome	Putative genes or phenotype	References
13	15	β2 microglobulin	(Hamilton-Williams et al., 2001)
14	13	None reported	(Brodnicki et al., 2003)
15	5	None reported	(McAleer et al., 1995)
16	17	MHC class 1	(Pomerleau et al., 2005)
17	3	May be involved in programmed cell death 1 (Pdcd-1)	(Wang et al., 2005)
18	3	*Vav3*	(Lyons et al., 2001)
19	6	Interacts with idd 6 and 20 to regulate T suppressor activity	(Morin et al., 2006)
20	6	Interacts with idd 6 and 19 to regulate T suppressor activity	(Morin et al., 2006)
21	18	None reported	(Hall et al., 2003)

Table 1.2   **idd loci (13 to 21) and candidate genes**

1.2.3 Is the NOD mouse a good model for human T1DM?

T1DM in humans is an extremely complex disease and results from a combination of environmental and genetic triggers. Although experimental animal models offer a way to dissect the relative importance of different aetiological influences, the data generated may only be interpretable in the context of the model. The clinical pattern of TIDM in humans and autoimmune diabetes in NOD mice share several features in common but there are also a few subtle differences (see table 1.3).

Association mapping using DNA from large numbers of individuals with T1DM and available family cohorts have identified a few of the genes that confer disease susceptibility in humans. There appears to be a remarkable level of concordance between the genes relevant to human T1DM and diabetes in NOD mice (reviewed by Wicker et al., 2005).

Class II loci within the MHC are without doubt the most important, with certain DR and DQ haplotypes conferring a relative risk of developing T1DM of between 3 and 50 times that of the general population (Maier and Wicker, 2005) and this is analogous to the NOD idd 1. Strikingly, the NOD MHC class II molecule I-A contains a non-aspartic acid substitution at position 57 of the β chain that is also seen in the human MHC class II molecule DQ β chain where it confers susceptibility to T1DM (Acha-Orbea and McDevitt, 1987).

As identified in NOD mice, non-MHC genes are now known to play a role in human T1DM and the promoter region of the insulin gene is important in humans. Although the same gene does not appear to have a NOD idd equivalent, perhaps because mice have 2 genes responsible for the production of insulin, there is accumulating evidence that insulin is an important autoantigen for autoimmune diabetes in NOD mice (reviewed by Maier and Wicker, 2005). The human gene CTLA4 encoding 2 isoforms is analogous to the NOD idd 5.1. (table 1.2). The human gene PTPN22 encoding the lymphoid protein tyrosine phosphatase has recently been confirmed to confer disease susceptibility in humans and the mouse orthologue ptpn8 appears to affect disease frequency in NOD mice (Wicker et al., 2005). There is increasing evidence that the IL-2 receptor α chain is similarly relevant to both human (Vella et al., 2005) and NOD disease where it is the major candidate for idd 3.

	Type 1 (autoimmune) Diabetes Mellitus	
	Human	NOD mouse
Weight loss	Present	Present
Polydipsia	Present	Present
Polyuria	Present	Present
Hyperglycaemia	> 15 mmol/l	20 – 30 mmol/l
Ketoacidosis	Common	Less severe
Serum insulin	Very low	Very low
Outcome without insulin	Lethal	Lethal
Sex preponderance	Female ≥ male	Female >> male

Table 1- 3   Comparison of clinical features present at the onset of autoimmune diabetes in humans and NOD mice
(adapted from Lampeter et al., 1989)

1.2.4 The evidence for lymphocytes in the pathogenesis of autoimmune diabetes in NOD mice

Diabetes in the NOD mouse was once regarded almost as a disease exclusively of T cell dysfunction following observations that $CD4^+$ and $CD8^+$ T cells reactive to islet antigens such as Glutamic Acid Decarboxylase (GAD), insulinoma associated protein 2 (IA-2) and Heat Shock Protein 60 (HSP-60) infiltrated pancreatic islets (reviewed by Lieberman and DiLorenzo, 2003). In addition, diabetes may be transferred by the adoptive transfer of either splenocytes (Wicker et al., 1986) or diabetogenic T cell clones (Haskins and Wegmann, 1996). Whilst $CD4^+$ T cells were originally considered essential for the disease transference, Susan Wong demonstrated that $CD8^+$ T cells could transfer diabetes in the absence of $CD4^+$ cells (Wong et al., 1996).

The possible role of $CD4^+CD25^+FOXP3^+$ regulatory T cell (T_{reg}) dysfunction leading to a breakdown of peripheral tolerance and thus autoimmunity in NOD mice has generated considerable interest but there is no hard evidence to date (as reviewed by Anderson and Bluestone, 2005). Cyclophosphamide has been used experimentally to accelerate the onset of diabetes in NOD mice (Harada and Makino, 1984) and it is possible that it acts by selectively targeting the T_{reg} cells (Brode et al., 2006). Furthermore, it has become clear that B cells as well as T cells are crucial for the development of autoimmunity in NOD mice. Whilst autoantibodies are a feature of autoimmune diabetes in NOD mice, it is thought the actions of B cells as antigen presenting cells are more important than antibody production (Tian et al., 2006). In addition, Natural Killer (NK) cell numbers and NK cell-mediated cytotoxicity are reduced in NOD mice compared to other strains with both phenotypes linked to diabetogenesis in NOD mice (Carnaud et al., 2001; Esteban et al., 2003).

1.2.5 Evidence that Mφ are important in the pathogenesis of autoimmune diabetes in NOD mice

Whilst lymphocytes are undoubtedly crucial to the development of autoimmunity within NOD mice (Anderson and Bluestone, 2005), increasing recognition has also been given to the role(s) played by the innate immune system and by Mφ in particular.

Monocyte chemoattractant protein-1 (MCP-1), an important chemokine for recruiting monocytes, is expressed within the islets of pre-diabetic NOD mice (Chen et al.,

2001) and there is extensive evidence, both by flow cytometry (Jarpe et al., 1990) and immunohistochemicy (O'Reilly et al., 1991; Reddy et al., 1993) that Mφ predominate amongst the first immunological cells to surround and then infiltrate the islets. Annemarie Jansen working with Drexhage in Paris described the progression from peri-insulitis through to full-blown invasive insulitis very clearly (Jansen et al., 1994) as summarised in table 1.4.

The importance of Mφ in the pathogenesis of autoimmune diabetes in the NOD mouse was recognised at an early stage. Ki-Up Lee, having appreciated that Mφ were the predominant leukocytes in the early insulitis observed in BB rats, demonstrated that Mφ ablation by intraperitoneal injections of silica prevented the development of diabetes in NOD mice (Lee et al., 1988). More recent evidence suggests that DC and Mφ are essential for the retention of lymphocytes within the insulitis (Nikolic et al., 2005) and Harry Georgiou working in Australia demonstrated that allogenic transfer of Mφ from CBA mice to new born NOD mice prevented disease progression (Georgiou et al., 1995).

Mφ and DC are the first and predominant source of Tumor Necrosis Factor (TNF) α within the pancreatic islets (Dahlen et al., 1998). In 1999 Shiva Reddy demonstrated the colocalisation of inducible nitric oxide synthase (iNOS) with Mφ within the pancreata of NOD mice (Reddy et al., 1999). Tiina Kipari in our group convincingly demonstrated the role of Mφ-derived iNOS to induce apoptosis of renal tubular epithelial cells in a murine model of renal inflammation (Kipari et al., 2006). Finally, Boris Calderon published evidence that Mφ were the key effectors of β cell death in the islets of Langerhan (Calderon et al., 2006).

Stage of Insulitis	Description
0 (Unaffected islets)	No Lymphocytic infiltration; all islets contained a few Mφ Observed in control mice and 60% of 3-week-old female NOD mice
1 (Swollen vessels adjacent to islets)	Numbers of Mφ in perivascular connective tissue doubled; no infiltration of islets. Observed in 40% of 3-week-old female NOD mice
2 (Early para-insulitis)	Accumulation of Mφ and DC; no infiltration of islets. Predominant in 7-week-old female / 10-week-old male NOD mice
3 (Para-insulitis)	↑ Accumulation of Mφ, DC, mixed $CD4^+$ & $CD8^+$ cells, some B cells in clusters. Few islets infiltrated by Mφ. Predominant in 10-week-old female / 22-week-old male NOD mice
4 (Late para-insulitis)	Islets were completely surrounded by this stage Apparent in > 17-week-old female or > 22-week-old male NOD mice
5 Lymphocytic insulitis	Para-insular accumulation of leukocytes apparent but massive infiltration of islets with Mφ, DC, and many T and B cells Only apparent in > 17-week-old female NOD mice
6 End-stage	No insulin producing cells remain Decreasing numbers of leukocytes Only apparent in > 17-week-old female NOD mice

Table 1- 4   Stages of insulitis observed in NOD or BALB/c pancreata as described by Annemarie Jansen (Jansen et al., 1994).

1.3 THE MACROPHAGE

Before describing abnormalities in Mφ populations from NOD mice, it is worth exploring the often conflicting roles Mφ play within the initiation, maintenance and resolution of inflammation.

The first description of 'macrophagocytes' came from the seminal work of Metchnikoff (1845 to 1916) who inserted rose thorns into starfish larvae and witnessed mesenchymal cells migrate into the wounds. He named the large cells macrophagocytes, later termed Mφ while the smaller 'microphagocytes' later became known as neutrophils or PMN (Segal, 2005).

There is recent evidence that monocytes and PMNs originate from common precursor cells in the bone marrow with circulating monocytes later differentiating into either DC, resident tissue Mφ or inflammatory Mφ (Fogg et al., 2006). There has been increasing evidence for different subsets of monocytes in humans, differentiated by their expression of CD14 and CD16. Approximately 90% of circulating monocytes are $CD14^{++}$ $CD16^{-}$ whilst the remaining monocytes are $CD14^{+}$ $CD16^{+}$. The $CD16^{+}$ monocytes are more proinflammatory with respect to their cytokine and chemokine profiles; in vitro studies on whole blood stimulated with LPS have shown they are responsible for the majority of TNFα (but almost no IL-10) production, despite relatively low numbers (Belge et al., 2002). $CD16^{+}$ monocytes also exhibit higher potency in antigen presentation and adhere more strongly to activated endothelium. Their precise role in infection and inflammation remains unclear (reviewed by Ziegler-Heitbrock, 2007).

A seminal paper by Frederic Geismann demonstrated 2 corresponding subsets of circulating murine monocytes, differentiated by their expression of 3 surface markers: CX_3CR1 (fractalkine receptor), CCR2 (MCP-1 receptor) and the epitope GR1. CX_3CR1^{LO} $CCR2^{HI}GR1^{HI}$ murine monocytes (analgous to the $CD14^{++}$ human monocytes) were actively recruited to sites of inflammation whereas CX_3CR1^{HI} $CCR2^{LO}GR1^{LO}$ murine monocytes (analgous to the $CD16^{+}$ human monocytes) remained within the circulation for longer periods and were recruited to non-inflamed tissues to replace resident tissue Mφ. Interestingly, both subtypes had the ability to differentiate into DC in vivo (Geissmann et al., 2003).

Resident tissue Mφ are ubiquitous and present in all organs where they act as sentinels for tissue injury or infection (Sean Eardley and Cockwell, 2005). Serosal Mφ form resident populations in peritoneal and pleural cavities whilst resident alveolar Mφ are present in non-inflamed lungs. Resident Mφ in liver, brain and bone are referred to as Kupffer cells, microglial cells and osteoclasts respectively. Local microenvironments, connective tissue matrices and apocrine secretion products from neighboring resident cells result in the phenotypes of these resident Mφ populations varying markedly (Gordon, 2003). Jean-Francois Cailhier has demonstrated that resident Mφ are critical to the initiation of both thioglycollate (TG) peritonitis (Cailhier et al., 2005) and Carrageenan (CG) pleurisy (Cailhier et al., 2006), with an almost complete failure to recruit PMN to these inflammatory models *in vivo* following Mφ depletion (see later).

There is extensive evidence that Mφ play key roles in the orchestration of inflammation, coordinating the early injurious, pro-inflammatory phase with the subsequent anti-inflammatory, resolution phase. During the injurious phase, inflammatory Mφ derived from $CCR2^{HI}GR1^{HI}$ monocytes (see above) infiltrate sites of inflammation where they are responsible for cell death and phagocytosis of invading microbial pathogens (where relevant) and also apoptotic resident cells. The actions of Mφ at this stage of the inflammatory process are thought to be responsible for the breakdown of tissue matrix. During the resolution phase Mφ activity results in the phagocytic clearance of apoptotic cells (AC) whether derived from senescent inflammatory cells such as PMN (Savill et al., 1989) or resident tissue cells (reviewed by Duffield, 2003).

In the carbon tetrachloride model of hepatic fibrosis, Mφ depletion at the height of the early injurious phase ameliorated hepatic scarring, but depletion during the later resolution phase resulted in failure of matrix degradation and persistent scarring (Duffield et al., 2005). Mφ may also be used as anti-inflammatory 'cell therapy' and David Kluth has demonstrated reduced inflammation by the adoptive transfer of IL-10 secreting Mφ to a rat model of nephrotoxic nephritis (Kluth et al., 2004; Wilson et al., 2002).

1.3.1 Opposing Mφ actions explained by different Mφ Phenotypes

How is it that a single cell type can have such apparent contradictory roles and be injurious at one time point and reparative at another? In somewhat of an oversimplification, 4 Mφ 'phenotypes' with different profiles of cytokine section and phagocytic capabilities have been described *in vitro*: classically activated, alternatively activated, type-2 activated, and the Mφ phenotype following phagocytosis of AC.

1.3.1.1 *Classically activated Mφ*

Classical activation occurs when a naïve resident tissue Mφ or monocyte derived Mφ is exposed to either IFNγ and pro-inflammatory cytokines, or microbial products that trigger a range of 'pattern recognition receptors' known as Toll-like receptors (TLR) e.g. the bacterial endotoxin lipopolysaccharide (LPS) triggers TLR 4.

IFNγ, produced *in vivo* by $CD4^+$ or NK cells, acts synergistically to potentiate classical activation (Erwig et al., 1998). Classically activated Mφ are typically injurious and produce large quantities of TNFα and nitric oxide (NO). They express high levels of MHC class II and CD86 (Mosser, 2003). Mφ production of chemokines recruits leukocytes whilst IL-12 production promotes a T_h1 response from nearby $CD4^+$ T cells, (figure 1.1).

1.3.1.2 *Alternatively activated Mφ*

If, on the other hand, naïve Mφ are initially confronted by T_h2 cytokines (e.g. IL-4 and IL-13) then they adopt a very different phenotype termed 'alternative' activation. These Mφ express high levels of mannose receptors and scavenger receptors and produce less NO and TNFα. They also exhibit an increased propensity for phagocytosis and antigen presentation (figure 1.1).

1.3.1.3 *Type 2 activated Mφ*

Type 2 activation is a relatively recent term for Mφ activation following exposure to CD40L in the presence of immunoglobulin G (IgG). These Mφ secrete high levels of IL-10 and reduced levels of IL-12 (Anderson and Mosser, 2002) and tend to promote T_h2 responses from nearby lymphocytes with increased T cell IL-4 production and IgG class switching among B cells (Mosser, 2003).

1.3.1.4 *Mφ phenotype following the phagocytosis of AC*

It is generally accepted that Mφ phenotype is determined by continuing initial cytokine exposure, making it resistant to re-programming (Erwig et al., 1998), an exception appears to be following the following AC phagocytosis. AC ingestion switches injurious, classically activated Mφ to a reparative anti-inflammatory phenotype exhibiting increased production of the anti-inflammatory cytokines transforming growth factor (TGF) β, IL-10 and prostaglandin E2 together with decreased production of TNFα and IL-6 (Fadok et al., 1998; Voll et al., 1997). It is thus pertinent that TGFβ1 is critical to the down-regulation of acute inflammation (Letterio and Roberts, 1998) and involved in wound repair (Border and Noble, 1994).

This switch in phenotype is specific to the phagocytosis of AC and is not seen following phagocytosis of either necrotic cells or opsonised particles both of which promote the classical activation. Elegant work by Huynh and colleagues demonstrated phosphatidylserine (PS) expressed on the surface of AC was critical to this switching of the Mφ phenotype and the production of TGFβ1 (Huynh et al., 2002). AC were instilled intra-tracheally during an *in vivo* model of acute lung injury and were phagocytosed by Mφ. Administration of PS expressing AC resulted in increased TGFβ1 production and enhanced resolution of the lung injury compared to those that received either control cells or AC from the non-PS-expressing PLB-985 cell line. The induction of TGFβ1 (and accelerated resolution of inflammation) could be rescued by instilling PS alongside AC from the PLB-985 cell line or by the instillation of liposomes expressing PS.

Current dogma suggests this mechanism of switching Mφ phenotype, from injurious to reparative after the ingestion of AC is fundamental to limiting the excessive 'collateral damage' that would otherwise be inflicted on host tissues by classically activated Mφ *in vivo*.

Classically activated Mφ

- Generation of pro-inflammatory cytokines & chemokines
- Killing cells by apoptosis
- Phagocytosis of pathogens, immune complexes & debris
- Matrix degradation

Monocyte

- Phagocytosis apoptotic cells

- Generation of anti - inflammatory cytokines & chemokines
- Matrix synthesis & repair
- Angiogenesis
- Antigen presentation

Alternatively activated Mφ

Figure 1- 1   Schematic diagram contrasting and comparing the functions of classically and alternatively activated Mφ.
(Adapted from Duffield, 2003)

1.3.2 Abnormalities in Mφ function apparent in NOD mice

Although numerous abnormalities in NOD Mφ phenotype and function have been described *in vitro*, it is unclear whether they are important *in vivo* and how they contribute to autoimmunity. The phenotypes of various NOD derived Mφ populations have been compared to various control Mφ populations by several research groups and a number of different defects have been identified. The data from different groups may appear conflicting and this may be explained in part by the use of differing control strains and subtly different Mφ populations.

It was initially demonstrated that TG elicited PMφ from NOD mice produced excessive amounts of IL-12, with a reduced IL-10 to TNFα ratio in response to LPS compared to a number of control strains including C57BL/6 and BALB/c mice (Alleva et al., 2000). In an extension of their work with NOD derived DC. Pradip Sen reported increased NFκB activity in response to LPS among splenic and BMDMφ from NOD mice using BALB/c mice among the control strains (Sen et al., 2003). A different series of experiments (Stoffels et al., 2004) reported that resident peritoneal Mφ (PMφ) from NOD mice produce increased levels of IL-1β and TNFα in response to AC , necrotic cells and LPS with C57BL/6 mice being used as controls. This consistent body of work supported the hypothesis that an increased pro-inflammatory response by NOD Mφ, together with a failure to switch phenotype following ingestion of AC resulted in a greater T_h1 response by CD4$^+$ cells and could thus underpin the autoimmune diseases seen in NOD mice.

In stark contrast however, Hanli Fan reported that TG elicited PMφ from NOD (and SLE-prone) mice were hypo-responsive to LPS in the presence of AC or Foetal Bovine Serum (FBS) and produce less IL-1β and other pro-inflammatory cytokines than control Mφ from various strains including C57BL/6 (Fan et al., 2004). This work was consistent with their previously published work using other autoimmune prone strains of mice (Koh et al., 2000). In a further series of experiments they demonstrated selective reduced activity of Rho, a cytoplasmic G protein and cytoskeletal regulator in Mφ derived from NOD and SLE-prone strains of mice (Fan et al., 2006) following exposure to AC or FBS.

In addition to the work examining the inflammatory phenotype(s) of NOD derived Mφ, it has been shown that PMφ and bone marrow derived Mφ (BMDMφ) from NOD mice do not up-regulate CD49d adequately in response to LPS stimulation and exhibit defective CD49d-mediated adhesion to fibronectin compared to C57BL/6 and BALB/c controls (Geutskens et al., 2004). It has also been reported that bone marrow precursor cells from NOD mice have a skewed maturation *in vitro* towards Mφ and away from DC, in response to GM-CSF compared to both BALB/c and C57BL/6 mice (Nikolic et al., 2005).

Defective AC phagocytosis, by resident PMφ from NOD mice, *in vitro*, was reported (O'Brien et al., 2002) in comparison to a range of control strains including C57BL/6 and BALB/c mice. The NOD PMφ phagocytic defect was specific for AC as it was not observed for polystyrene beads. It was more pronounced in female mice and appeared to diminish as mice aged. Although further work confirmed the phagocytic defect within the peritoneal cavity of NOD mice *in vivo* (O'Brien et al., 2006) no mechanism was identified.

Fc receptors (FcR) play an important role in phagocytosis (as described above), with FcγR2b inhibiting phagocytosis. Menna Clatworthy demonstrated that autoimmune prone strains of mice, including NOD mice, have an FcγR2b genetic haplotype that results in only 50% activity of this inhibitory receptor and as a consequence exhibit increased rates of phagocytosis of opsonised pneumococci *in vitro* (Clatworthy and Smith, 2004).

1.4 PHAGOCYTOSIS

The, phagocytosis of pathogens, cellular debris or AC, represents a key function of Mφ and is the singular action that gave them their name. Although it may seem a very straight forward function, phagocytosis is an extremely complex process. Mφ have to identify and differentiate particles to be phagocytosed from those that should remain intact. Particles identified for ingestion then have to be tethered or bound to the Mφ and then exquisitely intricate and coordinated movements of the actin cytoskeleton have to draw the particle into a phagosome within the Mφ. Finally lysosomes fuse with the phagosome to form a phagolysosome.

1.4.1 Receptors and ligands involved in phagocytosis

Mφ have an impressive array of surface receptors that identify and bind particles for phagocytosis. Several receptors relevant to phagocytosis by mammalian Mφ have been identified through elegant work with *Drosophila melanogaster* (as reviewed by Stuart and Ezekowitz, 2008). Several groups of receptors, particularly complement receptors (CR), FcR, scavenger receptors such as CD36 and pattern recognition molecules such as CD14 (the LPS receptor) are capable of identifying a range of proteins present on both AC and microbial pathogens whilst other receptors are more specific for invading microbes. Multiple epidermal growth factor-like domains (MEGF), CD91 (lipoprotein receptor related protein), scavenger receptor expressed by endothelial cells (SREC), and Stabilins 1 and 2 recognise are range of gram positive and negative bacteria including *Staphylococcus aureus*, *Listeria monocytogenes* and *Escherichia coli*. As the list of receptors involved in phagocytosis continually expands there is a growing understanding of how receptor involvement not only initiates phagocytosis but also influences the maturation of the resultant phagolysosome (Erwig et al., 2006).

Broadly speaking, receptors involved in the phagocytosis of AC can be divided into 3 groups (Savill et al., 2002): receptors that recognise non-self antigens, those that recognize altered (or damaged) self and finally receptors that recognise non-detaching self. Whilst the first group of receptors are involved in phagocytosis generally (as mentioned above), the latter 2 groups are particularly relevant to the phagocytosis of AC. Table 1.5 gives a summary of molecules shown to be important in the recognition of AC for phagocytosis.

1.4.1.1 *Recognition of non-self antigens*

Since AC become opsonised by complement and immunoglobulins (especially natural IgM antibodies), these receptors are also relevant to the clearance of AC.

The complement system is a cascade of enzymic proteins that will be discussed in greater detail later (chapter 1.6.3) Whilst later components of the complement system (C5 to C9) combine together to form the membrane attack complex that results in the lysis of target cells, earlier complement components, particular C3b decorate the surface of pathogens or AC. Professional phagocytes (Mφ and PMN) express complement receptors that recognise cell surface complement and trigger phagocytosis.

Pathogens, AC, or particles bearing epitopes recognised by the adaptive immune system will become coated with Ig. The membranes of Mφ are rich in receptors for the Fc component of Ig molecules. Most classes of FcR such as FcγRI and FcγRIII promote phagocytosis (Clynes et al., 1999). In contrast FcγRIIb is inhibitory and co-ligation of FcγRIIb with an activating FcR will inhibit phagocytosis (Clatworthy and Smith, 2004). Menna Clatworthy and colleagues have clearly identified how activatory and inhibitory Fcγ receptors combine to form a balancing act between the requirement of the immune system to promote inflammation and clear pathogens whilst avoiding autoimmunity (Floto et al., 2005).

Receptor	Ligand	References
CD14	LPS	(Devitt et al., 1998)
FcR	Fc component of opsonising Ig	(Clynes et al., 1999)
Complement Receptor 3 (CR3 / $\alpha_m\beta_2$)	Opsonic complement component inactivated C3b	(Savill et al., 2002)
Scavenger Receptor A (SRA)	Oxidised sites on AC	(Platt et al., 1996)
CD36	Oxidised sites on AC	(Savill et al., 1992)
LOX 1	Oxidised sites on AC	(Oka et al., 1998)
ABC1	Trans-membrane lipid rearrangement	(Hamon et al., 2000)
PS Receptor*	PS	(Bose et al., 2004; Fadok et al., 1992)
β2-Glycoprotein I Receptor	β2-Glycoprotein I	(Balasubramanian et al., 1997)
$\alpha_v\beta_3$ (Vitronectin Receptor)	Milk-fat globule epidermal growth factor 8	(Akakura et al., 2004)
Calreticulin	C1q & Mannose Binding Lectin	(Ogden et al., 2001)
$\alpha_v\beta_v$	bridging molecule Thrombospondin (TSP)	(Savill et al., 1992)
CD31	CD31	(Brown et al., 2002)

Table 1- 5   Receptors and molecules implicated in phagocytosis of AC
* role of the PS receptor is disputed (see text). Non-self receptors are high-lighted in yellow, altered self receptors in blue and non-detaching self in purple.

1.4.1.2 *Recognition of altered-self*

As cells undergo apoptosis a number of changes take place to the outer membrane as discussed in greater detail later in the chapter 1.5. Oxidised lipids are exposed (Kagan et al., 2002); PS on the internal surface of healthy cells, translocates to the outer surface (Fadok et al., 1992). Receptors that identify these changes are critical to the recognition and removal of AC. At one point it appeared that exposed PS was directly recognised by a PS-receptor on the surface of Mφ, triggering phagocytosis (Fadok et al., 2000; Fadok et al., 2001). Unfortunately the story is clearly much more complicated and PS-receptor deficient mice do not exhibit defective phagocytosis of AC either *in vitro* or *in vivo* (Bose et al., 2004) .

1.4.1.3 *Recognition of non-detaching self*

Elegant work by Simon Brown and colleagues demonstrated that cells actively communicate viability in order to escape phagocytosis since both AC and viable cells adhere (bind) to Mφ at 20°C but viable cells actively detach at 37°C. Although the exact mechanism has not been delineated, CD31 blocking antibodies prevented the detachment of viable cells thus implicating the involvement of CD31 (Brown et al., 2002).

1.4.2 Downstream signalling events

Once recognized particles have been bound to the Mφ, intricate, downstream signaling leads to carefully controlled changes of the actin cytoskeleton in order to implement phagocytosis. Different patterns of engulfment have been described (Kaplan, 1977): FcR mediated phagocytosis is thought to involve the extrusion of pseudopodia from the phagocyte that 'grab' the particle whereas the particle is seen to 'sink' into a phagosome during CR mediated phagocytosis.

The down-stream signaling events that result in these cytoskeletal movements have been the subject of much research with those following activation of FcγR and CR3 attracting the greatest interest. There is broad agreement regarding the classes of proteins involved, but slight variance in the exact role of certain signaling proteins (Castellano et al., 2001; Cougoule et al., 2006; Hall et al., 2006). Activation of either class of receptor appears to result in recruitment of small GTPases of the Rho family (Rho, Rac, and Cdc42) to the local area. These proteins cycle between inactive GDP

forms and an active GTP forms. Guanine-nucleotide exchange factors (GEF) cycle GTPases to the active state whilst GTPase activating proteins cycle the active form to the inactive state (see figure 1.2). The *Vav* family of proteins is an example of GEF that are crucial in the downstream signaling from these receptors. The activated GTPases, amongst other functions, recruit the Arp 2/3 complex to affect actin polymerisation and thus phagocytosis.

Castellano and colleagues (Castellano et al., 2001) argue that both Cdc42 and Rac are required for FcγR mediated phagocytosis with Cdc42 required for pseudopodia emission by the Mφ and Rac required for phagosome closure. In contrast to FcR signalling, they propose that Rho is the critical GTPase required for CR dependent phagocytosis.

The work of Cougoule and colleagues (Cougoule et al., 2006) on FcR signalling, whilst in agreement with the earlier published work of Castellano, went further to propose that the binding of IgG-opsonized particles to FcγR induced the activation of Src kinases, which phosphorylated 2 tyrosines in the receptor Immunoreceptor Tyrosine-based Activation Motif (ITAM) domain. These in turn recruited Syk whose kinase activity controlled *Vav* which controlled Rac activation. Rac and Cdc42 cooperated in inducing actin polymerisation at site of receptor activation and thus phagocytosis.

Hall and colleagues performed an elegant series of experiments using primary BMDMφ from knock-out (KO) mice. They found Mφ from *Vav* KO mice had a clear phagocytic defect for complement-opsonised sheep red blood cells (rbc) opsonised with complement but exhibited normal phagocytosis of IgG-opsonised rbc. They demonstrated that this was associated with a failure to recruit the Arp 2/3 complex to the nascent phagosome and hence construct the actin polymerisation during CR mediated signaling. Using Rac KO BMDMφ they demonstrated that Rac was required for actin polymerisation following both complement and Fcγ receptor activation. Furthermore, the transfection of *Vav* KO BMDMφ with constituitively active Rac rescued the phagocytic defect whilst constituitively active Cdc42 had no effect. Specific inhibition of Rho inhibited phagocytosis (but not actin polymerisation) following both CR and FcγR activation. Unlike the earlier descriptions that phagocytosis mediated via different receptors was visibly different,

they offered electron micrographs demonstrating pseudopodia and similar cytoskeletal movements following activation of both receptor pathways.

The data from Hall and colleagues (summarized in figure 1.3) is therefore subtly different from earlier published work as there was clear evidence *Vav* was not required, or at least was redundant, in FcR signaling, contrary to Cougoule and colleagues. Rho was required for both receptor pathways, although its function appears distinct to that of Rac and the necessity of Cdc42 was questionable, contrary to the earlier review by Castellano and colleagues. The reasons behind these subtle differences may be partly explained by the extensive use of immortalized cell lines and reconstructed phagocytic receptors in earlier work.
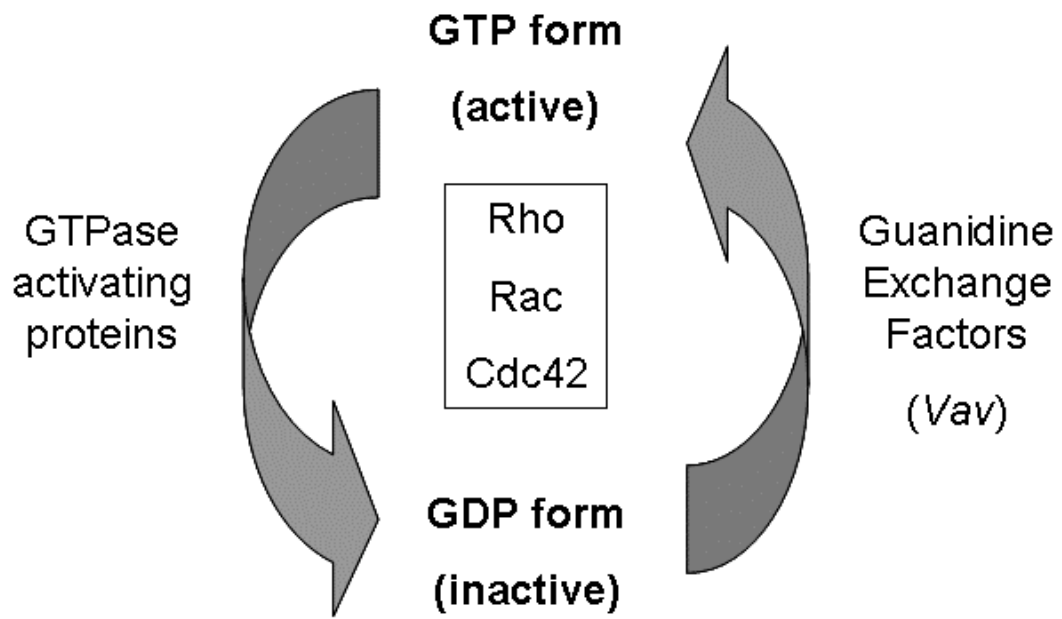
Figure 1- 2   Schematic diagram showing the activation / deactivation of the Rho family of small GTPases
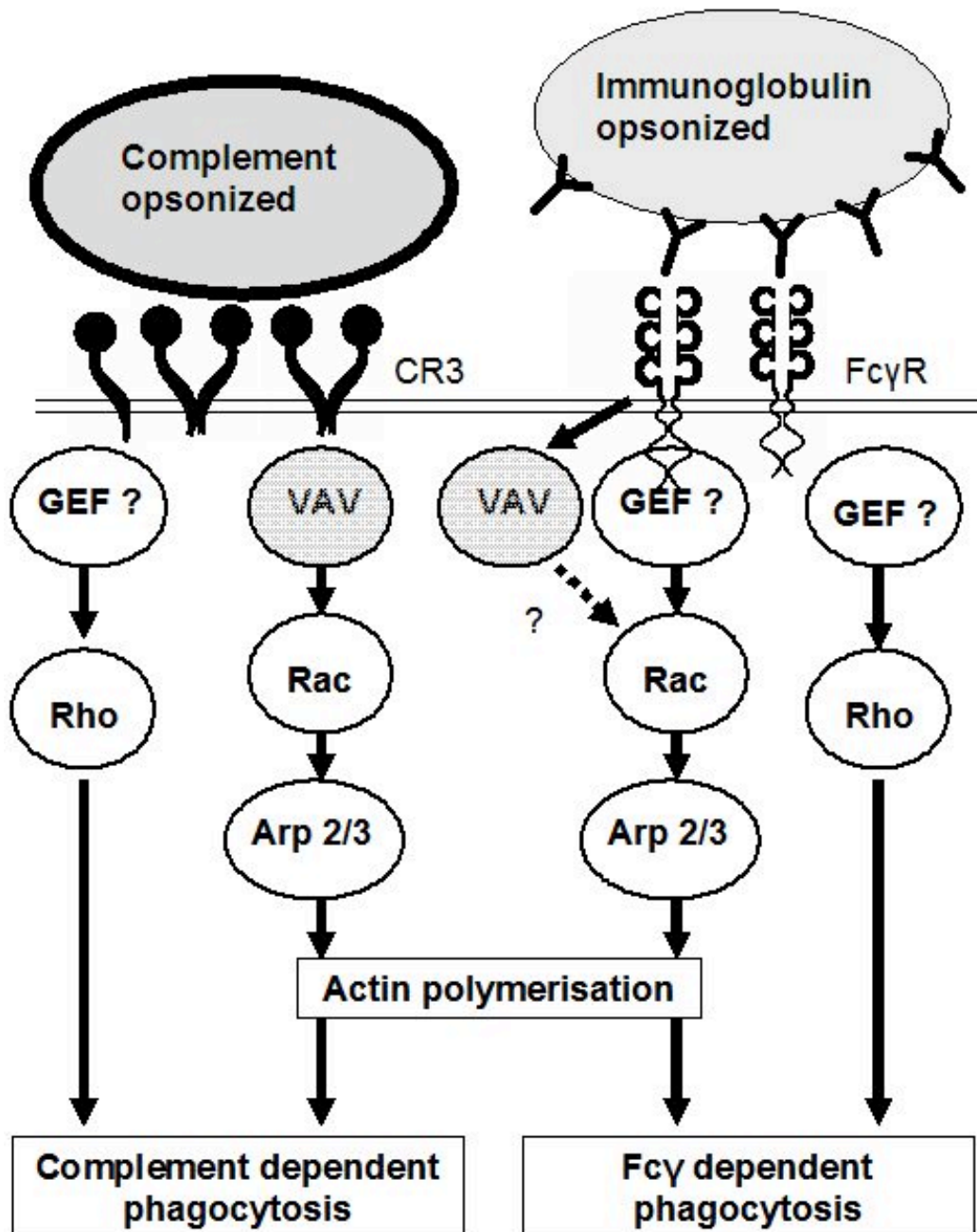
Figure 1- 3   Schematic diagram of the down-stream phagocytic signaling events
Following ligation of Complement Receptors and Fc Receptors in primary Mφ, Guanidine Exchange Factors (GEF) are recruited to the nascent phagosome. Vav is required to activate Rac following ligation of Complement, but not Fc Receptors. Rac recruits the Arp 2/3 complex to achieve actin polymerization. Activation of Rho is achieved via alternative GEF. Although Rho is not required for actin polymerization, activation of both GDPases is required for successful phagocytosis (Hall et al., 2006).

1.5 APOPTOSIS

Apoptosis was first described in a seminal paper by Kerr and colleagues and indeed their beautiful description of the defining morphological changes visible by light microscopy during apoptosis remain amongst the clearest available:

> "The earliest indication of pending [apoptosis] was found to be aggregation of condensed chromatin beneath the nuclear envelope. This is followed by breaking up of the nucleus, and cytoplasmic condensation and budding with the production of a number of compact, membrane-bounded cell fragments with relatively well preserved organelles." (Kerr et al., 1974).

Apoptosis has been shown to play a central role in embryogenesis where it helps to 'sculpt' the embryonic form into the adult shape (for example tadpoles' tails are 'trimmed' by apoptosis and in humans, inter-digital cells are removed to form discrete fingers by apoptosis). Within the early thymus autoreactive thymocytes are selected and die by apoptosis in order to prevent autoimmunity. Apoptosis is also fundamental to the maintenance of tissue homeostasis in adult life and facilitates the removal of senescent cells. During inflammation senescent PMN die by apoptosis, an act that limits tissue damage from the leaking of disrupted granules. Apoptosis is especially important for the removal of potentially cancerous cells that have sustained DNA damage.

The term apoptosis means 'leaves falling from a tree' and indicates that it was originally thought to be an immunologically silent in contrast to cell death by necrosis. Whilst apoptosis is ordered and programmed, necrosis is much more random. Necrosis is often the result of noxious stimuli such as ischemia or toxic substances and frequently affects whole fields of adjacent cells simultaneously. Necrotic cells lose membrane integrity as they 'fall apart' in a disorganised fashion, releasing cytoplasmic contents into the intercellular fluid where they may well prove to be inflammatory (Kanduc et al., 2002; Wyllie et al., 1980). As discussed earlier, phagocytosis of necrotic cells is frequently pro-inflammatory, inducing classical activation of Mφ whereas phagocytosis of AC induces an anti-inflammatory Mφ phenotype. AC are usually cleared rapidly by adjacent cells (Hughes et al., 1997) or professional phagocytes (Ren and Savill, 1998; Savill, 1997; Savill et al., 2002;

Savill et al., 1989) whilst those that are not cleared rapidly may undergo secondary necrosis with additional immunological consequences.

1.5.1 Apoptotic Pathways

As mentioned above, apoptosis is an orderly process. Kerr and colleagues described a regulated series of morphological changes that typically affected all cells undergoing apoptosis regardless of whether the cells were from a tadpole or human. Two distinct pathways have been described that initiate apoptosis: the intrinsic and extrinsic pathways. The extrinsic pathway of apoptosis is triggered by specific 'death receptors' displayed on the surface membrane of the cells whereas the intrinsic pathway is triggered as a result of noxious stimuli or by the loss of survival signals such as growth factors.

Fas (CD95) is a member of the Tumour Necrosis Factor Receptor (TNFR) superfamily and is among the best characterised of the death receptors. The ligand for Fas (FasL) may be expressed on the surface of leukocytes such as Mφ or T cells (Brown and Savill, 1999). Ligation of Fas ultimately results in activation of caspase-8 and then caspase-3. The intrinsic pathway will occur if a stimulus such as DNA damage recruits pro-apoptotic members of the Bcl family of proteins such as Bax to the outer mitochondrial membrane where they trigger the opening of mitochondrial pores. This results in the release of pro-apoptotic molecules such as Apoptosis Inducing factor (AIF) and cytochrome C into the cytoplasm. These molecules trigger a cascade of events involving the formation of the Apoptosome - a multimolecular complex comprising Apoptotic Protease Activating Factor 1 (APAF-1), cytochrome C and pro-caspase 9. This proteolytic complex converts pro-caspase-3 to active caspase-3 that is capable of cleaving many intracellular proteins. There are additional checks and balances on the intrinsic pathway to prevent inadvertent activation. For example, Inhibitor of Apoptosis Proteins (IAPs) act as an internal 'buffer' and can inhibit the activation of caspase-3. However in addition to pro-apoptotic molecules released from the mitochondria, Smac/DIABLO (second mitochondria-derived activator of caspase / direct inhibitor of apoptosis binding protein) is also released from the mitochondria following activation of the intrinsic pathway and Smac/DIABLO inhibits IAPs thereby ensuring that apoptosis ensues. A simplified, schematic diagram is offered in figure 1.4 whilst Hengartner describes the pathways in much greater detail in a comprehensive review (Hengartner, 2000). The activation

of caspase-3 is a key initial step of the final execution pathway that leads to cleavage of chromosomal DNA, nuclear condensation and apoptosis.

Caspases have a rather unique ability to activate each other merely by proximity (Hengartner, 2000) and most of the components required for activation and execution of the intrinsic pathway are pre-formed and 'ready to go' (Rich et al., 2000). Apoptosis is held in check by ensuring that the protagonists are separated and tightly controlled. The benefit of this arrangement is, of course, that when necessary apoptosis can be rapidly activated in an injured or dysfunctional cell.
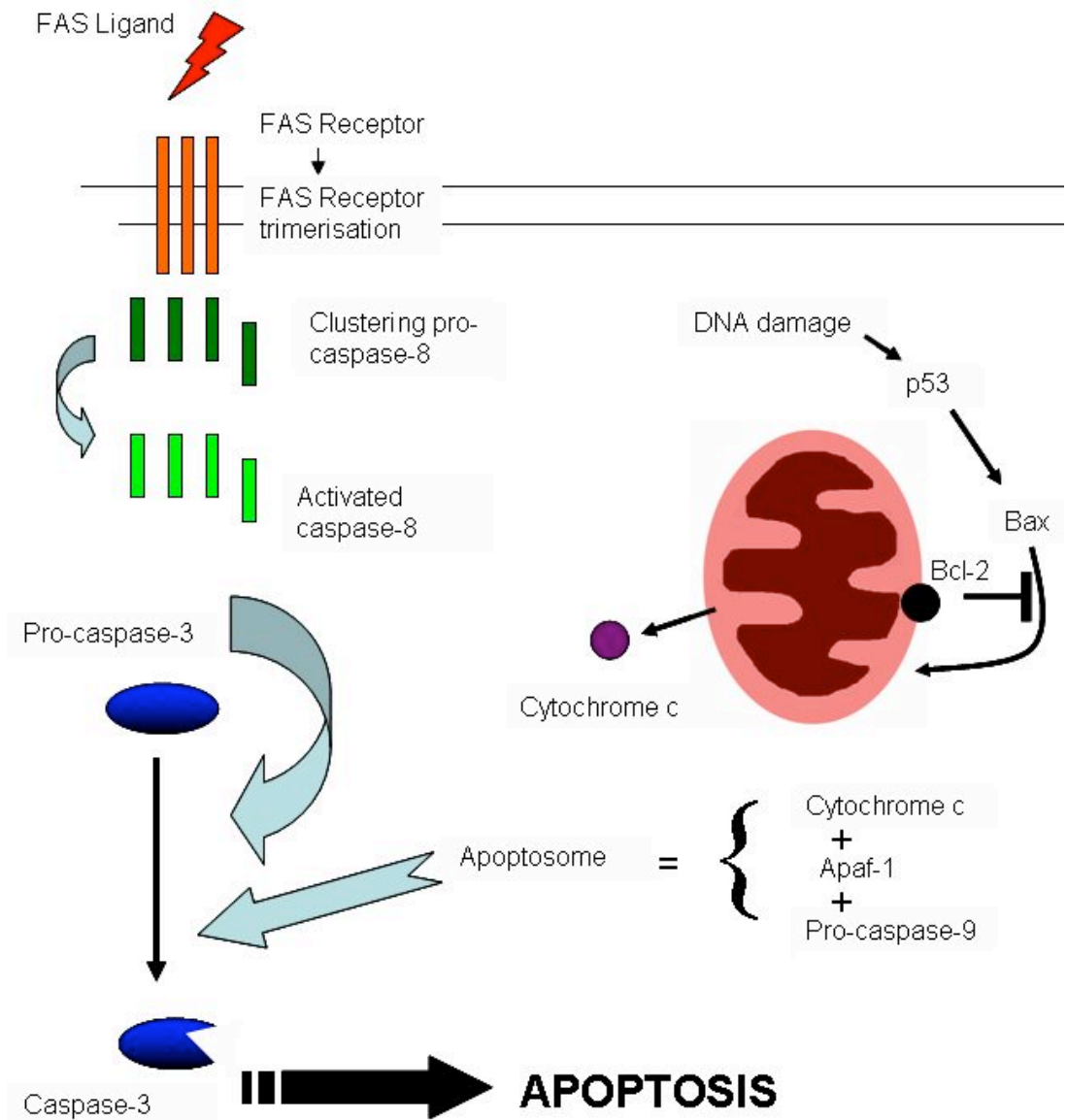
Figure 1- 4   Schematic diagram of apoptotic pathways
Apoptosis can be initiated via the extrinsic pathway via the4 cell surface Fas death receptor or via intrinsic mitochondrial pathway. Fas ligation by Fas ligand results in trimerisation of Fas and clustering of Fas-associated death domain and pro-caspase-8. Proximity activation results in the conversion of pro-caspase-8 to active caspase-8. Caspase-8 activates caspase-3 to initiate apoptosis. Injurious stimuli, including DNA damage will result in the release of p53 from the nucleus and translocation of pro-apoptotic members of the Bcl family of proteins such as Bax to the mitochondria. Pro-apoptotic and anti-apoptotic members of the Bcl family of proteins compete on the mitochondrial surface membrane. If the pro-apoptotic signal is dominant then pro-apoptotic such as cytochrome c will be released. Cytochrome c interacts in the cytosol with Apaf-1 and pro-caspase-9 to form the Apoptosome which can also activate caspase-3 to initiate the final execution phase of apoptosis. (Modified from Hengartner, 2000)

1.5.2 Failure to clear AC contributes to autoimmunity

In the previous paragraphs, phagocytosis and apoptosis have been discussed. It is evident that there are numerous receptors involved in the phagocytic clearance of AC. Whilst several of these receptors appear to be important *in vitro*, their absence *in vivo* using specific knockout mice, often produces a far less dramatic phenotype than predicted. For example, targeted disruption of SRA in murine thymic Mφ resulted in a 50% reduction in the phagocytosis of apoptotic thymocytes *in vitro* (Platt et al., 1996). However, analysis of thymuses from SRA knock out (KO) mice demonstrated no increased number of AC even following exposure of mice to gamma radiation that increases the rate thymocyte apoptosis (Platt et al., 2000). One explanation is that there is considerable redundancy built into the clearance of AC such that failure of a single receptor will not compromise the AC clearance system. Redundancy of this type underscores the evolutionary importance of phagocytic clearance of AC.

An exception to the above phenomenon is the C1qa KO mouse. C1q is the first component of the pathway of classical complement activation. The globular heads of C1q (often described as a bunch of tulips) bind to motifs on the surface of pathogens and AC, whilst the stalk binds to calreticulin on the surface of Mφ to facilitate phagocytosis (Ogden et al., 2001). Both *in vitro* and *in vivo* studies using peritoneal Mφ from C1q KO mice have demonstrated reduced clearance of AC with the intraperitoneal administration of C1qa replete serum to C1q KO mice restored the effective clearance of AC (Taylor et al., 2000). Interestingly, C1qa KO mice develop an autoimmune disease resembling Systemic Lupus Erythematosis (SLE) in humans, with autoantibodies targeting antinuclear antigens and a proliferative glomerulonephritis (Botto et al., 1998). The evidence that links the defective clearance of AC in these mice to the subsequent development of autoimmunity is largely circumstantial, but compelling nonetheless.

Increased numbers of free AC were apparent in the glomeruli of C1qa KO mice. In additional studies, C1qa KO mice developed more severe injury than wild-type mice following the induction of experimental nephrotoxic nephritis with increased numbers of free AC visible within the glomeruli. Importantly, mice lacking components of the alternative complement cascade or components of the classical

activation pathway downstream from C1q did not develop an aggravated form of inflammation thereby localising the phenotype to C1qa deficient mice with defective AC clearance (Robson et al., 2001). Furthermore, normal mice injected with irradiated, syngeneic AC have been shown to transiently develop low levels of anti-nuclear autoantibodies, anti-cardiolipin antibodies and anti-single-strand DNA autoantibodies, together with mild glomerular immunoglobulin deposition (Mevorach et al., 1998): potential hallmarks of SLE.

In humans, homozygous C1q deficiency is the strongest independent predictor for SLE development (Botto and Walport, 2002) and monocyte-derived Mφ isolated from patients with SLE have been shown to exhibit defect phagocytosis of AC *in vitro* (Herrmann et al., 1998). Autoantigens targeted in SLE such as Ro, La and nucleosomal DNA, have been identified on the surface of apoptotic blebs derived from keratinocytes undergoing apoptosis (Casciola-Rosen et al., 1994).

Taken together, the accumulated body of circumstantial evidence becomes quite compelling. The mechanisms by which AC persisting in an inflammatory milieu could contribute to autoimmunity remain largely speculative (as reviewed by Rosen and Casciola-Rosen, 1999). Phagocytosis and subsequent degradation of AC by Mφ is highly efficient, minimises the presentation of apoptotic material and induces an anti-inflammatory phenotype as previously discussed. They propose that ineffective Mφ clearance of AC may result in AC phagocytosis by DC. The caspase mediated cleavage of proteins during apoptosis produces novel autoantigens with a 'non-tolerized structure'. Impaired clearance of AC would permit these novel antigens to accumulate to 'suprathreshold levels' in the presence of co-stimulatory molecules and thus enter class II MHC presentation. Thus, following AC phagocytosis, DCs may subsequently present autoantigen resulting in T cell activation. As mentioned above, this remains speculative. Other data suggests that phagocytosis of AC by DC contributes to both induction and maintenance of immunological tolerance (Huang et al., 2000). In addition Lynda Stuart demonstrated that DC that phagocytosed AC were subsequently defective in their production of IL-12 and exhibited an inability to stimulate naïve T cells (Stuart et al., 2002). Furthermore, not all experimental mice with defects in the clearance of AC develop autoimmunity, for example CD14 KO mice. Lars-Peter Erwig has therefore argued that it is the context in which AC material is presented to lymphocytes that is critical with autoimmunity developing if

the AC material is presented in conjunction with "danger-signals" (Erwig and Henson, 2007).

Jacqueline Trudeau published how the neonatal pancreas undergoes a wave of apoptosis as it undergoes the tissue remodelling required for adult life with this wave of cell death occurring shortly before NOD mice develop signs of autoimmunity (Trudeau et al., 2000). Importantly, as mentioned above (O'Brien et al., 2002), PMφ from NOD mice appear to exhibit defective clearance of AC *in vitro*, consistent with the observations of Jaqueline Trudeau that increased numbers of free AC were visible in the neonatal pancreata of these mice (Trudeau et al., 2000).

There is convincing circumstantial evidence defective that defective AC clearance may lead to autoimmunity, but clearly more work is required to prove a causal link and identify the mechanism(s).

1.6 *IN VIVO* MODELS OF INFLAMMATION

It is clear, as illustrated by work with receptors involved in phagocytic clearance of AC, that whilst *in vitro* studies can offer valuable insights, it is still necessary to test hypotheses *in vivo*. Mφ function and phenotype can be examined *in vitro*, but this does not necessarily predict their behaviour during inflammation *in vivo*. Before describing the peritoneal and pleural models of inflammation used in this thesis and the rationale for their choice, it is useful to review some of the key cells, chemokines, cytokines and protein cascades involved.

Descriptions of inflammation date back over 2000 years, referring to rubor (redness), tumor (swelling), calor (heat) and dolor (pain) as the visible, cardinal signs (Celsius 30BC to 38AD). Following on from Virchow (1799 to 1878), more recent descriptions tend to concentrate on the tissue infiltration by various leukocytes, the leakiness of blood vessels and the release of various proteins and regard these as the processes that generate the cardinal signs recognised for so long. It is descriptions of these latter processes that this review will focus on.

1.6.1 Key cells involved in peritoneal and pleural inflammation

Following an inflammatory stimulus, resident leukocytes together with local mesothelial cells, produce chemokines and cytokines that act to recruit additional leukocytes in an attempt to clear the noxious stimulus and ensure tissue repair.

In the early stages of inflammation cytokines induce blood vessels to constrict then dilate, increasing the blood supply and hence ensuring the rapid arrival of additional leukocytes. Cytokines also stimulate the vascular endothelium to display various adhesion molecules such as selectins, integrins and immunoglobulin-like adhesion molecules (ICAMs). These enable circulating leukocytes to roll along the endothelium cell surface (selectin-mediated) prior to firm binding to the endothelial cells (integrin-mediated). The leukocytes then transmigrate between cells, cross the basement membrane and enter the extravascular connective tissue. Chemokines released locally form chemical gradients that attract specific classes of leukocyte towards the site of inflammation.

Initially there is a rapid influx of large numbers of inflammatory cells, primarily polymorphonuclear cells (PMN). Monocytes leave blood vessels and become inflammatory Mφ (or DC) as they cross the basement membrane. NK cells arrive a little later. These cells together constitute the 'innate' immune response that is not targeted to specific antigens but capable of rapid mobilisation and effective action against a broad spectrum of threats. If inflammation persists, T and B lymphocyte populations are activated and are recruited to promote the highly focused 'adaptive' immune response. What follows below is a brief overview of various key cell populations and their roles in the inflammatory process. Although not an exhaustive account, it is clear that the different cell types influence maturation and function of each other in complex and often poorly understood interactions.

1.6.1.1 *Mesothelial Cells*

Peritoneal and pleural cavities are lined by a monolayer of mesothelial cells which constitute a slippery, non-adhesive and protective barrier against physical and infectious injury (Mutsaers, 2004). However these cells are not mere inactive bystanders in inflammation but play an active role as they can produce significant amounts of pro-inflammatory cytokines such as IL-1β (Lanfrancone et al., 1992) and IL-6 (Topley et al., 1993) as well as anti-inflammatory cytokines such as IL-10 (Yao

et al., 2004). Human mesothelial cells have also been demonstrated to release chemokines such as IL-8, MCP-1 and Regulated upon Activation, Normal T Expressed and Secreted (RANTES) following stimulation (Li et al., 1998).

Fibroblasts are present beneath the mesothelial monolayer and have also been implicated in the inflammatory response with the production of chemokines (Loghmani et al., 2002; Witowski et al., 2001).

1.6.1.2 *Mφ*

The roles played by both resident and inflammatory Mφ, initiating and orchestrating different aspects of inflammation, have been described in detail elsewhere (chapter 1.3). It should be noted, however, that resident Mφ populations are crucial for the initiation of the inflammatory response in both TG peritonitis and CG pleurisy. If the resident Mφ populations are depleted, the subsequent inflammatory response is almost completely muted. The response can be rescued by adoptively transferring appropriate numbers of the relevant resident Mφ (Cailhier et al., 2005; Cailhier et al., 2006).

1.6.1.3 *DC*

Immature DC reside in almost all peripheral tissues and serosal cavities. They express low levels of both MHC class I/II molecules and lack co-stimulatory molecules such that they have a limited capacity to activate lymphocytes (Janeway et al., 2004). They have numerous surface receptors in common with Mφ, including pattern recognition receptors such as Toll-like receptors and are constantly sampling the microenvironment. Similar to Mφ, immature DC are proficient at recognising and phagocytosing pathogens, a process which leads to their activation and maturation.

Mature DC may produce large quantities of pro-inflammatory cytokines such as TNF α, and migrate through the lymphatic vessels to regional lymph nodes. Expression of MHC and co-stimulatory molecules is up-regulated and mature DC are thus highly effective stimulators of naïve T cells.

1.6.1.4 *Mast cells*

Like Mφ, mast cells originate in the bone marrow and enter tissues. Immature mast cells are agranular or poorly granular whilst mature mast cells are highly granular and have a characteristic appearance. They are highly specialised cells and express

Fcε receptors on their surface. Mast cell degranulation occurs within seconds of these Fcε receptors becoming cross-linked by antigen. Mast cells produce a wide array of biologically active substances (Janeway et al., 2004) including preformed enzymes (such as tryptases) and vasoactive mediators such as histamine. Pro-inflammatory cytokines such as TNFα or anti-inflammatory cytokines such as IL-4 or IL-13 are synthesised after activation. Peritoneal mast cells are also a source of chemokines and play an important role in the recruitment of PMN to sites of inflammation (Qureshi and Jakschik, 1988).

1.6.1.5 *Natural killer cells*

NK cells are large granular lymphoid-like cells and account for approximately 3% of resident peritoneal cells (Kawamura et al., 1999). As reviewed by Wilson and Delovitch (Wilson and Delovitch, 2003), NK cells can rapidly produce a broad spectrum of both T_h1 cytokines such as TNFα and IFNγ, as well as T_h2 cytokines such as IL-4 and IL-13. Production of IFNγ appears to be dependent on IL-12 production by Mφ (Kawamura et al., 1999) NK cells also mediate cytotoxicity directly either through Fas-Fas Ligand interactions or perforin/granzyme pathways. As such, they are thought to play important regulatory roles during both innate and adaptive immune responses. NK cells (via activation of B1 cells) are essential in the recruitment of T cells to delayed hypersensitivity reactions in the skin (Szczepanik et al., 2003).

1.6.1.6 *Lymphocytes*

T lymphocytes (T cells) are derived from the bone marrow but mature in the thymus. They are classified according to the markers expressed on the cell surface. The majority express the αβ T cell receptor (TCR), and these are then subdivided according to the expression of CD4 and CD8. $CD8^+$ cytotoxic (T_c) cells recognise antigens presented by MHC class I molecules present on all nucleated cells and then use perforin and granzyme to induce lysis of the targeted cell. $CD4^+$ T helper (T_h) cells recognise antigens presented by MHC class II molecules present only on specific antigen presenting cells such as DC, Mφ and B cells in conjunction with co-stimulatory molecules such as CD80 and CD86. They then provide a range of cytokines and chemokines important to the innate immune response and critical to development of the adaptive immune response. $CD4^+$ cells are further subdivided according to the pattern of cytokines they produce: T_h1 cytokines promote a typically

pro-inflammatory response whereas T_h2 cytokines are typically anti-inflammatory but tend to be important in the immune response generated against parasites such as filarial worms. Lower numbers of T cells express a γδ TCR and these cells do not express either CD4 or CD8.

T lymphocytes are present in the naive peritoneum and the majority express the typical αβ TCR. The majority of these peritoneal T cells in humans are $CD8^+$ T cells. Most of the T cells within the peritoneum appear to secrete T_h1 cytokines. Although only a minority of cells secrete T_h2 cytokines, they appear to play a vital role in supporting B cell differentiation and synthesis of IgA and IgG (Birkhofer et al., 1996). 17% of T cells in the peritoneum express the γδ TCR and interestingly this group of cells appears important in promoting differentiation of inflammatory monocytes to tissue Mφ as infection resolves (Skeen et al., 2004). They also appear to limit leukocyte recruitment early in the inflammatory response to *Bordetella pertussis* within the lung (Zachariadis et al., 2006).

B lymphocytes (or B cells) account for a substantial proportion of the cell population resident in either peritoneal or pleural cavities. Within the peritoneal cavity they account for up to 40% of total cells and can be divided into roughly equal numbers of either B1 or B2 cells (Hayakawa et al., 1985).

B2 cells are the circulating B cells derived from the bone marrow and matured in peripheral lymphoid tissue. They express a specific, membrane-bound immunoglobulin on their cell surface (the B cell receptor). Mature B cells circulate through the tissues until they encounter the specific antigen capable of stimulating their specific BCR, but they cannot become fully activated until they receive an additional signal from a T_h cell in a peripheral lymph node. Upon full activation these cells undergo clonal expansion and maturation to antibody producing plasma cells. B2 cells are also proficient antigen presenting cells, capable of recognising, processing and presenting antigen to T_h cells in conjunction with MHC class II. Although not as proficient as DC at T cell activation, they are frequently present in much greater numbers.

B1 cells are much rarer outside serosal cavities. An important function of B1 cells is the production of polyspecificity natural antibodies (IgM) that are synthesised and excreted prior to pathogen exposure. These antibodies bind other immunoglobulins,

self antigens and common bacterial polysaccharides. They are therefore effective at opsonising bacterial pathogens and AC thus facilitating phagocytosis. Unlike B2 cells, the B1 cell response is independent of T cells.

Mice deficient in B1 cells exhibit defective viral clearance, even if production of IgM by B2 cells is normal (Baumgarth et al., 2000). The presence of B1 cells is essential for subsequent T cell recruitment, both to delayed hypersensitivity reactions in the skin (Szczepanik et al., 2003) and also to filarial infections (Ramalingam et al., 2003) in the peritoneum. Interestingly secreted IgM from B cells appears effective in augmenting IgG responses to pathogens whilst reducing IgG autoantibodies (Boes et al., 2000).

1.6.1.7 *PMN*

PMN originate in the bone marrow from a common precursor cell shared with Mφ and DC (Fogg et al., 2006). Once released, PMN circulate between the vascular tree and the bone marrow until they either migrate into an inflammatory site or become senescent and are removed (Martin et al., 2003). There is therefore a pool of PMN, ready and waiting to react to inflammatory stimuli, enabling the rapid influx mentioned above. PMN do not appear to constitute a significant number of residential peritoneal cells but are rapidly recruited if required.

Once they arrive at the site of inflammation, PMN play an important part in the phagocytosis of pathogens opsonised with immunoglobulins or complement factors. Intracellular granules within the PMN, containing bactericidal substances such as proteases, myeloperoxidase, hydrolase enzymes and defensins, fuse with the phagosome surrounding the ingested bacteria. The PMN generates NO, the superoxide anion (O_2^-) and hydrogen peroxide (H_2O_2), in a 'respiratory burst' and these are also directly toxic to bacteria.

PMN are terminally differentiated cells and once they have crossed the vascular endothelium, entered a site of inflammation and become activated, they cannot return to the circulation. Either shortly after phagocytosis or once they become senescent, they die by apoptosis and in turn, are removed by phagocytosis. The ordered, controlled, death of infiltrating PMN by apoptosis is thought to be important to prevent the release of the highly toxic granules into surrounding tissues.

Having briefly reviewed the key cells involved in peritoneal and pleural inflammation, it is sensible to review some the cytokines and chemokines produced by these cells.

1.6.2 Cytokines

These can be defined as proteins released by cells that have an affect on other cells via specific receptors. They are released by tissues (mesenchymal cells) as well as leukocytes and together they affect a myriad of diverse outcomes. The functions of different cytokines can directly oppose each other, offering inflammatory processes a system of 'checks and balances' or they can have synergistic effects to amplify an inflammatory response. In the paragraphs that follow, the functions of important cytokines have been briefly reviewed. These are not intended to be exhaustive reviews and further reading may be desired.

1.6.2.1 *TNFα*

This is a potent pro-inflammatory cytokine that act through the NFκB intracellular pathway. It iss produced by a wide range of cells such as classically activated Mφ, NK cells, T cells and also epithelial cells. It acts locally to activate vascular endothelial cells, upregulate adhesion molecules and increase vascular permeability, thus increasing access of effector cells into inflamed tissue. Conversely it also works to increase drainage of fluid and the exit of cells such as maturing DC to lymph nodes. It contributes to local tissue damage and can provoke apoptosis. Systemically TNFα contributes to fevers and the systemic inflammatory response syndrome. TNFα also acts to increase production of other pro-inflammatory cytokines such as IL-1β and IL-6 (O'Shea et al., 2002).

1.6.2.2 *IFNγ*

This is predominantly produced by cells of lymphoid origin (NK and T cells), with production by cells of myeloid lineage being uncertain. As a member of the interferon family it has important functions in host defense against viral infection, but its actions are far broader. Like IL-1β and TNFα, it is a potent pro-inflammatory cytokine, but acts via the STAT-1 pathway. $CD4^+$ cells that mature in the presence of IFNγ will be committed to a T_h1 differentiation. It has also been shown to have a major impact on chemokine production (see below) and thus leukocyte recruitment as MCP-1 and RANTES are increased whilst IL-8 is decreased (Robson et al., 2001).

1.6.2.3 *IL-6*

IL-6 is a complex cytokine that exhibits a pro-inflammatory phenotype and recruits leukocytes to sites of inflammation (Cuzzocrea et al., 1999; Romano et al., 1997). Also circulating IL-6 acts upon hepatocytes and stimulates an acute phase response with the production of a range of proteins including the opsonins C-reactive protein and mannose-binding lectin (Janeway et al., 2004). IL-6 also displays anti-inflammatory properties and up-regulating the Mφ production of IL-1 receptor antagonist and soluble TNFα receptors, thus limiting the biological effect of these cytokines (Tilg et al., 1997). IL-6 KO mice exhibit much greater TNFα responses and PMN recruitment to endotoxin-exposed lungs than wild-type mice (Xing et al., 1998). The exact mechanisms or situations that determine whether IL-6 will act as a pro or anti-inflammatory cytokine remain unclear.

1.6.2.4 *IL-10*

IL-10, produced by Mφ, lymphocytes and keratinocytes is classified as an anti-inflammatory cytokine. By inhibiting IL-12 release from Mφ it tends to inhibit T_h1 and promote T_h2 responses. IL-10 inhibits PMN recruitment by downregulation of CXC chemokine production and appears to have a profound affect on PMN function, impairing phagocytic and bactericidal ability (Laichalk et al., 1996). In a murine model of Klebsiella pneumonia, neutralisation of IL-10 *in vivo* resulted in enhanced pro-inflammatory cytokine production, bacterial clearance and increased short and long-term survival (Standiford et al., 1996). In addition to being anti-inflammatory IL-10 seems to play a central role in the maintenance of peripheral tolerance as the activation of $CD4^+$ T cells by immature DCs induces the generation of IL-10 secreting $CD4^+CD25^+FOXP3^+$ T_{reg} cells. Conversely DCs exposed to IL-10 develop an alternatively activated state, resistant to maturation that induces expansion of the IL-10 secreting T_{reg} population (Lan et al., 2006). Thus there appears to be a "two-way relationship" between tolerogenic DC and T_{reg} (Mahnke et al., 2007).

1.6.2.5 *IL-12*

IL-12 links the innate and adaptive arms of the immune system. IL-12 is primarily produced by Mφ, DC and B cells and induces T_h1 differentiation of $CD4^+$ cells. As a result of skewing $CD4^+$ cells towards a Th1 phenotype IL-12 has marked pro-inflammatory consequences.

1.6.3 Chemokines

Chemokines are small proteins released by a wide range of cells to attract leukocytes bearing the relevant chemokine receptor as leukocytes migrate down a chemokine gradient towards the source of secretion. Differential receptor expression across leukocyte groups allows chemokines to achieve selective recruitment of different cell types at appropriate stages of the inflammatory process. Chemokines may have additional properties as outlined in tables 1.6 and 1.7.

Chemokines are classified into 4 groups according to the number of amino acids between the two cysteine residues nearest the N terminal position: CC, CXC, CX_3C and C. The former 2 groups make up the vast majority of known chemokines, with only one example of each of the latter 2 groups known. Broadly speaking CXC chemokines recruit PMN or lymphocytes whereas CC chemokines attract Mφ and DC (see tables 1.6 and 1.7).

Chemokine	Produced by	Receptors	Cells Attracted	Major effects
CXCL8 (IL-8) [closest analogue to KC in the mouse]	Monocytes, Mφ Fibroblasts Keratinocytes Endothelium	CXCR1 CXCR2	PMN Naïve T cells	Mobilises, activates & degranulates PMN Angiogenesis
CXCL7	Platelets	CXCR2	PMN	Activates PMN Clot resorption Angiogenesis
CXCL1 (GRO$_\alpha$) CXCL2 (GRO$_\beta$) [MIP-2 in the mouse] CXCL3 (GRO$_\gamma$)	Monocytes, Mφ Fibroblasts Endothelium	CXCR2	PMN	Activates PMN Fibroplasia Angiogenesis
CXCL10	Keratinocytes Monocytes Fibroblasts T cells Endothelium	CXCR3	Naïve T cells NK cells Monocytes	Anti-angiogenic Pro T$_h$1
CXCL12 (SDF-1)	Stromal cells	CXCR4	Naïve T cells Progenitor B cells Senescent PMN	B cell development Lymphocyte homing PMN retention in bone marrow
CXCL13 (BLC)	Stromal cells	CXCR5	B cells	Lymphocyte homing

Table 1- 6   Properties of selected CXC chemokines
(modified from Janeway et al., 2004).

Chemokine	Produced by	Receptors	Cells Attracted	Major effects
CCL3 (MIP-1α)	Monocytes, Mast Cells T cells Fibroblasts	CCR1,3,5	Monocytes DC NK & T cells Basophils	Pro T_h1
CCL4 (MIP-1β)	Monocytes, Mφ PMN Endothelium	CCR1,3,5	Monocytes DC NK & T cells	Competes with HIV-1
CCL2 (MCP-1)	Monocytes, Mφ Fibroblasts Keratinocytes	CCR2B	Monocytes DC NK & T cells Basophils	Activates Mφ Basophil histamine release
CCL5 (RANTES)	T cells Endothelium Platelets	CCR1,3,5	Monocytes DC NK & T cells Eosinophils Basophils	Degranulates basophils Acivates T cells Chronic Inflammation

Table 1- 7   Properties of selected CC chemokines
(modified from Janeway (Janeway et al., 2004)).

1.6.4 Additional inflammatory mediators

In addition to the cytokines and chemokines outlined previously, there are numerous additional immunologically active molecules produced during inflammation, including prostaglandins, prostacylins, thromboxanes and leukotrienes that are derived from arachidonic acid metabolism. Prostaglandins in particular effect several of cardinal signs of inflammation such as swelling and pain, whilst thromboxanes play important roles in platelet activation and clot formation.

The complement system was discussed earlier in relation to phagocytosis, but as a cascade of proteolytic enzymes it is intimately involved in several functions of the immune system. Figure 1.5 summarises the complement cascade, and the different pathways capable of initiating the system. The effects of some of the smaller cleavage products especially C3a, C4a and C5a are of particular relevance to this thesis since NOD mice have been shown to be completely deficient in C5 (Lynch and Kay, 1995), the most potent of them all. All 3 complement cleavage products induce smooth muscle contraction and increase vascular permeability. C5a and C3a can also induce expression of adhesion molecules enhancing the influx of inflammatory leukocytes (and the efflux of maturing DC). They activate mast cells to release histamine and pro-inflammatory cytokines such as TNFα. C5a also effects PMN and monocytes directly with a potent chemokine effect, and in addition enhances phagocytic abilities.
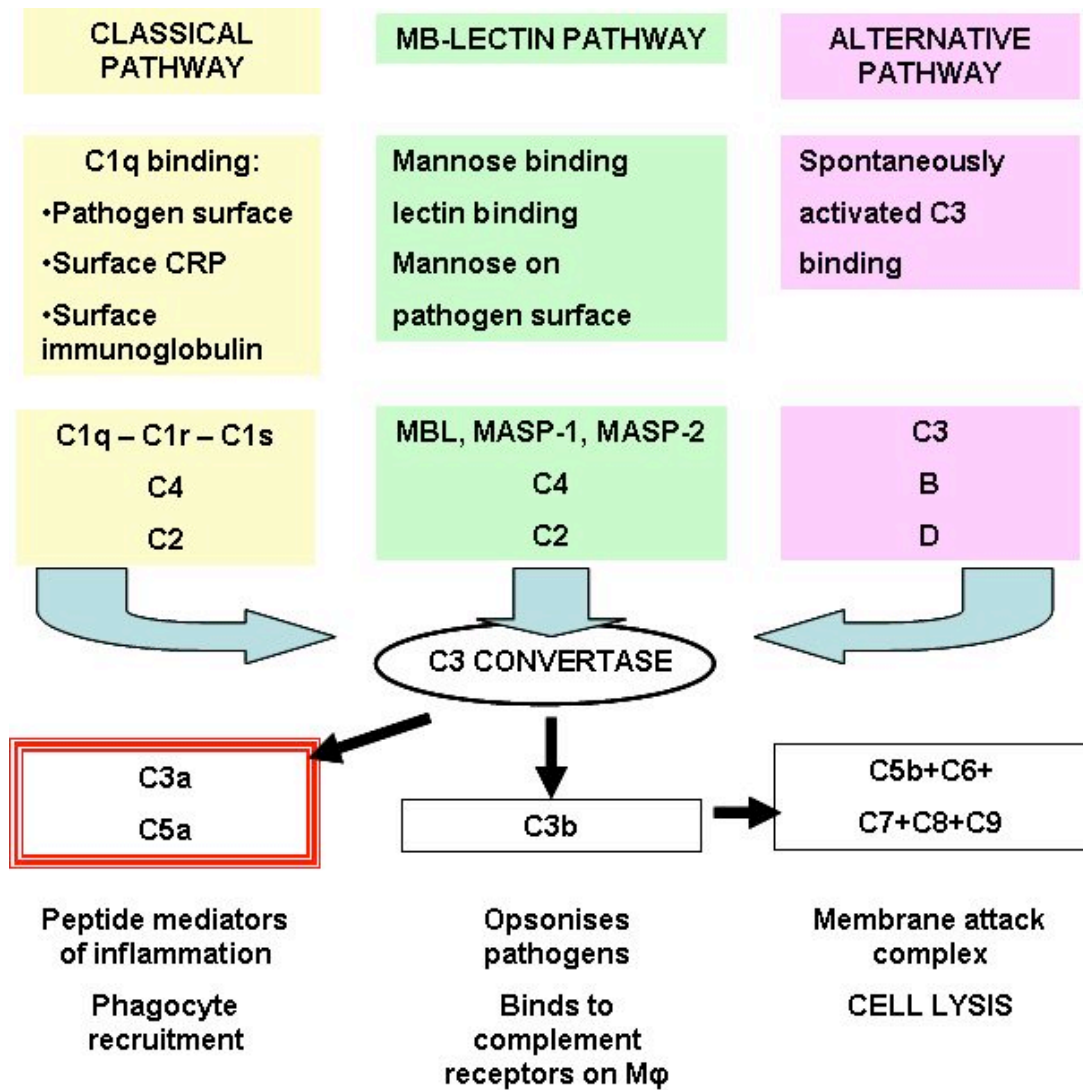
Figure 1- 5   Complement Pathways
The complement cascade can be activated by 3 distinct pathways. The classical pathway is initiated when the C1q complex binds the surface of a pathogen directly, or binds to either CRP or immunoglobulin adherent on the surface. C1q binding activates C1r to activate C1s. C1s then cleaves C4 and C2 to release C4b and C2b respectively and these components combine to form C3 convertase. The mannose binding lectin (MBL) pathway is initiated by MBL binding to mannose, activating MASP-2 to cleave C4 and C2 which then go on to form C3 convertase. The alternative pathway results from spontaneous hydrolysis of C3 enabling it to bind factor B which is then cleaved by factor D producing a soluble C3 convertase. C3 convertase, capable of cleaving C3 into C3a and C3b, unites the different arms of the complement cascade. C3b on the surface of pathogens can utilize components C5 through to C9 to form the membrane attack complex, which effectively punches holes in the cell membrane. Complement inhibitors on the surface of host cells act to limit complement-mediated injury to host cells. C3b itself is a potent opsonin and can interact with complement receptors on phagocytes. C3a and C5a are potent inflammatory mediators with chemotactic effects (modified from Janeway et al., 2004).

1.6.5 TG peritonitis

Brewer's thioglycollate (TG), originally devised as a culture medium, has long been used to generate a form of peritonitis in mice (TG peritonitis). It is a spontaneously resolving model of inflammation, characterised by a brisk influx of PMN that peaks at 6 to 12 hours after the intraperitoneal injection of TG and resolves by 36 hours (Baron & Procter, 1982). The monocytes influx is slower and more prolonged, peaking at 48 to 72 hours. The inflammatory response subsides by day 7 to 10 (Melnicoff et al., 1989).

The exact nature of the inflammatory stimulus is unknown and probably non-specific in view of the cocktail of ingredients! The solution of TG in sterile water is autoclaved during preparation, prior to injection raising the possibility that advanced glycation end-products (AGEs) and their receptor (RAGE) may be important (Chavakis et al., 2003; Li et al., 1997). Importantly, in light of the fact NOD mice lack C5, TG peritonitis appears to involve complement independent pathways (White et al., 2002). The main attraction of TG peritonitis over the years has been as a source of Mφ or PMN for use in *ex-vivo* experiments (Baron and Proctor, 1982; Gallily et al., 1964).

Within our laboratory, Jean-Francois Cailhier and colleagues, used a conditional Mφ-depletion system to demonstrate the critical importance of resident peritoneal Mφ in sensing the TG stimulus and initiating the subsequent inflammatory process, recruiting the initial PMN influx via the CXC chemokine MIP-2 (Cailhier et al., 2005). The model therefore has certain advantages over other, more 'disease relevant' models of inflammation when probing Mφ function *in vivo* in the NOD mouse model of autoimmune diabetes as it is reasonably well characterised and clearly profoundly dependent on resident Mφ function.

1.6.6 CG pleurisy

CG, an Irish sea moss, has become well established as an induction agent for pleural inflammation (Murai et al., 2003). When injected into the pleural cavity, it produces a self-limiting inflammatory process, generally considered an acute, complement-dependent, model of sterile inflammation. Akin to TG peritonitis, CG pleurisy is characterised by a brisk PMN influx followed by slower monocyte infiltration (Ackerman et al., 1980).

Frequent use has been made of the model by the pharmaceutical industry, using the PMN influx as an experimental read-out, to assess anti-inflammatory properties of their agents (Cuzzocrea et al., 2000; Cuzzocrea et al., 2004; Cuzzocrea et al., 1999). It has also been widely used to assess the importance of various established inflammatory mediators *in vivo*. (Cuzzocrea et al., 2000; Gilroy et al., 1999; Gilroy et al., 2004). Similar to TG peritonitis, the resident pleural Mφ has been shown to be critical for sensing the inflammatory stimulus and orchestrating the subsequent inflammatory process via the chemokine MIP-2 and a range of pro-inflammatory cytokines (Cailhier et al., 2006)

1.6.7 Delayed Type Hypersensitivity Pleurisy

Delayed Type Hypersensitivity (DTH), or Allergic Pleurisy, is used to examine aspects the adaptive immune system. Animals are actively sensitised to an antigen by subcutaneous or intra-dermal injection in conjunction with haptens. Langerhans cells within the dermis process the antigen and present it to $CD4^+$ cells with IL-12 thereby skewing a T_h1 response. A brisk adaptive immune response is initiated some days later when the animal is re-exposed to the antigen by an intra-pleural injection (see figure 1.6). Antigen presenting cells within the pleural cavity process the antigen and present it to the primed CD4+ cells which in turn produce large quantities of pro-inflammatory cytokines and CCL3 (MIP-1α) to recruit inflammatory Mφ. The Mφ, $CD4^+$ cells and local mesothelial cells all act to recruit additional inflammatory cells to the pleural cavity including PMN, mast cells and eosinophils resulting in an acute inflammatory response and local tissue damage.

Within the recent published literature, the DTH model of allergic pleurisy has been used to dissect mechanisms underpinning delayed hypersensitivity. The fact the inflammatory response takes place within a serosal cavity whereby the infiltrating cells are easily recoverable by lavage makes it extremely attractive for these uses. Cytokines and chemokines produced can be measured in the lavage fluid; blocking antibodies can introduced and their effects quantitatively measured (Aliberti et al., 2003; Klein et al., 2002; Klein et al., 2000; Pinho et al., 2003; Sampaio et al., 2000).

Although monocyte and Mφ recruitment is a major part of DTH, the process is not dependent on these cells for the initiation of the inflammatory response as the $CD4^+$

T cell is key. It is therefore a useful model to contrast with the Mφ-dependent models of TG peritonitis and CG pleurisy.
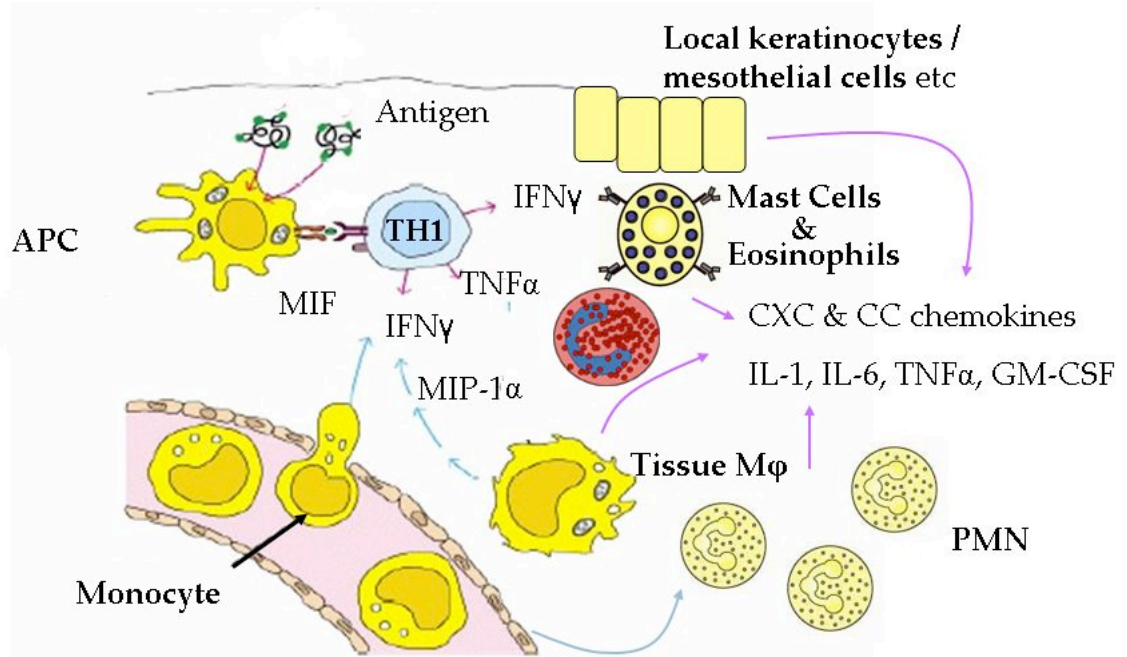
Figure 1- 6   Delayed-Type Hypersensitivity Pleurisy
The initial phase of the inflammatory response, sensitization, follows the intra-dermal or subcutaneous injection of antigen together with a hapten. The antigen is taken up by dendritic cells, processed and presented to $CD4^+$ cells to elicit a T_h1 response, memory T cells are formed. The second phase occurs when antigen alone is injected intra-pleurally several days later. It is quickly picked up by antigen presenting cells (APC) and presented to memory T cells, again eliciting a T_h1 response characterized by IFNγ, TNFα, macrophage inhibitory factor (MIF) and the important CC chemokine, MIP-1α. These chemokines and cytokines recruit inflammatory monocytes, mast cells and eosinophils. These leukocytes and the local mesothelial cells in turn produce a range of CC and CXC chemokines plus additional pro-inflammatory cytokines, recruiting PMN and provoking local tissue damage and oedema.

1.7 AIMS OF THE STUDY

The aims of this study were to examine the role(s), if any, that Mφ function played in the development of autoimmunity in general and autoimmune diabetes in particular within the NOD mouse.

The first aim was to confirm or refute the phagocytic defect observed in NOD Mφ during the clearance of AC *in vitro* and *in vivo*. If this defect was confirmed then what was the nature of the underlying mechanism and could this be linked to the development of diabetes?

The second aim of the project was to probe the apparent contradictory nature of the inflammatory phenotype of NOD-derived Mφ, both *in vitro* and *in vivo*.

Chapter 2. Methods

2.1 EXPERIMENTAL ANIMALS

Mice were housed in cages with free access to food and drinking water in a constant temperature room with a 12-hour light/dark cycle. All experiments were performed in accordance with the UK Government Home Office regulations.

2.1.1 Non Obese Diabetic Mice

NOD mice used in this thesis come from 3 distinct sources that may exhibit slight genetic differences. The NOD mice used for the *in vitro* phagocytosis experiments (chapter 3.2.1) were a gift from Dr FS Wong, Bristol University. Subsequently a breeding pair was purchased from Charles River (Italy), and a breeding colony established in the BRR animal facility, Little France, Edinburgh. NOD mice from this colony were used for all remaining experiments conducted at the Centre for Inflammation Research, Edinburgh University. *In vivo* phagocytosis assays and studies of sterile peritonitis were also conducted at the Cambridge Institute of Medical Research, Cambridge University (see chapter 5.2.3) and used NOD mice from their breeding colony which were originally obtained from Taconic Farms, USA.

All NOD mice were regularly tested for diabetes mellitus, either by blood or urine testing, as part of routine animal husbandry. Any NOD mice that tested positive for diabetes mellitus were immediately sacrificed and not used in any experimental procedure.

2.1.2 C57BL/6 Mice

C57BL/6 mice were bred at the BRR animal facility.

2.1.3 NOD.H2I^7 Congenic Mice

NOD.H2I^7 congenic mice were a gift from Dr FS Wong, Bristol University.

2.1.4 NOD.R320, NOD.R20, NOD.1591 and NOD.R905 Congenic Strains

Various congenic NOD strains including NOD.R320, NOD.R20, NOD.1591 and NOD.R905 were a gift from Professor L Wicker, Cambridge University.

2.2 CELLS

2.2.1 Resident Peritoneal Macrophages

2.2.1.1 *Recovering and Purifying Resident Peritoneal Macrophages*

The abdomen of a mice killed by schedule 1 was liberally sprayed with 70% ethanol and the abdominal skin reflected away from the intact peritoneal membrane by a midline incision and blunt dissection. Peritoneal cells were recovered by peritoneal lavage using 5ml of ice-cold phosphate buffered saline without cations (PBS). Depending on the experiment, samples of recovered lavage fluid (usually > 4ml/mouse) were either kept separate in 15ml tubes (BD Falcon, UK) or pooled according to strain in 50ml tubes (BD Falcon, UK). All tubes of lavage fluid were kept on ice pending further analysis.

Total leukocyte count of lavage fluid was obtained by haemocytometer. The samples were then centrifuged at 300g for 5 minutes at 4^oC and re-suspended at 1×10^6 cells/ml in Dulbecco's Modified Eagle medium with F12 (DMEM/12). Resident PMø were isolated from other peritoneal cells by adhesion to tissue culture plastic. Peritoneal cells were seeded into Costar plastic wells (Corning Life Sciences, Netherlands) and incubated for 1 hour at 37^oC with 5% CO_2. The numbers of cells and well size varied between experiments (see results chapters). Cells were then washed gently 3 times with warm DMEM/12 using a 1ml Pasteur pipette to remove non-adherent cells. After the 3rd wash the remaining adherent cells were incubated in DMEM/12 containing 100U/ml penicillin, 100U/ml streptomycin, supplemented with or without 10% Foetal Bovine Serum (FBS from Life Technologies, UK) as required.

2.2.1.2 *Assessing Purity of Resident Peritoneal Macrophages*

The purity of isolated PMφ was assessed by flow cytometry using F4/80, a murine marker with a high specificity for macrophages (McKnight et al., 1996). 1×10^6 peritoneal cells were seeded into 12-well plates and PMφ purified as described above. After the 3rd wash the media was replaced with 1ml ice-cold PBS and the adherent cells were scraped off using a cell scraper and transferred to chilled

polystyrene fluorescence-activated cell sorter (FACS) tubes (BD Falcon, UK). As a control, 200μl aliquots of peritoneal cells were placed directly in chilled FACS tubes and kept on ice. Cells were then centrifuged at 300g for 5 minutes at 4°C, re-suspended in 200μl blocking solution (PBS containing 10% mouse serum) and incubated for 30 minutes on ice. 50μl Allophycocyanin (APC) conjugated monoclonal rat-anti-mouse F4/80 (IgG2aκ, Caltag Laboratories, UK) diluted 1/100 in blocking solution, or the isotype control, was then added. Cells were mixed gently and incubated on ice for a further 30 minutes in the dark. Cells were then washed with cold PBS to remove excess antibody and re-suspended in 200μl of PBS. Analyses were performed using a FACScan instrument (Becton Dickinson, UK) and the results analysed by FlowJo software (Treestar, USA).

Over 86% of cells purified by adhesion were PMφ, characterized as F4/80^{HI}, whilst PMφ comprised ~50% of total resident peritoneal cells (figure 2.1).

2.2.2 RESIDENT PLEURAL MACROPHAGES

To avoid potential haemorrhage into the thoracic cavity from cervical dislocation, alternative methods of schedule 1 killing were employed such as rising concentrations of CO_2. The abdomen of the mouse was sprayed with 70% ethanol and the abdominal cavity opened by a wide transverse incision just below the rib cage. The abdominal organs were reflected away to expose the diaphragm. The diaphragm was punctured by a small, anterior, mid-line incision and the pleural cavities were lavaged with 1ml sterile 3.88% sodium citrate (Sigma, UK) in saline using a sterile Pasteur pipette. The recovered lavage fluid was either placed individually in 1.5ml Eppendorf tubes or placed in 15ml tubes (BD Falcon) and pooled according to strain, depending upon experimental requirements. Cells were kept on ice pending further analysis and/or purification of resident pleural macrophages (PLMφ) as detailed for PMφ above.
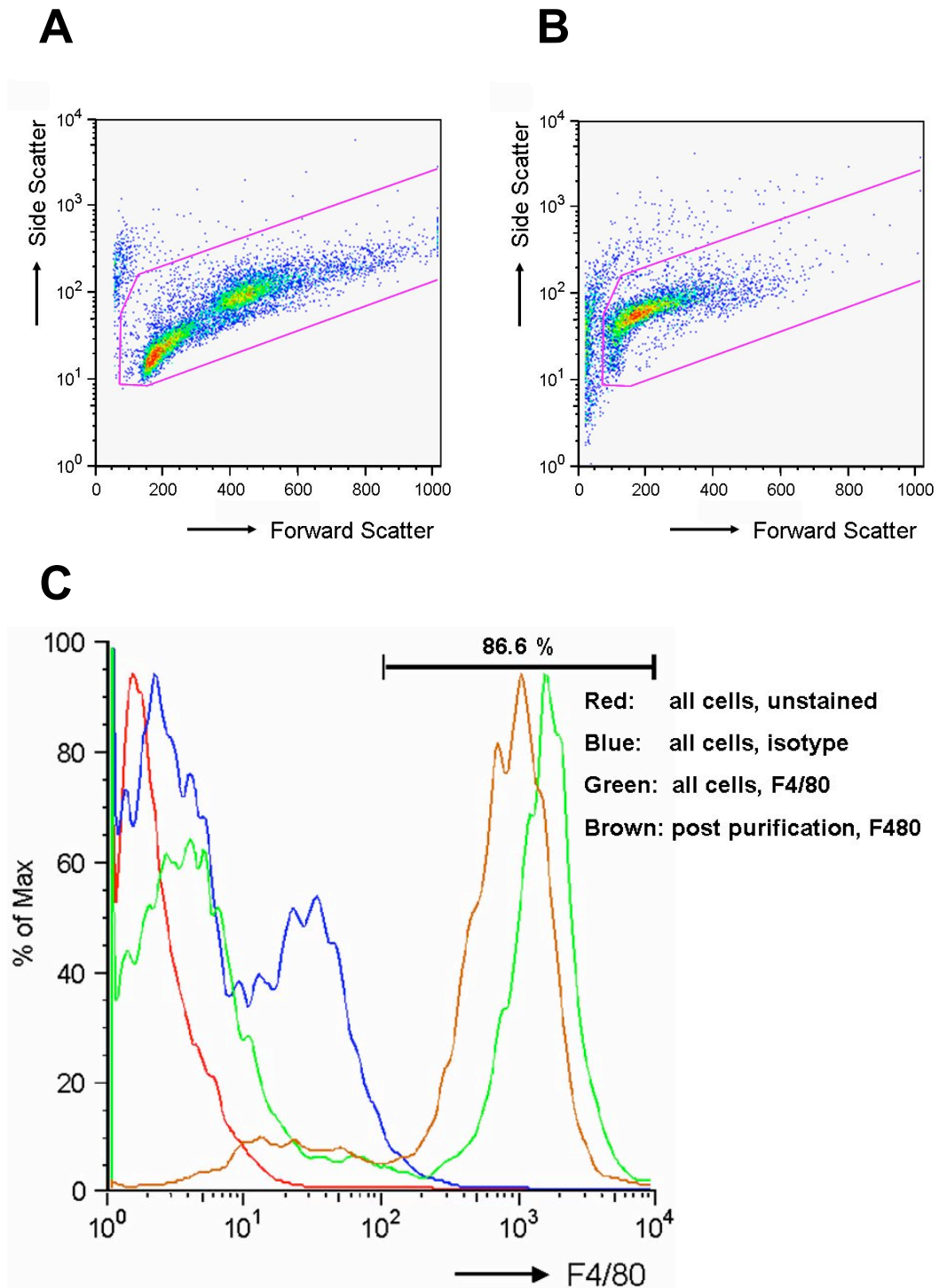
Figure 2- 1   Analysis of resident peritoneal macrophages purified by adhesion
Resident peritoneal cells recovered by lavage with ice-cold PBS were plated into plastic wells and left to adhere for 1 hour at 37°C. Non-adherent cells were removed by washing and adherent cells were mechanically removed by cell scraper and stained for the murine Mφ marker F4/80 before analysis by flow cytometry. (A) Forward and side scatter plots of peritoneal lavage fluid. (B) Forward and side scatter plots of peritoneal cells following purification by adhesion. (C) Over 86% of adherent cells (brown line) were strongly F4/80 positive indicating a high purity of Mφ achieved by this method of purification.

2.2.3 Bone Marrow Derived Macrophages

2.2.3.1 *Macrophage Colony Stimulating Factor from L929 cells*

Maturation of bone marrow derived macrophages (BMDMφ) requires the presence of macrophage colony stimulating factor (M-CSF) in the culture medium and this was derived in-house using medium conditioned by L929 cells. L929 cells are a malignant murine fibrosarcoma cell line and spontaneously secrete M-CSF into the supernatant. L929 cells were maintained in DMEM/12 medium supplemented with penicillin (100U/ml), streptomycin (100μg/ml) and 10% FBS (referred to as 'Mφ medium'). The cells were grown in Costar T162cm^2 flasks (Corning Life Sciences, Netherlands) with 25ml medium and split 1:30 when they reached confluency, usually after 7 days. Supernatants were harvested, filtered through a 0.45μm filter, aliquoted and then stored at -80ºC until required.

2.2.3.2 *Dissection of intact femurs and maturation of BMDMφ*

Mice were sacrificed and liberally spayed with 70% ethanol. Fur over the hind legs was removed by pulling from a transverse skin incision across the anterior abdomen to "de-trouser" the mouse. As much muscle as possible above and below the femur was carefully removed using sterile scissors. In order to free the femur, the tibia and fibula were cut distally whilst the pelvic bones were cut through proximally. Care had to be taken not to cut through the femur itself. Residual muscle was removed with disinfectant wipes and the femur dipped briefly in 70% ethanol before being placed in a sterile container with chilled Hank's Buffered Salt Solution (HBSS) containing 100U/ml penicillin and 100μg/ml streptomycin. The bones were placed on ice and transported to a sterile pre-cleaned tissue culture hood where the femurs were removed from the transport media and wiped thoroughly with a disinfectant wipe before being placed in a sterile Petri dish. Both ends of the femurs were removed with a sterile scalpel blade. A 25-gauge needle connected to a 10ml syringe filled with Mφ media supplemented with 20% L929 supernatant was inserted into the cavity of the femur and the bone marrow flushed into a 60ml Teflon pot (Roland Vetter Laboratory). This was repeated from both ends of the femur until the bone went translucent. Each femur was flushed into a separate Teflon pot. Further Mφ media supplemented with 20% L929 supernatant was added to each pot to bring the total volume to 40ml and the cells gently re-suspended. The pots were incubated at

37°C in 5% CO_2 for 7 days. 10ml of the fluid from the top of each pot was carefully aspirated (trying not to disturb the cells at the bottom) on days 2, 4 and 6 being was replaced each time with fresh medium.

2.2.3.3 *Characterisation of BMDMφ*

This method of maturing BMDMφ produces typically between 10 and 15 x 10^6 cells per femur. Aliquots of the cells thus matured were assessed for the purity of BMDMφ by 2 distinct methods: microscopy and flow cytometry.

Microscopic examination of BMDMφ using a cytospin

Cells were re-suspended in PBS containing 10% FBS at 1 x 10^6/ml. 200μl of the suspension was placed in the well of a cytospin holder and spun at 300g for 3 minutes using a Shandon Cytospin II (Shandon, UK). Cells were fixed with 100% methanol for 2 minutes, followed by staining in the Diff-quik Red solution for 1 minute and Diff-quik Blue solution for 1 minute (both from Gamidor Ltd, UK). Slides were air-dried overnight before being cover-slipped and mounted. As can be seen from figure 2.2, almost all the cells exhibit typical BMDMφ morphology.

Flow cytometric analysis of BMDMφ in suspension

Similar to PMφ, mature BMDMφ are also F4/80^{HI} whilst immature BMDMφ or monocytes are F4/80^{LO}or negative. Day 7 cells were harvested from the Teflon pots, washed in ice-cold PBS, resuspended at 1 x 10^6 cells/ml in blocking solution and stained with either anti-F4/80 monoclonal antibody (mAb) or isotype control as described previously. Greater than 93% of cells were F4/80^{HI} and therefore mature BMDMφ (figure 2.3).

A
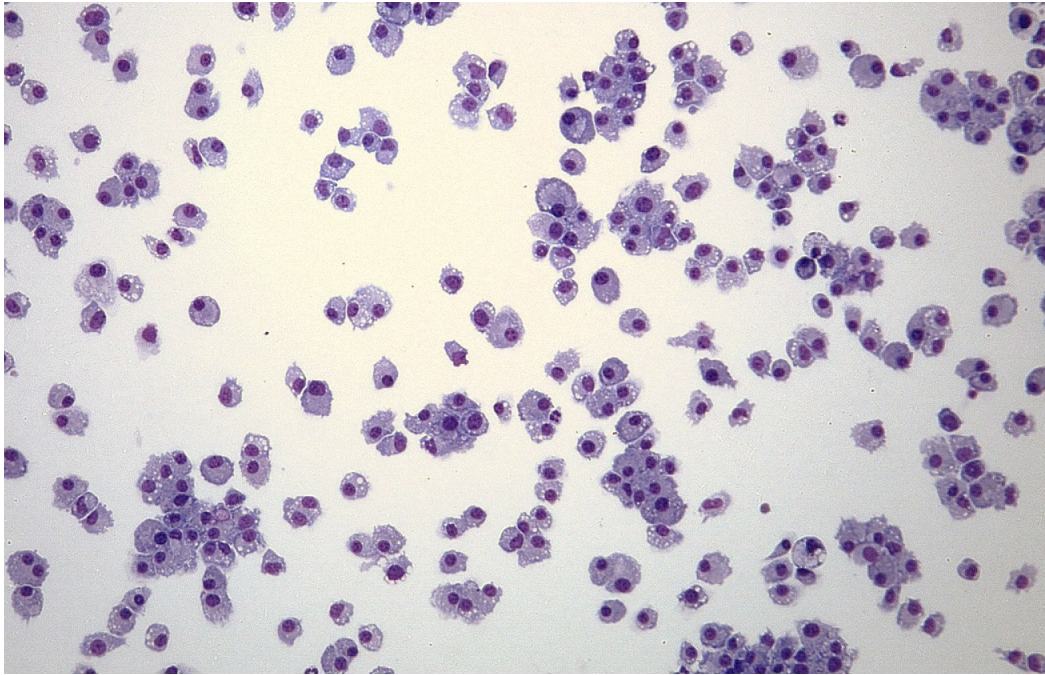
B
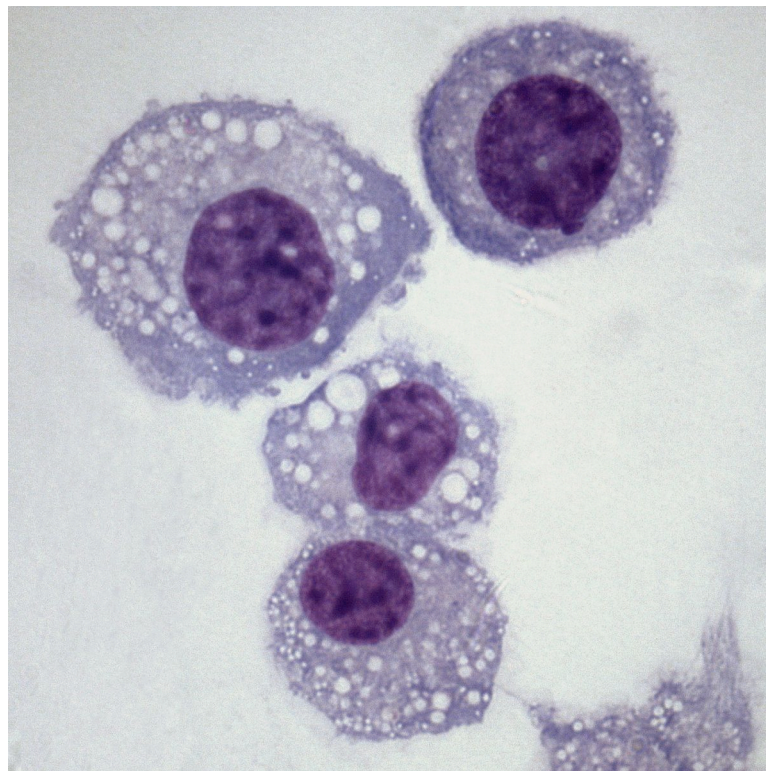
Figure 2- 2   Photomicrographs of typical cytospins of day 7 BMDMφ
Femurs were harvested and BMDMφ matured in teflon pots for 7 days in media containing 20% L929. Aliquot of BMDMφ were cytospun onto glass slides, fixed with methanol and stained with Diff-quik Red and Blue. (A) Low power view (x100) with numerous Mφ but no contaminating neutrophils. (B) High power view (x1000) from the same cytospin demonstrates the typical morphology of BMDMφ with a mononuclear nuclei and abundant cytoplasm.

A

B
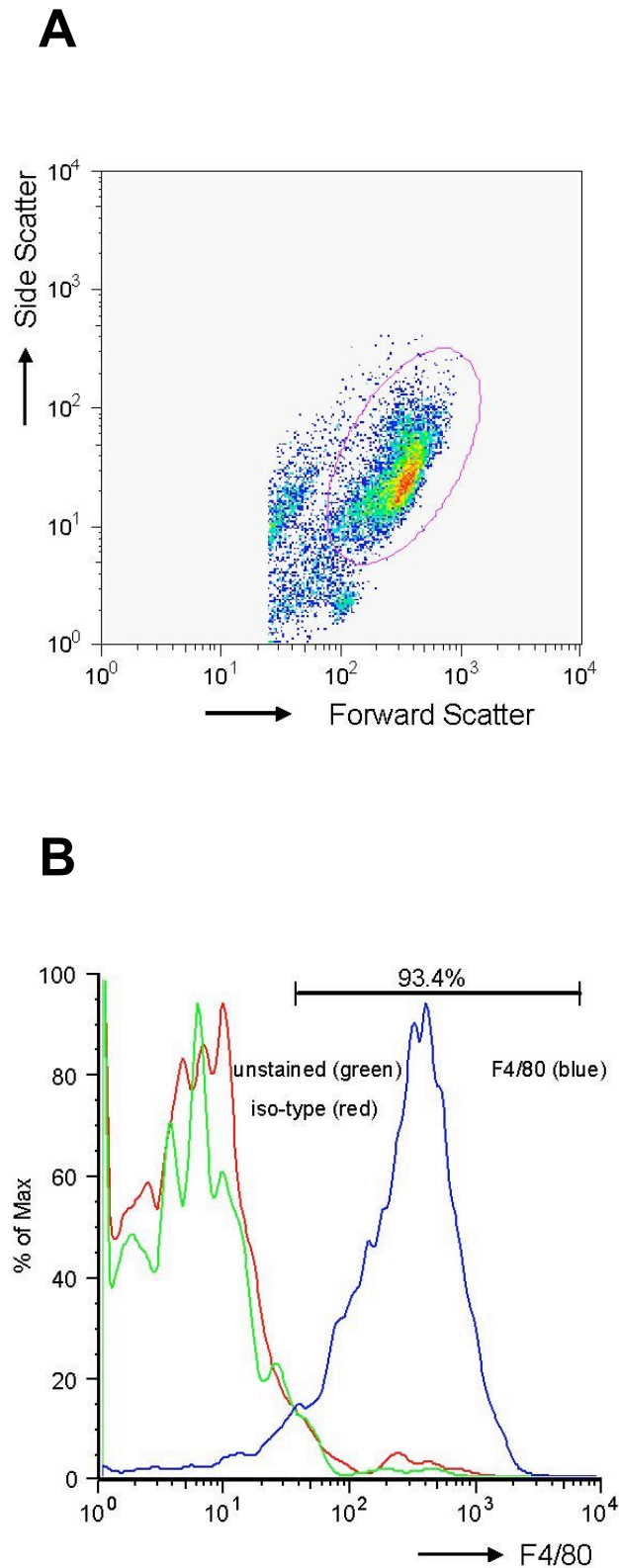
Figure 2- 3   Flow cytometric analysis of BMDMφ

Femurs were harvested and BMDMφ matured in teflon pots for 7 days in media containing 20% L929. Aliquots of cells were stained for the murine Mφ marker F4/80 and analysed by flow cytometry. (A) Mature BMDMφ lie in a characteristic position on the forward and side scatter plot as gated. (B) Over 93% of this population of cells is confirmed as F4/80^{HI}.

2.2.4 Apoptotic Cells

All AC used in the work described in this thesis were derived from 4 to 8 week old C57BL/6 mice.

2.2.4.1 *Preparation and labelling of apoptotic cells from thymocytes*

After sacrifice by cervical dislocation mice were liberally sprayed with 70% ethanol and the 4 limbs pinned to a polystyrene board. A longitudinal skin incision was made from the abdomen to the throat and the skin reflected to expose the underlying structures of the thorax and abdomen. A transverse incision was made through the peritoneum along the costal margin to expose the diaphragm. A further transverse incision through the entire width of the diaphragm was extended up each side of the thorax by longitudinal cuts through the ribs to form a flap that could be reflected superiorly thereby exposing the mediastinum. In young mice the thymus is easily visible as a pale grey, friable organ in the superior, anterior mediastinum. It is largest in young animals and becomes progressively smaller and less cellular as mice age. A sterile pair of fine, curved forceps was used to hold the thymus at its base and carefully 'pluck' it free, trying to avoid any haemorrhage that may result from a tear in the great vessels around the heart. The removed thymus was placed in a container with ice-cold Roswell Park Memorial Institute 1640 (RPMI) media and kept on ice for transport to a sterile tissue culture hood.

30ml of RPMI was added to a sterile Petri dish and within the tissue culture hood the thymus was gently ground between 2 sterile glass slides to release thymocytes into the media. When all thymocytes have been released, only a remnant of fibro-membranous tissue remains. The liberated thymocytes in RPMI were then passed through a 40μm filter into a Costar T75cm^2 flask. 1μl of Cell Tracker Green CMFDA dye (Invitrogen, UK) was added for every 1 x 10^6 cells within the suspension and the suspension incubated in the dark for 30 minutes at 37°C. 1ml of FBS was added to remove excess dye and the volume of RPMI was topped up to 100ml. Dexamethasone (Mayne Pharma, UK) was added to a final concentration of 1μM and the thymocytes incubated for a further 15 hours at 37°C in 5% CO_2. Following incubation the cell suspension was washed twice by centrifuging at 300g for 5 minutes at 4°C, decanting the supernatant and replacing it with fresh PBS in order to

remove any trace of lingering steroid. Finally, the cells were re-suspended at 10 x 10^6/ml in either media or PBS and kept on ice until used.

2.2.4.2 *Characterisation of apoptotic cells*

Typically each thymus yielded approximately 400 x 10^6 viable thymocytes at the outset, reducing to 50 x 10^6 AC following serum starvation and exposure to dexamethasone for 15 hours as above. The proportions of viable, apoptotic and necrotic cells remaining in suspension following aging of thymocytes was assessed by (i) microscopy following staining with Hoescht 33342 and trypan blue (both from Invitrogen, UK) and (ii) flow cytometry with annexin V conjugated to phycoerythrin (PE) and the vital dye 7-Amino-actinomycin (7-AAD) using the apoptosis detection kit I (BD Pharmingen, UK).

Microscopic examination of AC

The level of apoptosis was assessed by staining 0.5ml aliquots of the cell suspension with Hoescht 33342 (1µg/ml) for 15 minutes at room temperature. Hoescht 33342 is a blue fluorescent, cell permeable, nucleic acid stain that binds to double stranded DNA (Mocharla et al., 1987) The condensed pyknotic nuclei of AC can be distinguished from viable cells by their markedly bright fluorescence. Following staining the cells were photographed by inverted ultra-violet fluorescent microscopy on a Zeiss Axiovert microscope (Carl Zeiss Ltd, UK; original magnification x 400) using a blue filter. In general, greater than 95% of cells exhibited pyknotic nuclei (see figure 2.4) with very little variation between different preparations of AC. The level of necrosis was assessed by staining 0.5ml aliquots with 0.5ml 0.4% trypan blue and incubating for approximately 3 minutes at room temperature. Only cells that have lost membrane integrity (late apoptotic or secondarily necrotic cells) will stain blue. 10µl aliquots of the stained cells were added to a haemocytometer slide and the numbers of blue (necrotic) and clear (viable) cells were counted. Using this method of assessment approximately 45% of cells stained blue, again with little variation between different preparations of AC. Therefore only 5% of thymocytes remained viable with 50% exhibiting features of early apoptosis. The remaining 45% exhibited features of late apoptosis or secondary necrosis.

2.2.4.3 *Flow cytometric analysis of AC*

The membrane phospholipid, phosphatidylserine (PS) is translocated from the inner to the outer leaflet of the plasma membrane in AC, thereby exposing PS to the external cellular environment. Annexin V is a calcium dependent protein that has a high affinity for PS and binds to cells with exposed PS. Calcium rich binding buffer solution is supplied with the kit to facilitate the binding of annexin V to PS. Annexin V conjugated to PE fluoresces in the FL-2 channel of the flow cytometer. 7-AAD is a vital dye that only stains cells that have lost membrane integrity and fluoresces in the FL-3 channel. It is therefore possible to identify 3 distinct populations of cells:

- viable cells: annexin V negative and 7-AAD negative

- early apoptotic cells: annexin V positive but 7-AAD negative

- late apoptotic (secondarily necrotic) cells: annexin V positive and 7-AAD positive.

Apoptotic thymocytes were washed twice in PBS and resuspended in 1 x binding buffer solution at a concentration of 1×10^6 cells/ml as per the manufacturer's instructions. 100µl of the solution (1×10^5 cells) was transferred to a polystyrene FACS tube and 5µl of Annexin V-PE and 5µl of 7-AAD were added. Cells were gently vortexed and incubated for 15 minutes at room temperature in the dark. A further 400µl of 1x binding buffer solution was added to each tube prior to analysis. Typical findings are illustrated in figure 2.5.

The flow cytometric and microscopic analysis gave similar results. The cell suspension contains very few viable cells with the majority of cell population being split equally between early AC and late apoptotic or secondarily necrotic cells.
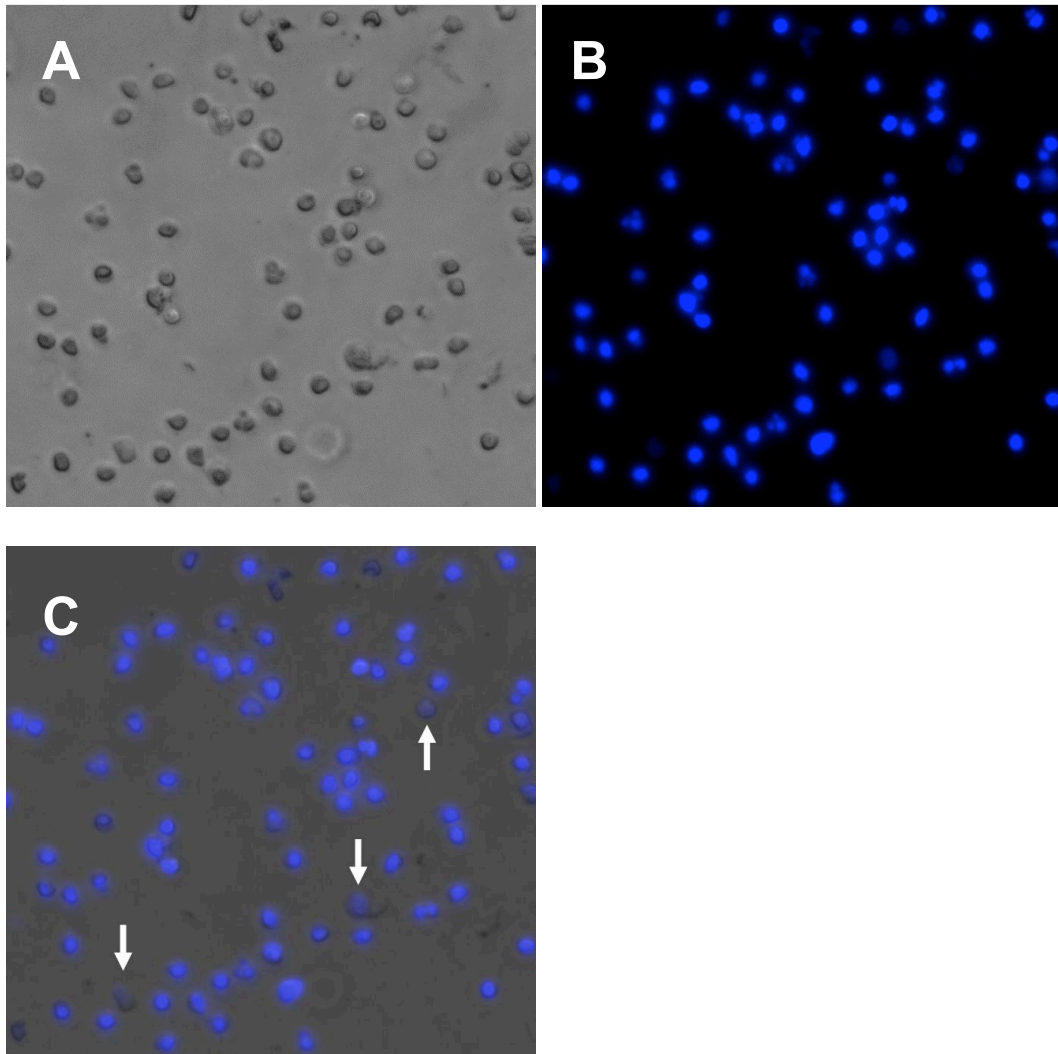
Figure 2- 4   Assessing the proportion of pyknotic nuclei by Hoescht 33342
Thymuses were harvested and thymocytes were aged for 15 hours in the absence of serum and in the presence of 1μM Dexamethasone. They were subsequently stained with 1μg/ml Hoescht 33342 and photographed (x 400) using an inverted fluorescence microscope. (A) The phase image taken with white light. (B) Image taken using a blue filter with ultraviolet (UV) light. (C) composite image of (A) and (B); whilst few viable cells are visible (white arrows), over 95% of cells have the typical pyknotic nuclei of apoptotic cells, fluorescing brightly under UV light when stained with Hoescht 33342.
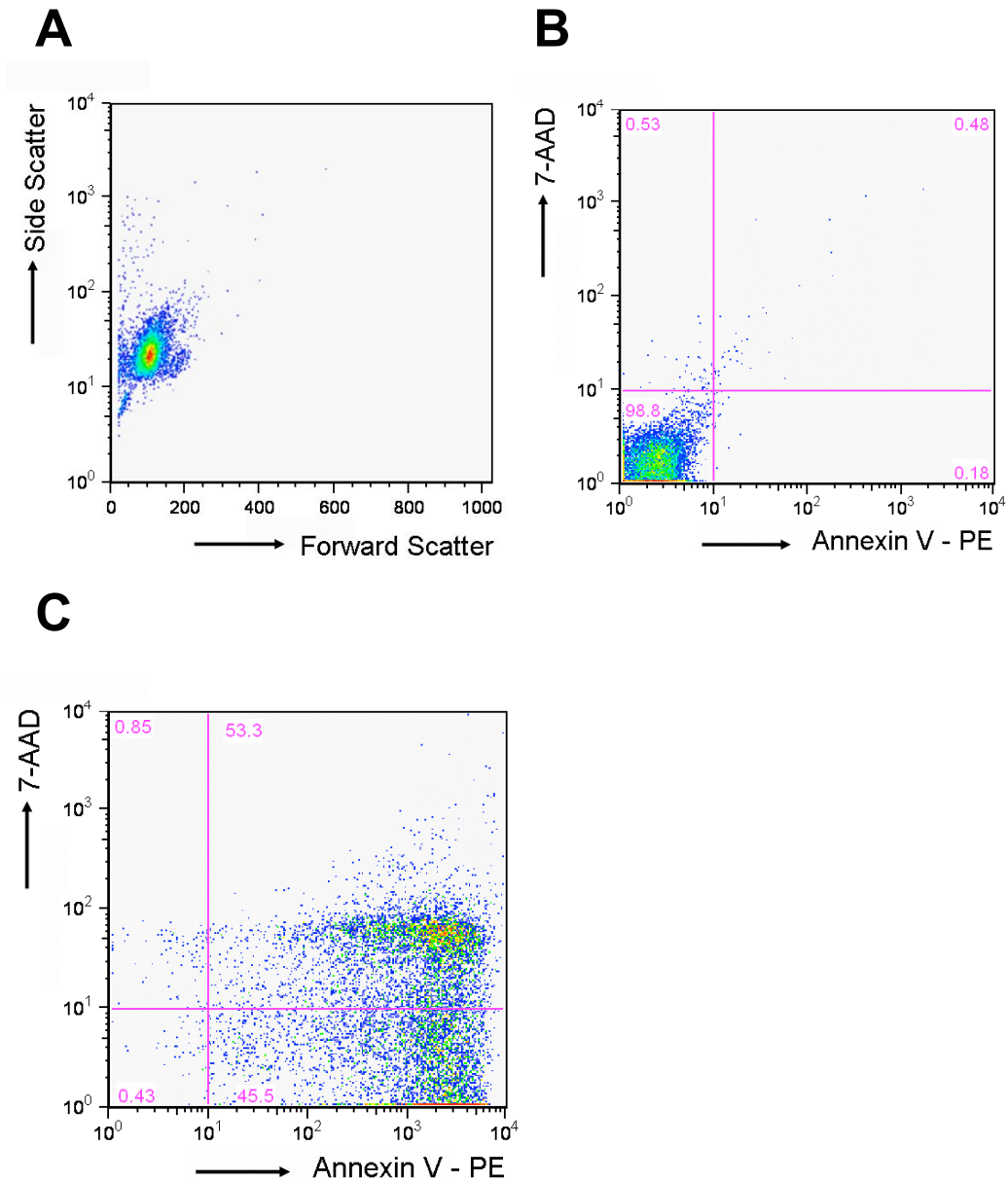
Figure 2- 5   Flow cytometric analysis of apoptotic thymocytes
Thymi were harvested and thymocytes aged for 15 hours in the absence of serum and in the presence of 1µM Dexamethasone. Aliquots of cells were dual stained with annexin V-PE and 7-AAD and assessed by flow cytometry. (A) Characteristic position on forward and side scatter plots occupied by thymocytes. (B) Unstained thymocytes used as a control sample. (C) the overwhelming majority of thymocytes were either early apoptotic (annexin V positive, 7-AAD negative) or late apoptotic/necrotic (dual positive).

2.2.5 Pneumococci

Fluorescein isothiocyanate (FITC) labeled, heat killed pneumococci, stored in PBS and kept at $-80^{o}C$ were a gift from Menna Clatworthy, Cambridge University. Aliquots of pneumococci were thawed immediately prior to use and washed twice in fresh PBS, centrifuged for 2 minutes at 10,000 rpm between washes, and finally resuspended in serum-free Mφ media at 1 x $10^{6}/\mu l$. When required, aliquots of pneumococci were opsonised in serum taken from mice 2 weeks after vaccination with the pneumovax vaccine (also a gift from Menna Clatworthy and stored at $-80^{o}C$). The pneumococci were thawed, centrifuged at 10,000 rpm and resuspended in PBS supplemented with 1% serum for 30 minutes at $37^{o}C$ in a water bath. They were then washed twice and resuspended in serum free Mφ media as described above

2.3 *IN VITRO* PHAGOCTOSIS ASSAYS

When assessing phagocytosis of particles by Mφ there is always a question as to whether the particle has been ingested, is bound to the Mφ or is merely 'overlying' the Mφ in a slightly different plane of view. Different strategies can be employed to answer this question. High magnification with confocal microscopy to assess a very narrow plane of view is extremely accurate but too prohibitively expensive and time consuming to be a practical solution. A particle could be regarded as phagocytosed if of the entire particle appears within the Mφ or alternatively, other investigators have argued they can identify the phagolysosome around a phagocytosed particle (O'Brien et al., 2002). A new strategy was developed for this project that effectively demonstrated whether or not a particle was phagocytosed.

2.3.1 *In vitro* phagocytosis assay using microscopic analysis

LysoTracker Red (Invitrogen, UK) is a vital dye that accumulates in intracellular compartments with a low internal pH such as lysosomes and fluoresces red under UV light. When added to the adherent Mφ that have been 'fed' either AC or beads, the dye is rapidly taken up by the Mφ and concentrates in lysosomes including phagolysosomes. If the 'phagocytic feed' has been pre-labeled with a green fluorescent dye, when located within a red phagolysosome the combined appearance would be predicted to be orange by fluorescence microscopy.

2.3.1.1 *Development and characterisation of a phagocytosis assay*

PMφ were harvested from an 8 week old male C57BL/6 mouse and purified as previously described (chapter 2.2) onto 1cm glass cover slips at the bottom of 24-well plates. After to the removal of non-adherent cells by washing, 0.5ml of Mφ media was left in each well and 2.5×10^6 AC re-suspended in 250μl Mφ media were added to each well giving a ratio of ~10 AC to each PMφ. Following incubation for 1 hour at 37^oC, 5% CO_2, wells were placed on ice and excess feed removed by gentle washing 3 times with ice-cold PBS. After the 3rd wash the cells were left in 200μl PBS and LysoTracker Red was added to a final concentration of 200nM. Cells were incubated for a further 15 minutes on ice. Immediately prior to microscopy, the cover-slips were removed from the PBS, inverted and placed onto a glass microscopy slide. Images were taken in turn with an Axioskop 2 microscope (Carl Zeiss Ltd, UK) using UV light with red and green filters (original x1000 magnification). A phase image was taken using white light and the 3 images were then merged using Photoshop software (Photoshop elements 2.0, Adobe USA) to produce a composite image. Figure 2.6 illustrates the accuracy of this technique, as one AC is clearly adjacent to a PMφ whilst another AC is located within a phagolysosome.

To test the hypothesis that the orange appearance indicated that an AC was within a phagolysosome, a series of 3 photographs (x 1000 magnification) were taken every 200μm through the presumed phagolysosome in order to form a 'Z' stack. The images were then deconvoluted and reconstructed into a 3-dimensional image using Velocity 2.5.1 software (Improvision, UK). Whilst one green apoptotic cell is clearly visible, the other AC is clearly located within a red phagolysosome (figure 2.7 and movie 2.1 on the supplementary CD ROM).

To obtain real-time video-microscopy of phagocytosis, PMφ were purified as above using 3×10^6 peritoneal cells per WillCo-dish®, glass bottom dishes (WillCo Wells, The Netherlands). Following purification of PMφ by adhesion, the cells were incubated in 1ml Mφ media containing 200nM LysoTracker Red. AC were prepared as before and re-suspended in Mφ media at 1×10^6 AC/ml. A Leica SP5C confocal laser scanning microscope was used (Leica Microsystems, UK) and the WillCo dish was placed on the stage heated to 37^oC within a climate control box maintaining 5% CO_2. Immediately prior to running the video microscopy AC were added to the PMφ

at a ratio of 10:1. Red and green fluorescent images together with a phase images were taken every minute for 30 minutes (original magnification x1000). The images were merged and run together to produce a short video using LAS AF software (Leica Microsystems, UK). It is possible to clearly see green AC being drawn into PMφ as red phagolysosomes form (movie 2.2 on supplementary CD ROM).

An assumption is made in the use of LysoTracker red dye that all phagolysosomes promptly acidify at a uniform rate. Recent data suggests that this may not be the case, with Mφ phagolysosomes containing material ingested via FcR maturing slower than those triggered by alternative receptors (Erwig et al., 2006). These factors are considered likely to be of relatively limited importance in assessing rates of phagocytosis and the addition of LysoTracker red dye to a conventional phagocytosis assay results in an extremely rigorous assay that is capable of assessing differences in the rates of phagocytosis of different Mφ populations.
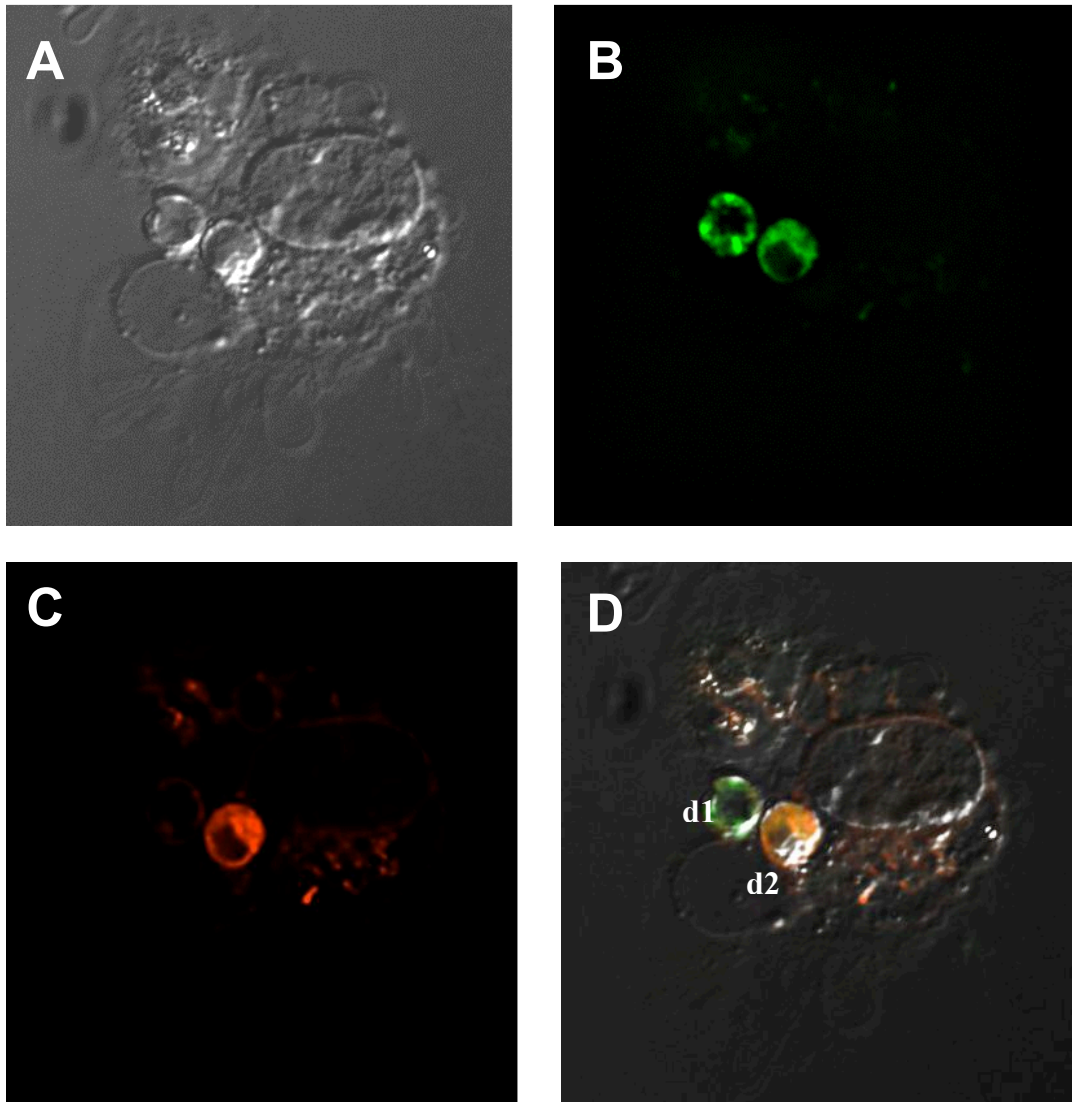
Figure 2- 6   Photomicrographs of PMφ and AC in the process of phagocytosis
Resident peritoneal Mφ were harvested, plated onto glass cover slips and purified. Fluorescent green apoptotic cells were added for 1 hour at 37oC before excess feed was washed away, leaving the cells bathed in PBS supplemented with 200nM LysoTracker Red dye. The cover-slips were inverted and placed onto glass microscope slides and viewed under fluorescent microscopy. (A) Image taken under phased white light. (B) Image taken under UV light with green filter. (C) Image taken under UV light with red filter. (D) Composite images were merged using Photoshop software; one adherent but non-ingested AC (d1) and one AC within a phago-lysosome (d2) are clearly visible.
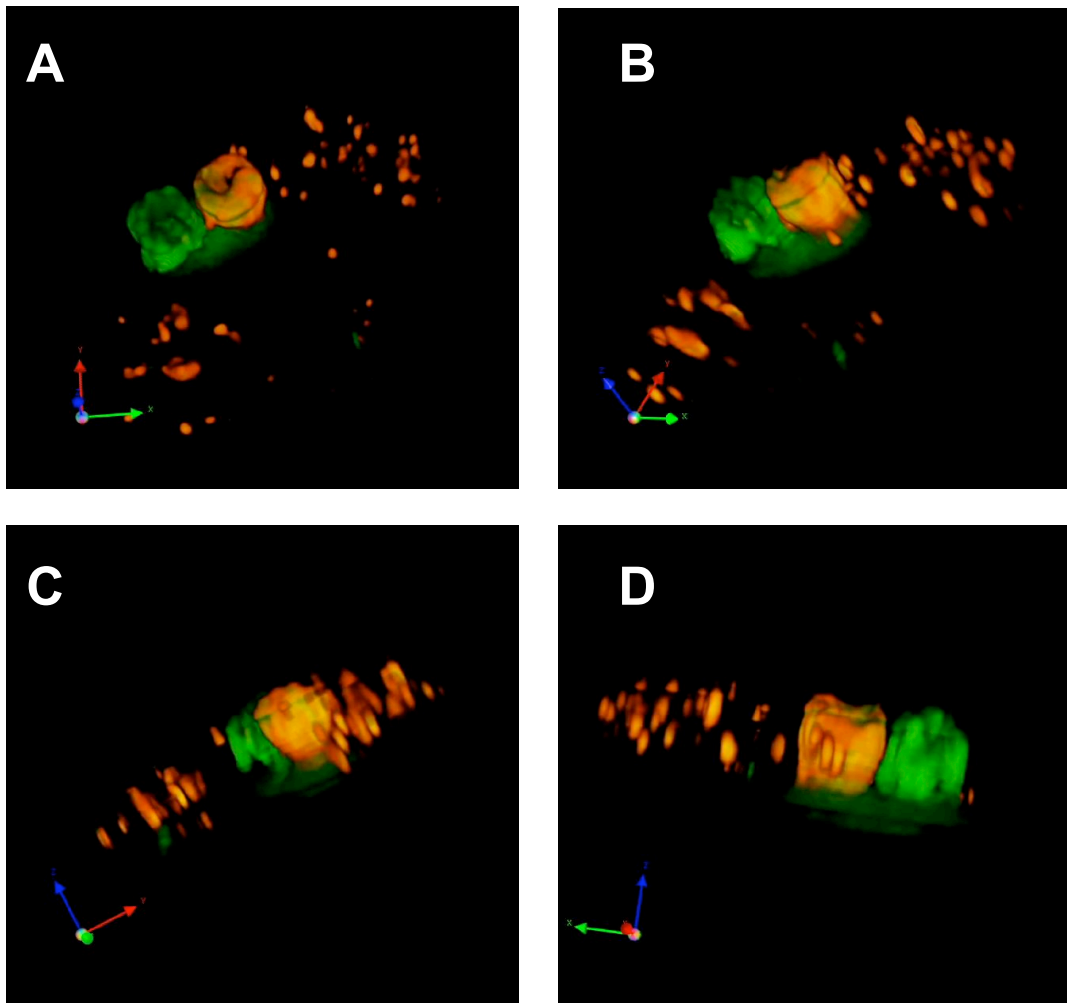
Figure 2- 7   Three dimensional analysis of PMφ following interaction with AC
Using ultraviolet light with the green and red filters as above, a series of images were taken every 200μm through the PMφ and AC seen in figure 2.6. The images were deconvoluted to remove extraneous light and then reconstructed into a 3-dimensional image using velocity software that could be viewed from different perspectives (images A to D). It is clearly apparent that one apoptotic cell (green) remains un-eaten, whilst the other is wrapped within a large phago-lysosome and appears orange.

2.3.1.2 *Performing phagocytosis assays using LysoTracker Red*

Resident peritoneal cells were harvested and PMφ purified by adhesion after seeding peritoneal cells into wells of costar plates. PMφ from individual mice were kept separate. After the 3rd wash, the PMφ were incubated in 200µl per well of warm Mφ media. The phagocytic 'feed' consisting of either fluorescent AC or 3µm fluorescent green latex beads (Polysciences Inc, Germany) were added to PMφ at a ratio of 10:1 in order to ensure that particle availability was not a rate limiting factor for phagocytosis. All strains of mice and different feed types were represented equally on any individual plate. The plates were gently agitated for a few seconds before they were incubated at 37°C, 5% CO_2 in the dark for 60 minutes. Following incubation the plates were placed on ice to terminate any ongoing phagocytosis and the excess feed removed by gently washing 3 times with ice-cold PBS, using a 1ml Pasteur pipette.

After the final wash the cells were left bathed in 200µl PBS containing 200nM LysoTracker Red and incubated for a further 15 minutes on ice in the dark. The plates were finally photographed by inverted fluorescent microscopy on a Zeiss Axiovert microscope using original magnification x 400. Phase and fluorescent images were taken as above and merged together to form composite images for assessment of phagocytosis. 3 or 4 random fields of view were taken per well, incorporating at least 300 PMφ.

The percent of PMφ exhibiting evidence of phagocytosis was calculated for each well expressed as the percentage of PMφ that had ingested at least one AC. The phagocytic index was calculated for each well by calculating the number of AC phagocytosed by 100 PMφ that had eaten at least one AC. In other words the phagocytic index is a measure of how well the phagocytically active PMφ have eaten. Both a low percent phagocytosis and phagocytic index would indicate a reduced phagocytic capacity for the PMφ. In contrast, a low percent phagocytosis with a normal phagocytic index would identify a sub-group of PMφ that exhibit a reduced phagocytic capacity whilst the remaining PMφ phagocytose normally.

2.3.2 *In vitro* phagocytosis assay using flow cytometric analysis

The phagocytosis assay described above is particularly robust and gives useful information regarding both the percentage of phagocytic cells and the phagocytic index. It is, however, not suitable for all particles such as bacteria which are difficult to visualise and count individually using light or fluorescent microscopy. Flow cytometry is capable of counting several thousand fluorescent events, such as fluorescently labeled bacteria, very rapidly and is an attractive method to assess phagocytosis. Dr Menna Clatworthy developed and validated a protocol for assessing the percentage phagocytosis of fluorescent pneumococci by PMφ using flow cytometry (Clatworthy and Smith, 2004) and this method was adapted to assess phagocytosis of pneumococci, beads and AC.

2.3.2.1 *Conduction of the phagocytosis assay*

PMφ were purified by adhesion following seeding 1 x 10^6 peritoneal cells into the wells of Costar 12-well plates. A typical peritoneal lavage yields approximately 3 x 10^6 cells and peritoneal lavages were pooled together in 50ml Falcon tubes according to strain to provide sufficient cells. Alternatively BMDMφ were seeded at 5 x 10^5 cells/well into Costar 12-well plates and incubated in 0.5ml of Mφ media either with or without 10% FBS according to the experimental requirements.

Phagocytic 'feed' particles were added to each well and the plate gently agitated. Pre-labeled AC or 3μm fluorescent green latex beads (Polysciences Inc, Germany) were added to Mφ at a ratio of 10:1 whilst 6 x 10^6 pneumococci were added to each well. Plates were then placed in a dark incubator for the specified time at 37^oC, 5% CO_2. One experimental plate was kept on ice in order to prevent phagocytosis and was used to assess non-specific binding. Wells containing Mφ alone were used to assess the auto-fluorescence of Mφ alone.

On completion of the incubation period, all plates were placed on ice and the wells washed vigorously 3 times with ice-cold PBS to remove excess feed. Mφ were then scraped off using a cell scraper and the cells were transferred into chilled polystyrene FACS tubes and stained for F4/80. Cells were analysed by FACScan with FlowJo software.

2.3.2.2 *Analysis of phagocytosis assay*

Mφ alone were used to draw a rough gate around the cells on the forward and side scatter plot (figure 2.8) and only F4/80^{HI} events within this gate were analysed. The initial gating by forward and side scatter prevented F4/80^{HI} fragments of Mφ created by the mechanical scraping of cells from potentially contaminating the analysis. The use of the F4/80 stain reliably excluded any cell types other than Mφ being assessed or any isolated feed such as clusters of AC that might have fallen into the original gate from the analysis. At least 2000 PMφ events were collected for each well.

AC, beads or pneumococci were all fluorescent in the FL-1 channel. The percentage of Mφ that shifted further than auto-fluorescence in FL-1 was recorded for each well (figure 2.9). These Mφ included those that had phagocytosed fluorescent feed or had feed bound to their surface. A measure of non-specific binding was obtained for each strain by analysing the plates kept on ice for the duration of the experiment to prevent phagocytosis. Binding of AC to Mφ at 37°C may well be higher than that achieved at 4°C, however the difficulties in separating out binding from phagocytosis at the higher temperature meant assessment of binding at 4°C was the pragmatic approach. The percent phagocytosis in each well was then calculated by subtracting the degree of binding obtained for the strain from the total percentage of Mφ shifting in FL-1. The number of wells per condition gave the experimental 'n' number.
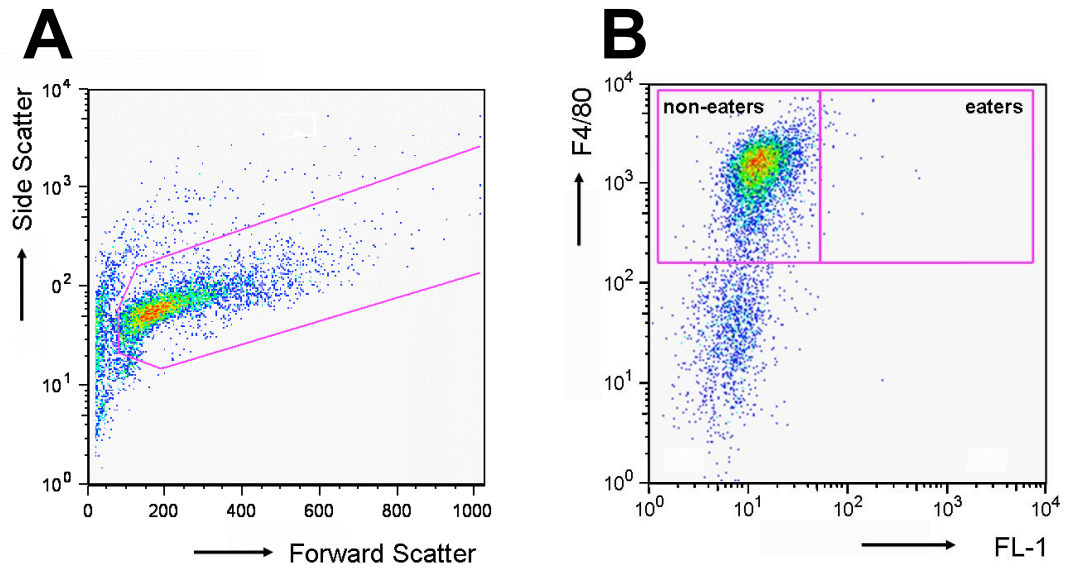
Figure 2- 8   Setting up gates to assess phagocytosis
Mφ were seeded into Costar 12-well plates and incubated for 1 hour at 37oC. The plates were then placed on ice and washed vigorously with ice-cold PBS. The cells were scraped off the plastic wells, transferred to chilled FACS tubes and stained with an anti-murine F4/80 antibody conjugated to APC prior to analysis by flow cytometry. (A) A gate was drawn around the cells by forward and side scatter to exclude debris. (B) Cells within this gate were analysed further. FL-4 (F4/80) was used to gate on Mφ alone. Autofluorescence in FL-1 was assessed and gates drawn to distinguish Mφ alone (non-eaters) from those associated with fluorescent feed (eaters).
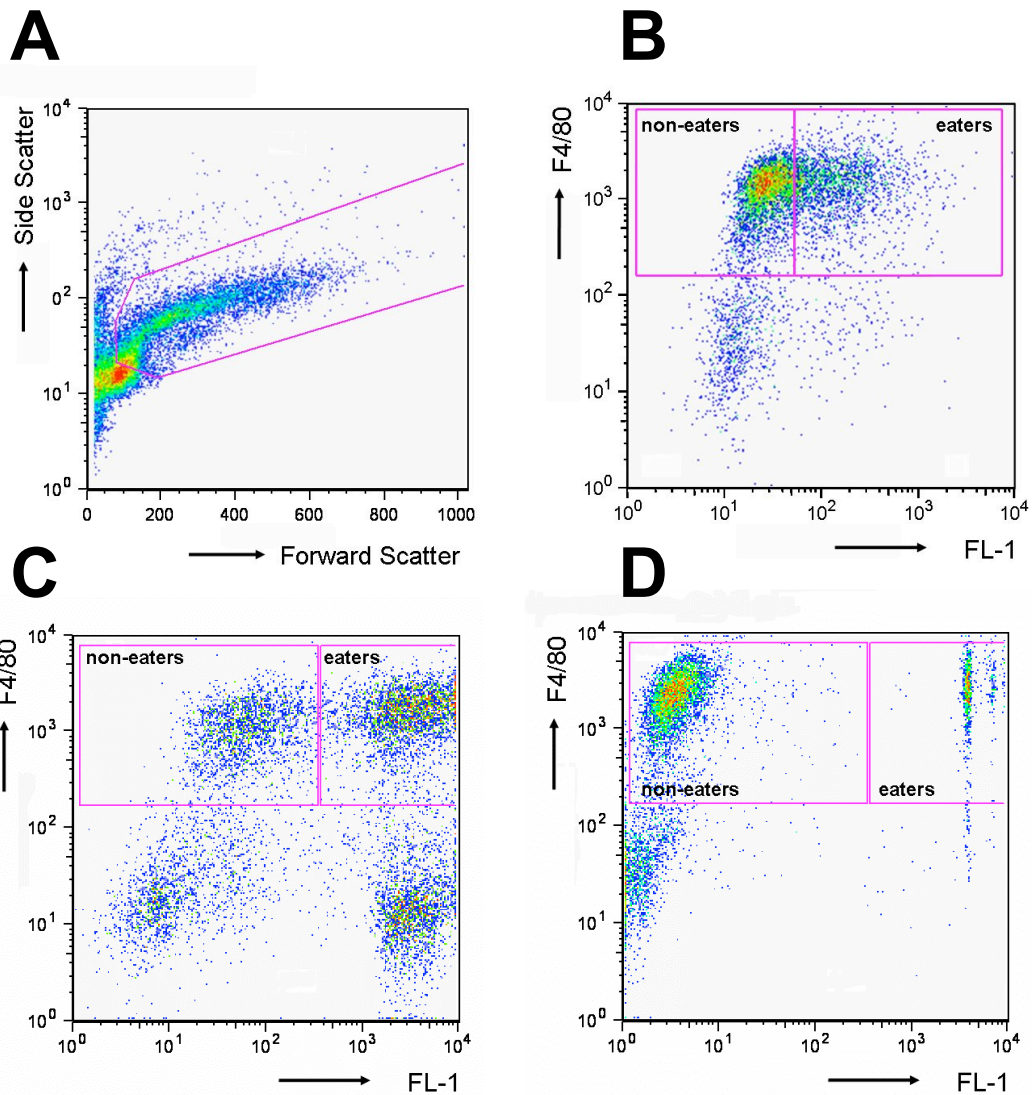
Figure 2- 9   Calculation of the percentage of Mφ exhibiting phagocytosis by flow cytometry

Mφ were seeded into Costar 12-well plates and feed was added. The plates were incubated for 1 hour at 37oC and then placed on ice and washed vigorously with ice-cold PBS. The cells were then scraped off the plastic wells, transferred to chilled FACS tubes and stained with an anti-murine F4/80 antibody conjugated to APC prior to analysis by flow cytometry. (A) An initial forward and side scatter gate excluded cell fragments and the majority of remaining feed (AC in this instance). Gated events were analysed by fluorescence in FL- 4 (F4/80) and FL- 1 (feed) using gates established for that experiment as previously shown. (B) Mφ incubated with pneumococci. (C) Mφ incubated with AC. (D) Mφ incubated with beads. Phagocytosis was assessed as the percentage of Mφ classified as 'eaters' at 37oC over and above the percentage of eaters seen with that strain of mice from experimental wells kept on ice to assess non-specific binding. N.B. examples are drawn from different experiments with different Mφ populations and FACScan settings and this is the reason for the different auto-fluorescence of Mφ evident.

2.4 *IN VIVO* PHAGOCYTOSIS ASSAY

The method used to assess phagocytosis *in vivo* in these studies is a modification of that developed by Philip Taylor (Taylor et al., 2000). AC were injected intraperitoneally (ip) and the loss of free AC from peritoneal lavage fluid was measured at various time points on the assumption that this represents AC clearance by phagocytosis. The same technique was also used to assess the phagocytosis of fluorescent green, 3μm latex beads *in vivo*.

2.4.1 Performing the *in vivo* phagocytosis assay

AC were resuspended in sterile PBS and kept on ice until used. The concentration of AC in PBS following resuspension was either 10 or 20 x 10^6 per ml, so that the numbers of AC required were contained in a final volume less than 0.5ml. Sterile 3μm latex beads were washed twice in sterile PBS, centrifuged at 10,000 rpm, and resuspended in sterile PBS at 10 x 10^6 per ml. Before injection the abdomen of the mouse was sprayed briefly with cleansing solution and wiped with a disinfectant wipe. The required numbers of AC or beads were drawn up into 1 ml syringe and injected ip via a 26-gauge needle.

Mice were sacrificed by cervical dislocation at various time points following injection. Immediately following death a peritoneal lavage was performed with 5ml ice-cold PBS. Due to the time taken for post mortem reflexes to subside, the lavage typically took place 1 minute after cervical dislocation. The time point used to measure the baseline numbers of AC or beads, when mice were sacrificed immediately following the ip injection, was therefore recorded as 1 minute and not zero. The strains of mice and the time points examined were scheduled such that any changes in the AC suspension would affect all strains and all time points equally. Lavage fluid recovered, usually in excess of 4ml, was immediately placed in a 15ml Falcon tube and kept on ice pending analysis.

2.4.2 Analysis of the *in vivo* phagocytosis assay following injection of apoptotic cells

2.4.2.1 *Microscopic analysis of peritoneal lavage fluid by cytospin*

Experimental data from our group has convincingly demonstrated that PMφ localise to the milky spots of the omentum and elsewhere following phagocytosis of AC and are not recoverable by peritoneal lavage (Simon Watson, PhD thesis, 2007). Initial samples of lavage fluid recovered were examined by cytospin. Analysis of these cytospins demonstrated readily identifiable individual PMφ without AC or with AC possibly bound to their surface in all samples. PMφ with a definite apoptotic body within a phagolysosome were extremely rare (figure 2.10) and accounted for less than 1% of PMφ identified, regardless of strain of mouse or time point examined. No further attempt was made to assess phagocytosis by microscopic analysis of cytospins and it was decided to use the loss of free recoverable AC from the peritoneal lavage fluid as a surrogate marker for the phagocytic clearance of AC or particles.
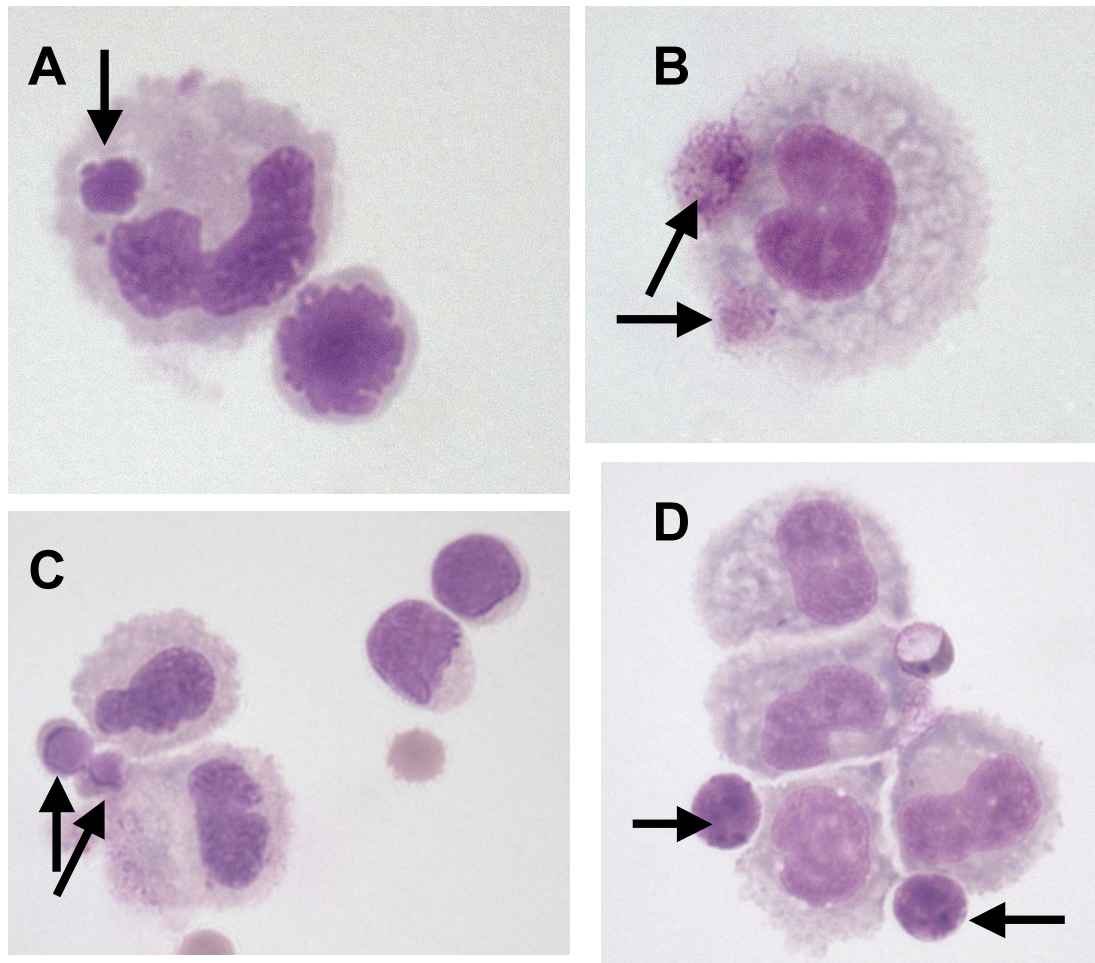
Figure 2- 10   Cytospin analysis of peritoneal Mφ following an ip injection of apoptotic cells

5 x 106 AC were injected ip and mice sacrificed 30 minutes later. Peritoneal lavages were performed immediately following death with 5ml ice-cold PBS. Samples of lavage fluid were cytospun onto glass slides, fixed with methanol and stained with Diff-quik Red and Blue. High power images (x1000 original magnification) were taken. (A) PMφ with a phagocytosed AC (black arrow). (B) PMφ with possible phagocytosed AC (black arrows). (C & D) Multiple PMφ with AC possible bound to their surface or in close proximity (black arrows).

2.4.2.2 *Assessment of phagocytosis of AC by flow cytometry*

Use of Flowcheck™ beads to count absolute numbers by flow cytometry

In order to assess the apparent loss of free AC and count the numbers of PMφ present within a sample of peritoneal lavage fluid it is necessary to be able to convert the numbers of events counted by flow cytometry to an absolute number of cells per ml of lavage fluid. A technique developed by Simon Watson was employed involving the spiking of samples with Flowcheck™ synthetic polystyrene beads (Flowcheck™ Beckman Coulter, UK) immediately prior to flow cytometric analysis analysis. Samples were spiked immediately prior to analysis to reduce potential binding of beads to Mφ. Samples were then thoroughly mixed by multiple pipetting by a 200µl Gilson pipette rather than vortex to avoid margination of the beads.

Each sample was spiked with a known number of beads and by counting the number of beads analysed it is possible to calculate the proportion of the aliquot analysed by the FACScan. By noting how many cellular events were counted from the sample it is then a simple calculation to determine how many cells were in the aliquot. If the size of the aliquot is known, it is possible to deduce the concentration of cells per ml of lavage fluid recovered. This can be summarized by the following formula:

$$\text{Cells per ml lavage fluid} = \frac{\text{Number of beads spiked} \quad \text{X} \quad \text{Number of cell events recorded}}{\text{Number of bead events recorded} \quad \text{X} \quad \text{Volume of lavage aliquot}}$$

For all experiments, 400µl aliquots of lavage fluid were spiked with 50,000 Flowcheck beads immediately prior to flow cytometric analysis. The formula therefore simplifies to:

$$\text{Cells per ml lavage fluid} = \frac{\text{Number of cell events recorded}}{\text{Number of bead events recorded}} \quad \text{X} \quad 125,000$$

Flowcheck™ beads fluoresce brightly in all FACScan channels, including FL-3 and this channel was kept reserved for beads. The flow cytometer was adjusted such that

the beads had FL-3 fluorescence around 10^3 on the log scale. With these settings, other cells had FL-3 fluorescence of 10^1 or less and beads were easily counted and excluded from further analyses (figure 2.11).

Counting PMφ and numbers of free apoptotic cells by flow cytometry

Following sacrifice of the mouse and peritoneal lavage, 400μl aliquots of fluid were transferred to chilled polystyrene FACS tubes, stained with F4/80 conjugated to APC as described previously. Samples were washed and spiked with 50,000 Flowcheck™ beads immediately prior to analysis by flow cytometry. Flowcheck™ beads were counted and gated out as described above. All of the remaining events were analysed according to fluorescence in FL-4 (F4/80 labeling PMφ) and FL-1 (Cell Tracker Green labeling AC). Quadrants were drawn separating 4 distinct populations (figure 2.12) and the numbers events counted in each:

- the quadrant with F4/80^{HI} FL-1^{LO} events represented PMφ with no AC involvement,

- the quadrant with F4/80^{HI} FL-1^{HI} events were considered to be PMφ associated with AC in some way (see below),

- the quadrant with F4/80^{LO} FL-1^{HI} events were free AC,

- the quadrant with F4/80^{LO} FL-1^{LO} events contained all other peritoneal cells such a B lymphocytes, mast cells and any contaminating red blood cells.

Using the formula described above, the numbers of free AC and total PMφ per ml of lavage fluid were calculated. Each peritoneal lavage used 5ml of PBS and an assumption made that the fluid flowed freely throughout the peritoneum mixing all cells equally. The numbers of cells per mouse were therefore estimated by multiplying the number of cells per ml by 5, regardless of actual volume of lavage fluid recovered. Phagocytosis of AC *in vivo* was estimated by the loss of free AC from lavage fluid. Different strains of mice, even if the same age, will vary in size and typically NOD mice are larger than their age and sex matched C57BL/6 controls. It is likely that the numbers of AC recovered at any given time point will be affected by the size and complexity of the peritoneal cavity as well as phagocytosis. To control for this variable, the loss of free AC was calculated by comparison to the

mean baseline numbers recovered for each strain and not from the numbers of AC injected.

A significant proportion of the F4/80^{HI} events (PMφ) were also FL-1^{HI}. Whilst some of these events represented AC within PMφ, some represented AC bound to PMφ (as in figure 2.10). Due to the dynamics of the interactions between AC and PMφ described by Simon Watson (PhD thesis 2007), with PMφ becoming non-recoverable following AC phagocytosis, it was considered that F4/80^{HI} FL-1^{HI} events were not a reliable measure of phagocytosis and they were not used in any calculations.
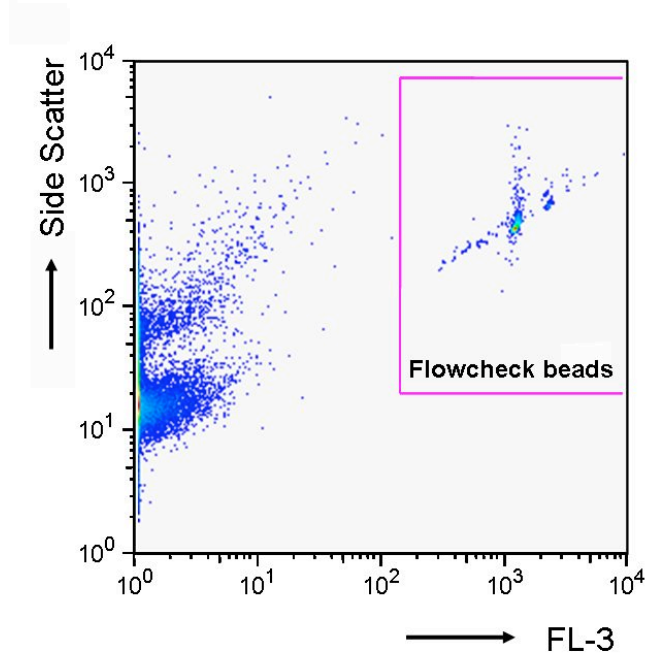
Figure 2- 11   Counting and gating out Flowcheck™ beads by flow cytometry
400µl aliquots of peritoneal lavage fluid were spiked with 50,000 Flowcheck™ beads immediately prior to flow cytometric analysis. Flow cytometry plot demonstrating how the Flowcheck™ beads are approximately 10^2 times brighter in FL-3 than other cells and are thus easily gated upon, counted and excluded from further analyses.
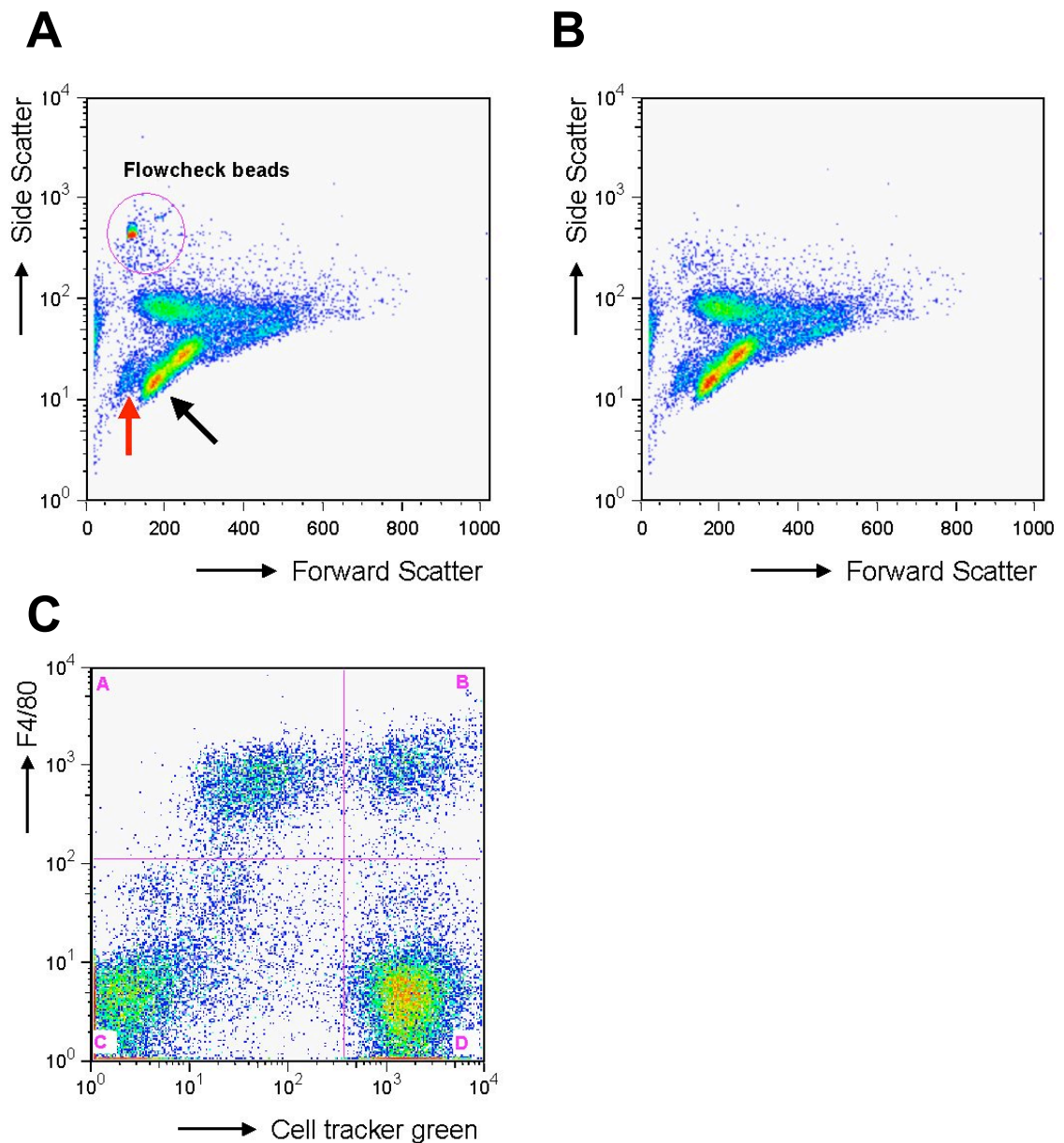
Figure 2- 12   Flow cytometric analysis of lavage fluid following an ip injection of AC
Mice were injected ip with 5 x 106 AC pre-labelled with Cell Tracker Green. They were sacrificed and peritoneal lavages performed at various time points. PMφ were stained with an anti-murine F4/80 antibody conjugated to APC. Immediately prior to analysis by flow cytometry, aliquots of lavage fluid were spiked with 50,000 Flowcheck™ beads. (A) Typical forward and side scatter profile of peritoneal lavage fluid: populations of red blood cells (grey arrow) and apoptotic cells (black arrow) are seen to partially overlie each other, Flowcheck™ beads are ringed. (B) Same lavage fluid once Flowcheck™ beads had been counted and excluded from further analyses. (C) All remaining events were analysed by their fluorescence in FL-4 (F4/80) and FL-1 (Cell tracker Green): Quadrant A = pure PMφ; quadrant B = PMφ associated with AC; quadrant D = free AC and quadrant C contains all other cells.

2.4.3 Analysis of the *in vivo* phagocytosis assay with beads

Analysis of the phagocytic clearance of 3μm fluorescent green latex beads was almost identical to assessing the clearance of labelled AC. The FACScan settings had to be altered to capture the extremely small size of the latex beads (smaller than the Flowcheck™ beads). Crucially, the latex beads were not as bright in FL-3 as the Flowcheck™ spheres and differentiation between beads and spheres was therefore straightforward. A gate was drawn around the Flowcheck™ beads in order to count them and exclude them from further analysis and quadrants were used to count the numbers of free latex beads and total PMφ (figure 2.13). Further analyses were as for AC.
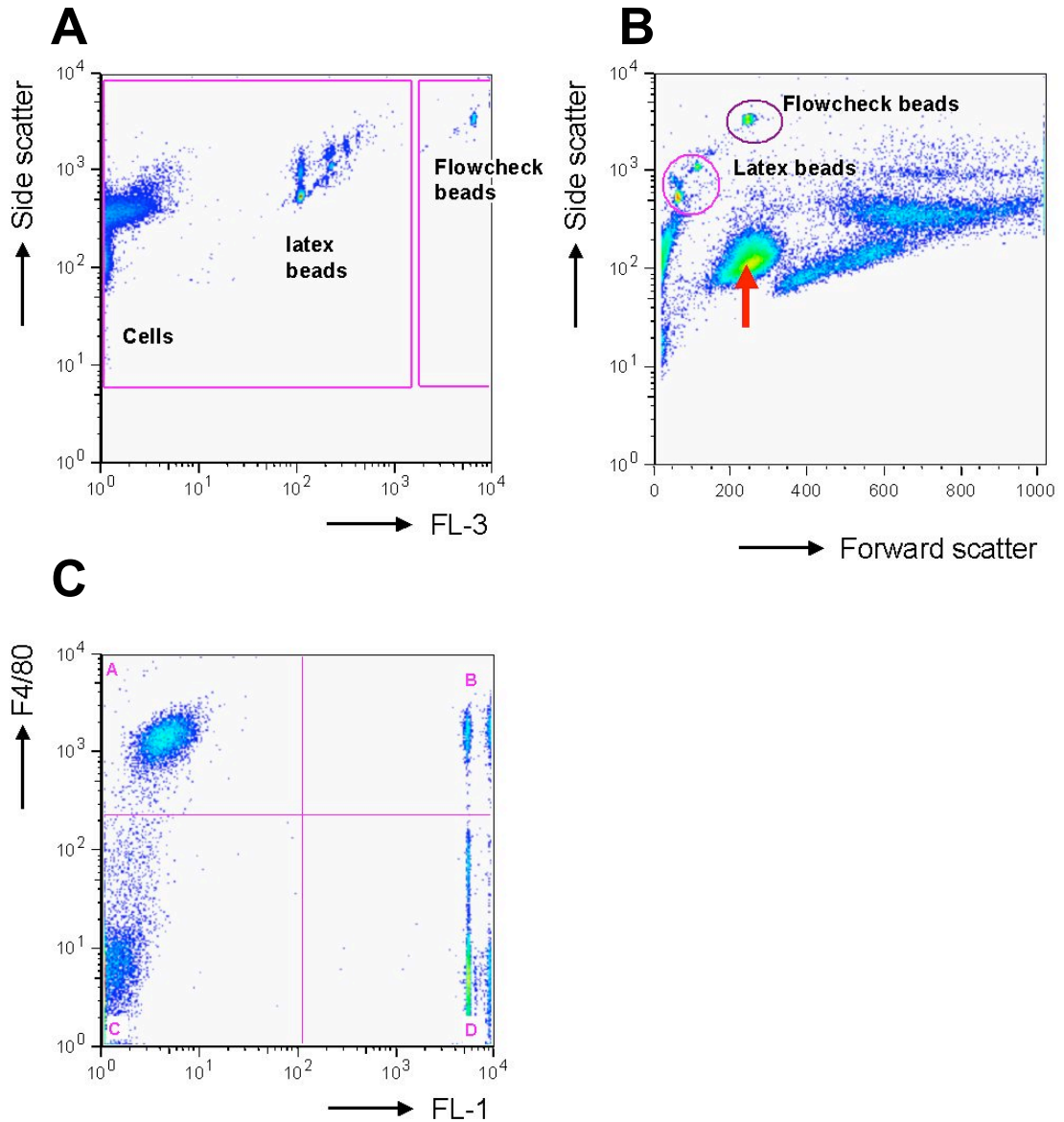
Figure 2- 13   Flow cytometric analysis of lavage fluid following an injection of latex beads

$3\mu m$, fluorescent green, latex beads were injected ip and the mice sacrificed 20 minutes later. Peritoneal lavages were performed immediately following death with 5ml ice-cold PBS and PMφ stained with an anti-murine F4/80 antibody conjugated to APC. Immediately prior to analysis by flow cytometry, aliquots of lavage fluid were spiked with 50,000 Flowcheck™ beads. Peritoneal cells, the latex beads used as feed' and the Flowcheck™ beads used for counting all particles exhibit different fluorescent properties in FL-3. (A) Gates were drawn using side scatter and FL-3 to count the FlowcheckTM beads and exclude them from further analyses. (B) Typical forward and side scatter profile of recovered lavage fluid: red blood cells are indicated by the arrow whilst cells and latex beads are labeled. (C) Events plotted according to fluorescence in FL-4 (F4/80) and FL-1. Quadrant A = pure PMφ; quadrant B = PMφ associated with beads; quadrant D = free beads and quadrant C contains all other cells.

2.4.4 Rationale for excluding samples from analysis

There were a number of reasons for excluding a small proportion of samples from analysis:

Occasionally no AC were identified within the lavage fluid, which to all intents and purposes resembled lavage fluid recovered from a naïve abdomen. It was assumed the ip injection had failed and been subcutaneous or missed the peritoneal cavity altogether (figure 2.13).

Occasionally the sample was very heavily blood stained presumably the result of bleeding occurring at the time of the ip injection. There are no data as to how additional serum proteins associated with excessive haemorrhage might affect the physiology of resident peritoneal cells or PMφ phagocytosis. The addition of a red cell lysis step to the protocol would require at least 2 additional washes and this would result in increased cell loss as some cells are lost from the pellet each time a wash step is introduced. This technique of assessing phagocytosis *in vivo* relies on counting the absolute numbers of AC and PMφ recovered and therefore would be very sensitive to the additional washes. It was decided to exclude heavily blood stained samples rather than subject all samples to a red cell lysis step and potentially reduce accuracy (see figure 2.14).

Very rarely a sample would appear to have lost virtually all injected AC and PMφ. Although this pattern is consistent with effective phagocytosis by PMφ leading to a brisk localisation to milky spots, it would also be consistent with a large proportion of the pellet being lost from the FACS tube during washing. These 2 options were distinguished by counting the lymphocytes within the samples. Numbers of lymphocytes are not affected by the MDR and remain reasonably constant. If the sample in question was also noted to have vastly reduced numbers of lymphocytes then it was excluded from analysis (figure 2.15).

For inexplicable reasons occasionally the data obtained by the flow cytometer for a particular sample was meaningless, showing a diffuse 'smear' on all channels. These samples were uninterpretable and were also excluded from analysis (figure 2.16).
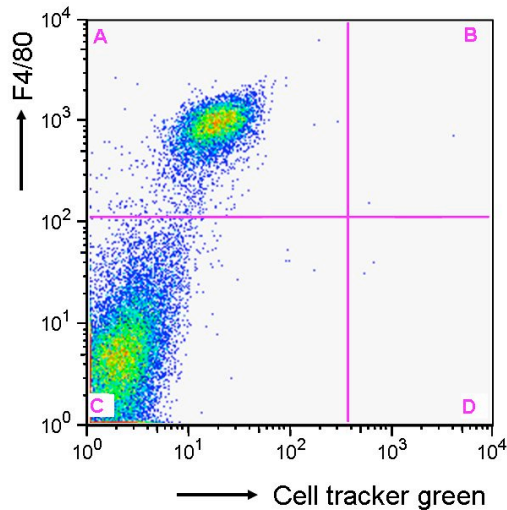
Figure 2- 14   No evidence of apoptotic cells in lavage fluid
Mice were injected ip with 5 x 10^6 AC pre-labelled with Cell Tracker Green, sacrificed at various time points thereafter and peritoneal lavages performed. Recovered PMφ were stained with an anti-murine F4/80 antibody conjugated to APC and fluid analysed by flow cytometry. Occasionally there would be no evidence of any AC within the lavage. An assumption was made that the ip injection had been sub-cutaneous and that particular sample would not be included in further analysis.
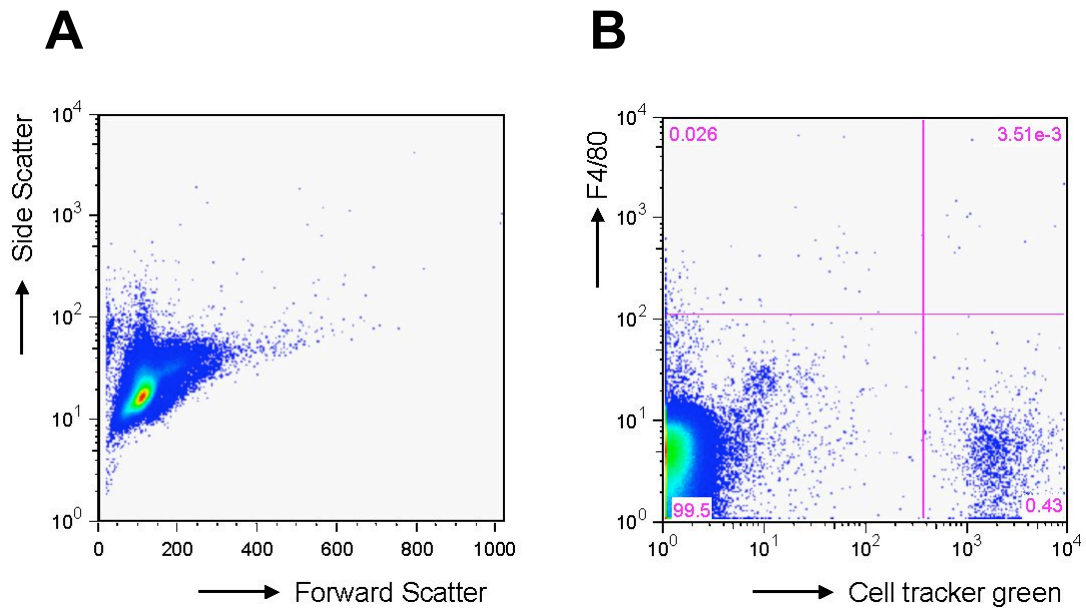
Figure 2- 15   Heavily blood stained lavage fluid
Mice were injected ip with 5 x 10^6 AC pre-labelled with Cell Tracker Green, sacrificed at various time points thereafter and peritoneal lavages performed. Recovered PMφ were stained with an anti-murine F4/80 antibody conjugated to APC and fluid analysed by flow cytometry. (A) Forward and side scatter profile of heavily bloodstained sample. (B) The same heavily bloodstained sample analysed by fluorescence in FL-4 and FL-1. Even with erythrocytes gated out as unstained in the bottom left quadrant PMφ numbers in particular appeared reduced.
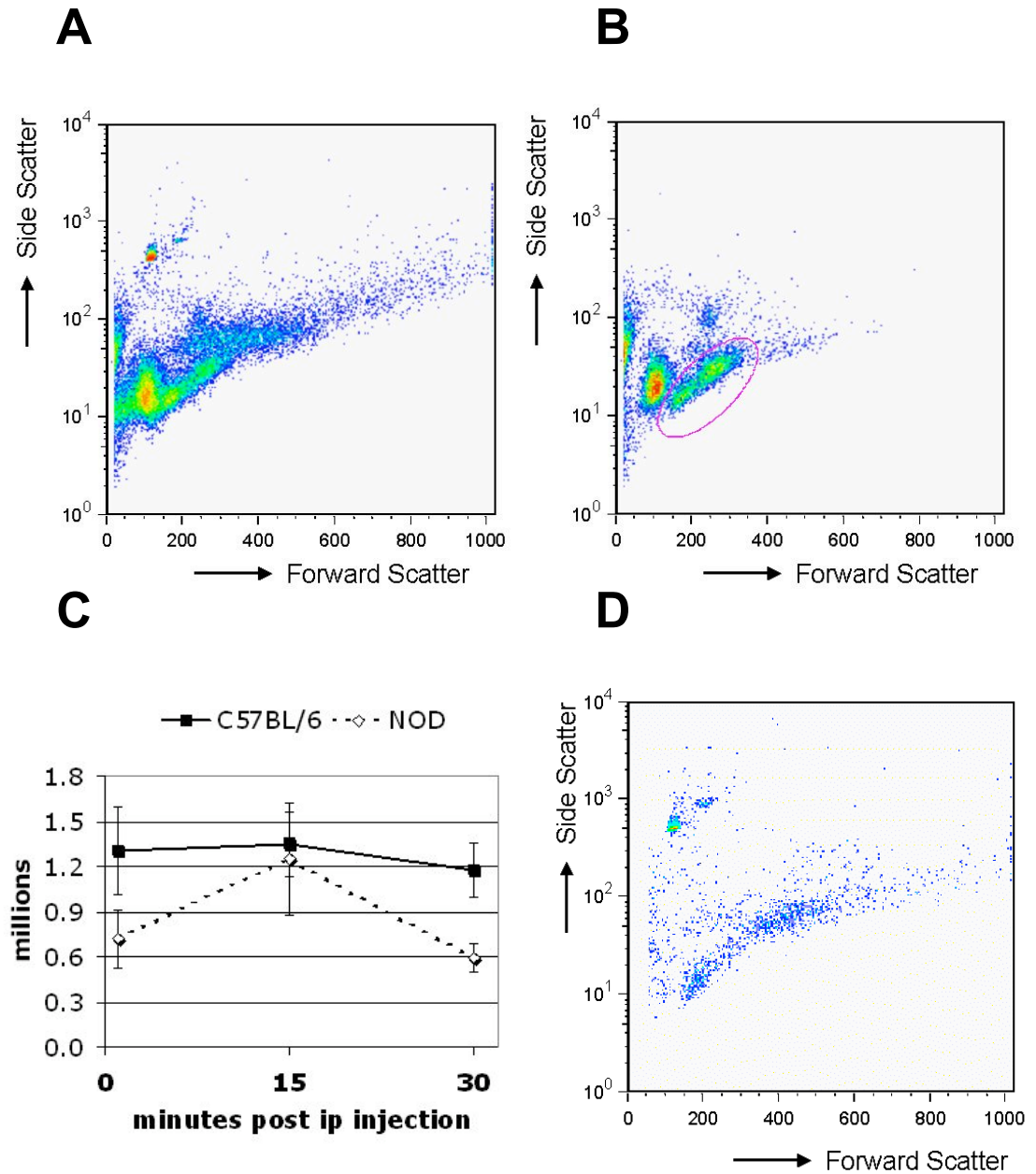
Figure 2- 16   Using analysis of lymphocyte numbers to assess partial loss of pellet
Mice were injected ip with 5 x 10^6 AC pre-labelled with Cell Tracker Green, sacrificed at various time points thereafter and peritoneal lavages performed. Recovered PMφ were stained with an anti-murine F4/80 antibody conjugated to APC and fluid analysed by flow cytometry. (A) Typical forward and side scatter plot of peritoneal lavage fluid. (B) Forward and side scatter plot of the same sample with PMφ, AC and Flowcheck™ beads gated out: lymphocytes are clearly visible and easily gated. (C) Lymphocyte numbers remained reasonably constant despite the Mφ disappearance reaction. (D) Occasionally a sample would be analysed with apparently very few PMφ or AC recovered. If lymphocyte numbers were also greatly reduced it was presumed that a significant part of the cellular pellet had been inadvertently lost during a washing step and the sample was excluded from further analysis.
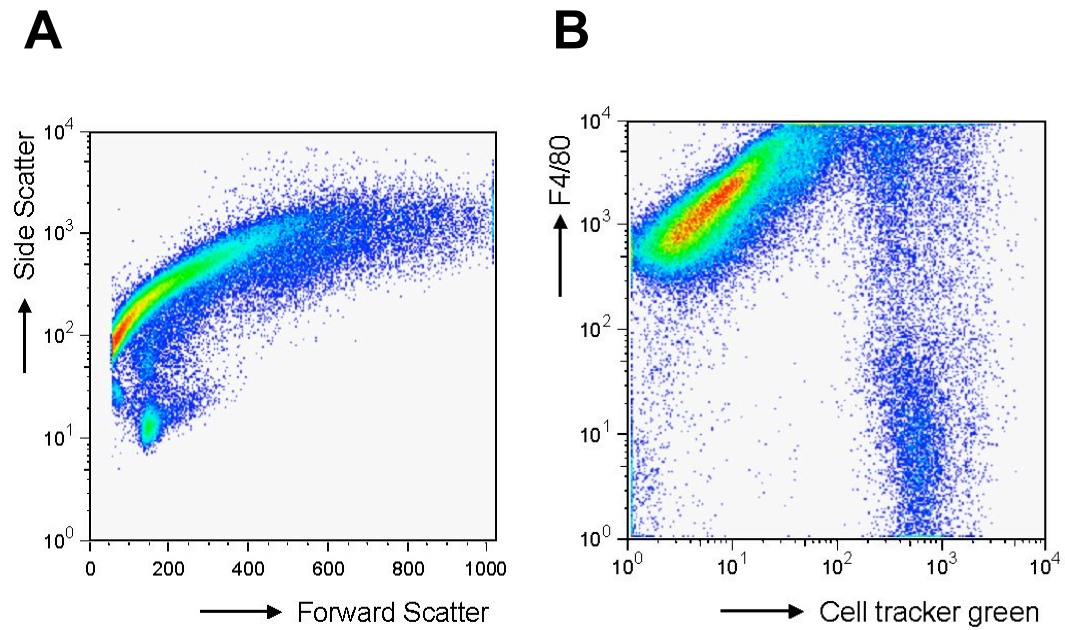
Figure 2- 17   Inexplicable smears
Mice were injected ip with 5 x 10^6 AC pre-labelled with Cell Tracker Green. Mice were sacrificed at various time points thereafter, peritoneal lavages performed and PMφ stained with an anti-murine F4/80 antibody conjugated to APC to fluoresce in FL-4. (A) Samples analysed by flow cytometry occasionally exhibited an inexplicable 'smear' on both forward and side scatter profiles. (B) The same sample analysed by fluorescence in FL-4 and FL-1. These samples were uninterpretable and not included in further analysis.

2.5 MEASURING MESSENGER RNA LEVELS WITHIN MACROPHAGES

Messenger RNA (mRNA) for a specific cellular protein can be measured within cell populations. The first step is to isolate the cells of interest and then extract total RNA from the cells ensuring separation from DNA present. The RNA is reverse transcribed to generate complimentary DNA (cDNA) and specific primers, targeting the signal for the requisite protein are used together with the Real Time Polymerase Chain Reaction (RT-PCR) to amplify and measure the signal.

2.5.1 Exracting mRNA using Trizol

RNA is very sensitive to RNAses which are ubiquitous. All plastic ware should be clean, (preferably from unopened bags or new racked Gilson pipette tips) or wiped with RNase inhibitor solution (Sigma, UK). Gloves must be worn at all times.

Resident PMφ or BMDMφ prepared as previously described were plated in wells of 6-well plates. For best results considerable numbers of cells are required and peritoneal cells pooled from 3 mice, or 3×10^6 BMDMφ, were used per well. One ml of Trizol solution (Gibco, UK) was added to the cells of each well. The Trizol/cell suspension mixture was passed through the Gilson pipette tip several times before transfer to a 1.5ml Eppendorf container and frozen at -80^oC pending RNA isolation.

To isolate the RNA, 0.2ml chloroform was added to each Eppendorf and vigorously mixed for several minutes at room temperature. Tubes were then centrifuged at 12,000 rpm for 15 minutes at 4^oC following which 2 liquid phases were evident - a clear aqueous phase containing the RNA, and a pink organic phase containing DNA and protein. The clear phase was extracted using a Gilson pipette and transferred to a fresh 1.5ml Eppendorf taking extreme care not to transfer any of the underlying phase. 0.5ml isopropranolol was added and samples incubated for 10minutes at room temperature to precipitate RNA from the aqueous phase. Samples were centrifuged at 12,000 rpm for 10 minutes at 4^oC and the supernatants discarded. The pellets were washed with 200μl 75% ethanol, vortexed gently and centrifuged at 7,500 rpm for 5 minutes at 4^oC. Excess ethanol was carefully aspirated and the remainder allowed to air dry at room temperature for 30 minutes. Once dry the RNA was dissolved in 20μl RNase free water (Sigma, UK) and frozen at -80^oC pending analysis. RNA concentration and purity were assessed by spectrophotometry by measuring OD at 260 and 280nm.

2.5.2 Reverse Transcription and Real Time PCR

The cDNA library was constructed using the TaqMan® Reverse Transcription kit (Applied Biosystems, USA) according to the manufacturer's instructions. Table 2.1 provides a summary of reagents and volumes used whilst Table 2.2 gives the program timings and temperatures required for reverse transcription. The resultant 100μl of cDNA solution was diluted 1:5 in RNase free water and stored at -80°C pending further RT-PCR analysis. TaqMan® Universal PCR Master Mix (Applied Biosystems, USA) was used to quantify the mRNA signal by RT-PCR according to manufacturer's instructions. Table 2.3 gives a summary of reagents used whilst Table 2.4 details the timings and temperature settings for the PCR cycles using an Applied Biosystems 7700 single reporter Real Time PCR machine. All sequence detection primers used (CD14, CD36, CD51, CD61, SRA, TSP and C1q) were a kind gift from Aili Zhang (Centre for Inflammation Research, Edinburgh).

2.5.3 Data Analysis

Two chemical reporters are incorporated within the TaqMan® RT-PCR mix. Each cycle of RT-PCR incorporates a reporter into the new DNA, cleaving it from its quencher and thus permitting it to fluoresce. RT PCR uses the accumulation of fluorescence as a measure of the quantity of the gene of interest present. In the system used, FAM was the reporter for the gene of interest and VIC for the house keeping gene 18s. The above system then counted the number of PCR cycles required to achieve a certain level of fluorescence for each reporter. $\Delta\Delta$CT represents the difference between the number of VIC cycles and number of FAM cycles required to achieve the set level of fluorescence and $\Delta\Delta$CT was calculated for each cDNA sample. The levels of each gene were therefore measured in comparison to 18s levels within each sample and not in absolute amounts thereby correcting for any minor differences that could occur between samples in the quantity of cDNA loaded into the RT-PCR mix.

Since the question of interest lay in the comparison between NOD Mφ and C57BL/6 Mφ, the data were normalised to the mean $\Delta\Delta$CT for the comparable C57BL/6 Mφ

and plotted on a logarithmic scale with the 95% confidence intervals. Statistical significance was determined by a student's t test between $\Delta\Delta$CT values.

Component	Volume (µl)	Final value
10 x TaqMan® Reverse Transcriptase buffer	10	1 x
25mM MgCl$_2$	22	5.5mM
deoxyNTPs mixture	20	500µM of each
Random Hexamer	5	2.5µM
RNase Inhibitor	2	0.4U/µl
MultiScribe Reverse Transcriptase (50U/µl)	2.5	1.25 U/µl
RNA Sample + RNase free water	38.5	200ng
Total	100	

Table 2- 1   Reagents and quantities used for Reverse Transcription PCR

Step	Incubation	Reverse Transcription	Reverse Transcription Inactivation
	HOLD	HOLD	HOLD
Time	10 minutes	1 hour	5 minutes
Temperature	$25^{o}C$	$48^{o}C$	$95^{o}C$

Table 2- 2   Temperatures and times used for Reverse Transcription

	Volume (µl)
TaqMan® Master Mixture (2x)	12.5
FAM mix	7
VIC mix (20x) Reagent	1.25
cDNA (1:5 dilution)	2.5
RNase free water	1.75
Total	**25µl**

Table 2- 3   Reagents and volumes used for Real Time PCR

Time	Temperature
2 minutes	50°C
10 minutes	95°C
15 seconds	95°C
1 minute	60°C
HOLD	4°C

CYCLE

Table 2- 4   Times and temperatures used for Real Time PCR

2.6 MEASURING CELL SURFACE EXPRESSION OF PROTEINS

Monoclonal antibodies are available that will bind to several of the various proteins on the surface of cells involved in the phagocytic process. An assumption was made that higher levels of protein expression would result in quantitatively more binding of the monoclonal antibody to the cell. If the primary monoclonal antibody is then linked to a fluorochrome this would result in a increased signal detectable by flow cytometry. An arbitrary measure of the expression of a particular protein on a particular cell type can thus be derived from the mean fluorescence of that cell type following immunolabeling with a particular monoclonal antibody.

Peritoneal cells were harvested from individual mice as previously described and kept separately on ice. 400µl aliquots of each lavage were placed in chilled FACS tubes and 50µl of mouse serum added to each sample as an Fc receptor blocker prior to incubation on ice for 30 minutes. Each sample was then dual stained with both a rat anti-mouse F4/80 monoclonal antibody conjugated to APC and either the monoclonal antibody targeting the cell surface receptor of interest or the appropriate isotype control. Monoclonal antibodies were diluted 1:100 with PBS containing 10% mouse serum. Table 2.5 provides a comprehensive list of the monoclonal antibodies and isotype controls used. 50µl of the antibody dilution was added to each sample prior to incubation on ice for a further 30 minutes in the dark. Cells were then washed in PBS to remove excess antibody. Alexa Fluor® 488 streptavidin (Invitrogen, UK) was added at a dilution 1:200 for a further 30 minutes on ice to samples using a biotinylated primary antibody or biotinylated isotype control and these samples were washed in PBS for a second time. Similarly samples immunolabeled with the primary antibody for CD36 were restained with a secondary antibody conjugated to FITC for a further 30 minutes on ice. All cells were resuspended in PBS containing 10% mouse serum immediately prior to analysis by flow cytometry using a FACScan instrument (Becton Dickinson, UK). Results were analysed by FlowJo software (Treestar, USA).

FITC and Alexa Fluor® 488 fluoresce in FL-1 and fluorescence in the FL-1 channel was therefore used as the measure of the expression of the protein of interest. Fluorescence in FL-1 was only assessed on F4/80^{HI} cells (PMφ). Because

fluorescence assessed by flow cytometry was measured using a logarithmic scale, a geometric mean rather than arithmetic mean was used.

Target Protein	Comment	Supplier	Isotype control	Supplier
CD 51 (α_V)	Biotinylated	eBioscience	Biotinylated Rat IgG1κ	eBioscience
CD 61 ($\beta 3$)	Biotinylated	eBioscience	Biotinylated Armenian Hamster IgG	eBioscience
Scavenger Receptor A (SRA)	Biotinylated	Serotec	Biotinylated Rat IgG2b	eBioscience
CD14	Conjugated FITC	Cambridge Bioscience	FITC Rat IgG2a	eBioscience
CD 36	Mouse anti mouse IgA 1° antibody	BD Pharmingen	Murine IgA	eBioscience
IgA	FITC conjugated 2° antibody	eBioscience	FITC Rat IgG2a	eBioscience
F4/80	Conjugated APC	eBioscience	APC Rat IgG2a	eBioscience

Table 2- 5   **List of antibodies used to target surface proteins involved in phagocytosis**

2.7 MEASURING *IN VITRO* PRODUCTION OF CHEMOKINES AND CYTOKINES

Different populations of Mφ including resident PMφ and PLMφ and BMDMφ were obtained as described in chapter 2.2. 1×10^6 peritoneal or pleural cells, or 0.5×10^6 BMDMφ were seeded into wells of 12-well plates. Plates were incubated for 1 hour at 37^oC, 5% CO_2 prior to removal of non-adherent cells by gentle washing with warm Mφ media using a sterile 1ml Pasteur pipette.

After the 3rd wash to remove non-adherent cells, the Mφ media was replaced by either:

1. Standard Mφ media without additional stimulation (quiescent)

2. Mφ media supplemented with 1μg/ml LPS (Sigma, UK)

3. Mφ media supplements with 0.5% thioglycollate (TG)

4. Mφ media supplemented with 0.25% carrageenan (CG)

Within the confines of a single experiment, all conditions arose from the same batch of quiescent Mφ media.

Plates were then incubated at 37^oC, 5% CO_2 and at the requisite time point (1, 4 or 24 hours later) plates were viewed by light microscopy (original magnification x 400) to assess cell morphology. Supernatants were carefully aspirated using a Gilson pipette into 1.5ml Eppendorf containers, trying not to disturb the cell layers adherent to the plastic. Supernatants were centrifuged at 12,000 rpm for 15 minutes at 4^oC to remove any cell debris. The resultant solutions, containing chemokines and cytokines produced by the cells, were decanted to fresh 1.5ml Eppendorf containers and frozen at -80^oC pending analysis.

Levels of chemokines (MIP-2, KC, and MCP-1) and cytokines (TNFα, IL-10 and IL-6) were measured either by ELISA (R&D, UK) or by cytometric bead array (CBA) (BD Biosciences, UK) according to manufacturer's instructions. The same methods were employed regardless of whether the chemokines and cytokines were produced *in vitro* (in supernatants as above) or *in vivo* and measured in lavage fluid or serum (see chapter 2.9 below).

Once supernatants had been aspirated from the wells, the plates were washed 3 times with ice-cold PBS and placed on ice. 0.5ml ice-cold cell lysis buffer (BD Pharmingen) containing proteinase inhibitors (Sigma, UK) was added to each well and vigorously agitated several times using a 1ml Gilson pipette. The solution, containing the contents of the lysed cells, was transferred to 1.5ml Eppendorf containers and centrifuged at 12,000 rpm for 15 minutes to remove cellular debris. The resultant solutions containing total cellular proteins were decanted to fresh 1.5ml Eppendorf containers and subsequently frozen at $-80^{o}C$ pending analysis.

Protein levels in the protein lysis buffer were measured by the detergent compatible (DC) protein assay (Bio Rad, USA) according to manufacturer's instructions for low protein concentration assays.

2.8 *IN VIVO* MODELS OF INFLAMMATION

2.8.1 Thioglycollate peritonitis

Brewer's Thioglycollate (TG) (Sigma, UK) was reconstituted in sterile, distilled water at either 3 or 10% weight/volume (w/v). The resultant solution was then aliquoted to 5ml sterile aliquots and stored at $4^{o}C$ until used.

Mice selected for zero time points were not injected with TG. The abdomens of all other mice were cleaned with a disinfectant wipe and TG Peritonitis initiated with an ip injection using either 1ml of 3% w/v or 0.5ml 10% w/v TG depending on the experiment. Mice were sacrificed at the appropriate time point by cervical dislocation. Peritoneal lavage was performed immediately following death with 5ml ice-cold PBS as previously described. Lavage fluid recovered, usually in excess of 4ml, was placed in 15ml falcon tubes and kept on ice pending analysis (Figure 2.17).

The samples were gently vortexed and 400µl aliquots removed to chilled FACS tubes. Remaining lavage fluid was centrifuged at 300g for 10 minutes at $4^{o}C$. The supernatant was then decanted off and stored at $-80^{o}C$ pending analysis of chemokines and cytokines as described above. Mouse serum was added to each FACS tube as an Fc receptor blocking agent and the cells incubated on ice for 30 minutes. The aliquots were then immunolabeled with rat-anti-mouse monoclonal antibodies (see table 2.6 for full details of antibodies and isotypes used) and incubated in the dark and on ice for a further 30 minutes. The cells were then washed

with PBS and analysed by flow cytometry. Different immunolabeling combinations and flow cytometry gates were used for different experiments as detailed below.

2.8.1.1 *Analysis of leukocyte cell kinetics: zero to 96 hours*

Three aliquots were removed from each sample of lavage fluid. The first aliquot was immunolabeled for F4/80 conjugated to APC and GR-1 conjugated to PE. The second sample was immunolabeled for B220 conjugated to PE and the third sample was stained for CD3 conjugated to PE.

Figure 2.18 illustrates the representative forward and side scatter plots of peritoneal lavage fluid recovered at zero, 24, 48 and 96 hour time points following the ip injection of TG. The gate used to define leukocytes, excluding debris and erythrocytes, is shown. Figure 2.19 demonstrates how the fluorescent profiles in FL-4 (F4/80) and FL-2 (GR-1) change with time over the 96 hours and the gates used to define and count Mφ and PMN at the various time points: Mφ were F4/80^{HI} whilst PMN were GR-1^{HI}/ F4/80^{NEG}. Figure 2.20 demonstrates how B and T lymphocytes were defined as B220^{HI}/Side scatter^{LO} and CD3^{HI}/Side scatter^{LO} respectively. Figure 2.21 demonstrates the characteristic profiles of Mφ, PMN and lymphocytes on the forward and side scatter plots;

The first set of aliquots from each mouse was spiked with 50,000 Flowcheck™ spheres immediately prior to analysis to facilitate counting absolute numbers of cells, as previously discussed. The absolute numbers of B cells and T cells in the second and third series of aliquots respectively were calculated as a percentage of total leukocytes number determined from the first aliquot.

2.8.1.2 *Analysis of leukocyte cell kinetics: zero to 24 hours*

TG peritonitis was initiated as described above using 0.5ml 10% TG in sterile distilled water and peritoneal cells harvested by peritoneal lavage at zero, 1, 4, 8 and 24 hour time points as previously described. Aliquots of lavage fluid were removed from each sample and triple stained for F4/80 conjugated to APC, GR-1 conjugated to PE, and CD11b conjugated to FITC.

The gates and flow cytometer settings used for the first series of time points (2.8.1.1 above) did not fit as well to the cells infiltrating the peritoneum in the early hours following initiation of inflammation as they did to the later time points. Separation of infiltrating monocytes, Mφ and PMN by flow cytometry at these time points required additional gating as some PMN express significant amounts of CD11b and some F4/80^{LO} monocytes express significant amounts of GR-1 (Geissmann et al., 2003) . For this series of time points, PMN were defined as forward scatter^{LO}/GR-1^{HI}. They were then counted and excluded from further analysis. Mature PMφ were defined as both CD11b^{HI} and F4/80^{HI}. Infiltrating monocytes were gated as CD11b^{MED} and F4/80^{LO} (see figure 2.22).
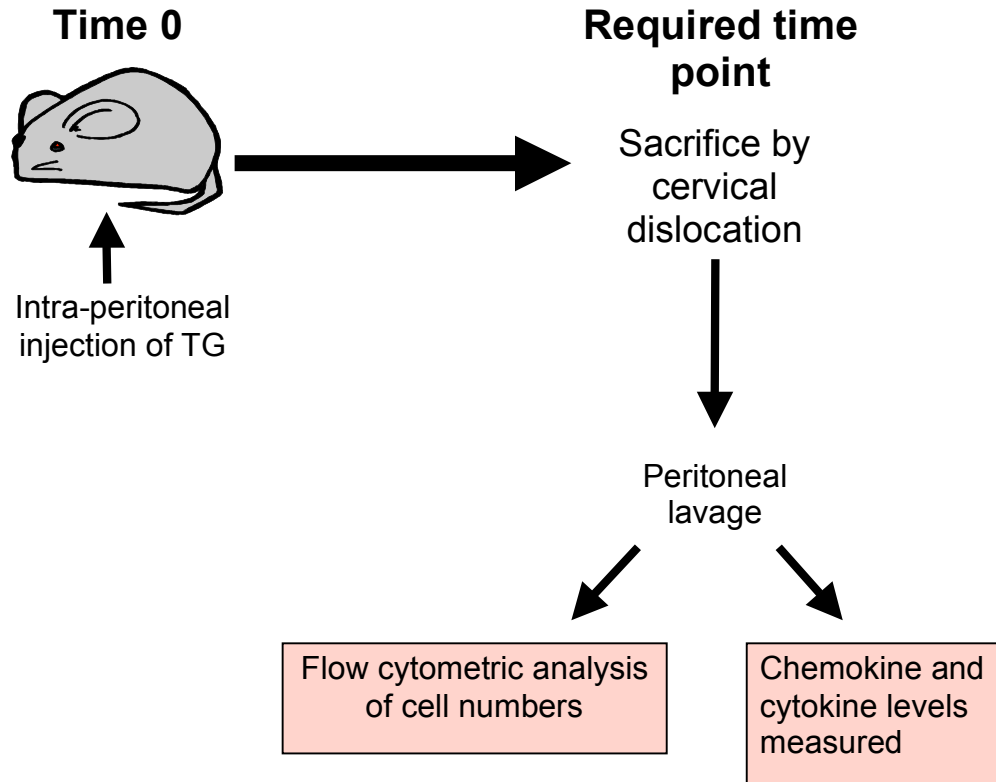
Figure 2- 18   Schematic diagram of Thioglycollate peritonitis studies

Target Protein	Comment	Supplier	Isotype control	Supplier
F4/80	Conjugated APC	eBioscience	APC Rat IgG2a	eBioscience
GR-1	Conjugated PE	eBioscience	PE Rat IgG2b	eBioscience
CD11b	Conjugated FITC	Caltag laboratories	FITC Rat IgG2b	Caltag laboratories
B220	Conjugated PE	eBioscience	PE Rat IgG2a	Caltag laboratories
CD3	Conjugated PE	Caltag laboratories	PE Rat IgG2a	Caltag laboratories
CD11c	Conjugated APC	Pharmingen	APC Hamster IgG	Pharmingen
CD4	Conjugated FITC	Caltag laboratories	FITC Rat IgG2a	eBioscience
CD8a	Conjugated APC	Caltag laboratories	APC Rat IgG2a	Caltag laboratories

Table 2- 6   **Monoclonal antibodies and isotypes used for flow cytometric analysis of leukocytes**
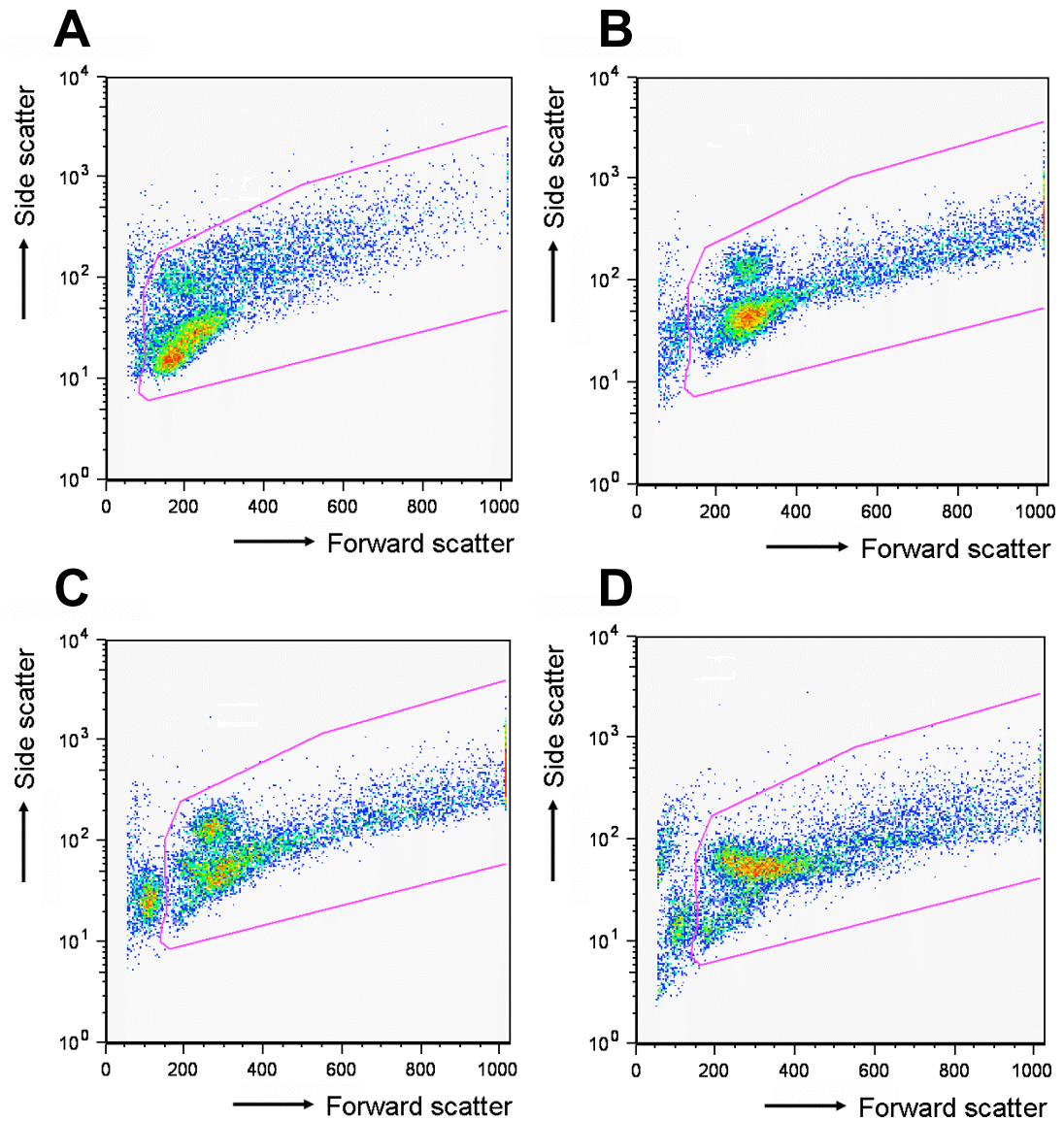
Figure 2- 19   Forward and side scatter plots of peritoneal cells during TG peritonitis
TG peritonitis was initiated by the injection of 1ml 3% TG. Peritoneal cells recovered at various time points by peritoneal lavage. Cells were immunolabeled and analysed by flow cytometry. Representative forward and side scatter profiles of peritoneal cells recovered are shown together with the gate used to count total leukocytes but exclude red blood cells (red arrow, image C) and debris. (A) Zero time point or resident cells. (B) 24 hours post TG injection. (C) 48 hours post TG injection. (D) 96 hours post TG injection. As the inflammatory process progresses, with different inflammatory cells entering and leaving the peritoneum, clear changes in the forward and side scatter profiles are apparent.
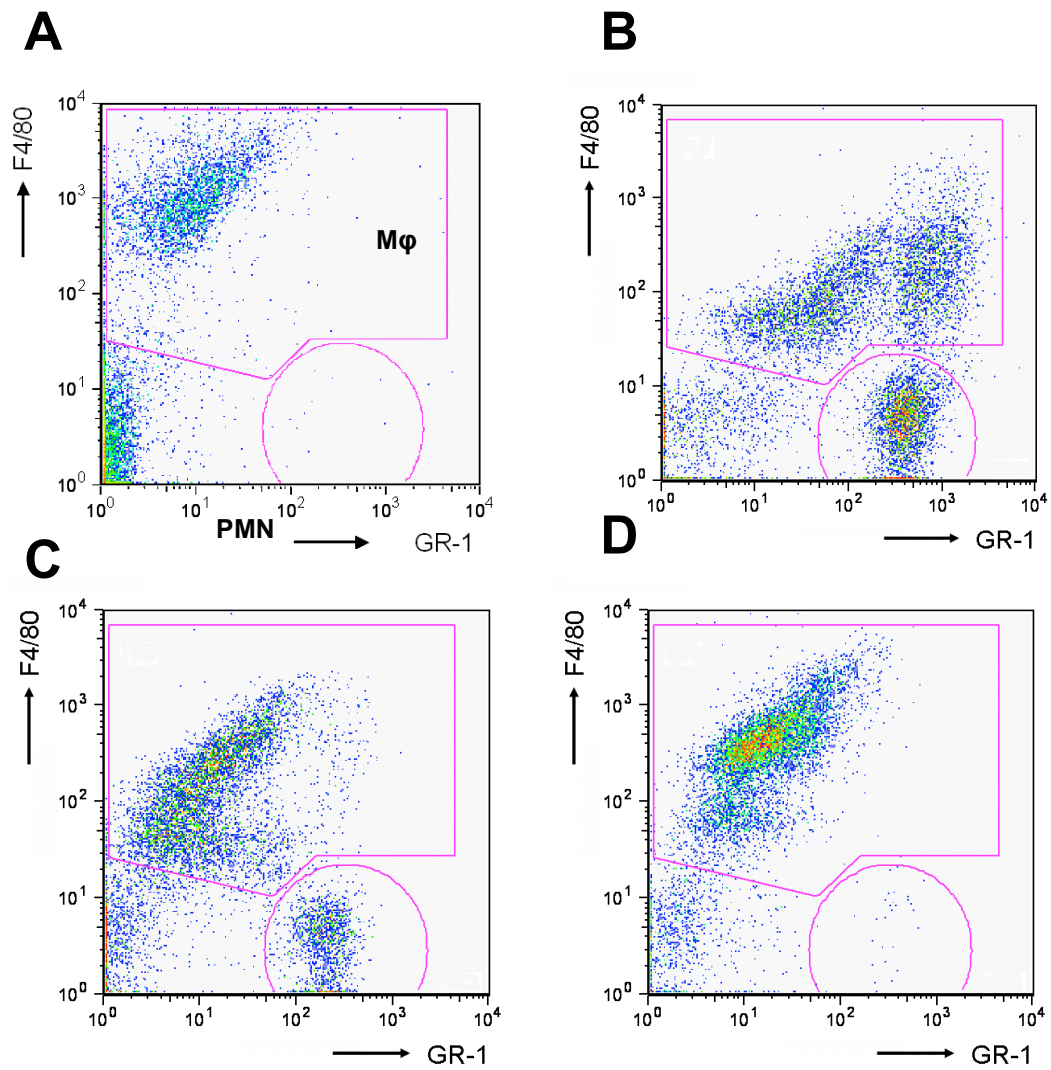
Figure 2- 20   Analysis of Mφ and neutrophil kinetics during TG peritonitis
TG peritonitis was initiated by the injection of 1ml 3% TG. Peritoneal cells were recovered at various time points by peritoneal lavage. Samples were immunolabelled for F4/80 conjugated to APC (FL-4) and GR-1 conjugated to PE (FL-2). Cells were then washed and analysed by flow cytometry. Leukocytes, gated as above, were analysed according to their F4/80 and GR-1 expression. Representative fluorescent profiles of leukocytes in FL-4 and FL-2 are shown together with the gates used to count Mφ (F4/80HI) and PMN (GR-1HI-F4/80NEG). (A) Zero time point or resident cells. (B) 24 hours post TG injection. (C) 48 hours post TG injection. (D) 96 hours post TG injection.
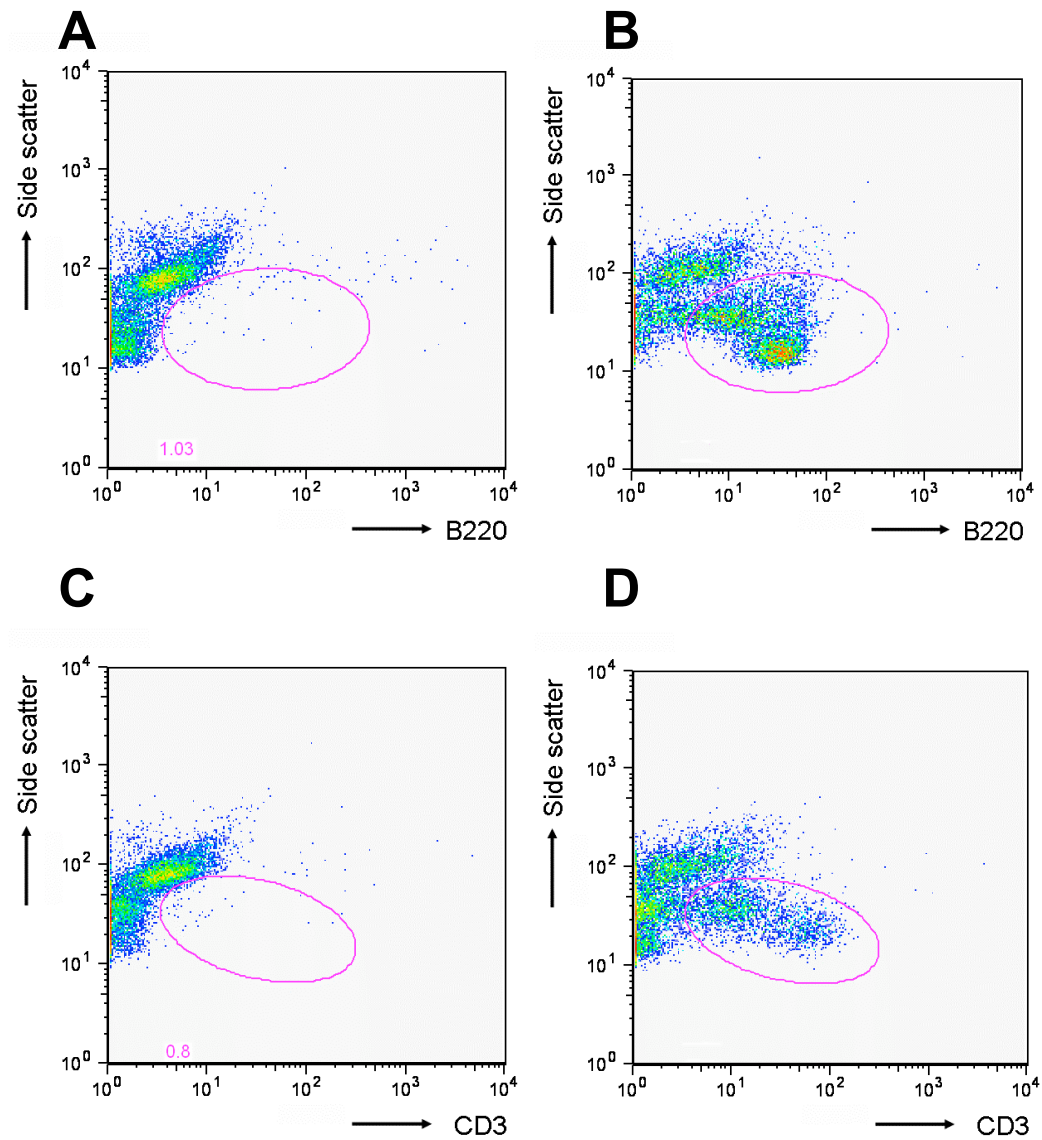
Figure 2- 21   Analysis of B and T lymphocyte numbers during TG peritonitis
TG peritonitis was initiated by the injection of 1ml 3% TG. Peritoneal cells were recovered at various time points by peritoneal lavage. Samples were immunolabeled either for B220 conjugated to PE (FL-2) or CD3 conjugated to PE or the appropriate isotype control. Cells were then washed and analysed by flow cytometry. Leukocytes, gated as above, were analysed according to their side scatter profile and FL-2 fluorescence. Representative side scatter / FL-2 plots of leukocytes are shown together with the gates used to count lymphocytes. (A) Peritoneal cells immunolabelled with B220 isotype control. (B) Peritoneal cells immunolabelled for B220. (C) Peritoneal cells immunolabelled with CD3 isotype control. (D) Peritoneal cells immunolabelled for CD3.
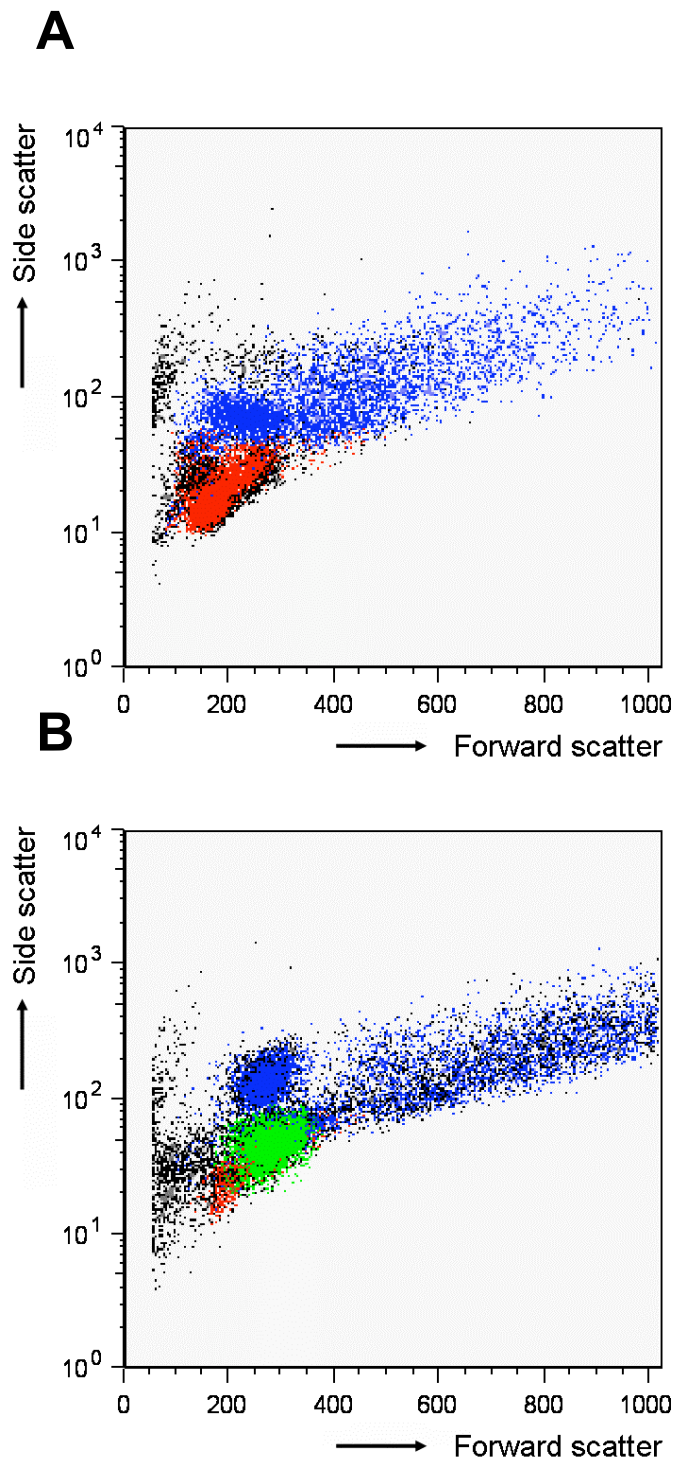
Figure 2- 22   Forward and side scatter profiles of leukocytes during TG peritonitis
TG peritonitis was initiated by the injection of 1ml 3% TG. Peritoneal cells recovered at various time points by peritoneal lavage. Samples were immunolabeled, washed and analysed by flow cytometry as above. Representative forward and side scatter plots of leukocytes are shown: Mφ in blue, lymphocytes in red and PMN in green. (A) Naïve peritoneal cells. (B) Peritoneal cells 24 hours after the initiation of TG peritonitis
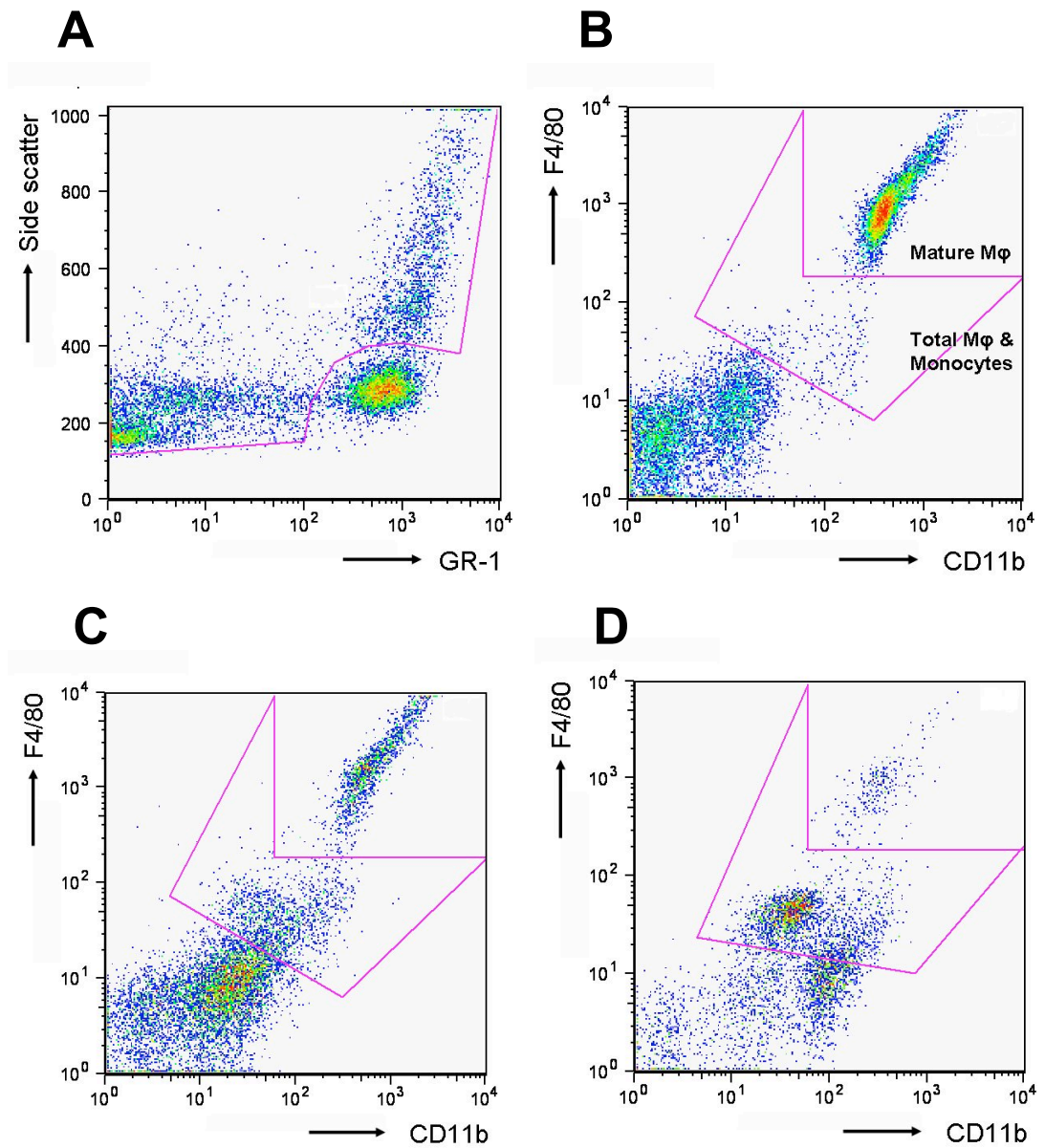
Figure 2- 23   Analysis of Mφ and neutrophil kinetics during TG peritonitis
TG peritonitis was initiated by the injection of 0.5ml 10% TG. Peritoneal cells were recovered at various time points by peritoneal lavage. Samples were immunolabeled for F4/80 conjugated to APC (FL-4), GR-1 conjugated to PE (FL-2) and CD11b conjugated to FITC (FL-1). Cells were then washed and analysed by flow cytometry. Leukocytes, gated as previously shown, were analysed according to their fluorescent profiles. (A) PMN were gated as forward scatter^{LO}/GR-1^{HI}, counted and excluded from further analyses. Mature Mφ (F4/80^{HI}/CD11b^{HI}) and monocytes (F4/80^{LO}/CD11b^{MED}) were then gated and counted from amongst the remaining cells. (B) Resident peritoneal cells. (C) 1 hour post TG injection. (D) 4 hours post initiation of TG peritonitis.

2.8.2 Carageenan pleurisy

Carrageenan (CG), a kind gift from Marine Colloids Inc, Philadelphia, USA, was reconstituted in sterile distilled water at 1% w/v immediately prior to use.

All mice, except those selected for the zero time point, were anaesthetised with isofluorothane gas. Whilst anaesthetised, the thoraces of the mice were sprayed with 70% ethanol and a small incision made through the skin between 6th and 8th intercostal muscles. 0.1ml CG was injected intrapleurally (i.pl) into all mice with a blunted 21G needle and the wound closed with a Michel clip.

Mice were sacrificed under general anaesthesia, at appropriate time points, by transection of the great vessels in the posterior abdominal cavity causing exsanguination. As much blood as possible was harvested into 1.5ml Eppendorf tubes and centrifuged at 14,000 rpm for 15 minutes at 4°C. The serum was then aspirated and frozen at - 80°C pending analysis of chemokines and cytokines as described previously.

Once death was confirmed a wide transverse incision just below the rib cage was made. The abdominal organs were reflected away to expose the diaphragm which was then punctured by a small, anterior, mid-line incision. The pleural cavities were lavaged with 1ml 3.88% sodium citrate (Sigma, UK) in saline using a sterile Pasteur pipette. Lavage fluid recovered was placed in 1.5ml Eppendorf tubes, weighed accurately to measure the volume recovered and kept on ice pending further analysis.

The samples were gently vortexed prior to removal of 50μl aliquots to chilled FACS tubes. The remaining fluid was centrifuged at 2000 rpm for 5 minutes at 4°C. Supernatants were again decanted off and stored at -80°C pending analysis of chemokines and cytokines as described above.

Mouse serum was added to each FACS tube as an FcR blocking agent and the cells incubated on ice for 30 minutes. The aliquots were then immunolabeled with monoclonal antibodies (see table 2.6 for full details of antibodies used) and incubated in the dark, on ice, for a further 30 minutes following which the cells were washed with PBS and analysed by flow cytometry.

2.8.2.1 *Analysis of cell kinetics: zero to 72 hours*

A schematic diagram of an experiment studying carrageenan pleurisy is given in figure 2.23. Two aliquots were removed from each pleural lavage sample. The first aliquot was immunolabeled for F4/80 conjugated to APC, GR-1 conjugated to PE and CD11b conjugated to FITC. The second sample was immunolabelled for CD11c conjugated to APC.

Figure 2.24 illustrates representative flow cytometry plots of pleural lavage fluid recovered at both the zero and 24 hour time points following the intrapleural injection of CG. In a similar fashion to PMφ, PLMφ were defined as F4/80^{HI}, CD11b^{HI} whilst PMN were defined as GR-1^{HI}, F4/80^{NEG} cells. DC were defined as CD11c^{HI} and were counted as demonstrated in figure 2.25.
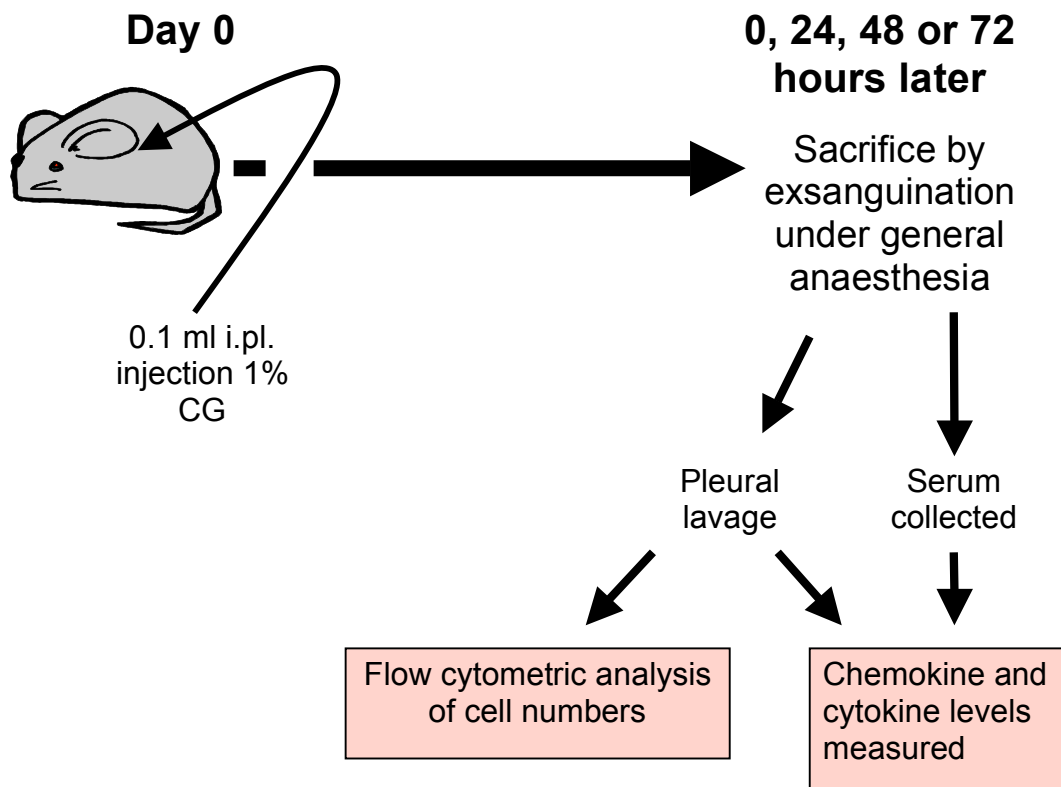
Figure 2- 24   Schematic diagram of Carrageenan pleurisy
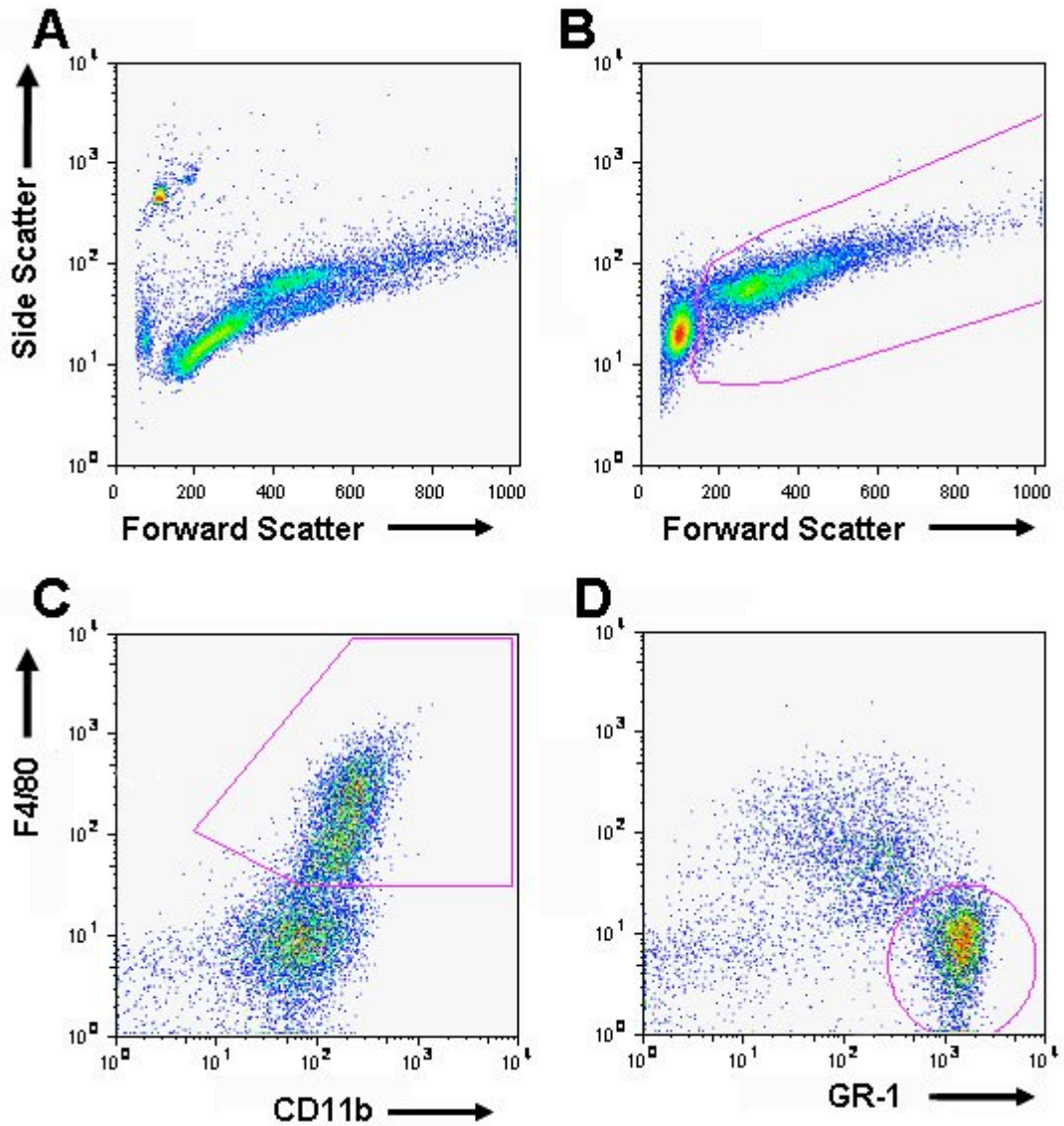
Figure 2- 25   Analysis of leukocytes recruited to CG pleurisy
CG pleurisy was initiated by the injection of 0.1ml 1% CG i.pl. Pleural cells were recovered by pleural lavage at various time points and immunolabeled for F4/80 conjugated to APC (FL-4), GR-1 conjugated to PE (FL-2) and CD11b conjugated to FITC (FL-1). Samples were analysed by flow cytometry. (A) Representative forward and side scatter plot of naïve pleural cells and Flowcheck™ beads. (B) Representative forward and side scatter plot of pleural cells 24 hours after initiation of pleurisy with gate used to count leukocytes, excluding red blood cells and debris. (C) Representative plot of pleural cells 24 hours after initiation of pleurisy analysed by fluorescence in FL-1 and FL-4, demonstrating gate used to count Mφ (F4/80^{HI}, CD11b^{HI}). (D) Representative plot of pleural cells 24 hours after initiation of pleurisy analysed by fluorescence in FL-2 and FL-4, demonstrating gate used to count PMN (GR-1^{HI}, F4/80^{NEG}).
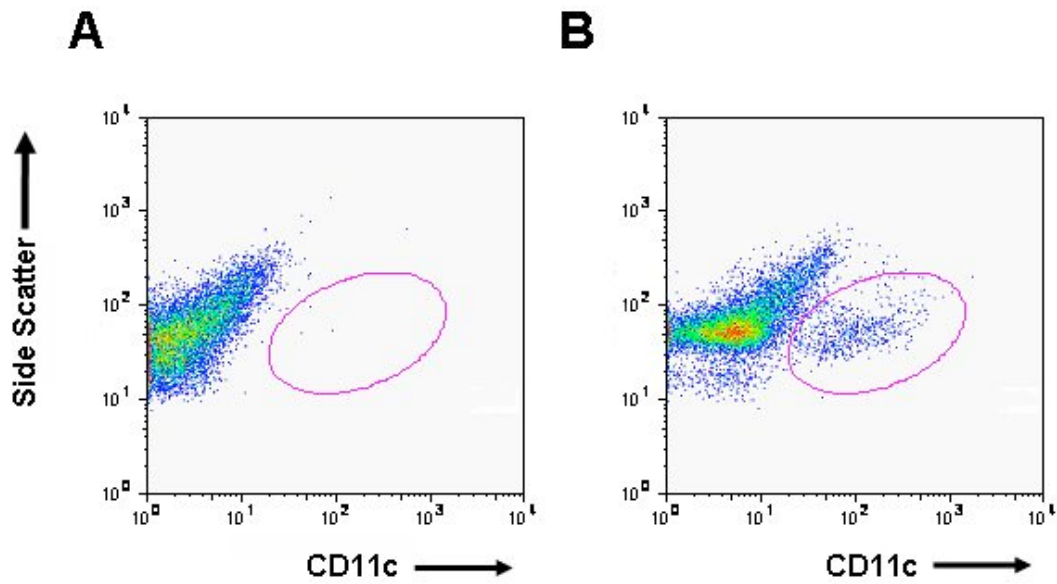
Figure 2- 26   Analysis of dendritic cells in CG pleurisy
CG pleurisy was initiated by the injection of 0.1ml 1% CG i.pl. Pleural cells were recovered by pleural lavage at various time points and immunolabelled either for CD11c conjugated to APC (FL-4), or the isotype conjugated to APC. Samples were analysed by flow cytometry. (A) Side scatter, FL-4 plot of pleural cells 24 hours after initiation of pleurisy following immunolabeling with the isotype antibody: the gate used to count CD11c^{HI} dendritic cells is illustrated. (B) Representative side scatter, FL-4 plot of pleural cells 24 hours after initiation of pleurisy following immunolabeling for CD11c conjugated to APC.

118

2.8.3 Delayed-Type Hypersensitivity Pleurisy

Initiation of delayed-type hypersensitivity pleurisy (DTH pleurisy) required 2 phases undertaken 12 days apart. Phase 1 was the sensitisation of the mice to Methylated Bovine Serum Albumin (Meth'BSA). Phase 2, was initiation of pleurisy by the i.pl. injection of meth'BSA.

1% meth'BSA was homogenised in complete Freud's adjuvant (CFA) immediately prior to use. Mice to be sensitised were anaesthetised with isofluorothane gas and the base of their tails carefully shaved using an electric razor. Whilst still under general anaesthesia the skin was wiped with a medicated swab and 0.1ml of meth'BSA in CFA was injected intradermally using a sterile 26g needle. Care was taken to avoid a subcutaneous injection. Mice were then allowed to recover from the anaesthesia. DTH pleurisy was initiated 12 days later in exactly the same way as for CG pleurisy except that 0.1ml of 1% meth'BSA in sterile distilled water was injected.

Whilst all mice were sensitised, those for the zero time point (i.e. naïve mice) were not injected i.pl. with meth'BSA. Mice were again sacrificed by exsanguination under general anaesthesia to permit collection of blood for serum analysis. Pleural lavages were collected, leukocyte numbers together with cytokine and chemokine levels were analysed as for CG pleurisy. A schematic diagram of an experiment studying DTH pleurisy is given in figure 2.26.
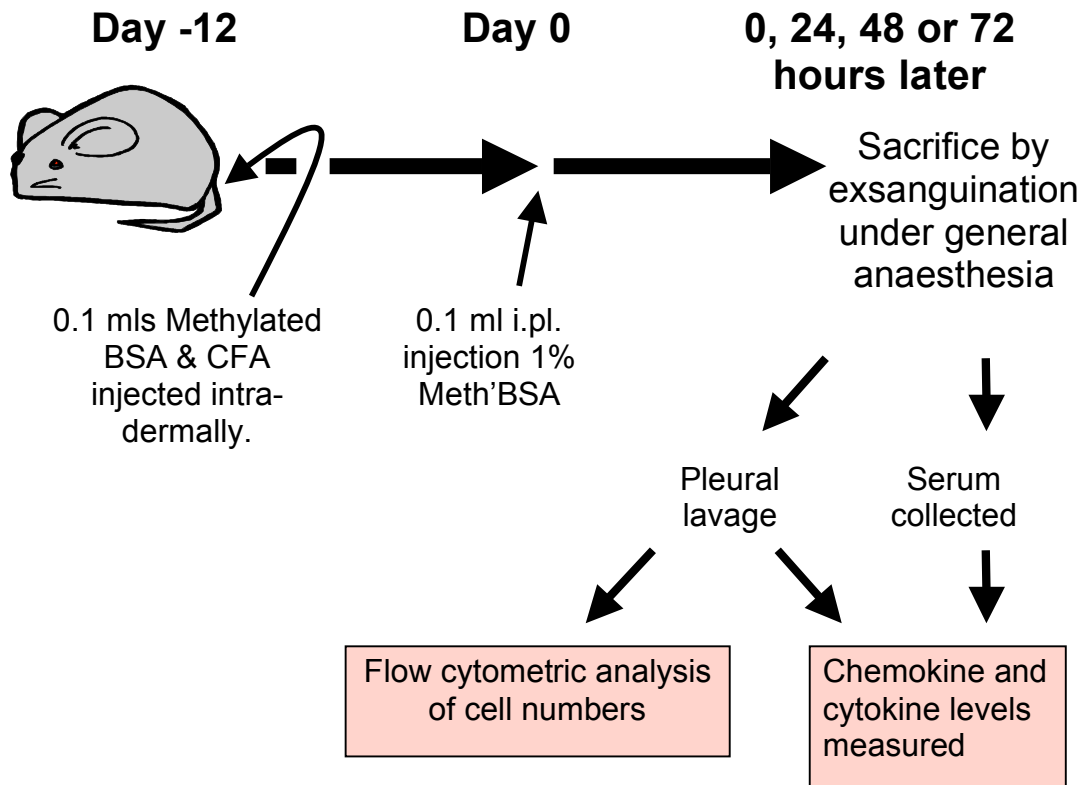
Figure 2- 27   Schematic diagram of Delayed Hypersensitivity pleurisy

120

2.9 ANALYSIS OF CIRCULATING LEUKOCYTES

Attempts were made to use blood retrieved from the abdominal cavity during exsanguination under general anaesthesia following transection of the great vessels (see models of CG pleurisy and DTH pleurisy above). Blood recovered using that technique however clotted extremely rapidly such that data collected could be inaccurate. The whole blood used in this thesis to analyse circulating leukocytes came from a tail bleed. Mice were warmed gently under a lamp and restrained gently. A small nick was made near the base of the tail using a sterile scalpel. Once a large droplet of blood had formed, 50μl was collected using a sterile 200μl Gilson pipette and immediately mixed vigorously with 100μl of 3.88% citrate in a 500μl Eppendorf. The resultant mixture was then split equally between 2 chilled FACS tubes labeled A and B and kept on ice. Each tube was then immunolabeled with 50μl of a solution containing 3 monoclonal antibodies, each diluted 1:100 in PBS with 10% mouse serum. Tube A was immunolabeled for F4/80 conjugated to APC, GR-1 conjugated to PE and CD11b conjugated to FITC. Tube B was immunolabeled for CD8a conjugated to APC, B220 conjugated to PE and CD4 conjugated to FITC. Cells were incubated on ice, in the dark, for 30 minutes and then washed in PBS. Pharm Lyse™ lysing solution (BD Biosciences) was used according to manufacturer's instructions to remove red blood cells from the analysis.

Following red cell lysis, leukocytes were resuspended in PBS with 10% mouse serum. Samples were spiked with 50,000 Flowcheck™ beads immediately prior to analysis by flow cytometry. Representative dot plots of total leukocytes and gates used to define monocytes and PMN are illustrated in figures 2.27. Gates used to count lymphocytes are shown in figure 2.28. The numbers of events were translated into absolute numbers of leukocytes by comparison to beads counts as previously described.
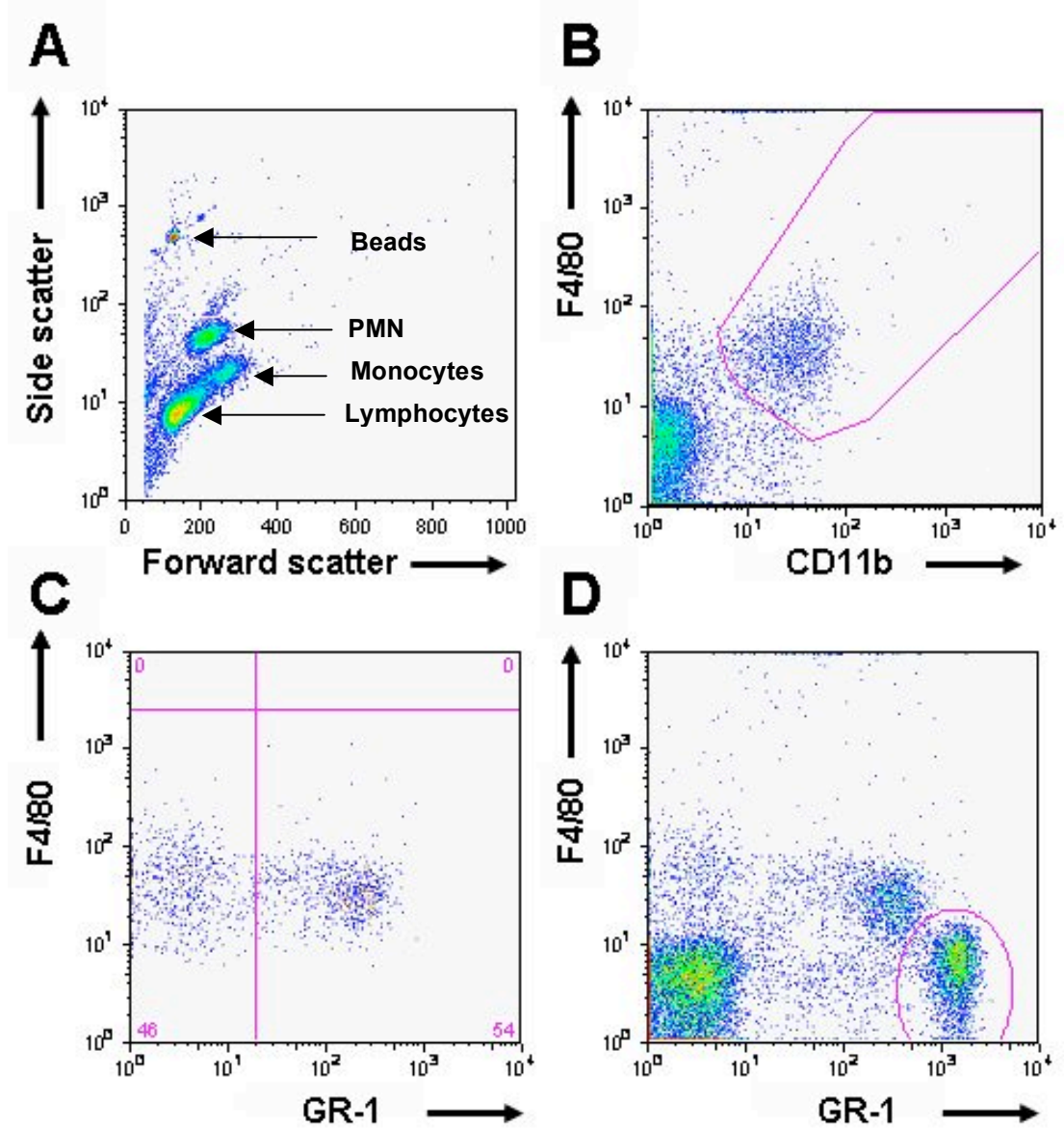
Figure 2- 28   Analysis of circulating monocytes and PMN
Blood was collected from a tail bleed into 3.88% citrate. Leukocytes were immunolabeled and red cells lysed using a lysis buffer. Cells were analysed by flow cytometry using Flowcheck[TM] beads to count absolute circulating numbers. (A) Representative forward and side scatter plot demonstrating the positions occupied by the major leukocyte groups (labeled). (B) Representative plot of all leukocytes assessed by fluorescence in FL-4 (F4/80) and CD11b (FITC). The gate used to count monocytes is shown. (C) Representative plot of monocytes alone when assessed by fluorescence in FL-4 (F4/80) and FL-2 (GR-1): 2 distinct groups of monocytes (GR-1[HI] and GR-1[LO]) were easily distinguished and counted as shown. (D) Representative plot of all leukocytes examined by fluorescence in FL-4 (F4/80) and FL-2 (GR-1). The gate used to count PMN is shown.
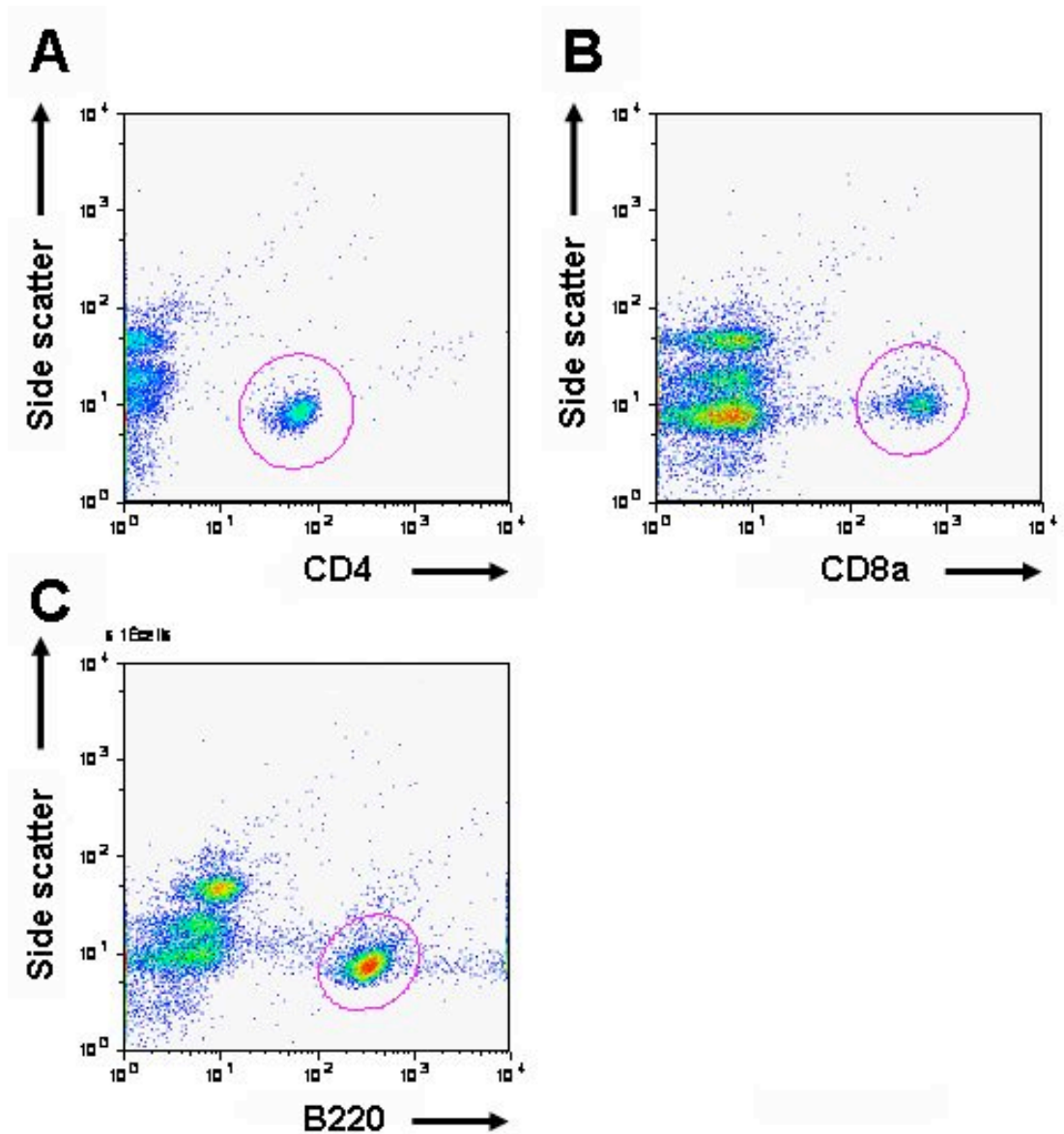
Figure 2- 29   Analysis of circulating lymphocytes
Blood was collected from a tail bleed into 3.88% citrate. Leukocytes were immunolabeled and red cells lysed using a lysis buffer. Cells were analysed by flow cytometry using Flowcheck[TM] beads to count absolute circulating numbers. (A) Representative plot of all leukocytes assessed by side scatter profile and fluorescence in FL-1 (CD4). The gate used to count CD4 T lymphocytes is shown. (B) Representative plot of all leukocytes assessed by side scatter profile and fluorescence in FL-4 (CD8a). The gate used to count CD8 T lymphocytes is shown. (C) Representative plot of all leukocytes assessed by side scatter profile and fluorescence in FL-2 (B220). The gate used to count B lymphocytes is shown.

2.10 STATISTICAL ANALYSIS

All statistical analyses were done using PRISM 4 (GraphPad, San Diego, USA). Student's t tests were used to compare an individual pair of mean values whilst Analysis of variance (ANOVA) was used to compare differences across several mean values. 2 way ANOVA was used to compare the effects of 2 variables such as strain of mouse and duration of inflammation. Bonferonni post tests were used to compare individual means within the context of an ANOVA.

Chapter 3. NOD Macrophages Exhibit Reduced Phagocytic Clearance *In Vitro*

3.1 INTRODUCTION

Apoptotic cells are usually rapidly cleared by Mφ, regarded as a 'professional' phagocyte, as well as other non-professional phagocytic cells within tissues. The defective clearance of AC has been linked with a predisposition to autoimmunity (Casciola-Rosen et al., 1994). It is hypothesised that the persistence of AC may result in the presentation of autoantigen to T cells by DC and that this might contribute to a breakdown in peripheral tolerance and the generation of autoimmune responses. For example, C1q knockout mice exhibit a well documented defect in AC clearance and have a tendency to develop glomerulonephritis that is characterised by the presence of AC (Robson et al., 2001). Similarly other strains of mice prone to develop autoimmune diseases such as SLE exhibit defective clearance of AC by Mφ. In 2002 O'Brien et al demonstrated that Mφ from NOD mice phagocytosed AC less effectively *in vitro* compared to Mφ from a number of other control strains that do not develop autoimmune diabetes (O'Brien et al., 2002). The impaired ability to ingest AC was age-dependent and was most pronounced in mice as young as one week old and was almost undetectable in mice at 12 weeks of age. They also noted that Mφ from female NOD mice cleared AC less effectively than those from male NOD mice and that the defective clearance was more apparent among resident PMφ than BMDMφ. In their experiments, they found that the phagocytic ingestion of polystyrene beads was comparable across all strains studied, thereby suggesting the defect was specific to AC and did not result from a generalised phagocytic defect. They argued that these data fitted the observations that diabetes develops with a much higher incidence in female rather than male NOD mice and occurs shortly after a wave of apoptosis in the neonatal pancreas as it is remodelled in preparation for adult life.

In the studies described in this thesis, C57BL/6 mice were chosen as the main control strain for 2 reasons. Firstly, O'Brien et al (O'Brien et al., 2002) demonstrated that Mφ from C57BL/6 mice exhibited the level of phagocytosis that was closest to NOD Mφ. As a result, it was felt this would make them the most rigorous control strain to use. Secondly, congenic NOD strains usually have C57BL/6 chromosomal segments replacing parts of their NOD genome. The H-2[i7] is a congenic NOD strain that differs from the NOD genome only in its MHC genes which are derived from C57BL/6 mice. It does not, however, develop insulitis or autoimmune diabetes.

3.2 RESULTS

3.2.1 NOD and H-2^{i7} PMφ demonstrate reduced phagocytic clearance of AC and latex beads *in vitro*.

Peritoneal cells were harvested from 6 female NOD mice aged 5 weeks together with age and sex matched C57BL/6 and H-2^{i7} control mice (see above). Phagocytosis assays were performed as previously described in chapter 2.3. In brief, PMφ were exposed to either fluorescently labelled AC or 3μm latex beads (at a ratio of one PMφ to ten particles) for one hour in the presence of 10% FBS. The percentage phagocytosis and phagocytic index were assessed by fluorescence photography followed by manual counting. Over 300 PMφ were counted to give values per well and 3 to 4 wells were examined to give values per mouse. Since 6 mice were assessed from each strain, each value therefore represents at least 5400 PMφ. Statistical analysis was by 2-way analysis of variance (ANOVA) with Bonferroni post tests.

In accordance with the previously published work of O'Brien et al (O'Brien et al., 2002), NOD PMφ exhibited both a lower percentage phagocytosis and phagocytic index compared to C57BL/6 PMφ following exposure to AC *in vitro*. These data indicate that fewer NOD PMφ phagocytosed AC and, of those that did ingest AC, they ingested fewer in the allotted time than the C57BL/6 control PMφ (figure 3.1). In marked contrast to the published data, however, defective clearance of latex beads by NOD PMφ was also evident. As expected, since the MHC is not implicated in phagocytosis, H-2^{i7} PMφ behaved in an identical fashion to NOD PMφ following exposure to either AC or 3μm latex beads *in vitro* and exhibited a significantly lower percentage phagocytosis and phagocytic index than C57BL/6 derived PMφ (figure 3.1). These mice develop neither insulitis nor diabetes and thus these data do not support the hypothesis that it is the impaired phagocytic clearance of AC, specifically of apoptotic beta cells in the pancreas, by NOD Mφ in the second and third weeks of life that predisposes to organ specific autoimmune diabetes in NOD mice. The data, however, are consistent with a hypothesis that impaired phagocytosis contributes to the predisposition to generalised autoimmunity seen in NOD mice.

A

B
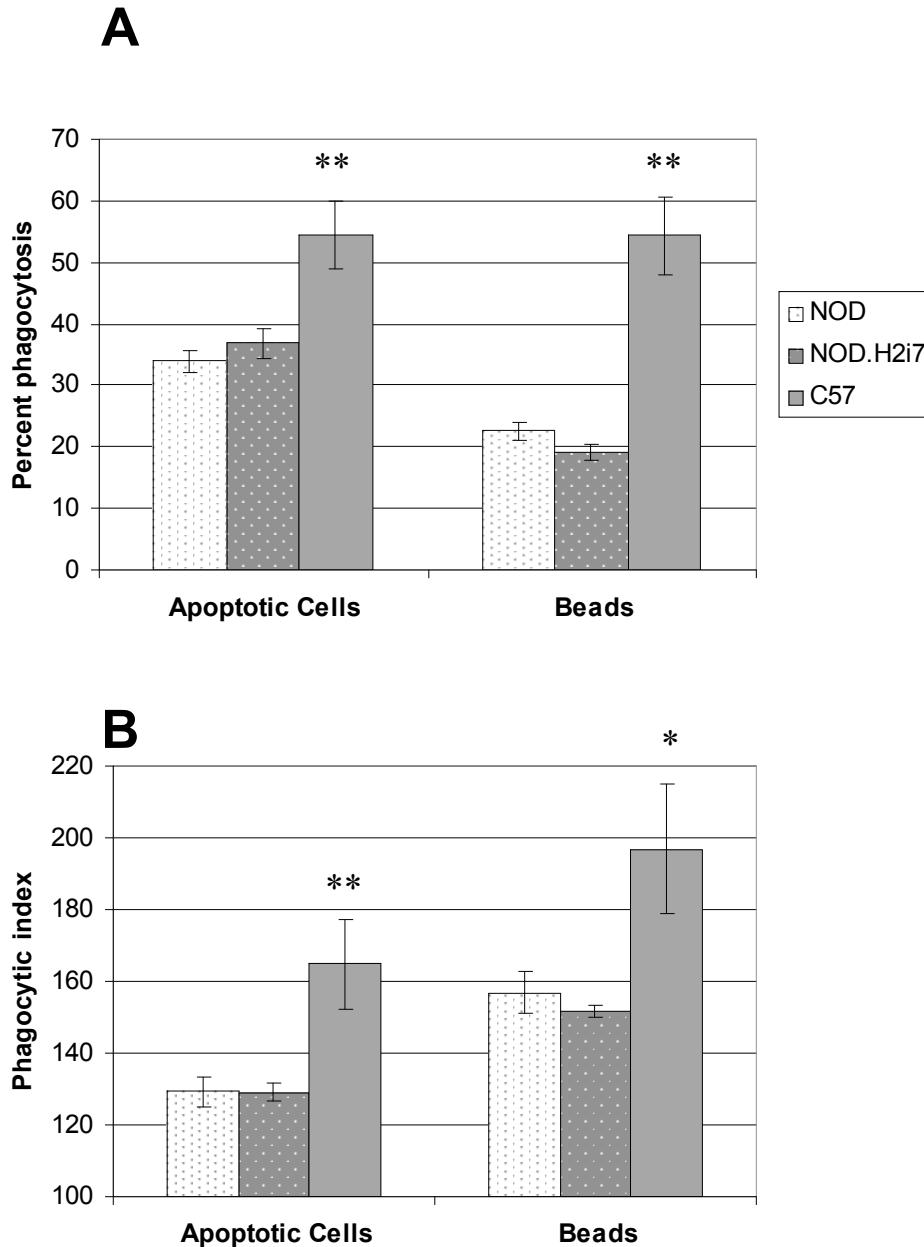
Figure 3- 1   Analysis of phagocytosis of AC and 3µm latex beads *in vitro*
Resident peritoneal cells were harvested from C57BL/6 mice, NOD mice and the congenic NOD mouse strain H2^{i7}. PMφ were purified by adhesion and fed AC at a ratio of 10:1 for 60 minutes at 37°C. Phagocytosis was analysed by microscopy following the addition of LysoTracker Red. Percentage phagocytosis was defined as the percent of PMφ that had ingested at least 1 AC whilst phagocytic index was defined as the number of AC eaten by 100 PMφ that had eaten at least 1 AC. (A) PMφ from NOD and the congenic NOD strain H2^{i7} exhibit reduced percentage phagocytosis *in vitro* compared to C57BL/6 PMφ (B) PMφ from NOD and the congenic NOD strain H2^{i7}, exhibit reduced phagocytic index *in vitro* compared to C57BL/6 PMφ; * $p < 0.05$, ** $p < 0.01$; C57BL/6 vs. NOD and H2^{i7}; 2-way ANOVA with Bonferroni post tests.

3.2.2 NOD Mφ *in vitro* do not exhibit reduced clearance of opsonised pneumococci

Having demonstrated that NOD PMφ demonstrate impaired phagocytic clearance of both AC and latex beads *in vitro*, it was felt important to assess whether this was generalised to all particles, or whether under certain conditions NOD PMφ would clear particles at comparable rates to a control strain. It has been convincingly demonstrated that C57BL/6 mice lacking the inhibitory FcγR2b exhibit enhanced clearance of opsonised pneumococci (Clatworthy and Smith, 2004). Many lupus-prone strains of mice as well as NOD mice have a genetic haplotype that results in an approximately 50% reduced expression of FcγR2b on the cell surface of Mφ compared to control strains including C57BL/6 Mφ (Clatworthy and Smith, 2004). It would therefore be reasonable to hypothesise that NOD PMφ would exhibit increased phagocytosis of opsonised pneumococci compared to C57BL/6 PMφ.

The small size of pneumococci makes the assessment of percentage phagocytosis and phagocytic index by direct microscopy as described above extremely difficult. An alternative method of assessing phagocytosis by flow cytometry described and validated by Menna Clatworthy (Clatworthy and Smith, 2004) and described previously in chapter 2.3 was therefore employed. In brief, fixed, fluorescent pneumococci were either opsonised in serum from mice vaccinated with pneumovax 2 weeks previously or left non-opsonised. Pooled PMφ from 6 week old female NOD mice or C57BL/6 control mice were 'fed' opsonised or non-opsonised pneumococci or fluorescently labeled AC for one hour at 37^0C. The phagocytosis assay was performed in serum-free media in order to avoid unintentional opsonisation of pneumococci. Control wells were kept on ice for the duration of the phagocytosis assay in order to assess non-specific binding. PMφ were removed from the plastic by scraping, placed in FACS tubes, stained with anti-murine F4/80 antibodies conjugated to APC to fluoresce in FL-4 and assessed by flow cytometry. Since all phagocytosed particles were fluorescent in FL-1, the percentage phagocytosis was assessed as the percentage of PMφ that shifted in FL-1 over and above the rate of non-specific binding. Twelve mice from each strain were used to supply sufficient PMφ for 4 wells per strain for AC (n = 4) and 6 wells per strain for opsonised and non-opsonised pneumococci (n = 6). Over 5000 PMφ events were recorded per well.

The phagocytic defect for AC seen with NOD PMφ compared to C57BL/6 PMφ was consistent with phagocytosis being reduced by 32% despite the alternative method of assessing phagocytosis and the use of serum-free media. A small, but statistically significant, defect was detected for the phagocytosis of non-opsonised pneumococci but no difference between the 2 strains was detected for the phagocytosis of opsonised pneumococci (see figure 3.2)

Thus, the *in vitro* phagocytic defect seen with NOD PMφ is neither limited to AC, nor is it dependent on the presence or absence of serum. It can however be corrected by opsonising the feed, thereby bringing different factors into play, such as FcR.
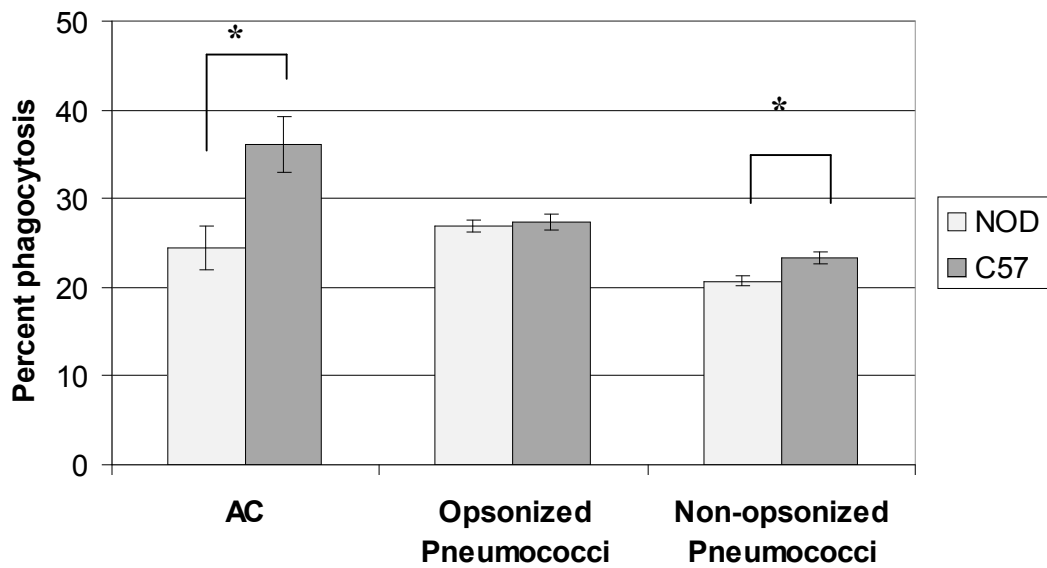
Figure 3- 2   **Analysis of *in vitro* phagocytosis of opsonised pneumococci**
Resident peritoneal cells from NOD and C57BL/6 mice were harvested by peritoneal lavage, pooled according to strain, plated into plastic wells and purified by adhesion. PMφ were 'fed' either apoptotic cells at a ratio of 10:1 or an excess of pneumococci (opsonised or non-opsonised) in the absence of serum. Phagocytosis was assessed after 1 hour. Cells were washed, scraped from the plastic and immunolabeled for F4/80 prior to analysis by flow cytometry. NOD mice exhibited reduced clearance of both AC and non-opsonised pneumococci but not opsonised pneumococci; * p < 0.05; 2-way ANOVA with Bonferroni post tests.

3.2.3 Both BMDMφ and PMφ from 15-week-old female NOD mice exhibit a marked *in vitro* phagocytic defect for AC

Having demonstrated the *in vitro* phagocytic defect was clearly apparent in very young NOD mice, it was considered important to examine whether the defect was still apparent in much older but still pre-diabetic NOD mice. It was also important to know whether it is indeed more pronounced in resident, sentinel Mφ such as PMφ or whether alternative Mφ populations such as BMDMφ exhibit a similar phagocytic defect.

PMφ were harvested from 15-week-old female NOD and C57BL/6 mice. Femurs were harvested and BMDMφ matured in Teflon pots for 7 days as described previously (chapter 2.2) and plated for 24 hours prior to use. Phagocytosis assays were performed using pooled Mφ and assessed by flow cytometry as described above (and chapter 2.3). Six NOD and 8 C57BL/6 mice were used, providing sufficient PMφ for 8 wells per strain (n = 8) and BMDMφ for 12 wells per strain (n = 12). Over 5000 Mφ events were recorded per well. Statistical analysis was by 2-way ANOVA with Bonferroni post tests.

Even with 15 week old mice there was a clear, albeit somewhat reduced, phagocytic defect still apparent in NOD PMφ compared to controls. However, BMDMφ from the same mice exhibited a marked reduction in phagocytosis of AC (see figure 3.3).

O'Brien's original paper had argued that defective clearance of AC by NOD Mφ, although still evident in BMDMφ, was more pronounced in PMφ and that the defect became less apparent as NOD mice aged to the point of almost resolving by 12 weeks. These data were used to support the hypothesis that defective clearance of apoptotic Beta cells, at a very specific time point during the development of neonatal mice when the pancreas undergoes a wave of apoptosis, lead to the development of organ specific autoimmunity. The data from the studies outlined in this thesis suggests that the phagocytic defect is present in a much broader context.
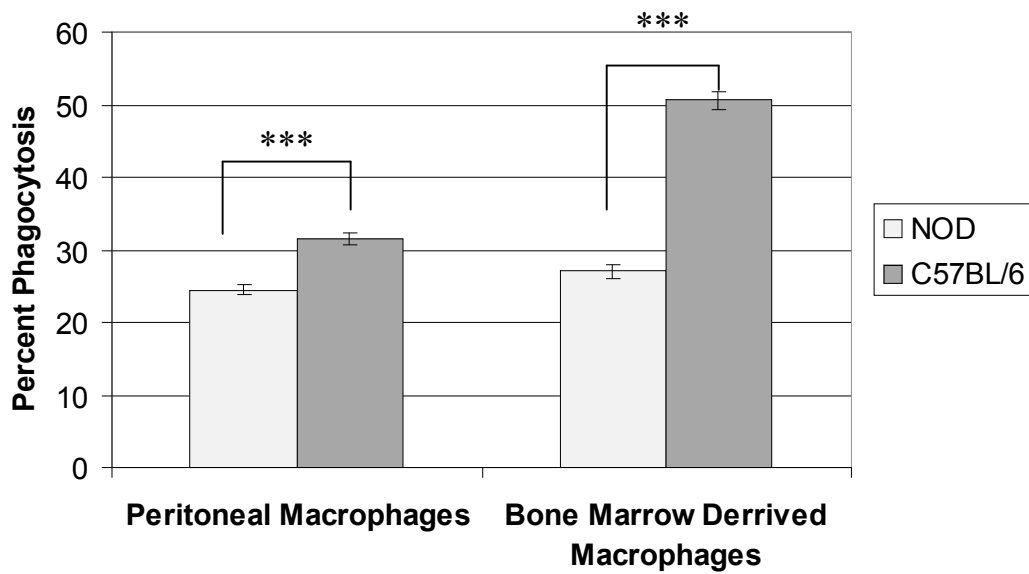
Figure 3- 3   Analysis of in vitro phagocytosis by PMφ from 15 week old NOD mice and BMDMφ from the same mice
Resident peritoneal cells from NOD and C57BL/6 mice were harvested by peritoneal lavage, pooled according to strain, plated into plastic wells and purified by adhesion. Femurs were harvested from the same mice and BMDMφ matured in Teflon pots for 7 days in the presence of 20% L929. Mature BMDMφ were plated into plastic wells 24 hours prior to analysis. Mφ were 'fed' AC at a ratio of 10:1 in the absence of serum and phagocytosis was assessed after 1 hour. Cells were washed, scraped from the plastic and immunolabeled for F4/80 prior to analysis by flow cytometry. PMφ and BMDMφ from NOD mice exhibited reduced phagocytosis of AC; ***$p < 0.001$; 2-way ANOVA with Bonferroni post tests.

3.2.4 The phagocytic defect for AC is clearly apparent with both 30 and 60 minute feed times

Having demonstrated that the phagocytic defect was clearly apparent in 15-week-old as well as very young NOD mice and was just as marked in BMDMφ as PMφ, it was felt important to examine whether the duration of the *in vitro* phagocytosis assay was important. Did NOD Mφ initially ingest AC at a rate comparable to controls, but then "fatigue" or "saturate" at an early stage?

BMDMφ were harvested from 9-week-old female NOD mice and C57BL/6 controls. An *in vitro* phagocytosis assay was performed as described above (and chapter 2.3) using pooled Mφ and assessment by flow cytometry. AC were used as 'feed' at a ratio to Mφ of 10:1 with 'feed' times of either 30 or 60 minutes. Once again, NOD BMDMφ exhibited a marked reduction in the percentage phagocytosis of AC that was clearly apparent at both 30 and 60 minutes (figure 3.4).

These data therefore suggest that the defective phagocytosis of AC by NOD Mφ *in vitro* is not merely due to early saturation of the phagocytic capacity of Mφ for AC.
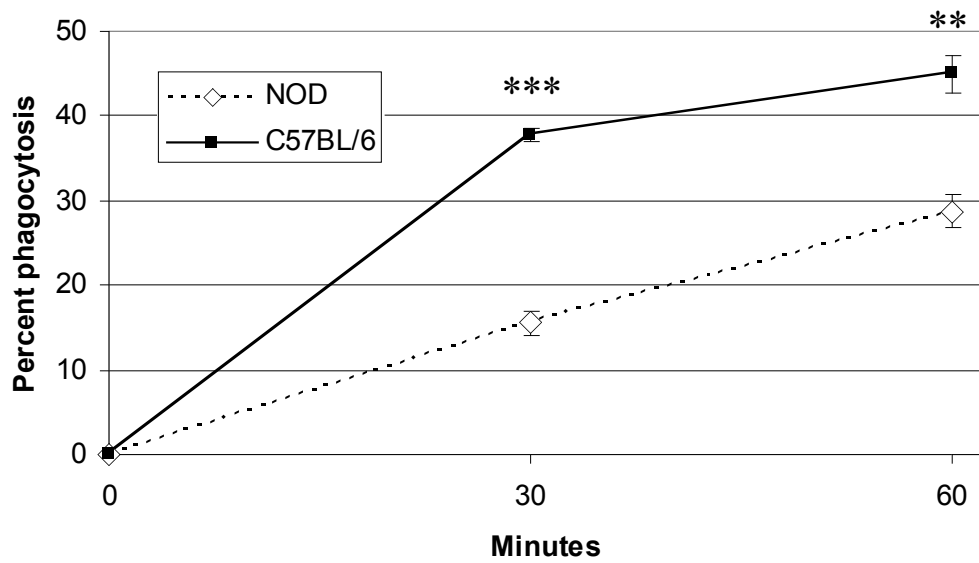
Figure 3- 4   Analysis of the effect of incubation time on *in vitro* phagocytosis
Femurs were harvested and BMDMφ matured in Teflon pots for 7 days in the presence of 20% L929. Mature BMDMφ were plated into plastic wells 24 hours prior to analysis. Mφ were 'fed' AC at a ratio of 10:1 in the absence of serum and phagocytosis assessed after 30 or 60 minutes. Cells were washed, scraped from the plastic and immunolabeled for F4/80 prior to analysis by flow cytometry. BMDMφ from NOD mice exhibited reduced phagocytosis of AC by 30 minutes with the defect being maintained at 60 minutes; *** p < 0.001, ** p < 0.01; NOD vs. C57BL/6; 2-way ANOVA with Bonferroni post tests.

3.3 SUMMARY

PMφ and BMDMφ from NOD mice exhibit a striking phagocytic defect in vitro.

The defect is apparent for AC, 3μm latex beads and non-opsonised pneumococci, but not opsonised pneumococci.

The defect is evidently independent of the presence or absence of FBS.

The defect is clearly present in older pre-diabetic NOD mice as well as very young mice.

The defect is clearly demonstrable by 30 minutes.

Chapter 4. NOD Macrophages Exhibit Reduced Phagocytic Clearance of Apoptotic Cells *In Vivo*

4.1 INTRODUCTION

The work outlined in Chapter 3 confirmed the previously published work that NOD mice exhibit a marked phagocytic defect for AC *in vitro* and extended this by demonstrating that the defect is neither limited to AC nor confined principally to young mice (chapter 3). It was now crucial to determine whether the defect was present *in vivo*.

O'Brien, having originally published data regarding defective clearance of AC by NOD Mφ *in vitro* in 2002 (O'Brien et al., 2002), published further work in 2006 trying to demonstrate an AC clearance defect *in vivo* (O'Brien et al., 2006). They described 2 experimental techniques to address the question. In the first experiment, AC were injected ip and at various time points resident peritoneal PMφ were recovered by peritoneal lavage. These cells were cytospun, stained and examined by light microscopy to assess the percentage phagocytosis and phagocytic index. In the second technique the mice were injected with dexamethasone to induce thymocyte apoptosis. The mice were subsequently sacrificed and the thymi removed. Tissue sections were then stained and examined by light microscopy. Free AC were counted as a measure of the phagocytic capability of resident thymic Mφ.

There are theoretical problems with both these techniques used to examine phagocytosis *in vivo*. It is well documented that injecting thioglycollate or LPS ip results in the rapid disappearance of PMφ from the peritoneal cavity, a phenomenon termed the Mφ Disappearance Reaction (MDR) (Nelson and Boyden, 1963).Simon Watson clearly demonstrated that the ip administration of AC elicited a profound and rapid MDR such that very few PMφ could be obtained by peritoneal lavage 30 mins following AC administration (PhD, University of Edinburgh 2007). Furthermore, he demonstrated that PMφ that had phagocytosed an AC preferentially 'disappeared' by localising to Mφ-rich milky spots of the omentum. Thus, performing a cytospin of the cells that are retrieved from the peritoneum by peritoneal lavage after ip AC administration fails to appreciate the dynamic nature of the peritoneal cavity *in vivo* and examining the low number of retrievable PMφ could be extremely misleading. It has also been documented that thymocytes from NOD mice are resistant to apoptosis induced by dexamethasone *in vitro* (Bergman et al., 2003) although the susceptibility *in vivo* is unknown. The assessment of phagocytic capacity using this model is

difficult to interpret unless the level of apoptosis induced among the thymocytes of NOD and control strains *in vivo* are equal.

Bearing in mind the limitations above, it was decided to use the *in vivo* phagocytosis assay employed by Taylor et al (Taylor et al., 2000) that had been adapted by Simon Watson (PhD, University of Edinburgh 2007). Fluorescently labeled AC were injected ip and phagocytosis was assessed by the relative numbers of free AC recovered by peritoneal lavage at various time points. Unlike Taylor et al, no attempt was made to quantify phagocytosis by examining cytospins of retrieved PMφ.

4.2 RESULTS

4.2.1 Similar numbers of AC are recovered from NOD and C57BL/6 mice, despite increased numbers of resident PMφ present in the peritonea of NOD mice

Having demonstrated that the NOD phagocytic defect for AC *in vitro* was pervasive, male mice aged 8 to 12 weeks were selected with age and sex matched C57BL/6 controls. *In vivo* phagocytosis assays were performed as previously described (chapter 2.5). In brief, 5 million pre-labelled AC (prepared as described in chapter 2.2) were injected ip and mice subsequently sacrificed after 1, 15 or 30 minutes. Free AC and remaining peritoneal cells were recovered by peritoneal lavage. Aliquots of lavage fluid were kept on ice and stained with anti-murine F4/80 antibodies conjugated to APC. Cells recovered were assessed by flow cytometry. The absolute numbers of AC and PMφ were calculated by spiking the sample with a known number of fluorescent beads immediately prior to analysis as described in chapter 2.4. Eight mice of each strain were used for each time point (n = 8). Statistical analysis was by 2-way ANOVA with Bonferroni post tests.

Occasionally a sample was excluded from the analysis either because the injection of AC had not been into the peritoneal cavity, intraperitoneal bleding, loss of the cell pellet during washing or because the FACS plot was uninterpretable (explained in great detail in methods chapter 2.5). Once these samples were excluded there were between 6 and 8 mice per group per time point.

NOD mice had significantly more PMφ recovered by peritoneal lavage than C57BL/6 controls after 1 minute and a trend to more PMφ at both later time points (figure 4.1(A)). However, despite the presence of almost twice as many PMφ initially present to phagocytose and clear AC, strikingly similar numbers of free AC were recovered from the 2 strains of mice at all 3 time points assessed (see figure 4.1(B)).

Since it is highly likely that there was no influx of Mφ into the peritoneal cavity during this period, the implication of these data is that each NOD PMφ cleared AC less efficiently than each C57BL/6 PMφ.

4.2.2 Adjusting clearance of free AC for numbers of resident PMφ unmasks a marked *in vivo* phagocytic defect within NOD mice

The different strains of mice frequently differ in size despite matching for sex and age. There may well be other complexities between the peritonea of the 2 strains that are poorly understood and could not be anticipated that may affect recovery of AC by peritoneal lavage. These differences mean that although similar numbers of AC are injected ip, there is a difference in the numbers of AC recovered from each strain, even at time zero when no phagocytic clearance has taken place. Using the clearance of free AC by each strain at each time point makes some allowance for these complexities. The numbers of free AC cleared by each mouse at each time point are estimated by comparing the numbers of AC recovered at each time point to the mean baseline number of AC recovered from that particular strain.
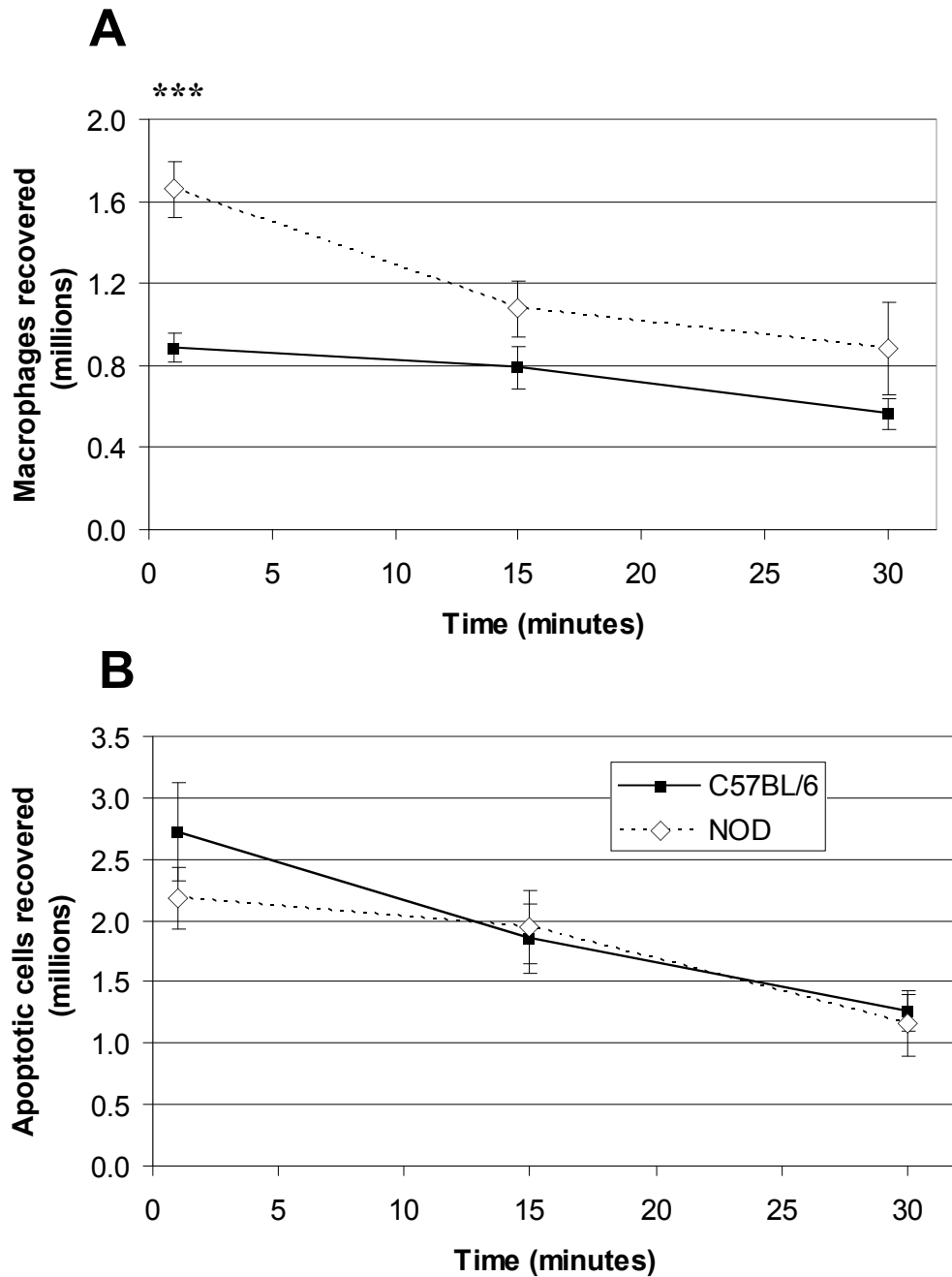
Figure 4- 1   Analysis of free AC and PMφ numbers recovered
5×10^6 AC were injected ip. Mice were sacrificed either immediately post injection of ip cells (1 minute) or after 15 or 30 minutes. Free AC and remaining peritoneal cells were recovered by peritoneal lavage with ice-cold PBS. Aliquots of lavage fluid were immunolabeled for F4/80 and analysed by flow cytometry. Samples were spiked with 50,000 Flowcheck[TM] beads immediately prior to analysis to facilitate counting absolute numbers of free AC and PMφ recovered. (A) NOD mice had significantly higher numbers of resident PMφ at baseline to participate in phagocytic clearance of AC. (B) No differences were observed in the numbers of free AC recovered at any time point; *** $p < 0.001$; NOD vs. C57BL/6; 2-way ANOVA with Bonferonni post tests

There are different ways to adjust the clearance of free AC to compensate for differing numbers of PMφ present in naïve peritonea of NOD and C57BL/6 mice. Assuming there is no influx of Mφ into the peritoneal cavity to contribute to the loss of AC, the simplest method is to adjust the clearance of free AC according to the number of PMφ present in the naïve abdomen at the start of the experiment. Using clearance of free AC as a surrogate marker for phagocytosis, an estimate is thus made of the mean number of AC phagocytosed per PMφ. The mean number of PMφ recovered from that strain at 1 minute was used to estimate numbers of PMφ present in the naïve peritoneal cavity.

One potential source of error present is the assumption that Mφ do not enter the peritoneal cavity (a reasonable assumption since in the time frame of these experiments it would be a monocyte influx and these would be expected to be inefficient phagocytes). An additional source of error is that the arithmetic means of AC and PMφ numbers recovered at 1 minute provide only an estimate of baseline numbers. Nonetheless, accepting these limitations a defect in the clearance of AC starts to emerge with NOD mice exhibiting markedly reduced phagocytosis of AC per PMφ at both 15 minutes and 30 minutes (figure 4.2).

A similar pattern emerged when larger numbers (10×10^6) of AC were injected ip, using 8 female mice aged 6 to 8 weeks old per group (figure 4.3) suggesting that despite the increased numbers of resident PMφ found in NOD mice, the phagocytic defect can not be explained merely by AC availability being a rate limiting factor for phagocytosis by NOD PMφ.
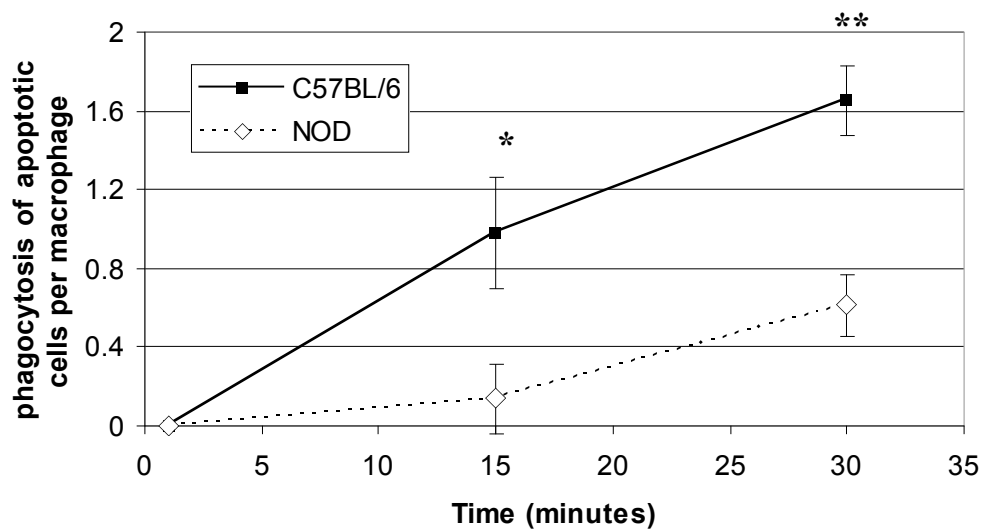
Figure 4- 2   Analysis of AC phagocytosis, adjusted for baseline numbers of PMφ
5×10^6 AC were injected ip. Mice were sacrificed either immediately post injection of ip cells (1 minute) or 15 or 30 minutes later. Free AC and remaining peritoneal cells were recovered by peritoneal lavage with ice-cold PBS. Aliquots of lavage fluid were immunolabeled for F4/80 and analysed by flow cytometry. Samples were spiked with 50,000 Flowcheck^{TM} beads immediately prior to analysis to facilitate counting the absolute numbers of free AC and PMφ recovered. Clearance of AC was calculated for each strain by comparing numbers of free AC recovered from each mouse to mean baseline numbers of recovered AC. The clearance of AC was then adjusted for numbers of resident PMφ present; * $p < 0.05$, ** $p < 0.01$; NOD vs. C57BL/6; 2-way ANOVA with Bonferonni post tests
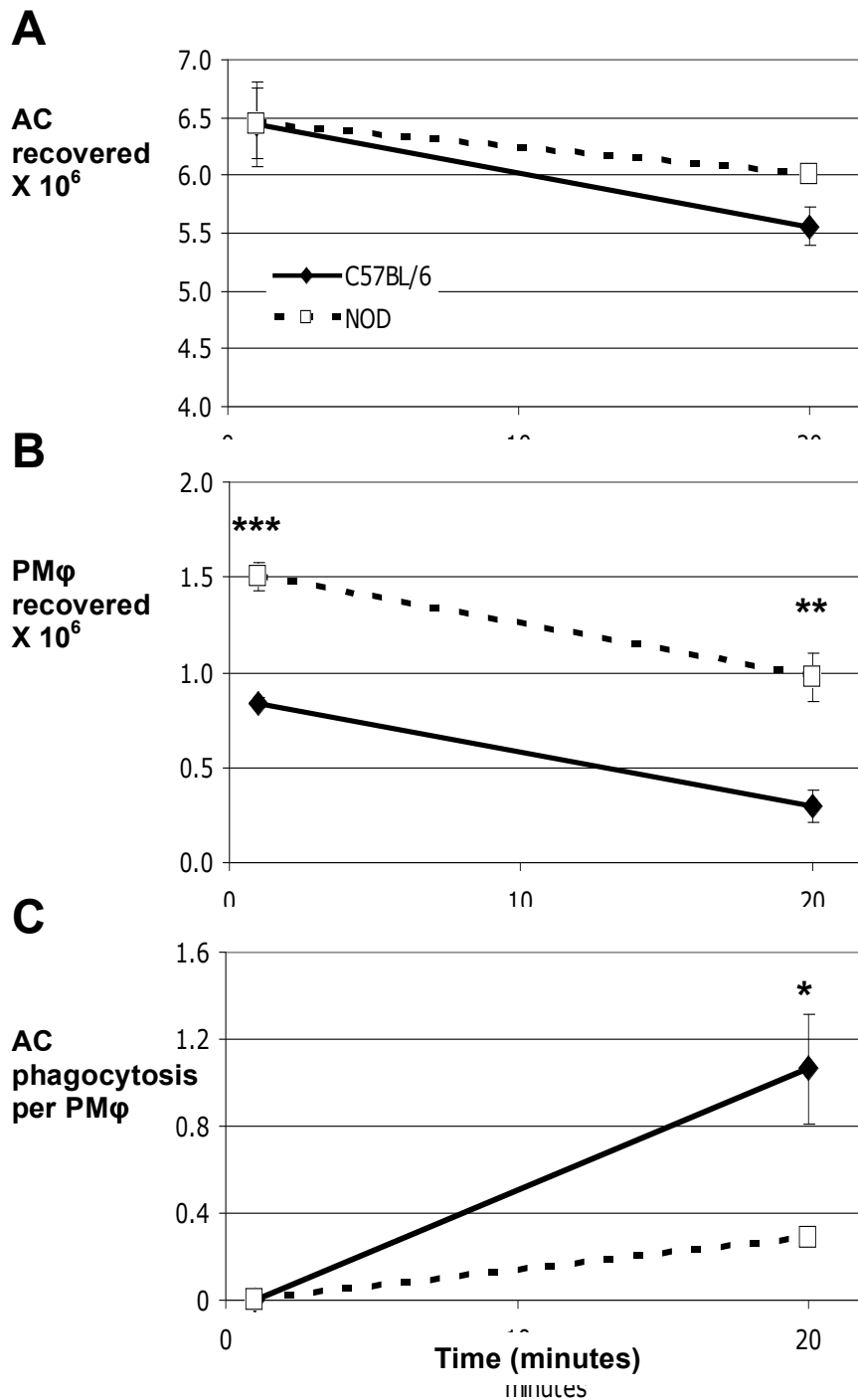
Figure 4- 3 Analysis of *in vivo* phagocytosis following ip administration of 10 x 10^6 AC
10 x 10^6 AC were injected ip. Mice were sacrificed either immediately post injection of ip cells (1 minute) or 20 minutes later; 8 mice per group. Free AC and remaining peritoneal cells were recovered by peritoneal lavage with ice-cold PBS. Aliquots of lavage fluid were immunolabeled for F4/80 and analysed by flow cytometry. Samples were spiked with 50,000 Flowcheck^{TM} beads immediately prior to analysis. (A) No difference was seen in the number of free AC recovered (B) Higher numbers of free PMφ were recovered from NOD mice. (C) Clearance of AC was calculated for each strain by comparing numbers of free AC recovered from each mouse to mean baseline numbers of recovered AC; the clearance of AC was then adjusted for numbers of resident PMφ present; C57BL/6 mice cleared more AC per PMφ. * $p < 0.05$, ** $p < 0.01$, *** $p < 0.001$; NOD vs. C57BL/6; 2-way ANOVA with Bonferonni post tests

4.2.3 Relating the numbers of free AC recovered to the numbers of resident PMφ recovered at each time point

Professor Sherratt (Professor of Mathematics, Heriot-Watt University, Edinburgh) was consulte in the light of the potential sources of error inherent in the above method of analysing the available data as he specialises in mathematical modelling of biological systems. Professor Sherratt's analysis indicated that the clearance of AC by PMφ can be accurately described using a mathematical model:

$$\delta A/\delta t = -k_1 PA / (k_3 + A) \qquad A \qquad \text{AC number}$$

$$\delta P/\delta t = -k_2 PA / (k_3 + A) \qquad P \qquad \text{PMφ number}$$

$$k_{1\text{-}3} \qquad \text{constants}$$

This model assumes that the rates of clearance of AC and the disappearance of PMφ are proportional to the numbers of PMφ and AC present (see figure 4.4). He fitted the data points from the above experiment to these equations using a least squares method to make two separate and interesting predictions (see figure 4.5).

The first prediction concerns rate of clearance of AC. Because in this general form of the model the clearance rate depends on the number of apoptotic cells, he took the clearance rate when $A = 2$ (million) as a specific statistic with which to compare the models. The best-fit parameters gave rates of 0.065 (units: per minute) for the C57BL/6 strain and 0.032 for the NOD strain. These numbers indicate that, when there are 2×10^6 AC present, the average time taken by a PMφ to locate and clear one of these cells is 1 / 0.065 or approximately 15 minutes for the C57BL/6 mice and 1 / 0.032 or approximately 31 minutes for the NOD mice.

The second prediction concerned the parameter k_3. The best-fit value was quite different for the two cases. For the C57BL/6 strain the data implied k_3 was very large (effectively infinite). This would mean that the time needed to find an AC was significantly greater than the time needed to clear it i.e. an increase in the numbers of AC present would result in a further increase in the clearance rate. On the other hand, for the NOD strain the best fit was with $k_3 = 0$. This would indicate that the time needed to locate an AC was insignificant compared to the time needed to clear it i.e. increasing the numbers of AC present would have no impact on the clearance rate.

Therefore, this mathematical analysis and modeling of the experimental data suggested a very different behaviour between the PMφ of the two strains.

4.2.4 NOD mice exhibit reduced *in vivo* phagocytosis of beads

Having clearly identified the phagocytic defect of NOD mice for AC *in vivo*, it was important to examine whether the clearance 3μm latex beads *in vivo* was also impaired in the light of the defective clearance of 3μm latex beads *in vitro* outlined in Chapter 2. The method was very similar to that employed for AC above and described in detail in chapter 2.5. In brief, 10×10^6 fluorescent green, latex beads were injected ip into 8 week old female NOD or age and sex matched C57BL/6 control mice. Mice were sacrificed by cervical dislocation either immediately (n = 4 per group) or 20 minutes later (n = 8 per group). Peritoneal cells and latex beads were recovered by peritoneal lavage, PMφ were immunolabeled for F4/80 and samples analysed by flow cytometry. Aliquots were again spiked with 50,000 Flowcheck^{TM} beads immediately prior to analysis to facilitate counting absolute numbers of beads and PMφ recovered.

Even though, once again NOD mice had higher numbers of resident PMφ (2.9 ± 0.2 vs. 2.0 ± 0.14; NOD vs. C57BL/6; p < 0.01), the C57BL/6 mice were strikingly more efficient at clearing the latex beads (figure 4.6). This confirmed the *in vitro* data suggesting the phagocytic defect of NOD mice is not confined to AC as previously published.
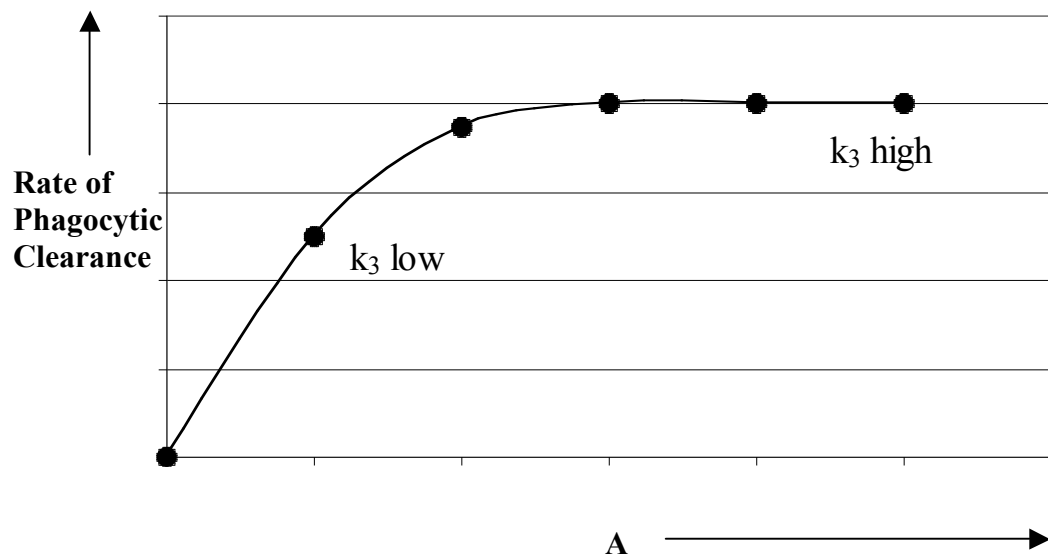
$$\delta A/\delta t = -k_1 PA / (k_3 + A)$$

$$\delta P/\delta t = -k_2 PA / (k_3 + A)$$

Figure 4- 4   Explanation of the meaning behind constant k_3

The model implies that the rate of phagocytic clearance of apoptotic cells is dependent on the availability of apoptotic cells i.e. their numbers present. When the numbers of apoptotic cells increases, the rate of clearance will increase. The size of the constant k_3 indicates where on the above graph the rate of clearance lies for a given number of AC (A).
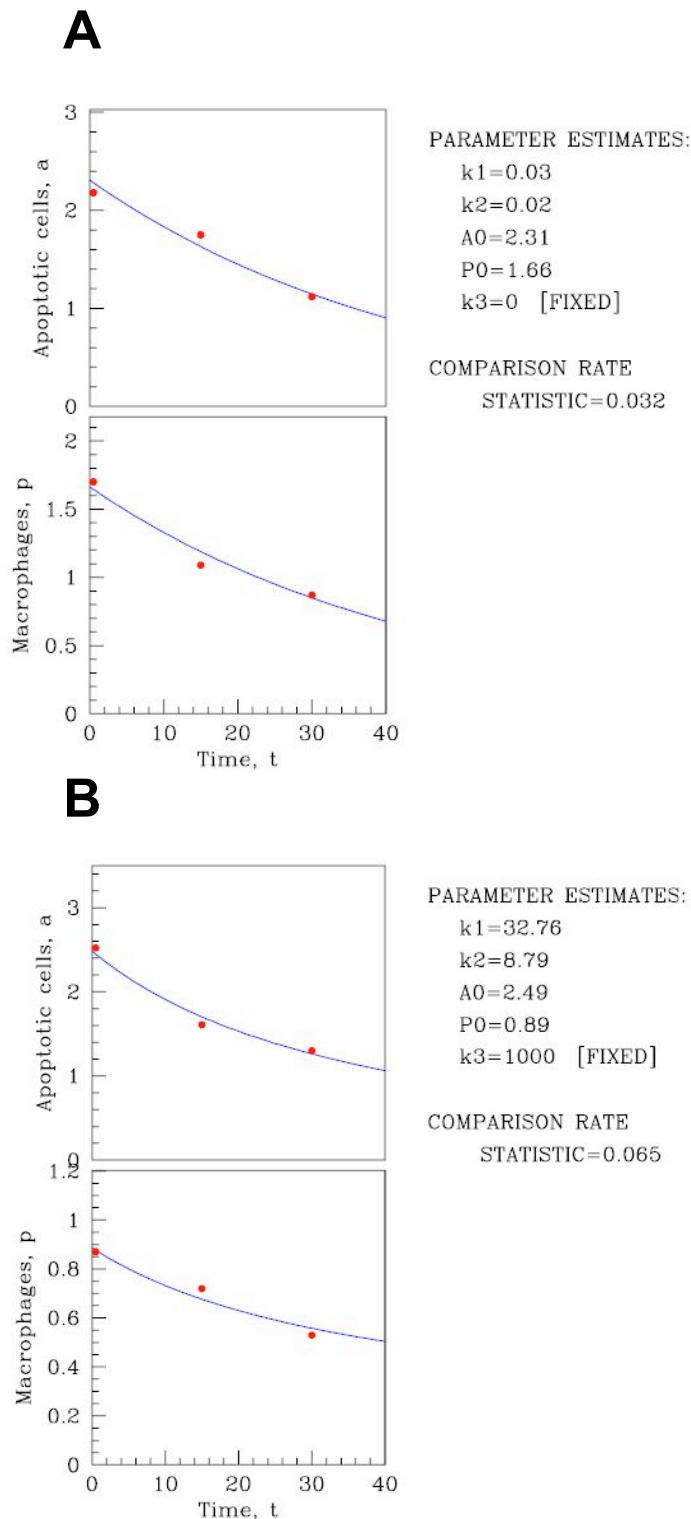
Figure 4- 5   Illustrations of the 'best fit' lines used to analyse experimental data
(A) Best fit parameters for the NOD strain of mice require k_3 to be effectively zero. (B) Best-fit parameters for the C57BL/6 strain of mice require k_3 to be effectively infinite
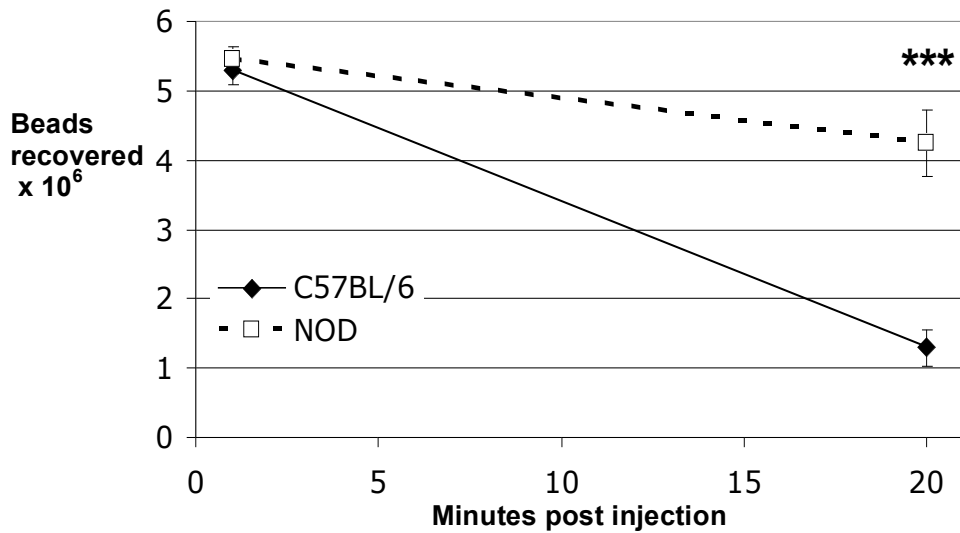
Figure 4- 6   NOD mice exhibit defective clearance of latex beads *in vivo*
10×10^6 fluorescent green 3µm latex beads were injected ip. Mice were sacrificed either immediately post injection of ip cells (n = 4) or 20 minutes later (n = 7). Free latex beads and remaining peritoneal cells were recovered by peritoneal lavage with ice-cold PBS. Aliquots of lavage fluid were immunolabeled for F4/80 and analysed by flow cytometry. Samples were spiked with 50,000 Flowcheck^{TM} beads immediately prior to analysis. After 20 minutes significantly fewer latex beads were recovered from the peritonea of C57BL/6 mice compared to NOD mice. *** $p < 0.001$; NOD vs. C57BL/6; 2-way ANOVA with Bonferonni post tests

4.3 SUMMARY

Resident peritoneal macrophages from NOD mice exhibit a striking defect in the phagocytic clearance of AC compared to C57BL/6 mice in vivo

Results of mathematical modelling imply that NOD resident peritoneal macrophages take twice as long to clear an apoptotic cell in vivo as C57BL/6 controls

The mathematical modelling also implies that the defect lies with the phagocytosis of the apoptotic cell as suspected from the in vitro data and not locating the apoptotic cell

Defective phagocytosis of 3μm latex beads, as well as AC is evident in vivo

Chapter 5. The *in vivo* phagocytic defect of NOD mice localises to idd18 & *Vav3*

5.1 INTRODUCTION

Data presented in chapters 3 and 4 demonstrated a clear defect in the phagocytic clearance of AC and latex beads by Mφ of NOD mice compared to C57BL/6 mice. This defect was clearly present in BMDMφ and resident PMφ *in vitro* and was also evident in PMφ *in vivo*. These experiments, however, did not provide any insights into the underlying cause of the defect. Contrary to the implication of the work done by Simon Levine's group in Boston, USA (Fan et al., 2006) the *in vitro* phagocytic defect was found to be present irrespective of the presence or absence of FBS. Also, in contrast to the work of O'Brien et al (O'Brien et al., 2002) the phagocytic defect was clearly present in pre-diabetic NOD mice of all ages tested. Furthermore, the phagocytic defect was not limited to AC alone and did diminish with age. In addition, mathematical modelling of the data generated from the *in vivo* experiments suggested that the rate at which NOD PMφ could physically engulf and clear an AC was the key rate-limiting step. These data support the hypothesis that the slower phagocytic clearance of NOD Mφ is the result of a defect in one of the many crucial steps that are required for efficient phagocytosis.

It was decided to explore this issue by two distinct approaches. The first approach was to examine the expression of surface receptors previously documented to play an important role in the phagocytic clearance of AC seeking a clear difference between the Mφ from NOD and C57BL/6 mice. This strategy will detect a difference in the level of expression of receptors and will give no indication regarding function. The second approach was to compare the efficiency of *in vivo* phagocytosis in various congenic strains of NOD mice in an attempt to localise the defect to a specific idd locus. Whilst this genetic approach may not identify a single responsible gene, it may narrow it down to a few candidate genes within an idd locus. Furthermore, within the candidate genes suggested by such an approach, a limited number that might play a role in the regulation of phagocytosis. The advantage of this approach is that it gives functional information and, if it can be demonstrated that the phagocytosis defect does localise to an idd locus, gives a strong indication that the defect plays an aetiological role in the development of type 1 diabetes mellitus in NOD mice.

5.2 RESULTS

5.2.1 No consistent differences were identified between NOD and C57BL/6 Mφ in the production of mRNA for several key phagocytic receptors

Real Time PCR makes it possible (as described in chapter 2.6), to assess quantitatively the amounts of mRNA coding for a specific protein present within a given a population of cells. It was decided to use this approach to analyse the production of mRNA for a range of key receptors known to play a role in the phagocytic process, comparing PMφ and BMDMφ from NOD mice to those from C57BL/6 mice. The receptors chosen were the scavenger receptors CD36 and SRA, the integrins CD51 (αV), CD61 (β3) and CD29 (β1), the LPS receptor CD14, the complement protein C1q and thrombospondin (TSP).

RNA was isolated and quantified by Real Time PCR as previously described. In brief, PMφ were harvested by peritoneal lavage from either 6 week old female NOD mice or age and sex matched C57BL/6 controls. Due to the paucity of mRNA available from the PMφ of a single mouse, peritoneal cells from 3 mice were pooled together, plated in 6-well plates for 1 hour and the PMφ purified by adhesion. Nine individual mice from each strain were therefore required to give 3 RNA samples for analysis (n = 3). RNA was extracted from cells using Trizol and frozen at -80°C until further analysis. BMDMφ from the same mice (4 of each strain, n = 4) were matured in Teflon pots for 7 days as previously described (chapter 2.2). 3 x 10^{6} BMDMφ were plated into the wells of a 6-well plate for 1 hour before non-adherent cells were removed by gentle washing with warm media. RNA was again extracted from cells using Trizol and frozen at -80°C until further analysis. A cDNA library was then constructed by Reverse Transcription and the samples assessed by Real Time PCR. Each result was expressed as a fraction of the 18s housekeeping gene mRNA. NOD Mφ and C57BL/6 Mφ were then compared directly and plotted on a logarithmic scale with 95% confidence intervals. Statistical analysis was by student's t test.

Figure 5.1 illustrates the data for BMDMφ whilst figure 5.2 illustrates the data for PMφ. As can be seen, analysis of mRNA from BMDMφ indicated that NOD Mφ underexpressed TSP but overexpressed CD14. In contrast, analysis of mRNA from PMφ indicated no difference in the expression of these 2 proteins but overexpressed CD61. Since the phagocytic defect of NOD mice compared to C57BL/6 mice was

clearly evident in both PMφ and BMDMφ, these inconsistent differences in mRNA are unlikely to be significant.

Rather than continue comparing the production of mRNA for an ever greater number of receptors, it was decided to examine the expression of receptors on the cell surface using flow cytometry. It could be argued that surface expression, rather than expression of mRNA is physiologically more important.
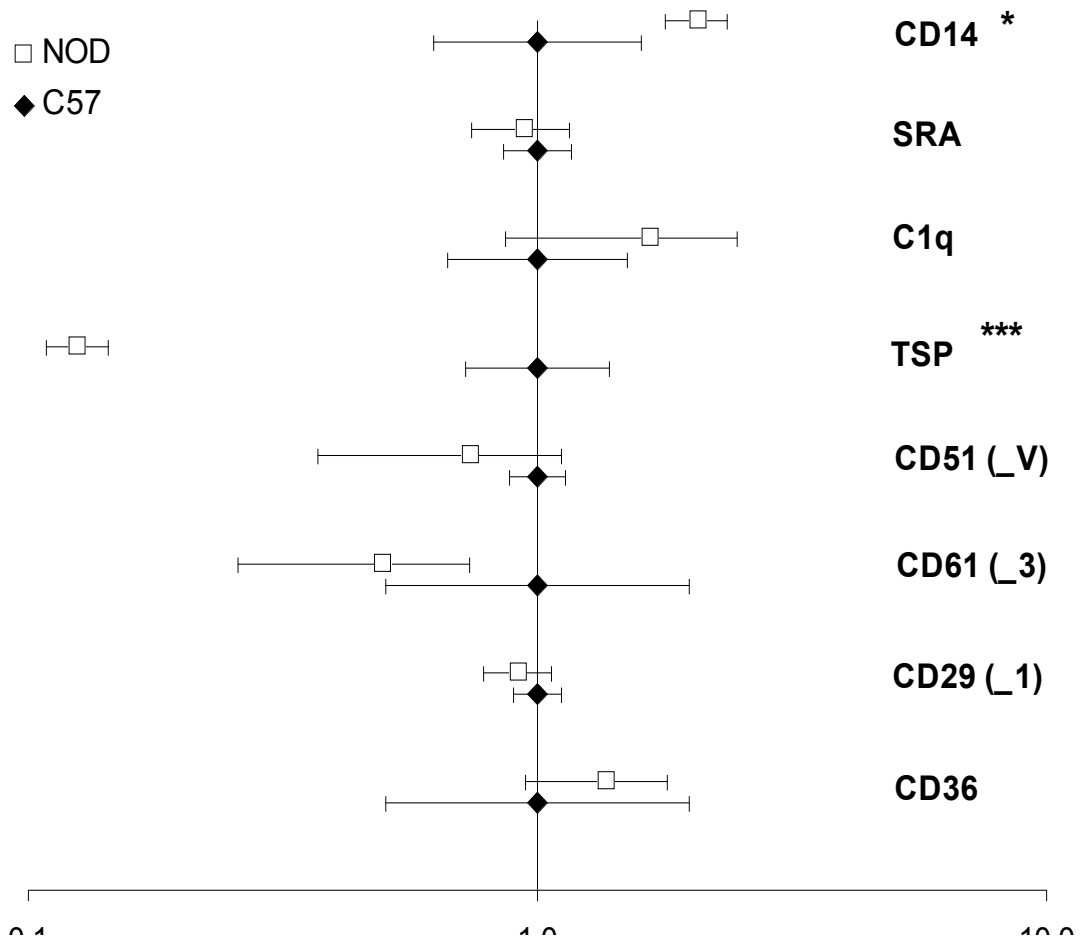
Figure 5- 1   mRNA expression by NOD and C57BL/6 BMDMφ
Femurs were harvested and BMDMφ matured for 7 days in Teflon pots prior to plating into plastic wells. mRNA was extracted and isolated using Trizol and cDNA was obtained by Reverse Transcription. mRNA for specific cell surface receptors was quantified by Real Time PCR relative to the housekeeping gene 18s mRNA. Levels of each receptor found in NOD BMDMφ are expressed relative to C57BL/6 BMDMφ, 95% confidence intervals are shown. * $p < 0.05$, *** $p < 0.001$; NOD vs. C57BL/6; Student's t test.
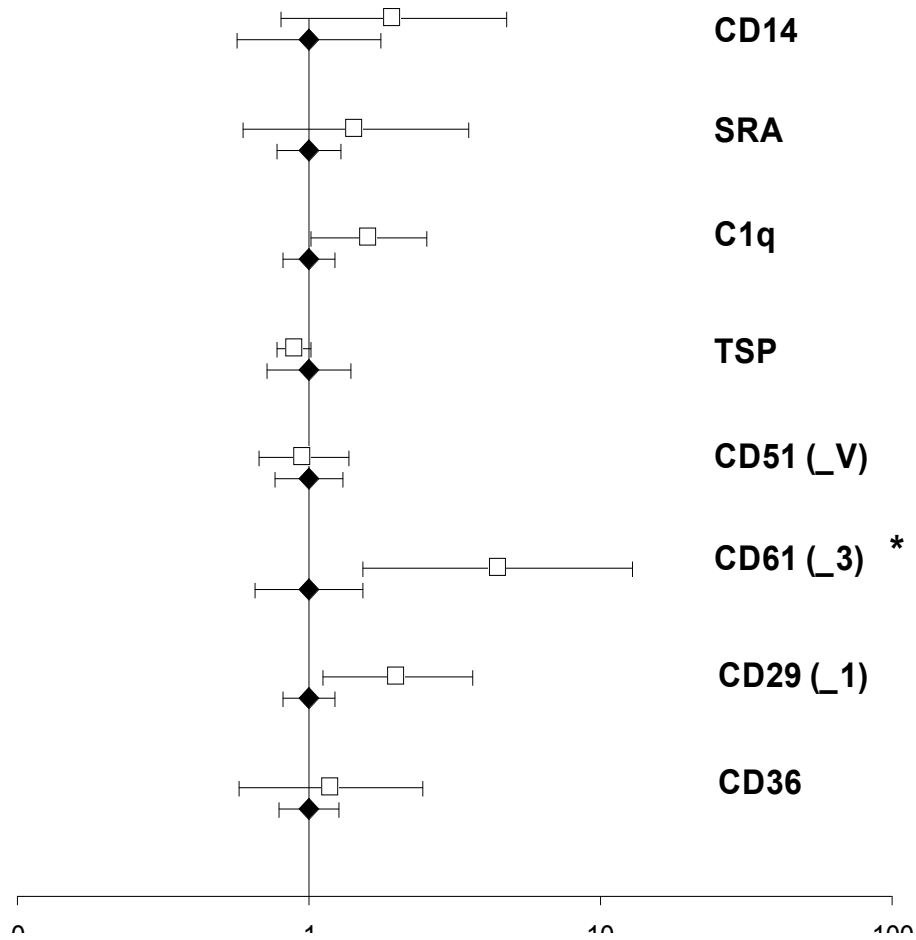
Figure 5- 2   mRNA production by NOD and C57BL/6 PMφ
Peritoneal cells NOD and C57BL/6 mice were harvested by peritoneal lavage with 5ml ice-cold PBS. 9 mice of each strain were used. Lavages from the same strain were pooled together in groups of 3 and cells plated into wells of 6-well plates. PMφ were purified by adhesion and mRNA was extracted and isolated using Trizol. cDNA was obtained by Reverse Transcription. mRNA for specific cell surface receptors was quantified by Real Time PCR relative to the housekeeping gene 18s mRNA. Levels of each receptor found in NOD PMφ are expressed relative to C57BL/6 PMφ, 95% confidence intervals are shown. * p < 0.05; NOD vs. C57BL/6; Student's t test.

5.2.2 No real differences were identified between NOD and C57BL/6 PMφ in the surface expression of several key phagocytic receptors

Antibody availability limited the examination of the surface expression of receptors involved in phagocytosis to 5 key receptors involved in apoptotic cell ingestion: CD14, SRA, CD36, CD51 and CD61. Expression was assessed by flow cytometry as previously described (chapter 2.7). In brief, PMφ were harvested by peritoneal lavage from either 5-week-old female NOD or age and sex matched C57BL/6 control mice. The harvested cells were kept on ice and aliquots from each mouse were immunolabelled for the murine Mφ marker F4/80 and each of the surface receptors in turn. The anti-F4/80 antibody was conjugated to APC to fluoresce in FL-4 whilst the anti-receptor antibodies were chosen to fluoresce in FL-1. Appropriate isotype controls were used. Levels of surface receptor expression were assessed on F4/80 positive cells only to ensure specificity and measured as the geometric mean fluorescence in FL-1 (arbitrary units). Six mice of each strain were used and statistical analysis undertaken using the student's t-test.

Although the expression of CD14 by NOD PMφ appeared significantly reduced compared to that of C57BL/6 PMφ (14.2 ± 0.7 vs. 18.0 ± 0.7; NOD vs. C57BL/6; $p < 0.01$), the FL-1 shifts for PMφ of both strains were small and this may have been secondary to limited efficiency of antibody binding (see figure 5.3). Thus, 2 additional anti-murine CD14 antibodies (clones 4C6 and 61D3, kind gifts of John Hall, CIR, Edinburgh) were assessed. Unfortunately, despite using increasing concentrations of each antibody, these antibodies bound CD14 slightly more efficiently than the original antibody: 4C6 (24.4 ± 0.86 vs. 19.1 ± 0.26; NOD vs. C57BL/6; $p < 0.001$) and 61D3 (25.1 ± 1.0 vs. 21.3 ± 0.5; NOD vs. C57BL/6; $p < 0.01$). Although the data regarding CD14 was consistent it remains tentative. Similar results were obtained with the anti-murine CD36 antibodies used. The shifts in FL-1 achieved for both strains of PMφ were very small and, although the differences between them reached statistical significance, the pathophysiological importance of the finding remains unclear (see figure 5.4). In order for this line of inquiry is to be pursued additional antibodies with increased binding to these receptors will be required.

The surface expression of SRA by NOD PMφ was significantly higher (see figure 5.5) and was almost twice that of the control strain (35.6 ± 4.1 vs. 22.3 ± 0.8; NOD vs. C57BL/6; $p<0.01$). It is unlikely that increased expression of the SRA receptor would lead to diminished phagocytosis and this result may also be a statistically significant finding but not a key biological finding that sheds light upon the underlying mechanism of defective phagocytosis of NOD PMφ.

As expected, both strains of mice expressed high levels of CD61, with NOD PMφ expressing slightly more than controls (79.7 ± 3.04 vs. 62.2 ± 2.89; NOD vs. C57BL/6; $p < 0.01$). Whilst this difference reached statistical significance, it was very small and again most unlikely to result in any altered physiological functions such as phagocytosis (see figure 5.6).

Both NOD and C57BL/6 PMφ expressed reasonably high levels of CD51 (32.2 ± 0.54 vs. 31.0 ± 1.12; NOD vs. C57BL/6; ns), but no differences were evident between the 2 strains (see figure 5.7).

The use of Real Time PCR and flow cytometry to assess mRNA production and surface expression of selected proteins had proved to be unfruitful. This could be because the relevant proteins had not been selected for analysis as study is limited by the availability of PCR probes, monoclonal antibodies and time. It might also reflect the fact that the defect lies in the functionality of a receptor rather than protein production or cell surface expression. Alternatively the defect could lie within the intracellular pathways necessary for efficient phagocytosis and not with cell surface receptors at all.

Microarray technology, searching for relative differences between the strains in the expression of thousands of genes, was considered. However the opportunity arose to try the alternative strategy of using congenic NOD strains. This approach had 3 advantages: (i) if successful it would highlight only a few candidate genes, (ii) it would prove that at least one of the implicated genes was responsible for the phagocytic defect and (iii) it would strongly implicate the defect in the aetiology of diabetes in NOD mice.
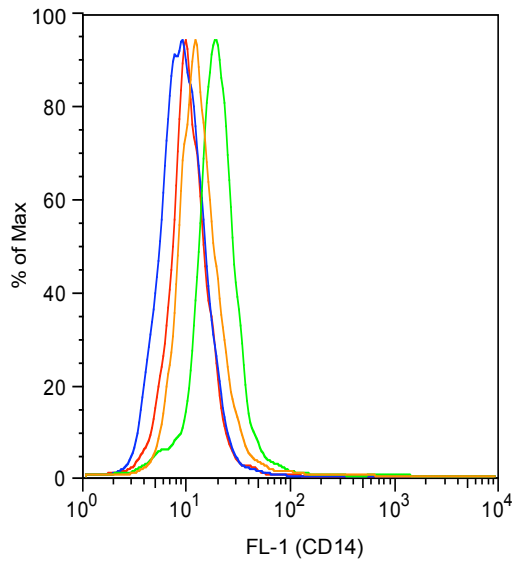
Figure 5- 3   Representative histograms of CD14 expression of PMφ
PMφ were harvested by peritoneal lavage and immunolabelled for F4/80 (conjugated to APC to fluoresce in FL-4) and CD14 or correct isotype antibody (conjugated to fluoresce in FL-1). The fluorescence in FL-1 of the F4/80 positive PMφ was then assessed. Representative plots are shown above: unstained in blue, isotype control in red, C57BL/6 PMφ with monoclonal antibody in green and NOD PMφ with monoclonal antibody in brown.
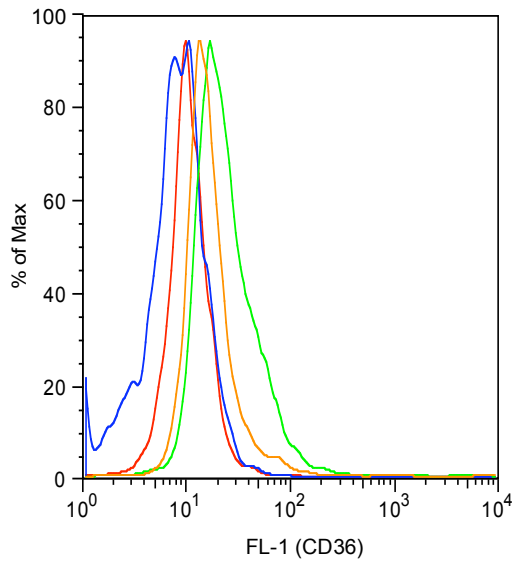
Figure 5- 4   Representative histograms of CD36 expression of PMφ
PMφ were harvested by peritoneal lavage and immunolabelled for F4/80 (conjugated to APC to fluoresce in FL-4) and CD36 or correct isotype antibody (conjugated to fluoresce in FL-1). The fluorescence in FL-1 of the F4/80 positive PMφ was then assessed. A representative plot is shown above: unstained in blue, isotype control in red, C57BL/6 PMφ with monoclonal antibody in green and NOD PMφ with monoclonal antibody in brown.
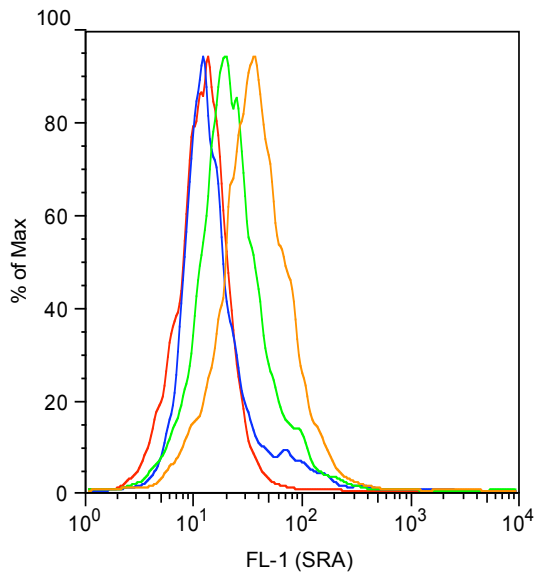
Figure 5- 5   Representative histograms of SRA expression of PMφ
PMφ were harvested by peritoneal lavage and immunolabelled for F4/80 (conjugated to APC to fluoresce in FL-4) and SRA or correct isotype antibody (conjugated to fluoresce in FL-1). The fluorescence in FL-1 of the F4/80 positive PMφ was then assessed. A representative plot is shown above: unstained in blue, isotype control in red, C57BL/6 PMφ with monoclonal antibody in green and NOD PMφ with monoclonal antibody in brown.
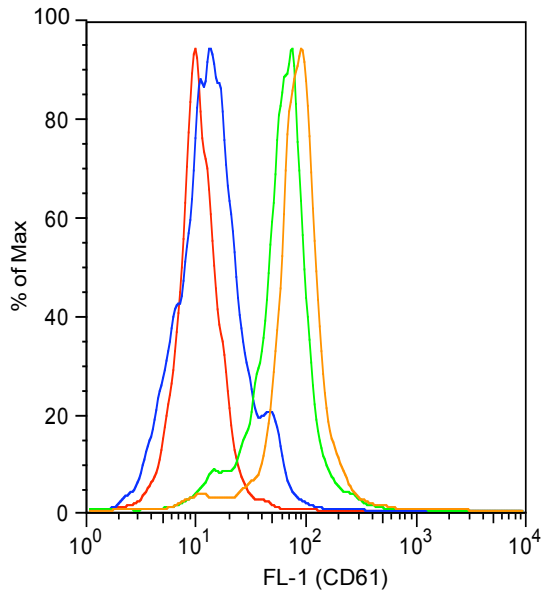
Figure 5- 6   Representative histograms of CD61 expression of by PMφ
PMφ were harvested by peritoneal lavage and immunolabelled for F4/80 (conjugated to APC to fluoresce in FL-4) and CD61 or correct isotype antibody (conjugated to fluoresce in FL-1). The fluorescence in FL-1 of the F4/80 positive PMφ was then assessed. A representative plot is shown above: unstained in blue, isotype control in red, C57BL/6 PMφ with monoclonal antibody in green and NOD PMφ with monoclonal antibody in brown.
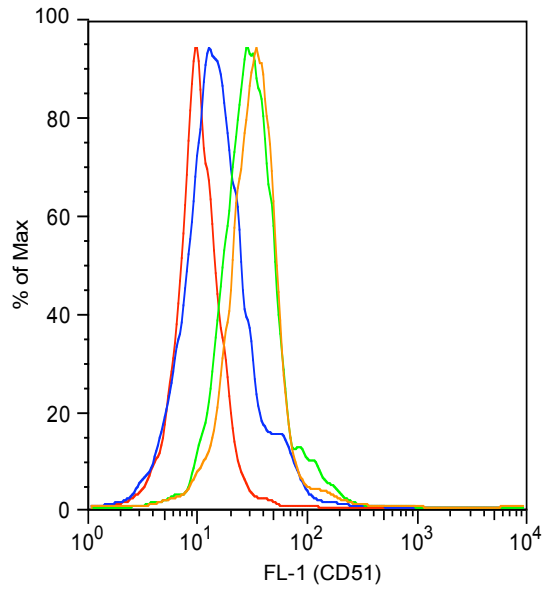
Figure 5- 7   Representative histograms of CD51 expression of PMφ
PMφ were harvested by peritoneal lavage and immunolabelled for F4/80 (conjugated to APC to fluoresce in FL-4) and CD51 or correct isotype (conjugated to fluoresce in FL-1). The fluorescence in FL-1 of the F4/80 positive PMφ was then assessed. A representative plot is shown above: unstained in blue, isotype control in red, C57BL/6 PMφ with monoclonal antibody in green and NOD PMφ with monoclonal antibody in brown.

5.2.3 Using congenic NOD strains, the *in vivo* phagocytic defect is localised first to idd 3/10/18 and subsequently to idd 18

Idd loci within the NOD genome that convey susceptibility to type 1 diabetes mellitus have been identified through linkage studies. NOD congenic strains have been developed with small sections of NOD genome within these idd loci replaced by chromosomal material from other strains of mice, usually C57BL/6 or C57BL/10. The R323 strain has C57BL/6 material on chromosome 3 replacing idd 3/10/18 regions; R20 has C57BL/6 material only replacing idd 3/10; R905 has C57BL/10 genetic material replacing idd 9 on chromosome 4 whilst the 1591 strain has C57BL/6 material replacing idd 3 on chromosome 3 and C57BL/10 material replacing idd 5 on chromosome 1 (see table 5.1).

5.2.3.1 *The phagocytic defect localises to idd 10/18*

In vivo phagocytosis assays were performed as previously described (chapter 2.5) at the University of Cambridge. Seven-week old female NOD mice were used with age and sex matched C57BL/6, R323 and 1591 mice. The number of time points examined was reduced in order to accommodate the simultaneous assessment of 4 strains of mice. In brief, 5 million AC pre-labelled with cell-tracker green were injected ip and mice sacrificed 1 or 30 minutes later. Free AC and peritoneal cells were recovered by peritoneal lavage. Aliquots of lavage fluid were kept on ice and stained with anti-murine F4/80 antibodies conjugated to APC. Cells recovered were assessed by flow cytometry. Absolute numbers of AC and PMφ were calculated by spiking the sample with a known number of fluorescent beads immediately prior to analysis. Four mice of each strain were used for the initial 1 minute time point and 6 mice of each strain for the 30 minute time point. Statistical analysis was by 1 or 2 way ANOVA with Bonferroni post tests as appropriate.

There were similar numbers of PMφ present in the peritoneal cavities of NOD and NOD congenic strains. As expected, fewer PMφ were recovered from C57BL/6 mice than from NOD or either congenic strain assessed (see figure 5.8), although the differences between C57BL/6 and NOD mice did not reach statistical significance. In this experiment the C57BL/6 mice and the R323 congenic strain effectively cleared

all AC from the peritoneal cavity in the allotted time scale. The NOD and 1591 congenic strain failed to clear any AC, (see figure 5.9).

This highlights certain subtle differences between different NOD colonies. The 'Edinburgh' NOD mice were purchased from Charles River, France whilst the 'Cambridge' NOD mice originated from the Taconic sub-strain in the USA. The two colonies were separated approximately 30 years ago. 'Edinburgh' NOD mice had increased numbers of PMφ compared to C57BL/6 mice but cleared comparable numbers of AC such that the phagocytic defect was therefore implicit. In contrast 'Cambridge' NOD mice had statistically comparable levels of PMφ but had an explicit phagocytic defect *in vivo* with fewer AC cleared.

As explained in chapter 2.4, the numbers of AC recovered by peritoneal lavage is affected by factors other than phagocytic clearance alone. For example, the size and complexity of the peritonea being lavaged may vary across different strains of mice. This can be controlled for to some extent by calculating the clearance of AC from peritonea i.e. the numbers of AC recovered at the later time point are compared to mean numbers recovered at baseline for that particular strain. The C57BL/6 and R323 strains cleared significantly more AC than either NOD or 1591 mice with no differences in AC clearance observed between C57BL/6 and R323 mice (figure 5.10).

The replacement of NOD chromosomal material on chromosome 3 across idd regions 3, 10 and 18 in R323 mice completely corrected the phagocytic defect. It is reasonable to hypothesis that any gene(s) responsible for the defect are located within this region. It is also reasonable to infer that since replacing both idd 3 and idd 5 with C57BL/6 and C57BL/10 material respectively (the 1591 congenic strain) did not correct the phagocytic defect, that idd 3 is not involved and that the defect therefore localises to idd 10/18.

Strain	idd Loci	Chromosome	Source of replacement DNA	Defective Apoptotic cell Phagocytosis?
C57BL/6	n/a	n/a	n/a	NO
NOD	n/a	n/a	n/a	YES
R323	3/10/18	3	C57BL/6	NO
R20	3/10	3	C57BL/6	YES
1591	3/5	3 & 1	C57BL/6 & C57BL/10	YES
R905	9	4	C57BL/10	YES

Table 5- 1   **Summary of NOD congenic strains used and the presence or absence of an apoptotic cell phagocytosis defect**
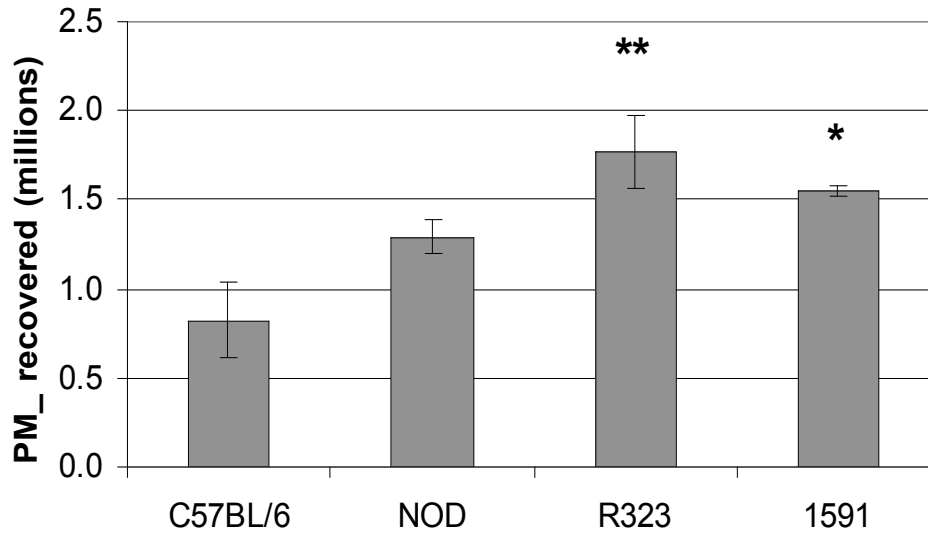
Figure 5- 8 **Analysis of the numbers of resident PMφ recovered**
5 x 10^{6} AC were injected ip into 4 age and sex matched mice of each strain. Mice were sacrificed immediately by cervical dislocation and peritoneal cells recovered peritoneal lavage. Aliquots of lavage fluid were immunolabelled for the murine Mφ marker F4/80 to identify PMφ, spiked with Fowcheck[TM] beads to enable counting of absolute cell numbers and assessed by flow cytometry. C57BL/6 mice have fewer resident peritoneal macrophages than the NOD congenic strains of mice, * $p < 0.05$, ** $p < 0.01$ vs. C57BL/6; 1 way ANOVA. No significant differences were elicited either between NOD and NOD congenic strains, or between NOD and C57BL/6 mice.
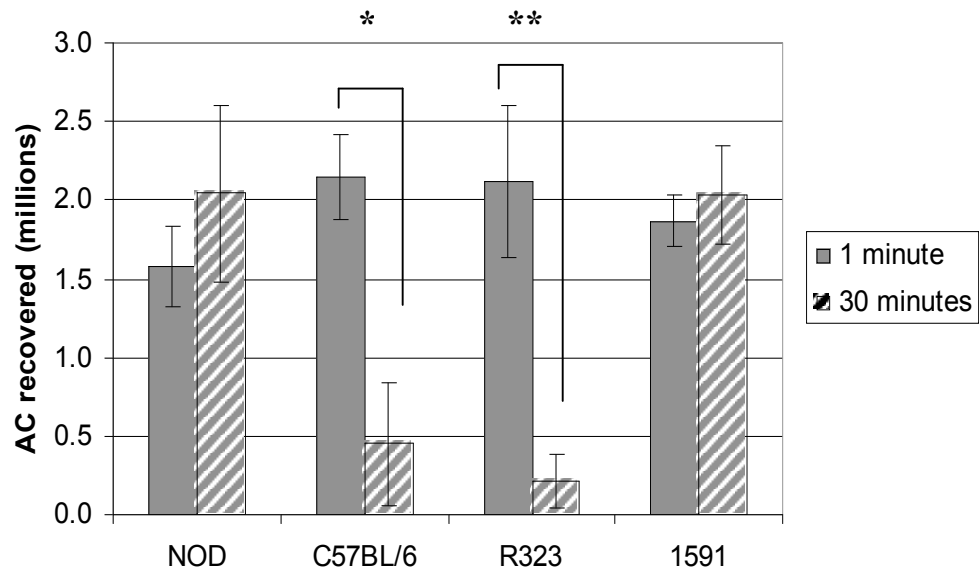
Figure 5- 9   Analysis of AC numbers recovered by different strains of mice
5×10^6 pre-labeled AC were injected ip into age and sex matched mice of each strain. Mice were sacrificed either immediately (n = 4 per group) or 30 minutes later (n = 6 per group) by cervical dislocation. Peritoneal cells were recovered peritoneal lavage. Aliquots of lavage fluid were spiked with Flowcheck[TM] beads to enable counting of AC numbers and assessed by flow cytometry. Significant numbers of AC were cleared by C57BL/6 and R323 mice, in sharp contrast to NOD and 1591 mice. * $p < 0.05$, ** $p < 0.01$; 1 vs. 30 minute dwell times; 2 way ANOVA with Bonferroni post tests.
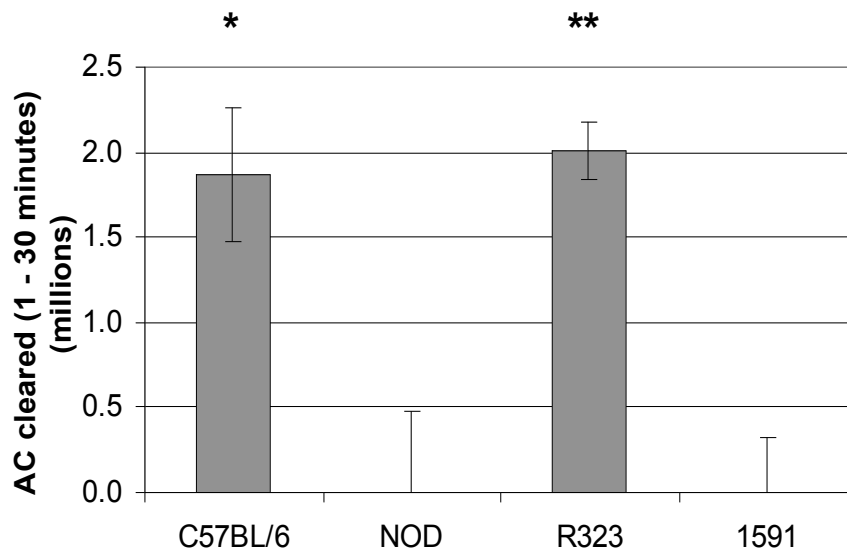
Figure 5- 10   Analysis of AC clearance by different strains of mice
5×10^6 pre-labeled AC were injected ip into age and sex matched mice of each strain. Mice were sacrificed either immediately (n = 4 per group) or 30 minutes later (n = 6 per group) by cervical dislocation. Peritoneal cells were recovered peritoneal lavage. Aliquots of lavage fluid were spiked with Fowcheck^{TM} beads to enable counting of AC numbers and assessed by flow cytometry. AC clearance was calculated by comparing numbers of AC recovered at 30 minutes to baseline numbers recovered for that strain. C57BL/6 and R323 mice cleared significantly more AC than NOD and 1591 mice. * $p < 0.05$, ** $p < 0.01$; vs. NOD or 1591 mice; no significant differences were identified between C57BL/6 and R323 mice; 1 way ANOVA with Bonferroni post tests.

5.2.3.2 *The phagocytic defect localises to idd 18*

A further series of *in vivo* phagocytosis assays was performed using a different panel of congenic mice for comparison: R20 (idd 3/10) and R905 (idd 9) strains. If the R20 congenic did not exhibit a phagocytic defect, then the gene(s) underlying the defective AC clearance would localise to idd 10. Conversely, if the R20 congenic exhibited an AC phagocytic defect then gene(s) would be localise to idd 18. The R905 strain was included as a negative control with C57BL/6 remaining as a positive control for the experiment.

Female NOD mice aged 6 to 7 weeks with age and sex matched controls were selected. Because the C57BL/6 mice had effectively cleared all available AC by 30 minutes in the previous experiment, their clearance rates towards the end of the experiment were limited by AC availability. Rather than inject more AC, a shorter time point of 20 minutes was selected. Four mice were again used at the 1 minute time point and 6 mice were used at the 20 minute time point. Statistical analysis was by 1 or 2 way ANOVA as appropriate with Bonferroni post tests.

On this occasion there were similar numbers of PMφ present in all strains of mice (figure 5.11). Nevertheless, only C57BL/6 mice cleared significant numbers of AC (figure 5.12), clearing significantly more than the NOD and congenic strains; AC clearance was similar between NOD mice and R20 and R905 congenic strains (figure 5.13). Thus, the phagocytic defect was not corrected by replacement of idd 3/10 with C57BL/6 chromosomal material.

From the previous experiment replacing idd 3, 10 and 18 on chromosome 3 with material from C57BL6 mice corrected the defective phagocytosis present in NOD mice to levels comparable to C57BL/6 mice. From this latter experiment, replacement of idd 3 and 10 alone with chromosomal material from C57BL/6 mice did not correct the phagocytic defect. These data suggest that the phagocytic defect localises to idd 18 although this specific experiment has yet to be undertaken: this would require importation of additional congenic mice from USA and was possible through lack of time.
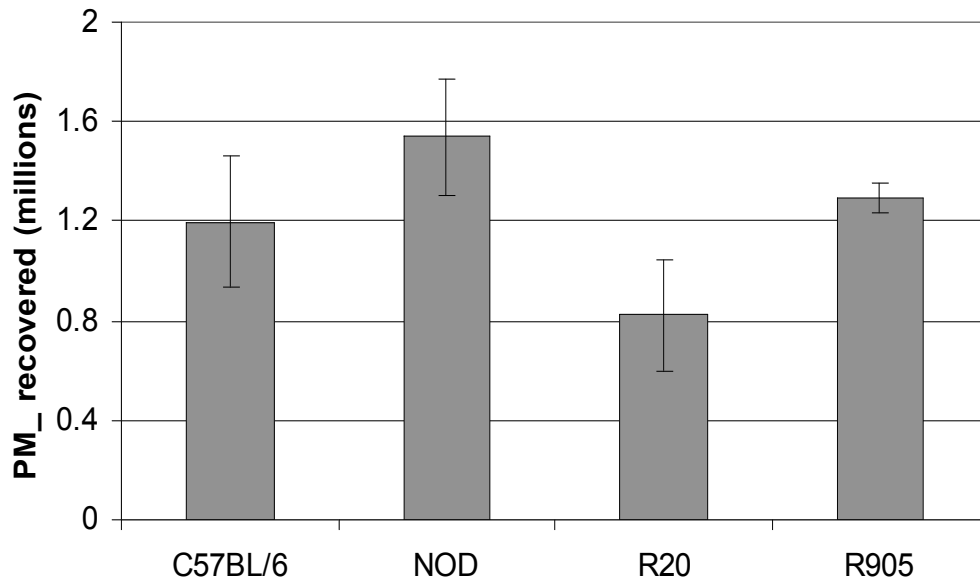
Figure 5- 11   Analysis of resident PMφ numbers recovered
5×10^6 AC were injected ip into 4 age and sex matched mice of each strain. Mice were sacrificed immediately by cervical dislocation and peritoneal cells recovered peritoneal lavage. Aliquots of lavage fluid were immunolabelled for the murine Mφ marker F4/80 to identify PMφ, spiked with Flowcheck[TM] beads to enable counting of absolute cell numbers and assessed by flow cytometry. No significant differences were elicited between any of the strains of mice investigated.
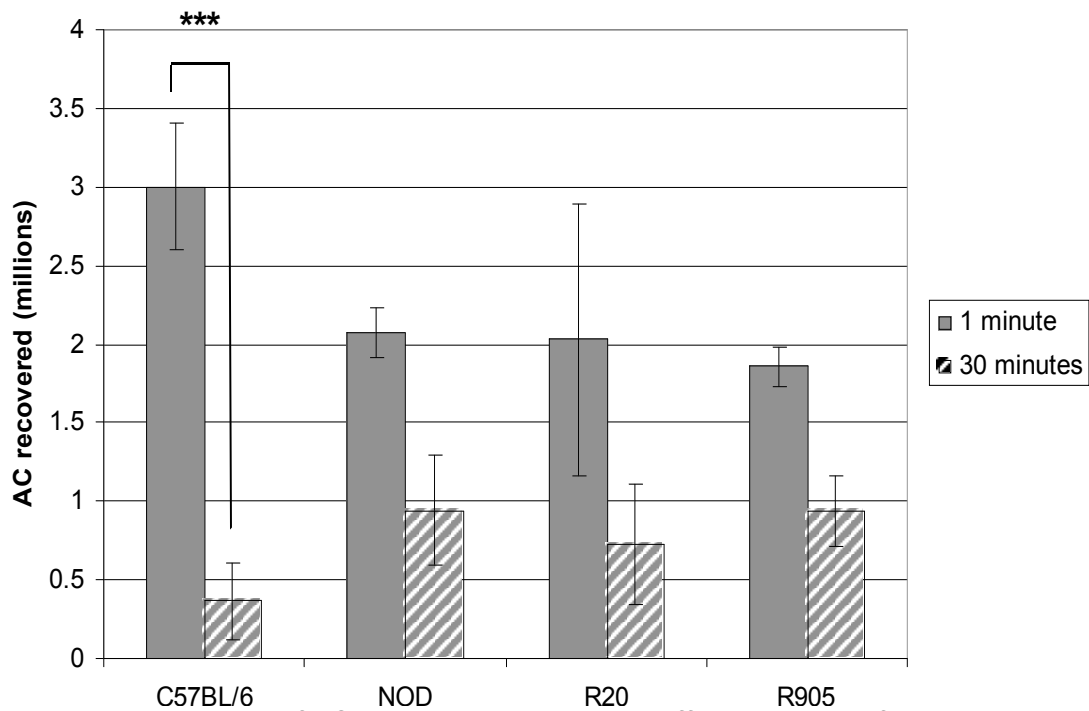
Figure 5- 12   Analysis of AC numbers recovered by different strains of mice

5×10^6 pre-labeled AC were injected ip into age and sex matched mice of each strain. Mice were sacrificed either immediately (n = 4 per group) or 20 minutes later (n = 6 per group) by cervical dislocation. Peritoneal cells were recovered peritoneal lavage. Aliquots of lavage fluid were spiked with Flowcheck[TM] beads to enable counting of AC numbers and assessed by flow cytometry. Significant numbers of AC were cleared by C57BL/6 mice, in contrast to NOD, R20 and R905 mice. *** $p < 0.001$; 1 minute vs. 20 minute dwell times; 2 way ANOVA with Bonferroni post tests.
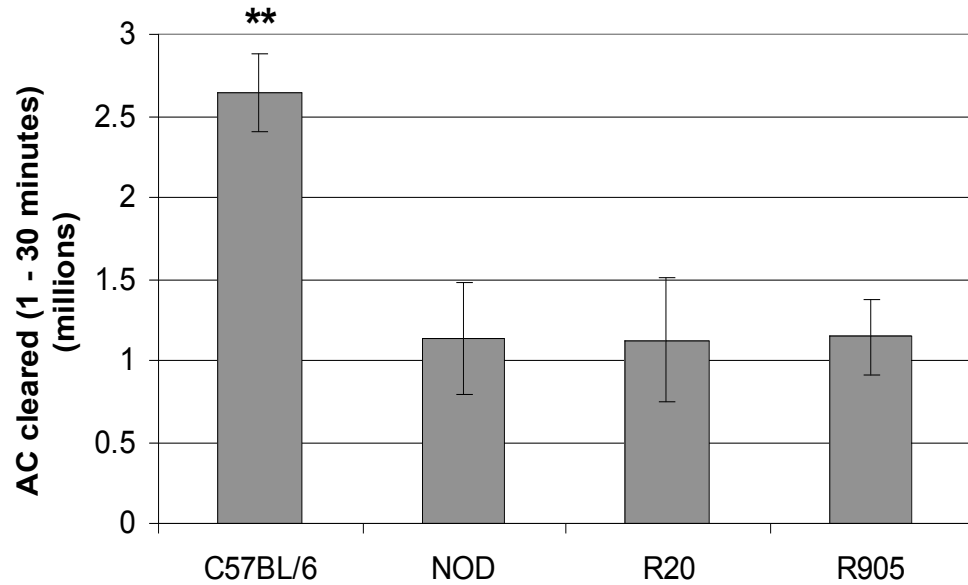
Figure 5- 13   Analysis of AC clearance by different strains of mice
5 x 10^{6} pre-labeled AC were injected ip into age and sex matched mice of each strain. Mice were sacrificed either immediately (n = 4 per group) or 20 minutes later (n = 6 per group) by cervical dislocation. Peritoneal cells were recovered peritoneal lavage. Aliquots of lavage fluid were spiked with Flowcheck[TM] beads to enable counting of AC numbers and assessed by flow cytometry. AC clearance was calculated by comparing numbers of AC recovered at 30 minutes to baseline numbers recovered for that strain. C57BL/6 cleared significantly more AC than NOD, R20 or R905 mice. ** $p < 0.01$; vs. NOD, R20 or R905 mice; 1 way ANOVA with Bonferroni post tests.

5.3 SUMMARY

Real Time PCR analysis of both BMDMφ and PMφ found no consistent difference between NOD and C57BL/6 mice in the mRNA production for CD36, C1q, TSP, CD61, CD51 and CD29. These molecules are unlikely candidates for the mechanism underlying defective AC phagocytosis by NOD Mφ

PMφ of mice possibly express less CD14 and CD36, but the cell surface antibody binding was extremely low for both strains of mice

PMφ of mice possibly express more SRA on their surface as assessed by flow cytometry, but again antibody binding was low for both strains of mice

A key finding is that the NOD congenic strain R323 (idd 3/10/18) cleared AC from the peritoneal cavity with the same efficiency as C57BL/6 mice. The R20 congenic mice (idd 3/10) cleared AC from the peritoneal cavity at a similar rate to NOD mice. These results suggest that the genes underlying the defective peritoneal clearance of AC localise to idd 18 on chromosome 3. Analysis of the known genes within the idd 18 locus yields only one functional gene that importantly has several single nucleotide polymorphisms: *Vav3* (Maier and Wicker, 2005) a GEF that has been shown to be involved in phagocytosis (Hall et al., 2006).

Chapter 6. *In vitro* analysis of the inflammatory phenotype of NOD macrophages

6.1 INTRODUCTION

Having demonstrated a clear phagocytic defect in Mφ from NOD mice *in vitro* and *in vivo*, it was felt important to examine other functions of NOD Mφ. An important function of resident Mφ is to act as sentinel cells that sample the microenvironment and, if required, initiate the inflammatory response by producing pro-inflammatory chemokines and cytokines (Cailhier et al., 2005; Cailhier et al., 2006). Although previous work has compared the responsiveness of NOD Mφ to Mφ from various control strains *in vitro*, there is no clear consensus in the literature.

Jerrold Levine's group from Boston, USA reported that, in the presence of either serum or opsonised AC, TG elicited PMφ from NOD mice produced less pro-inflammatory cytokines (principally IL-1β) than TG elicited PMφ from either DBA or C57BL/6 control mice following stimulation with LPS (Fan et al., 2004). This was consistent with and extended their previous work with SLE prone strains of mice (Koh et al., 2000). It was, however, in stark contrast with 2 previously published papers by different groups that found various Mφ populations from NOD mice to be hyper-responsive to inflammatory stimuli.

Sen et al in North Carolina, USA reported that the NFκB pathway in both BMDMφ and splenic Mφ from NOD mice was hyperactive compared to Mφ from either BALB/c or NOR mice with a consequent increased production of pro-inflammatory cytokines (Sen et al., 2003). This extended their previously published work examining NOD derived DC *in vitro* (Poligone et al., 2002).

Stoffels et al (Stoffels et al., 2004) in Leuven, Belgium reported that resident PMφ from NOD mice produced significantly more pro-inflammatory cytokines (IL-1β and TNFα) in response to necrotic cells or LPS compared to Mφ from either C57BL/6 or NOR mice Also, unlike Mφ from either C57BL/6 or NOR control strains, resident PMφ from NOD mice failed to downregulate cytokine production in the presence of AC. In contrast the pro-inflammatory response of NOD Mφ to IFNγ was diminished compared to control strains. Consistent with these findings they demonstrated hyperactivity of the NFκB signalling pathway and reduced STAT1α activity.

As the literature regarding an important aspect of Mφ function was controversial, it was felt crucial to examine the inflammatory phenotype of different NOD Mφ

populations *in vitro* and *in vivo*. BMDMφ and 2 resident Mφ populations (PMφ and PLMφ) were used in the *in vitro* experiments and TG peritonitis and CG pleurisy were utilised as 2 models of *in vivo* inflammation. These models had been well established within our laboratory and previously shown to be Mφ-dependent (Cailhier et al., 2005; Cailhier et al., 2006). Lastly, the DTH model of pleurisy, a less Mφ-dependent *in vivo* model of inflammation, was used.

C57BL/6 mice were used as the control strain for similar reasons as outlined in previous chapters. They are widely used in the literature as a control strain for NOD mice and both strains are considered to lean more towards a T_h1 inflammatory response. Also, for any work undertaken with NOD congenic strains most of the transgenic material comes from C57BL/6 mice.

6.2 RESULTS: BMDMΦ

6.2.1 BMDMφ derived from NOD and C57BL/6 mice are comparable

Nikolic et al, working in the Netherlands, suggested that when bone marrow precursor cells are matured in the presence of GM-CSF, those from NOD mice preferentially differentiate into Mφ, with defective maturation into DC, compared to those of C57BL origin (Nikolic et al., 2005). Prior to comparing chemokine and cytokine production from NOD and C57BL/6 BMDMφ, it was therefore essential to demonstrate equal levels of maturity between the 2 strains of BMDMφ when used at day 7.

Femurs were harvested from 4 male NOD mice aged 8 weeks together with age and sex matched C57BL/6 controls. BMDMφ were matured in Teflon pots as previously described (chapter 2.2) until day 7. The cells were resuspended by vigorous agitation using a Pasteur pipette, following which 10μl aliquots were removed and cell numbers counted by haemocytometer. Aliquots of containing 2×10^5 cells were then placed in chilled FACS tubes on ice, washed in PBS and triple stained for CD11b conjugated to FITC, F4/80 conjugated to PE and CD11c conjugated to APC (see table 2.6) for full details of monoclonal antibodies used) as previously described. The cells were then analysed by flow cytometry.

No differences were seen in the number of the cells yielded from a single femur of each strain of mice at day 7 ($13 \pm 1.1 \times 10^6$ vs. $12.6 \pm 1.5 \times 10^6$; C57BL/6 vs. NOD; ns). No differences were seen in the proportion of cells that were BMDMφ defined as F4/80^{HI} / CD11b^{HI} cells ($91.5 \pm 4.9\%$ vs. $87.0 \pm 9.5\%$; C57BL/6 vs. NOD; ns). Geometric mean fluorescence in each channel was used as a measure of protein expression. No differences between the strains were seen in CD11b, F4/80 or CD11c expression by the cell populations recovered at day 7 (see figure 6.1).

It was therefore considered reasonable to compare cytokine and chemokine production between day 7 BMDMφ derived from NOD and C57BL/6 mice in response to a variety of stimuli.
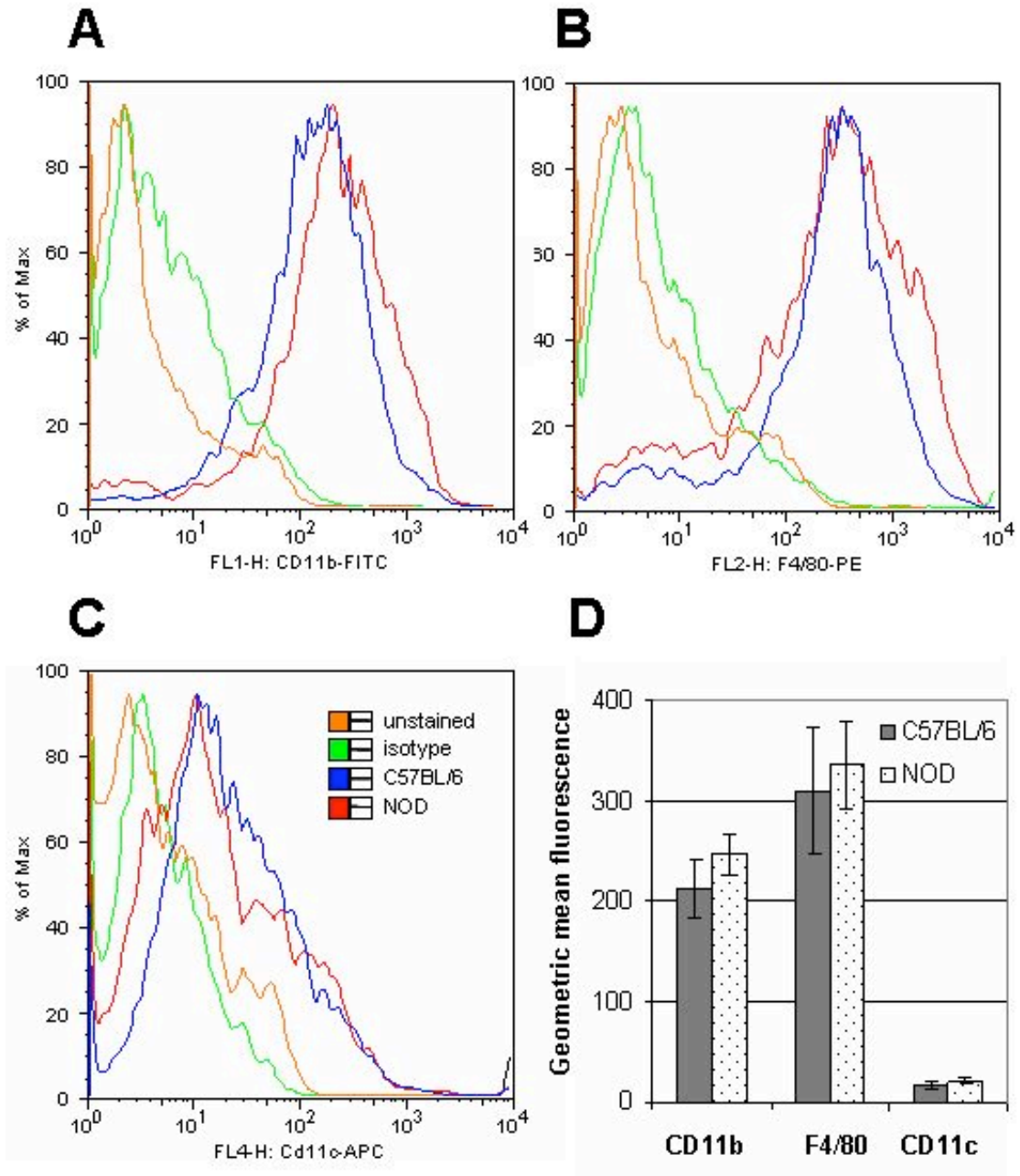
Figure 6- 1 **Mφ derived from the bone marrow of NOD and C57BL/6 mice exhibit comparable surface expression of macrophage markers**
BMDMφ from NOD and C57BL/6 mice were matured for 7days in Teflon pots in the presence of 20% L929 supernatant. Aliquots were removed on day 7, stained for CD11b, F4/80 and CD11c and examined by flow cytometry. Whilst the majority of cells from both strains expressed high levels of CD11b (**A**) and F4/80 (**B**), few cells expressed significant levels of CD11c (**C**). No differences were seen between the strains in the expression of each protein as assessed by the geometric mean fluorescence (**D**).

6.2.2 NOD BMDMφ exhibit a marked hyper-inflammatory response

12 male NOD mice aged 8 to 12 weeks, together with 15 age and sex matched C57BL/6 controls were sacrificed by rising levels of CO_2. Resident pleural and peritoneal cells were harvested by lavage, pooled according to strain and kept on ice pending further analysis (chapters 6.3 and 6.4). A femur was harvested from the first 6 mice of each group and BMDMφ were matured in Teflon pots for 7 days as previously described using media supplemented with 10% FBS and 20% L929 supernatant (chapter 2.2). Mature BMDMφ were pooled according to strain and 0.5 x 10^6 cells were plated into the wells of 12-well plates. Non-adherent cells were removed after 1 hour by gentle washing and the remaining cells were incubated in 0.5ml of either standard media (quiescent control) or media containing either 1μg/ml LPS, 0.25% CG or 0.5% TG.

Cells were inspected visually by light microscopy (x 400 magnification) and the supernatants from each well were aspirated after 1, 4 or 24 hours. Supernatants were centrifuged and stored at -80^oC prior to analysis of cytokine and chemokine levels. 4 wells were used for each condition. The concentrations of MIP-2 and KC were measured by ELISA whilst MCP-1, TNFα, IL-6, IFNγ and IL-10 levels were measured by CBA as described in chapter 2.8

Following the aspiration of supernatants, all remaining cells were lysed using 0.5ml lysis buffer and the protein concentration was measured for each well and used as a surrogate for cell number. Cytokine and chemokine levels recorded in each well were then adjusted, to take into account the protein content of the well. Mean protein levels extracted from the wells were not significantly different across the 2 strains (613 ± 12μg/ml vs. 580 ± 13μg/ml; NOD vs. C57BL/6; p = ns).

6.2.2.1 *Quiescent BMDMφ produce negligible levels of chemokines or cytokines*

BMDMφ incubated in standard Mφ media, without stimulation, produced very low levels of all chemokines and cytokines measured. Although, as expected levels increased with time in culture and differences were observed in the levels of KC detected between the strains. It should be noted, however, that the production of all chemokines and cytokines examined (including KC) remained negligible compared to stimulated Mφ (data from the 24 hour time point is displayed in table 6.1, data

from other time points is not shown). This confirmed the non-stimulatory quiescent nature of the media used throughout the experiment.

6.2.2.2 *Neither NOD nor C57BL/6 BMDMφ produce IFNγ*

Since Mφ are not thought to produce IFNγ, this was a useful negative control, and indeed no significant production of IFNγ was detected at any time point (see table 6.2) irrespective of the stimulus used.

6.2.2.3 *BMDMφ from NOD mice are hyper-inflammatory in response to LPS*

No differences in the production of any chemokine or cytokine measured were apparent at the 1 hour time point (see table 6.3). At the 4 hour time point NOD BMDMφ produced significantly more KC and MIP-2 (both CC chemokines) and MCP-1 (CXC chemokine) compared to control Mφ. However, the production of MIP-2 was comparable between the 2 strains at the 24 hour time point with production by C57BL/6 BMDMφ apparently having 'caught up' (see figure 6.2).

Similarly, by 4 hours BMDMφ from NOD mice produced considerably increased levels of the pro-inflammatory cytokines TNFα and IL-6 compared to the C57BL/6 controls as well as less of the anti-inflammatory cytokine IL-10. These differences were either maintained or increased at the 24 hour time point (see figure 6.3).

This pattern is entirely consistent with NOD BMDMφ exhibiting an exaggerated pro-inflammatory phenotype compared with C57BL/6 controls, in keeping with the published work of Sen et al ((Sen et al., 2003).

	NOD BMDMφ		C57BL/6 BMDMφ	
	pg/ml	(sem)	pg/ml	(sem)
MIP-2	667.6	(66.7)	542.9	(82.3)
KC	1,064[***]	(108.3)	342.7	(66.5)
MCP-1	65.6	(9.9)	50.9	(12.4)
TNFα	0.0	(0.0)	8.0	(9.8)
IL-6	12.7	(4.5)	11.0	(4.4)
IFN γ	1.0	(1.2)	0.0	(0.0)
IL-10	3.8	(2.3)	3.0	(3.7)

Table 6- 1   Chemokine and cytokine production by quiescent non-activated BMDMφ after 24 hours

BMDMφ from NOD mice and C57BL/6 control mice were matured for 7 days in Teflon pots with media supplemented with 20% L929 medium. 0.5×10^6 BMDMφ were seeded into 12-well plastic plates, gently washed and incubated in 0.5ml quiescent media for 24 hours. Supernatants were harvested and the remaining cells washed with PBS, lysed and the protein content of each well measured. Levels of chemokines and cytokines measured in the supernatants of individual wells were adjusted for the protein contents extracted from each well. Data shown are the mean levels of 4 wells. Trivial levels of all chemokines and cytokines were detected in the supernatants. *** $p < 0.001$, NOD vs. C57BL/6 by 2-way ANOVA across the whole time course. No other differences were significant.

Time	NOD BMDMφ		C57BL/6 BMDMφ	
(hours)	pg/ml	(sem)	pg/ml	(sem)
LPS STIMULATION				
1	0.0	(0.0)	0.7	(0.8)
4	2.4	(1.7)	3.9	(2.9)
24	1.0	(1.2)	0.0	(0.0)
CG STIMULATION				
1	1.5	(1.0)	1.6	(1.0)
4	10.7	(7.1)	5.2	(6.0)
24	5.2	(6.0)	19.1	(7.4)
TG STIMULATION				
1	0.0	(0.0)	0.5	(0.0)
4	9.5	(0.0)	6.1	(0.7)
24	0.0	(7.0)	10.9	(7.0)

Table 6- 2   Negligible interferon γ production by BMDMφ stimulated with either LPS, CG or TG
BMDMφ from NOD mice and C57BL/6 control mice were matured for 7 days in Teflon pots with media supplemented with 20% L929 medium. 0.5×10^6 BMDMφ were seeded into 12-well plastic plates, gently washed and incubated in 0.5ml media containing either 1µg/ml LPS, 0.25% CG or 0.5% TG for 1, 4 or 24 hours. Supernatants were harvested and the remaining cells washed with PBS, lysed and the protein content of each well measured. Levels of interferon-γ measured in the supernatants were adjusted for the protein content of each well. Data shown are the mean levels of 4 wells. No significant differences identified between NOD and C57BL/6 mice by 2-way ANOVA.

	NOD BMDMφ		C57BL/6 BMDMφ	
	pg/ml	(sem)	pg/ml	(sem)
LPS STIMULATION at 1 hour				
MIP-2	1325.8	(54.4)	859.4	(53.0)
KC	2320.5	(83.9)	738.8	(31.8)
MCP-1	510.5	(117.7)	280.2	(67.1)
TNFα	642.4	(37.3)	372.9	(40.7)
IL-6	60.4	(24.3)	66.3	(28.4)
IL-10	110.7	(80.2)	83.0	(23.4)
CG STIMULATION at 1 hour				
MIP-2	193.1	(28.3)	132.3	(29.2)
KC	127.7	(27.5)	19.1	(11.1)
MCP-1	55.3	(12.2)	20.3	(16.7)
TNFα	7.0	(8.5)	12.5	(9.2)
IL-6	5.6	(3.5)	7.8	(7.0)
IL-10	13.5	(8.3)	16.7	(20.5)
TG STIMULATION at 1 hour				
MIP-2	60.5	(4.1)	94.8	(41.1)
KC	0.0	(1.8)	0.0	(15.6)
MCP-1	27.1	(9.9)	15.3	(9.6)
TNFα	0.0	(0.0)	0.0	(0.0)
IL-6	6.7	(1.1)	4.5	(1.4)
IL-10	6.1	(6.2)	0.7	(0.9)

Table 6- 3   Chemokine and cytokine production by stimulated BMDMφ after 1 hour
BMDMφ from NOD mice and C57BL/6 control mice were matured for 7 days in Teflon pots with media supplemented with 20% L929 medium. 0.5×10^6 cells were seeded into 24-well plastic plates, gently washed and incubated in 0.5ml media containing either 1μg/ml LPS, 0.25% CG or 0.5% TG for 1 hour. Supernatants were harvested and the remaining cells washed with PBS, lysed and the protein content of each well measured. Levels of chemokine and cytokine measured in the supernatants were adjusted for the protein content of each well. Data shown are the mean levels of 4 wells. No significant differences identified between NOD and C57BL/6 mice by 2-way ANOVA.
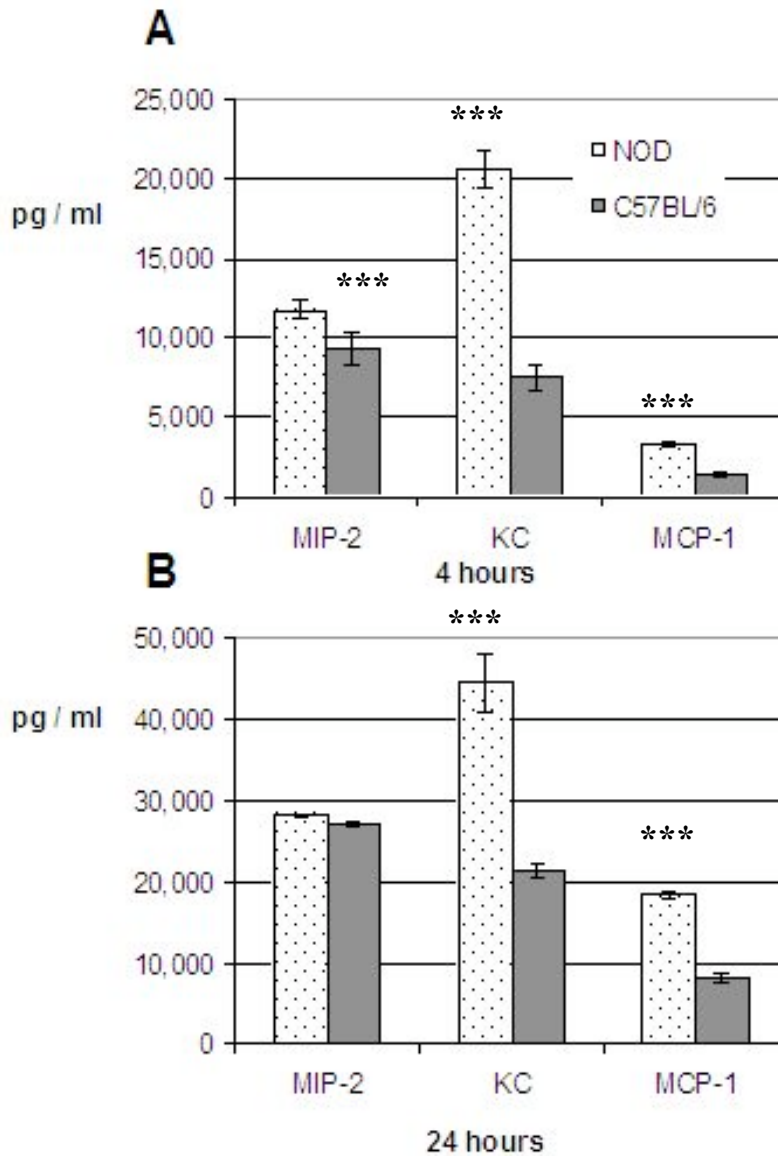
Figure 6- 2   Chemokine levels produced by BMDMφ stimulated with LPS

BMDMφ from NOD mice and C57BL/6 control mice were matured for 7 days in Teflon pots with media supplemented with 20% L929 medium. 0.5×10^6 cells were seeded into 12-well plastic plates, gently washed and incubated in 0.5ml media containing 1µg/ml LPS. Supernatants were harvested and the remaining cells washed with PBS, lysed and the protein content of each well measured. Levels of chemokines measured in the supernatants were adjusted for the protein content of each well. Data shown are the mean levels of 4 wells. Histograms show the normalised levels; NOD in polka dots, C57BL/6 in solid bars. (A) Chemokines at 4 hours. (B) Chemokines at 24 hours. *** $p < 0.001$; NOD vs. C57BL/6; 2-way ANOVA across each time course.

Figure 6- 3   Cytokine levels produced by BMDMφ stimulated with LPS
BMDMφ from NOD mice and C57BL/6 control mice were matured for 7 days in Teflon pots with media supplemented with 20% L929 medium. 0.5×10^6 cells were seeded into 12-well plastic plates, gently washed and incubated in 0.5ml media containing 1µg/ml LPS. Supernatants were harvested and the remaining cells washed with PBS, lysed and the protein content of each well measured. Levels of cytookines measured in the supernatants were adjusted for the protein content of each well. Data shown are the mean levels of 4 wells. Histograms show the normalised levels; NOD in polka dots, C57BL/6 in solid bars. (A) Cytokines at 4 hours. (B) Cytokines at 24 hours. *** $p < 0.001$, * $p < 0.05$; NOD vs. C57BL/6; 2-way ANOVA across each time course.

6.2.2.4 *BMDMφ from NOD mice are hyper-inflammatory in response to Carrageenan*

Once again no significant production of IFNγ was detected at any time point (see table 6.2), and no differences in chemokine or cytokine production were apparent by 1 hour (see table 6.3). However, at the 4 and 24 hour time points, the broad pattern of hyper-inflammatory increased chemokine and cytokine production by NOD BMDMφ compared to CB57BL/6 BMDMφ in response to CG was similar or even more exaggerated to that exhibited in response to LPS (see figures 6.4 and 6.5).

6.2.2.5 *BMDMφ from NOD mice secrete higher levels of MIP-2, KC and TNFα in response to Thioglycollate*

The overall levels of stimulation achieved with 0.5% TG appeared significantly less than that obtained with 1μg/ml LPS or 0.25% CG as the levels of all cytokines and chemokines measured were significantly lower. Nevertheless although no differences in chemokine or cytokine production were apparent at 1 hour (see table 6.2), the differences increased with time and by 24 hours a broadly similar pattern emerged. NOD derived BMDMφ produced higher levels of MIP-2, KC and TNFα than CB57BL/6 BMDMφ although similar (but very low) levels of MCP-1, IL-6 and IL-10 were noted (see figures 6.6 and 6.7).
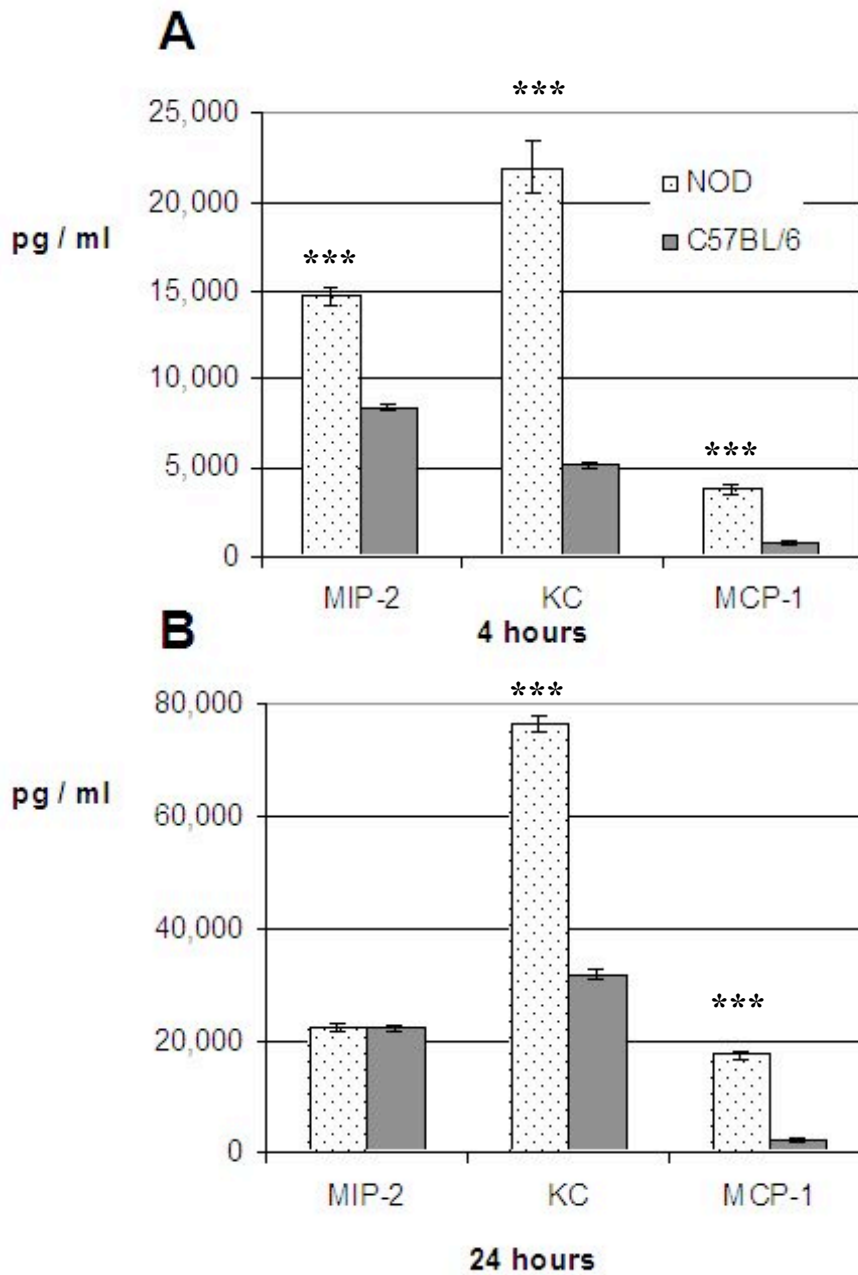
Figure 6- 4   Chemokine levels produced by BMDMφ stimulated with CG
BMDMφ from NOD mice and C57BL/6 control mice were matured for 7 days in Teflon pots with media supplemented with 20% L929 medium. 0.5 x 10^6 cells were seeded into 12-well plastic plates, gently washed and incubated in 0.5ml media containing 0.25% CG. Supernatants were harvested and the remaining cells washed with PBS, lysed and the protein content of each well measured. Levels of chemokines measured in the supernatants were adjusted for the protein content of each well. Data shown are the mean levels of 4 wells. Histograms show the normalised levels; NOD in polka dots, C57BL/6 in solid bars. (A) Chemokines at 4 hours. (B) Chemokines at 24 hours. *** $p < 0.001$; NOD vs. C57BL/6; 2-way ANOVA across each time course.

Figure 6- 5   Cytokine levels produced by BMDMφ stimulated with CG
BMDMφ from NOD mice and C57BL/6 control mice were matured for 7 days in Teflon pots with media supplemented with 20% L929 medium. 0.5×10^6 cells were seeded into 12-well plastic plates, gently washed and incubated in 0.5ml media containing 0.25% CG. Supernatants were harvested and the remaining cells washed with PBS, lysed and the protein content of each well measured. Levels of cytokines measured in the supernatants were adjusted for the protein content of each well. Data shown are the mean levels of 4 wells. Histograms show the normalised levels; NOD in polka dots, C57BL/6 in solid bars. (A) Cytokines at 4 hours. (B) Cytokines at 24 hours. *** $p < 0.001$, ** $p < 0.01$; NOD vs. C57BL/6; 2-way ANOVA across each time course.
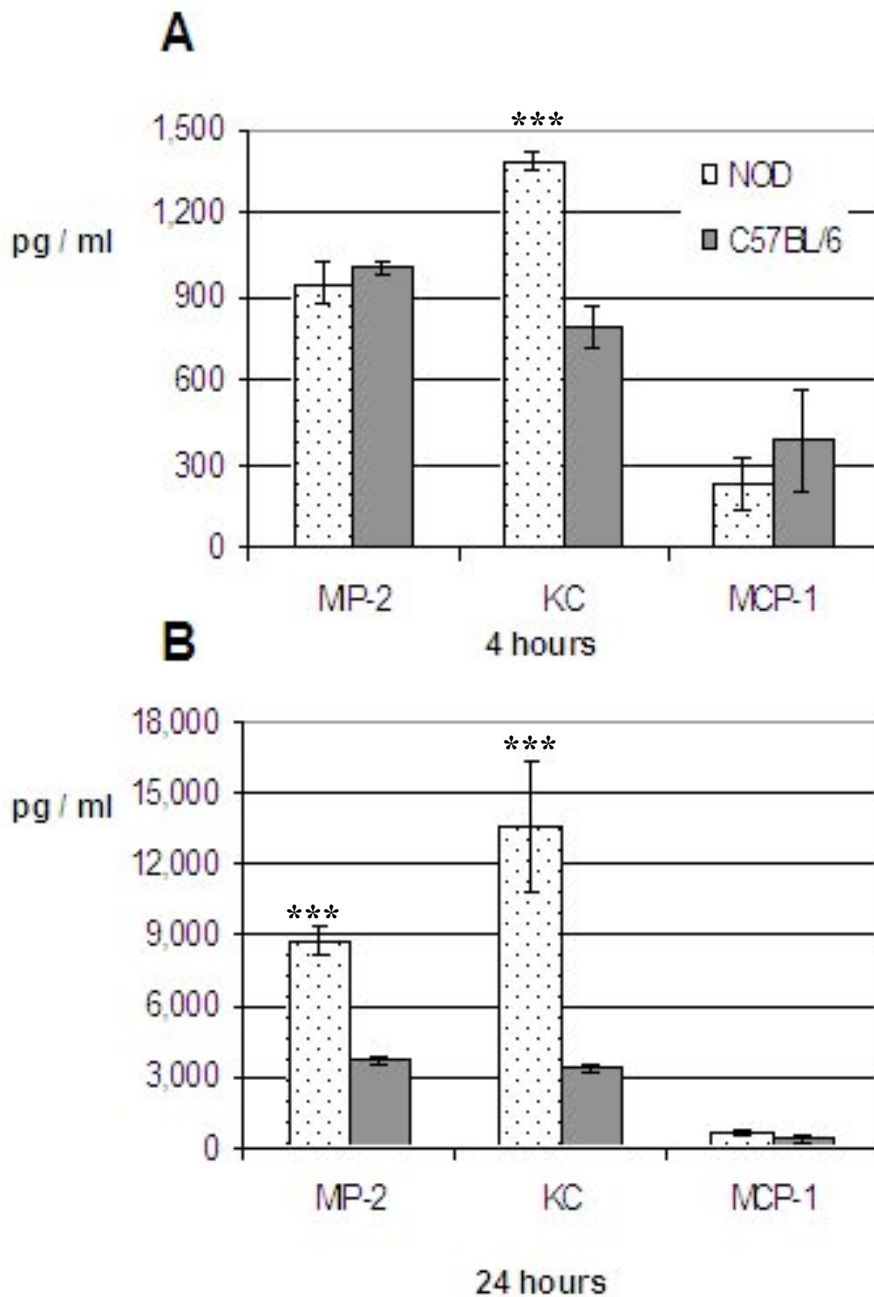
Figure 6- 6   Chemokine levels produced by BMDMφ stimulated with TG
BMDMφ from NOD mice and C57BL/6 control mice were matured for 7 days in Teflon pots with media supplemented with 20% L929 medium. 0.5×10^6 cells were seeded into 12-well plastic plate, gently washed and incubated in 0.5ml media containing 0.5% TG. Supernatants were harvested and the remaining cells washed with PBS, lysed and the protein content of each well measured. Levels of chemokines measured in the supernatants were adjusted for the protein content of each well. Data shown are the mean levels of 4 wells. Histograms show the normalised levels; NOD in polka dots, C57BL/6 in solid bars. (A) Chemokines at 4 hours. (B) Chemokines at 24 hours. *** $p < 0.001$; NOD vs. C57BL/6; 2-way ANOVA across each time course.
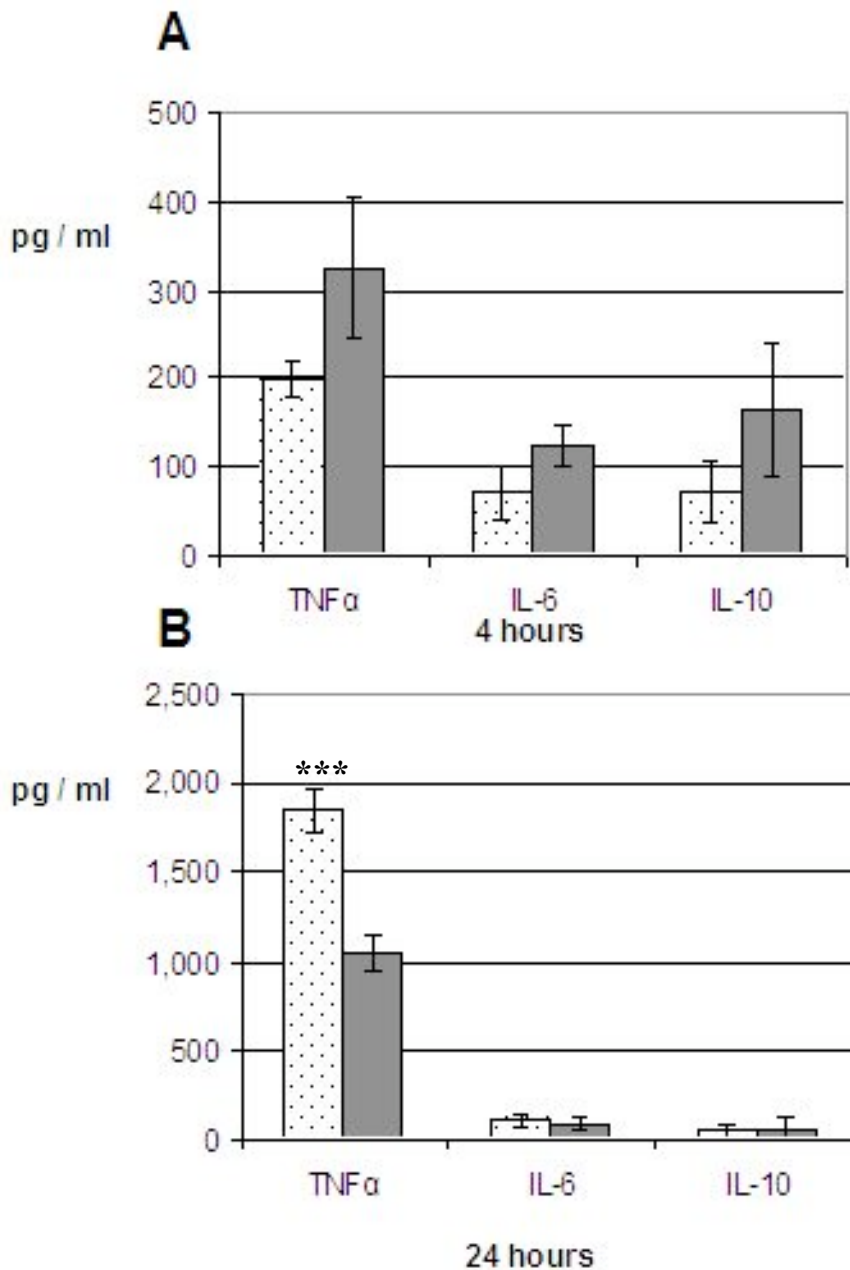
Figure 6- 7   Cytokine levels produced by BMDMφ stimulated with TG
BMDMφ from NOD mice and C57BL/6 control mice were matured for 7 days in Teflon pots with media supplemented with 20% L929 medium. 0.5 x 10^6 cells were seeded into 12-well plastic plates, gently washed and incubated in 0.5ml media containing 0.5% TG. Supernatants were harvested and the remaining cells washed with PBS, lysed and the protein content of each well measured. Levels of cytokines measured in the supernatants were adjusted for the protein content of each well. Data shown are the mean levels of 4 wells. Histograms show the normalised levels; NOD in polka dots, C57BL/6 in solid bars. (A) Cytokines at 4 hours. (B) Cytokines at 24 hours. *** $p < 0.001$; NOD vs. C57BL/6; 2-way ANOVA across each time course.

6.3 RESULTS: RESIDENT PLEURAL MACROPHAGES

6.3.1 NOD PLMφ are strikingly hypo-responsive compared to C57BL/6 PLMφ

Resident pleural cells were obtained by pleural lavage from the same mice as those sacrificed for the BMDMφ used above (chapter 6.2.2) i.e. 12 male NOD mice aged 8 to 12 weeks and 15 ag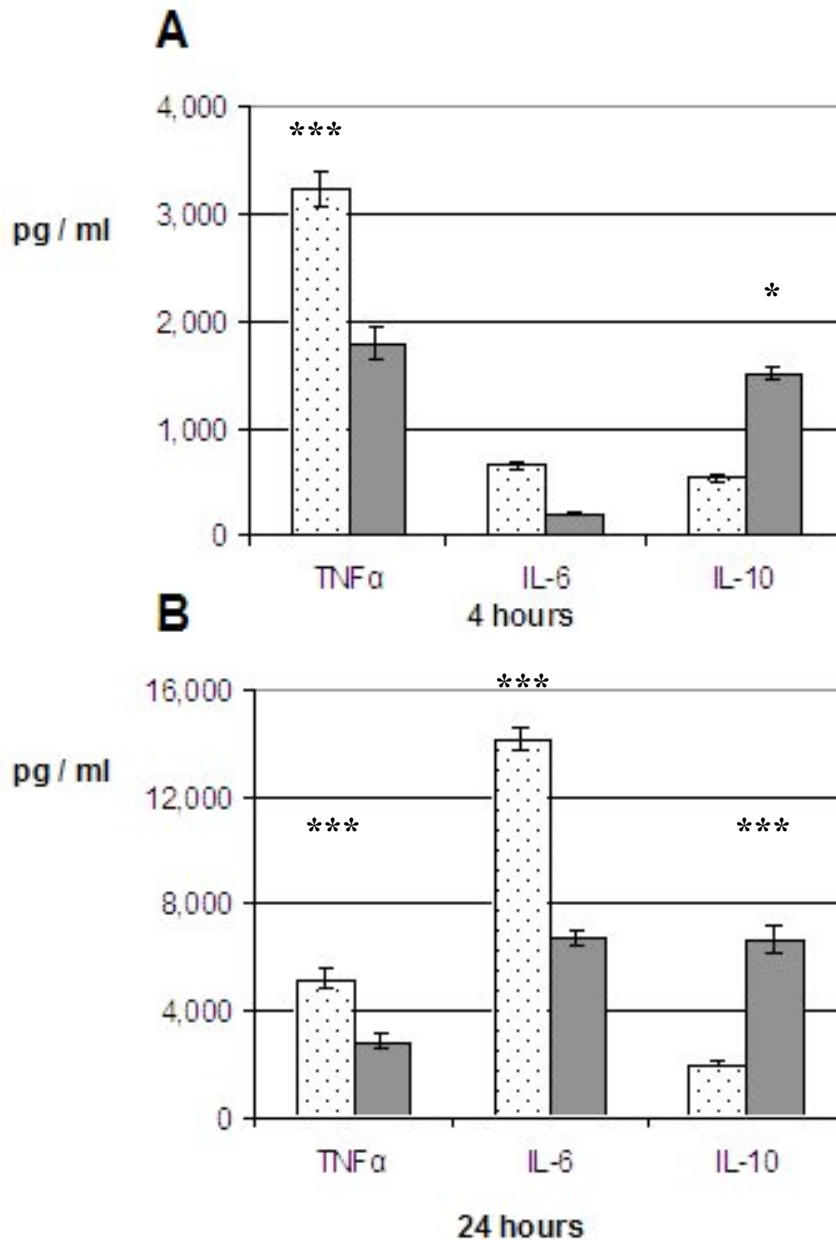e and sex matched C57BL/6 controls. 0.25×10^6 cells were plated into plastic wells of 12-well plates and non-adherent cells removed after 1 hour by gentle washing with warm media. The remaining PLMφ were incubated in 0.5ml of either standard media (quiescent non-stimulatory) or media containing 1μg/ml LPS or 0.25% CG. As above, cells were inspected visually by light microscopy (x 400). Supernatants from each well aspirated at 1, 4 or 24 hours and analysed in an identical fashion to those above. The cells were lysed and the protein content of each well analysed as before. Individual cytokine and chemokine levels recorded in each well were again adjusted for the protein to compensate for differences in cell numbers across conditions and time points. Protein levels were significantly higher in the wells seeded with resident pleural cells from NOD mice compared to C57BL/6 controls (214 ± 18μg/ml vs. 135 ± 5.8μg/ml; NOD vs. C57BL/6; $p < 0.001$ student's t test). For this experiment, leukocyte numbers were counted by haemocytometer and a set number of leukocytes (0.25×10^6) plated into each well. Although this might reflect increased cell loss amongst the C57BL/6 PLMφ, an alternative explanation is more likely. In a series of pleural lavages from male mice, aged 8 to 12 weeks (6 per group), analysed by flow cytometry (chapter 7.3), NOD mice had a much higher proportion of PLMφ among their resident pleural cells (74.5 ± 4.1% vs. 53.5 ± 2.0%; NOD vs. C57BL/6; $p < 0.001$ student's t test). This is sufficient to explain the difference in protein levels and reinforces the importance of adjusting recorded levels of cytokines and chemokines for either the adherent cell number or a surrogate marker such as protein levels.

6.3.1.1 *Quiescent PLMφ produce low levels of chemokines and cytokines*

As previously, the levels of all chemokines and cytokines produced by PLMφ incubated in quiescent non-inflammatory Mφ media increased over time. The levels produced were, however, extremely low compared to the stimulated groups, once

again confirming the non-inflammatory nature of both cells and the quiescent Mφ media (see table 6.4).

6.3.1.2 *PLMφ from NOD mice are hypo-responsive to both LPS and CG*

Once again, no significant production of IFNγ was detected at any time point regardless of stimulation (table 6.5).

Although no differences in the production of any chemokine or cytokine measured were apparent at the 1 hour time point (see table 6.6), striking differences emerged between NOD and C57BL/6 PLMφ by the 4 hour time point. In response to LPS, PLMφ harvested from NOD mice produced significantly less of all chemokines and cytokines than the C57BL/6 controls (see figures 6.8 and 6.9 respectively), although the difference in MCP-1 levels in response to LPS (figure 6.8 (B)) did not reach statistical significance at the 4 hour time point by 2-way ANOVA with Bonferroni post hoc tests due to the variance at later time points within the time course. Similarly, in response to CG, PLMφ harvested from NOD mice produced significantly less of the chemokines and cytokines measured than the C57BL/6 controls (see figures 6.10 and 6.11 respectively). There were no obvious differences in the state of the cells on inspection by light microscopy between the 2 strains of mice used to explain this dramatic difference with the PLMφ from each strain being uniform in size and appearance. This pattern, in stark contrast to that seen with BMDMφ above, is thought to reflect the hypo-responsive nature of NOD derived resident Mφ populations compared to C57BL/6 derived controls.

Although levels of MCP-1 and KC produced by PLMφ continued to accumulate up to the 24 hour time point, as seen with the BMDMφ preparations above, levels of MIP-2, TNFα, IL-10 and IL-6 appeared to fall dramatically (see table 6.7). Since no supernatant (and therefore no chemokine or cytokine) was removed from the wells it is thought this may reflect degradation of chemokines and cytokines by enzymes specifically produced by the resident cells *ex vivo* and not BMDMφ *in vitro*.

	NOD PLMφ		C57BL/6 PLMφ	
	pg/ml	(sem)	pg/ml	(sem)
MIP-2	4,249***	(723)	6,755	(873)
KC	3,528	(504)	2,665	(482)
MCP-1	58.9	(38.1)	45.9	(65.0)
TNFα	12.4	(7.7)	26.4	(3.2)
IL-6	769.4	(415.4)	439.8	(75.6)
IFN γ	1.2	(1.5)	2.9	(2.0)
IL-10	29.6	(20.1)	72.3	(59.0)

Table 6- 4   Chemokine and cytokine levels produced by quiescent PLMφ after 24 hours

Pleural cells from NOD mice and C57BL/6 control mice were harvested by pleural lavage. 0.25×10^6 cells were seeded into 12-well plastic plates and the PLMφ purified by adhesion and incubated in 0.5ml media for 24 hours. Supernatants were harvested and the remaining cells washed with PBS, lysed and the protein content of each well measured. Levels of chemokines and cytokines measured in the supernatants were adjusted for the protein content of each well. Extremely low levels of all chemokines and cytokines measured were detected. Data shown are the mean levels of 4 wells, *** $p < 0.001$, NOD PLMφ vs. C57BL/6 PLMφ by 2-way ANOVA across the whole time course. All other differences were not significant.

Time	NOD PLMφ		C57BL/6 PLMφ	
(hours)	pg/ml	(sem)	pg/ml	(sem)
	LPS STIMULATION			
1	0.9	(0.7)	1.3	(0.5)
4	0.9	(0.4)	0.0	(0.0)
24	0.0	(0.0)	0.0	(0.0)
	CG STIMULATION			
1	1.8	(0.7)	1.9	(0.3)
4	0.6	(0.5)	6.5	(1.6)
24	0.7	(0.5)	1.8	(2.0)

Table 6- 5   Negligible amount of interferon γ levels are produced by PLMφ
Pleural cells from NOD mice and C57BL/6 control mice were harvested by pleural lavage. 0.25×10^6 cells were seeded into 12-well plastic plates and the PLMφ purified by adhesion and incubated in 0.5ml Mφ media containing either 1µg/ml LPS, or 0.25% CG for 1, 4 or 24 hours. Supernatants were harvested and the remaining cells washed with PBS, lysed and the protein content of each well measured. Levels of interferon-γ measured in each supernatant were adjusted for the protein content of each well. Data shown are the mean levels of 4 wells, no significant differences identified between PLMφ from NOD mice and C57BL/6 mice, 2 way ANOVA.

	NOD PLMφ		C57BL/6 PLMφ	
	pg/ml	(sem)	pg/ml	(sem)
LPS STIMULATION at 1 hour				
MIP-2	58.3	(7.4)	374.9	(57.5)
KC	90.4	(7.5)	841.3	(92.6)
MCP-1	0.0	(0.0)	22.8	(26.4)
TNFα	2.2	(1.6)	35.1	(3.7)
IL-6	15.0	(0.6)	107.3	(13.7)
IL-10	3.9	(4.5)	18.5	(9.3)
CG STIMULATION at 1 hour				
MIP-2	70.5	(7.7)	55.2	(4.9)
KC	99.3	(6.6)	87.8	(20.3)
MCP-1	0.0	(0.0)	0.0	(0.0)
TNFα	5.5	(2.4)	7.5	(1.4)
IL-6	23.1	(2.2)	14.8	(1.4)
IL-10	23.1	(7.9)	26.6	(6.3)

Table 6- 6   Chemokine and cytokine production by PLMφ after 1 hour of stimulation
Pleural cells from NOD mice and C57BL/6 control mice were harvested by pleural lavage. 0.25 x 106 cells were seeded into 12-well plastic plates and the PLMφ purified by adhesion and incubated in 0.5ml Mφ media containing either 1µg/ml LPS or 0.25% CG for 1 hour. Supernatants were harvested and the remaining cells washed with PBS, lysed and the protein content of each well measured. Levels of chemokines and cytokines measured in the supernatants were adjusted for the protein content of each well. Data shown are the mean levels of 4 wells, no significant differences identified between PLMφ from NOD mice and C57BL/6 mice, 2-way ANOVA.
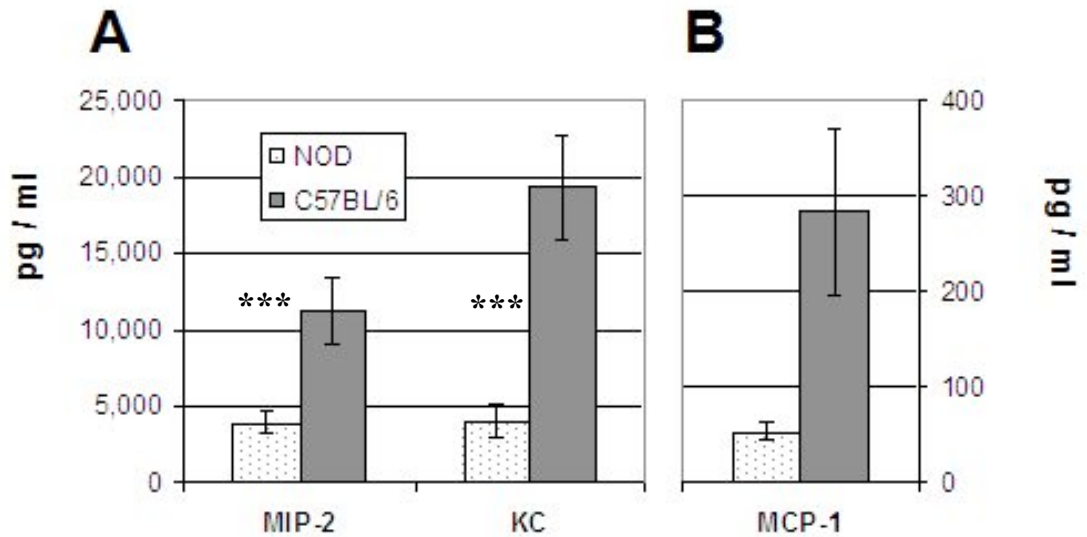
Figure 6- 8   Chemokine levels produced by PLMφ after 4 hours stimulation with LPS

Pleural cells from NOD mice and C57BL/6 control mice were harvested by pleural lavage, 0.25 x 106 cells were seeded into 12-well plastic plates and the PLMφ purified by adhesion and incubated in 0.5ml Mφ media containing 1µg/ml LPS for 4 hours. Supernatants were harvested, the remaining cells washed with PBS, lysed and the protein content of each well measured. Levels of chemokine measured in the supernatants were adjusted for the protein content of each well. Data shown are the mean levels of 4 wells. Histograms show the adjusted levels, NOD PLMφ in polka dots, C57BL/6 PLMφ in solid bars. (A) MIP-2 and KC levels. (B). MCP-1 levels. *** $p < 0.001$; NOD vs. C57BL/6; 2-way ANOVA across each time course.

Figure 6- 9   Cytokine levels produced by PLMφ after 4 hours stimulation with LPS
Pleural cells from NOD mice and C57BL/6 control mice were harvested by pleural lavage, 0.25 x 106 cells were seeded into 12-well plastic plates and the PLMφ purified by adhesion and incubated in 0.5ml Mφ media containing 1μg/ml LPS for 4 hours. Supernatants were harvested, the remaining cells washed with PBS, lysed and the protein content of each well measured. Levels of chemokine measured in the supernatants were adjusted for the protein content of each well. Data shown are the mean levels of 4 wells. Histograms show the adjusted levels, NOD PLMφ in polka dots, C57BL/6 PLMφ in solid bars. (A) TNFα and IL-10 levels. (B). IL-6 levels. *** $p < 0.001$, **$p < 0.01$; NOD vs. C57BL/6; 2-way ANOVA across each time course

Figure 6- 10   Chemokine levels produced by PLMφ after 4 hours stimulation with CG
Pleural cells from NOD mice and C57BL/6 control mice were harvested by pleural lavage, 0.25×10^6 cells were seeded into 12-well plastic plates and the PLMφ purified by adhesion and incubated in 0.5ml Mφ media containing 0.25% CG for 4 hours. Supernatants were harvested, the remaining cells washed with PBS, lysed and the protein content of each well measured. Levels of chemokine measured in the supernatants were adjusted for the protein content of each well. Data shown are the mean levels of 4 wells. Histograms show the adjusted levels, NOD PLMφ in polka dots, C57BL/6 PLMφ in solid bars. (A) MIP-2 and KC levels. (B). MCP-1 levels. *** $p < 0.001$, **$p < 0.01$; NOD vs. C57BL/6; 2-way ANOVA across each time course.

Figure 6- 11   Cytokine levels produced by PLMφ after 4 hours stimulation with CG
Pleural cells from NOD mice and C57BL/6 control mice were harvested by pleural lavage, 0.25 x 106 cells were seeded into 12-well plastic plates and the PLMφ purified by adhesion and incubated in 0.5ml Mφ media containing 0.25% CG for 4 hours. Supernatants were harvested, the remaining cells washed with PBS, lysed and the protein content of each well measured. Levels of cytokine measured in the supernatants were adjusted for the protein content of each well. Data shown are the mean levels of 4 wells. Histograms show the adjusted levels, NOD PLMφ in polka dots, C57BL/6 PLMφ in solid bars. (A) TNFα and IL-10 levels. (B). IL-6 levels. *** $p < 0.001$; NOD vs. C57BL/6; 2-way ANOVA across each time course.

	NOD PLMφ		C57BL/6 PLMφ	
	pg/ml	(sem)	pg/ml	(sem)
LPS STIMULATION at 24 hours				
MIP-2	3,788	(416)	4,314	(588)
KC	18,165***	(2,746)	51,115	(10,039)
MCP-1	690	(166)	976	(80)
TNFα	26	(4)	85	(9)
IL-6	4256*	(506)	8185	(926)
IL-10	101*	(35)	231	(26)
CG STIMULATION at 24 hours				
MIP-2	3,915	(444)	6,170	(1,612)
KC	12,531**	(1,184)	19,752	(2,070)
MCP-1	204***	(23)	414	(33)
TNFα	44	(7)	124	(47)
IL-6	1354**	(134)	2931	(406)
IL-10	291	(31)	542	(50)

Table 6- 7   Chemokine and cytokine levels produced by PLMφ after 24 hours stimulation

Pleural cells from NOD mice and C57BL/6 control mice were harvested by pleural lavage, 0.25 x 106 cells were seeded into 12-well plastic plates and the PLMφ purified by adhesion and incubated in 0.5ml Mφ media containing either 1µg/ml LPS or 0.25% CG for 24 hours. Supernatants were harvested, the remaining cells washed with PBS, lysed and the protein content of each well measured. Levels of chemokine and cytokine measured in the supernatants were adjusted for the protein content of each well. Data shown are the mean levels of 4 wells. *** $p < 0.001$, **$p < 0.01$, * $p < 0.05$; NOD PLMφ vs. C57BL/6 PLMφ; 2-way ANOVA across each time course.

6.4 RESULTS: RESIDENT PERITONEAL MACROPHAGES

6.4.1 NOD PMφ are hypo-responsive compared to C57BL/6

Resident peritoneal cells were obtained by peritoneal lavage from the same mice as those sacrificed for the PLMφ and BMDMφ used above (chapter 6.2 and 6.3) i.e. 12 male NOD mice aged 8 to 12 weeks and 15 age and sex matched C57BL/6 controls. Once again 0.25×10^6 cells were plated into plastic wells of 24-well plates and non-adherent cells removed after 1 hour by gentle washing with warm media. Remaining PMφ were incubated in 0.5ml of either standard media (quiescent) or media containing 1µg/ml LPS or 0.5% TG. As above, cells were inspected visually by light microscopy (x 400). Supernatants from each well were aspirated after 1, 4 or 24 hours and analysed in an identical fashion to those above. Remaining cells were lysed and the protein content of each well analysed as before. Individual cytokine and chemokine levels recorded in each well were again normalised to the mean protein content to compensate for differences in cell numbers across conditions and time points.

The mean protein level measured across all wells was 145 ± 5.8µg/ml. No differences were identified between the 2 strains (166 ± 8.1µg/ml vs. 153 ± 8.2µg/ml; NOD vs. C57BL/6; p = ns)

6.4.1.1 *Quiescent PMφ produce low levels of chemokines and cytokines*

It was noted once again that levels of all chemokines and cytokines produced by PMφ bathed in Mφ media without stimulation increased with time. Although the levels produced were noted to be extremely low compared to the LPS stimulated wells, (see table 6.8) the levels were perhaps higher than those achieved with quiescent BMDMφ or PLMφ and similar to the TG stimulated wells (tables 6.1 6.4 and 6.10 respectively). Whilst it is possible this was due to contamination of the media with LPS the same batch of Mφ media was used throughout the experiment for all 3 different Mφ phenotypes examined. In addition, sterile needles and sterile PBS were used for all peritoneal lavages. Alternatively it may reflect the increased sensitivity of PMφ to stimulation by their external environment and the low stimulatory capacity of the 0.5% TG used.

	NOD PMφ		C57BL/6 PMφ	
	pg/ml	(sem)	pg/ml	(sem)
MIP-2	10,375	(1,597)	9,043	(1,876)
KC	3,772	(956.2)	7,199	(1,385)
MCP-1	165.7	(13.5)	726.5	(632.8)
TNFα	60.4	(7.2)	416.7	(113.5)
IL-6	3,116	(29.4)	1,310	(145.2)
IFN γ	3.43	(0.75)	2.28	(1.12)
IL-10	55.2	(16.4)	73.2	(20.9)

Table 6- 8   Chemokine and cytokine levels produced by quiescent PMφ after 24 hours

PMφ from NOD and C57BL/6 controls were harvested by peritoneal lavage and 0.25×10^6 cells were seeded into 12-well plastic plates, purified by adhesion and incubated in 0.5ml media for 24 hours. Supernatants were harvested and the remaining cells washed with PBS, lysed and the protein content of each well measured. Levels of chemokines and cytokines measured in the supernatants were adjusted for the protein content of each well. Low levels were detected of all chemokines and cytokines measured. Data shown are the mean levels of 4 wells.

6.4.1.2 *PMφ from NOD mice are hypo-responsive to LPS in comparison to C57BL/6 PMφ*

Once again, no significant production of IFNγ was detected at any time point regardless of stimulation (table 6.9).

Unfortunately, as mentioned previously, the 0.5% TG stimulation failed to elicit an inflammatory response from PMφ of either strain. Levels of all chemokines or cytokines measured were equal to, or even below, those achieved by quiescent PMφ (data from the 24 hour time point is displayed in table 6.10; data from earlier time points is not shown). Although the explanation is unclear, the inflammatory response achieved by stimulation of BMDMφ by 0.5% TG was far less than achieved with 0.25% CG or 1μg/ml LPS. Thus it is possible that on this occasion 0.5% TG was too dilute to be an effective an *in vitro* stimulus. No further analysis of these data was attempted.

Whilst 1μg/ml LPS was sufficient to provoke a significant inflammatory response from PMφ, no significant production of any of the chemokines or cytokines measured was apparent until the 24 hour time point (see table 6.11). At 24 hours a broadly similar pattern to that obtained from PLMφ emerged with PMφ from NOD mice appearing hyporesponsive compared to the C57BL/6 controls (see figures 6.12 and 6.13).

Time	NOD PMφ		C57BL/6 PMφ	
(hours)	pg/ml	(sem)	pg/ml	(sem)
	LPS STIMULATION			
1	0.0	(0.0)	2.4	(2.3)
4	0.0	(0.0)	0.0	(0.0)
24	2.6	(2.0)	1.7	(1.1)
	TG STIMULATION			
1	0.0	(0.0)	0.0	(0.0)
4	0.0	(0.0)	0.0	(0.0)
24	3.2	(1.0)	5.8	(1.5)

Table 6- 9   Negligible interferon γ levels produced by PMφ
PMφ from NOD and C57BL/6 controls were harvested by peritoneal lavage and 0.25 x 10⁶ cells were seeded into 12-well plastic plates, purified by adhesion and incubated in 0.5ml media containing either 1µg/ml LPS, or 0.5% TG for 1, 4 or 24 hours. Supernatants were harvested and the remaining cells washed with PBS, lysed and the protein content of each well measured. Levels of interferon-γ measured in the supernatants were adjusted for the protein content of each well. Data shown are the mean levels of 4 wells; no significant differences identified between NOD and C57BL/6 mice, 2-way ANOVA.
.

	NOD PMφ		C57BL/6 PMφ	
	pg/ml	(sem)	pg/ml	(sem)
MIP-2	1,757	(154)	2,291	(325)
KC	1,467	(218)	1,721	(272)
MCP-1	87	(43)	89	(41)
TNFα	53	(13)	71	(19)
IL-6	42	(14)	125	(44)
IFN γ	106	(15)	126	(8)
IL-10	1,757	(154)	2,291	(325)

Table 6- 10   Chemokine and cytokine production by PMφ after 24 hours TG stimulation
PMφ from NOD and C57BL/6 controls were harvested by peritoneal lavage and 0.25×10^6 cells were seeded into 12-well plastic plates, purified by adhesion and incubated in 0.5ml media supplemented with 0.5% TG for 24 hours. Supernatants were harvested and the remaining cells washed with PBS, lysed and the protein content of each well measured. Levels of chemokines and cytokines measured in the supernatants were adjusted for the protein content of each well. Data shown are the mean levels of 4 wells; no significant differences identified between NOD and C57BL/6 mice, 2-way ANOVA.
.

	NOD PMφ		C57BL/6 PMφ	
	pg/ml	(sem)	pg/ml	(sem)
LPS STIMULATION at 1 hour				
MIP-2	1,162	(154.9)	991.9	(103.5)
KC	1,115	(202.9)	1,311	(237.7)
MCP-1	0.0	(0.0)	139.8	(141.2)
TNFα	92.3	(14.3)	135.0	(16.1)
IL-6	376.2	(53.0)	252.9	(25.3)
IL-10	22.9	(26.4)	73.5	(71.0)
LPS STIMULATION at 4 hours				
MIP-2	9,131	(871)	5,998	(699)
KC	13,659	(986)	5,088	(556)
MCP-1	113	(22)	74	(11)
TNFα	46	(5)	52	(4)
IL-6	325	(71)	335	(56)
IL-10	2,521	(370)	1,533	(178)

Table 6- 11   Chemokine and cytokine production by PMφ after 1 or 4 hours LPS stimulation
PMφ from NOD and C57BL/6 controls were harvested by peritoneal lavage and 0.25 x 10^6 cells seeded, purified by adhesion and incubated in 0.5ml media containing either 1µg/ml LPS for 1 or 4 hous. Supernatants were harvested and the remaining cells washed with PBS, lysed and the protein content of each well measured. Levels of chemokines and cytokines measured in the supernatants were adjusted for the protein content of each well. Data shown are the mean levels of 4 wells; no significant differences identified between NOD and C57BL/6 mice, 2-way ANOVA across time course.
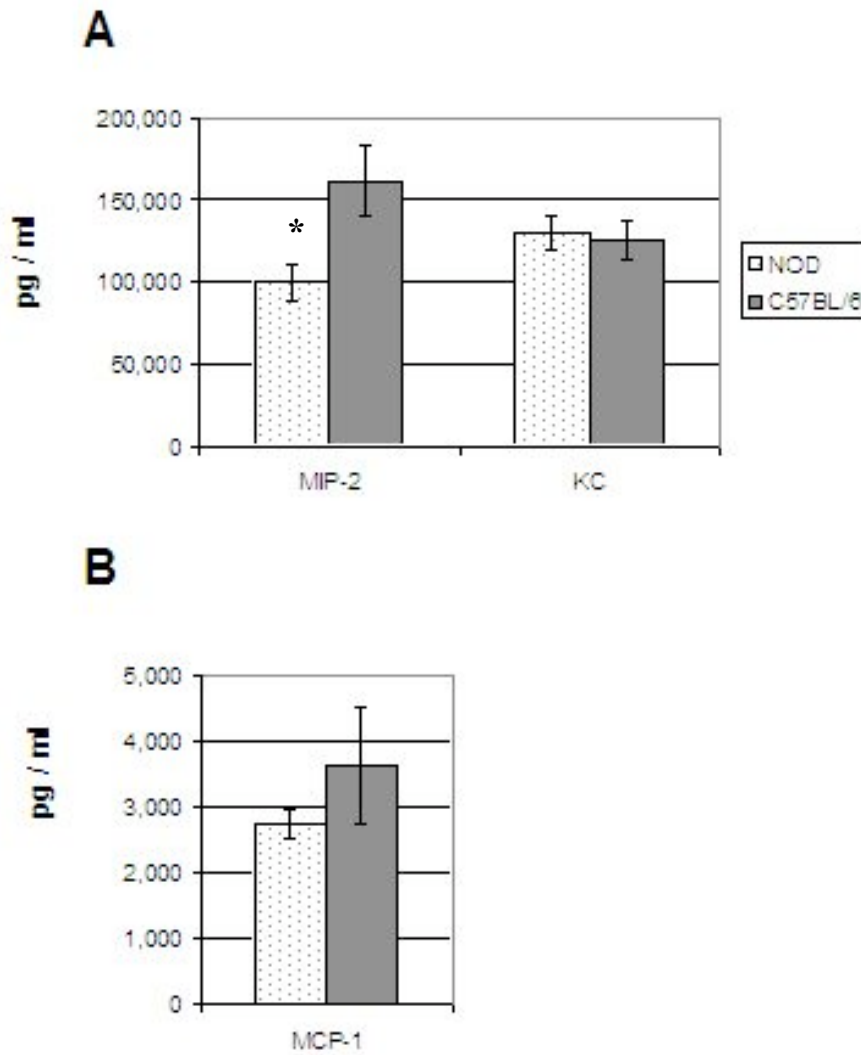
Figure 6- 12   Chemokine production by PMφ after 24 hours of LPS stimulation
PMφ from NOD and C57BL/6 controls were harvested by peritoneal lavage and 0.25×10^6 cells were seeded into 12-well plastic plates, purified by adhesion and incubated in media containing 1µg/ml LPS for 24 hours. Supernatants were harvested, the remaining cells washed with PBS, lysed and the protein content of each well measured. Levels of chemokine measured in the supernatants were adjusted for the protein content of each well. Data shown are the mean levels of 4 wells Histograms show the adjusted levels, NOD PMφ in polka dots, C57BL/6 PMφ in solid bars. (A) MIP-2 and KC levels. (B) MCP-1 levels. * p < .05; 2-way ANOVA across each time course.

Figure 6- 13   Cytokine production by PMφ after 24 hours of LPS stimulation
PMφ from NOD and C57BL/6 controls were harvested by peritoneal lavage and 0.25×10^6 cells were seeded into 12-well plastic plates, purified by adhesion and incubated in media containing 1µg/ml LPS for 24 hours. Supernatants were harvested, the remaining cells washed with PBS, lysed and the protein content of each well measured. Levels of cytokine measured in the supernatants were adjusted for the protein content of each well. Data shown are the mean levels of 4 wells Histograms show the adjusted levels, NOD PMφ in polka dots, C57BL/6 PMφ in solid bars. (A) TNFα and IL-10 levels. (B) IL-6 levels. *** $p < 0.001$, * $p < .05$; 2-way ANOVA across each time course.

6.4.2 NOD PMφ are hyporesponsive compared to C57BL/6 PMφ

Although the above experiment with TG stimulation of PMφ failed to achieve levels of chemokines and cytokines over and above those produced by quiescent PMφ, the data is reminiscent of an earlier, smaller study that examined the effect on PMφ phenotype of stimulation with TG and LPS for 4 hours *in vitro*.

PMφ were harvested from 5 female NOD mice aged 6 weeks together with 8 age and sex matched C57BL/6 control mice. Cells were pooled according to strain and 1 x 10^6 resident peritoneal cells were plated into wells of 12 well plates. PMφ were purified by adhesion, with non-adherent cells removed by gentle washing after 1 hour. The remaining PMφ were incubated for 4 hours in 1ml of standard media (quiescent) or media containing either 1μg/ml LPS or 0.5% TG (this experiment used the same batch but a different aliquot of 10% TG from the experiment above). Cytokine and chemokine levels were determined by ELISA according to the manufacturer's instructions but IL-6 was not measured. The remaining cells were lysed with cell lysis buffer and protein levels in the buffer were assessed as in the experiment above. Levels of all cytokines and chemokines were adjusted to the mean protein level for all wells (314μg/ml). No differences were noted in the protein levels assessed from wells seeded with NOD PMφ as opposed to C57BL/6 PMφ (318 ± 27μg/ml vs. 311 ± 22μg/ml; NOD vs. C57BL/6; p = ns)

On this occasion, quiescent PMφ produced much less cytokines or chemokines than PMφ stimulated with either TG or LPS (levels shown in table 6.12). Production of the CXC chemokines, MIP-2 and KC in response to LPS was similar between the 2 strains although surprisingly, MCP-1 production was actually higher by NOD PMφ (see figure 6.14). Both TNFα and IL-10 production by NOD PMφ in response to LPS was markedly reduced in comparison to PMφ derived from C57BL/6 mice (see figure 6.15). NOD PMφ produced less of all and cytokines measured than C57BL/6 PMφ in response to TG (see figure 6.8).

	NOD PMφ		C57BL/6 PMφ	
	pg/ml	(sem)	pg/ml	(sem)
MIP-2	2,778	(232.2)	2,413	(252.3)
KC	1,582**	(162.7)	671	(99.1)
MCP-1	5	(0.3)	3	(1.6)
TNFα	46	(1.4)	50	(3.7)
IL-10	56	(37.1)	43	(10.7)

Table 6- 12   Chemokine and cytokine production by quiescent PMφ
Peritoneal cells from NOD mice and C57BL/6 mice were harvested by peritoneal lavage and 0.25×10^6 cells were seeded into 12-well plastic plates. PMφ were purified by adhesion and incubated in 0.5ml media for 4 hours. Supernatants were harvested and the remaining cells washed with PBS, lysed and the protein content of each well measured. Levels of chemokines and cytokines measured in the supernatants were adjusted for the protein content of each well. Data shown are the mean levels of 4 wells. ** $p < 0.01$ NOD PMφ vs. C57BL/6 PMφ; student's t test.
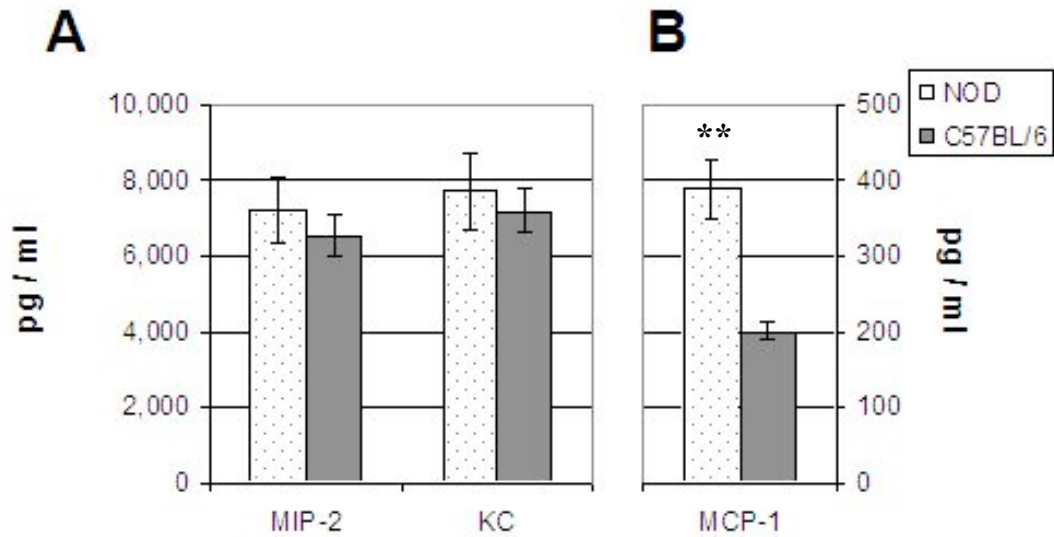
Figure 6- 14   Chemokine production by PMφ after 4 hours of LPS stimulation
Peritoneal cells from NOD mice and C57BL/6 control mice were harvested by peritoneal lavage. 0.25 x 10^6 cells were seeded into 12-well plastic plates. PMφ were purified by adhesion and incubated in media containing 1µg/ml LPS for 4 hours. Supernatants were harvested, the remaining cells washed with PBS, lysed and the protein content of each well determined. Chemokine levels measured in the supernatants were adjusted for the protein content of each well. Data shown are the mean levels of 4 wells. Histograms show the adjusted levels, NOD PMφ in polka dots, C57BL/6 PMφ in solid bars. (A) MIP-2 and KC levels. (B) MCP-1 levels. **$p < 0.01$; NOD PMφ vs. C57BL/6 PMφ; student's t test.
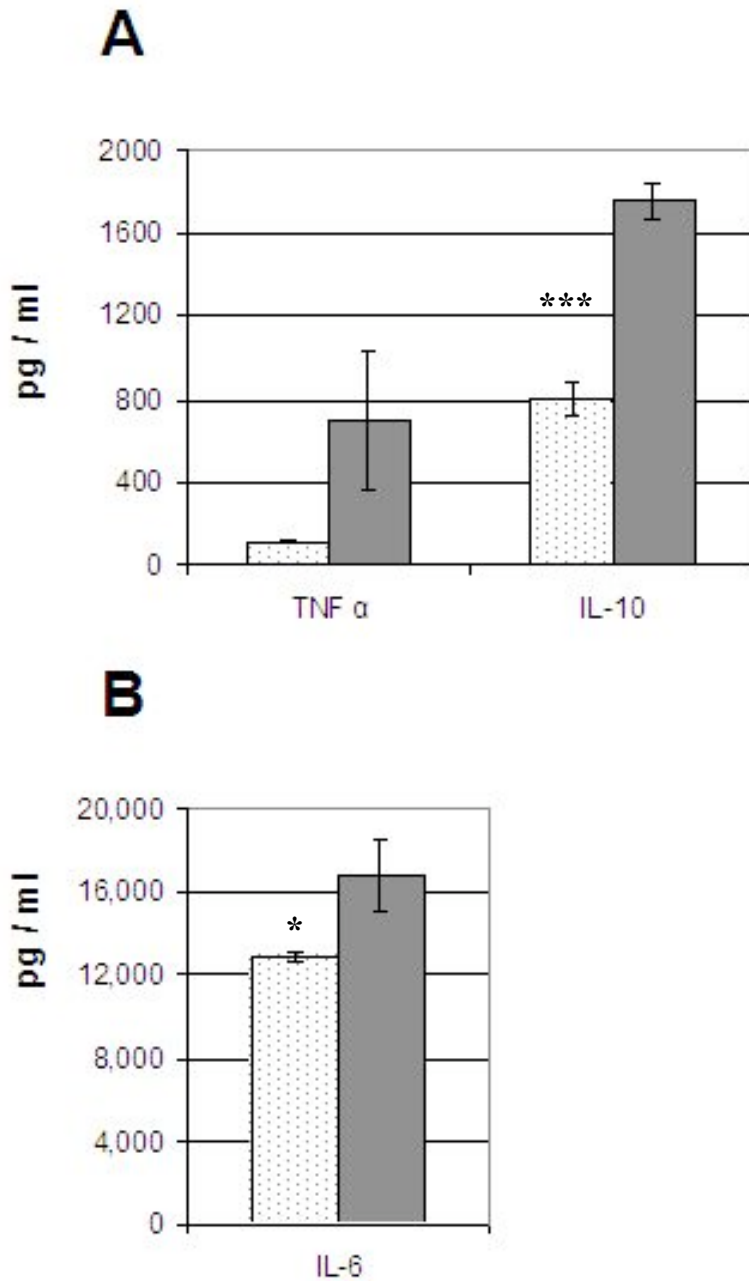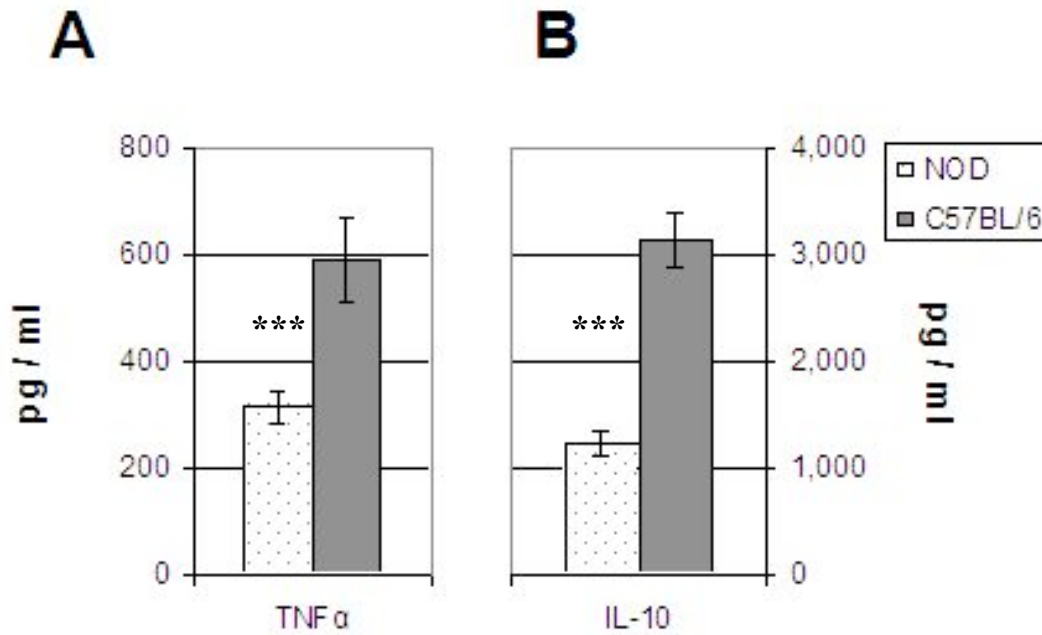
Figure 6- 15   Cytokine production by PMφ after 4 hours of LPS stimulation
Peritoneal cells from NOD mice and C57BL/6 control mice were harvested by peritoneal lavage. 0.25 x 10^6 cells were seeded into 12-well plastic plates. PMφ were purified by adhesion and incubated in media containing 1µg/ml LPS for 4 hours. Supernatants were harvested, the remaining cells washed with PBS, lysed and the protein content of each well determined. Cytokine levels measured in the supernatants were adjusted for the protein content of each well. Data shown are the mean levels of 4 wells. Histograms show the adjusted levels, NOD PMφ in polka dots, C57BL/6 PMφ in solid bars. (A) TNFα levels. (B) IL-10 levels. ***p < 0.001; NOD PMφ vs. C57BL/6 PMφ; student's t test.

Figure 6- 16   Chemokine production by PMφ after 4 hours of TG stimulation
Peritoneal cells from NOD mice and C57BL/6 control mice were harvested by peritoneal lavage. 0.25 x 10^6 cells were seeded into 12-well plastic plates. PMφ were purified by adhesion and incubated in media containing 0.5% TG for 4 hours. Supernatants were harvested, the remaining cells washed with PBS, lysed and the protein content of each well determined. Chemokine levels measured in the supernatants were adjusted for the protein content of each well. Data shown are the mean levels of 4 wells. Histograms show the adjusted levels, NOD PMφ in polka dots, C57BL/6 PMφ in solid bars. (A) MIP-2 and KC levels. (B) MCP-1 levels. * $p < 0.05$, **$p < 0.01$; NOD PMφ vs. C57BL/6 PMφ; student's t test.
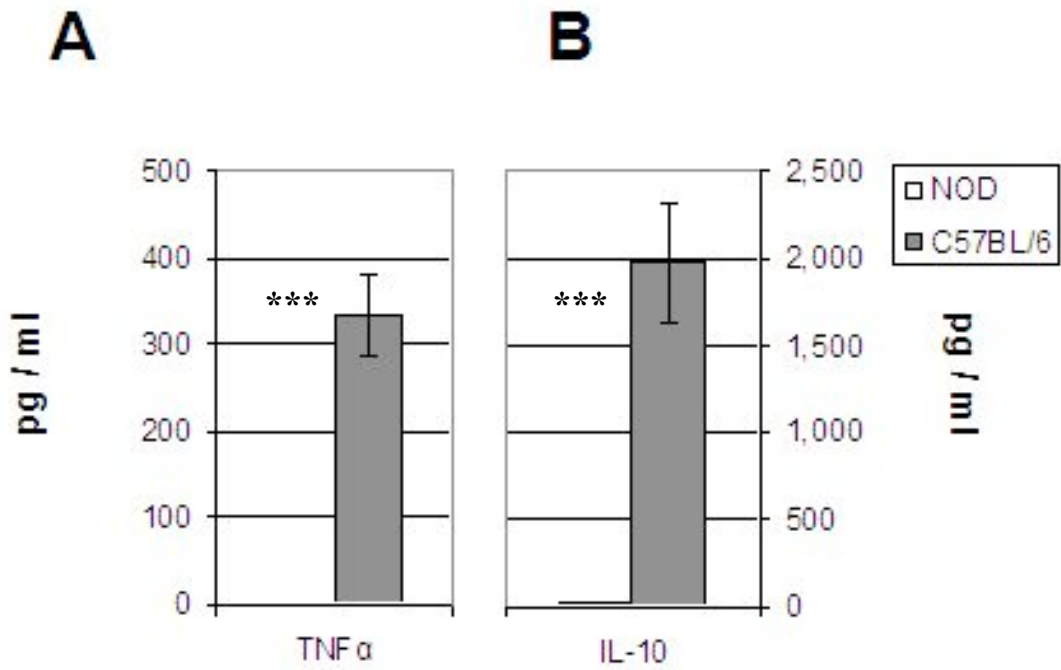
Figure 6- 17   Cytokine production by PMφ after 4 hours of TG stimulation
Peritoneal cells from NOD mice and C57BL/6 control mice were harvested by peritoneal lavage. 0.25 x 106 cells were seeded into 12-well plastic plates. PMφ were purified by adhesion and incubated in media containing 0.5% TG for 4 hours. Supernatants were harvested, the remaining cells washed with PBS, lysed and the protein content of each well determined. Cytokine levels measured in the supernatants were adjusted for the protein content of each well. Data shown are the mean levels of 4 wells. Histograms show the adjusted levels, NOD PMφ in polka dots, C57BL/6 PMφ in solid bars. (A) TNFα levels. (B) IL-10 levels. ***$p < 0.001$; NOD PMφ vs. C57BL/6 PMφ; student's t test.

6.5 SUMMARY

In this chapter, it was demonstrated that NOD BMDMφ are pro-inflammatory in comparison to C57BL/6 controls following stimulation with LPS, TG or CG.

In contrast, PMφ and PLMφ from NOD mice were significantly less responsive than C57BL/6 control Mφ to LPS, and either TG or CG stimulation.

It should be noted, however, that the pattern was less consistent and less clear with *ex-vivo* resident Mφ than with the BMDMφ. This may reflect the greater cellular heterogeneity in *ex-vivo* Mφ populations or perhaps greater sensitivity to their external environment and therefore any inadvertent contamination of tissue culture media.

This divergent response between *ex-vivo* Mφ and BMDMφ may help explain the apparent discord between data published by different research groups.

The next important question was to determine which phenotype appeared to influence the inflammatory process *in vivo*?

Chapter 7. Analysis of the NOD inflammatory response *in vivo*

7.1 INTRODUCTION

Following examination of the patterns of chemokine and cytokine production by NOD and C57BL/6 Mφ *in vitro*, it was important to examine the inflammatory responses of these mice *in vivo*. Three models of inflammation were chosen for analysis: TG peritonitis, CG pleurisy and DTH pleurisy.

7.2 THIOGLYCOLLATE PERITONITIS

TG peritonitis is a well characterised model of sterile inflammation, frequently used to elicit inflammatory Mφ for *ex vivo* experimentation (Fan et al., 2004). Our group has previously demonstrated that TG peritonitis is markedly dependent on the function of resident peritoneal Mφ (Cailhier et al., 2005). From the hyper-responsive, pro-inflammatory phenotype of NOD BMDMφ *in vitro*, it could be hypothesised that NOD mice would exhibit an exaggerated inflammatory response and greater leukocyte recruitment. Conversely, the hypo-responsive phenotype of NOD PMφ would suggest a diminished inflammatory response with reduced PMN and Mφ recruitment as a result of reduced production of key chemokines and cytokines. Indeed, Potter et al reported that several 'autoimmune prone' strains of mice exhibit a muted inflammatory response in TG peritonitis (Potter et al., 2003). In addition, Bouma et al (Bouma et al., 2005) reported that NOD mice exhibited markedly impaired leukocyte recruitment to TG peritonitis that was more marked than that evident in lupus-prone strains. The mechanism was unexplained by either group although Bouma et al suggested that an impaired migratory ability of NOD PMN may underlie the defect.

It was decided to explore the inflammatory response of NOD mice to TG peritonitis in greater detail. The study of similar time points to previous reports would corroborate (or refute) the reported muted inflammatory phenotype exhibited by NOD mice. In addition, focus on the first 24 hours would facilitate study of the levels of important chemokine and cytokines at time points previously shown to be important for leukocyte recruitment in order to determine whether the PMφ of NOD mice exhibited an abnormal pattern of chemokine and cytokine production *in vivo*.

7.2.1 NOD mice recruit fewer leukocytes in thioglycollate peritonitis

Peritonitis was initiated with TG in male NOD mice aged 8 to 12 weeks and age and sex matched C57BL/6 controls as previously described (chapter 2.9.1). In brief, 1ml of TG (3% w/v in sterile distilled water) was injected ip to all mice with the exception of those selected for the zero hour (naïve) time point. Mice were sacrificed at baseline (naïve) and 24 (n=8 mice), 48 (n=5 mice) and 96 (n=5 mice) hours following TG administration. Mice underwent peritoneal lavage with 5ml ice-cold PBS immediately after death. Aliquots were removed from each sample and placed in chilled FACS tubes. After immunolabeling with various leukocyte markers (F4/80 [Mφ], GR1 [PMN], B220 [B cells] and CD3 [T cells]) peritoneal cells were analysed by flow cytometry as described in chapter 2.9.1.1. The remaining fluid was centrifuged to remove cells and aliquots frozen at -80°C pending further analysis.

Analysis of the peritoneal cells recovered revealed a striking reduction in the total numbers of leukocytes recruited by NOD mice during TG peritonitis (see figure 7.1A) despite increased numbers of PMφ present in the naïve peritoneum at baseline ($1.16 \pm 0.26 \times 10^6$ vs. $0.52 \pm 0.08 \times 10^6$; NOD vs. C57BL/6; $p < 0.02$ by student's t test of individual time point although not significant in context of the full experimental time course and analysis by 2 way ANOVA). A marked reduction in the numbers of Mφ and PMN was evident in NOD mice compared to C57BL/6 control mice (figure 7.1B and C).

In a pattern highly reminiscent of the lupus-prone mice strains (Potter et al., 2003), NOD mice recruited markedly fewer Mφ overall. Whilst Mφ numbers peaked at 48 hours and started to fall by 96 hours in C57BL/6 mice, they were still increasing in NOD mice by the end of the experimental time course (figure 7.1B). The peak in PMN numbers occurred at 24 hours in both strains with numbers markedly reduced by 48 hours. Although the profile of PMN infiltration was similar between NOD and C57BL/6 mice, the peak PMN number was significantly lower in NOD mice (figure 7.1C). In addition, NOD mice recruited fewer B and T lymphocytes figure 7.2). Indeed, unlike C57BL/6 mice, NOD mice did not exhibit a significant increase in either B or T lymphocyte numbers at any time point.
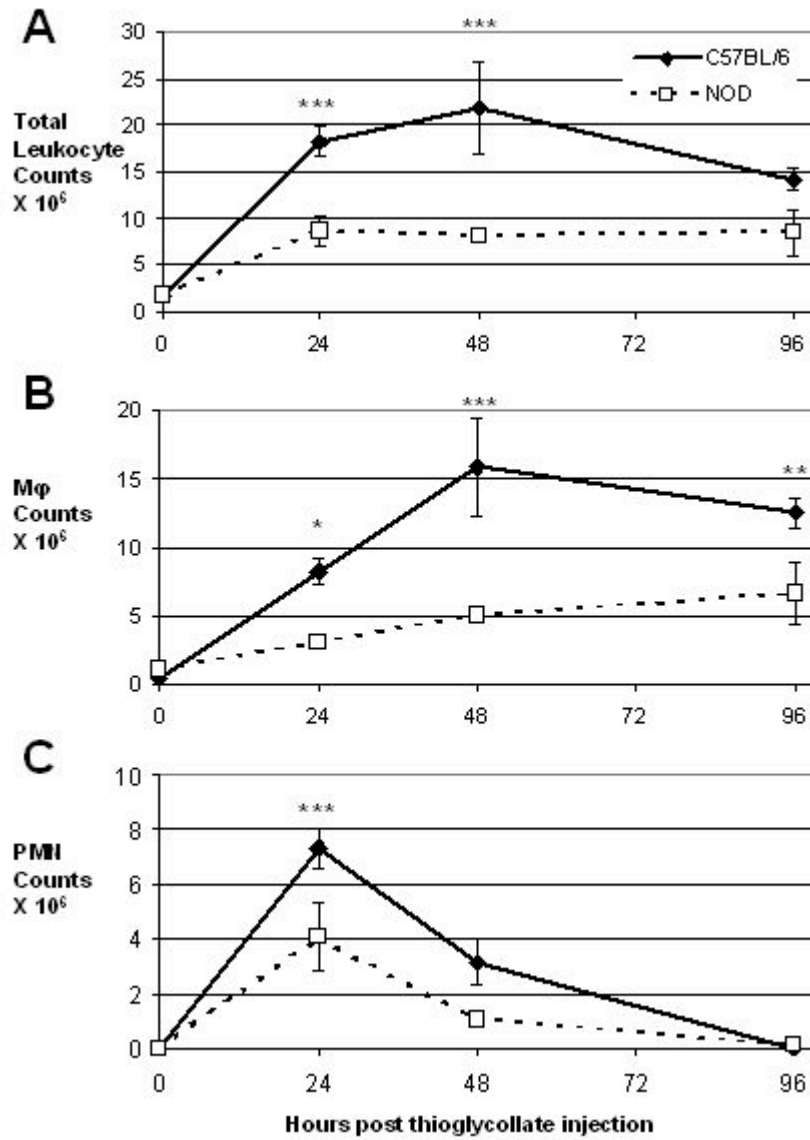
Figure 7- 1   NOD mice recruit fewer leukocytes during thioglycollate peritonitis
Peritonitis was induced with an ip injection of 1ml 3% TG. Peritoneal cells were recovered by lavage, immunolabeled and then analysed by flow cytometry. 8 mice were used for the 24-hour time point, 5 mice per strain for all other time points. C57BL/6 mice in solid lines, NOD in dashed lines. NOD mice exhibit a marked defect in the recruitment of leukocytes to the peritoneum (A). The defective recruitment was most striking for Mφ (B), although reduced recruitment of PMN (C) is also clearly apparent. *** $p < 0.001$, ** $p < 0.01$, * $p < 0.05$; C57BL/6 vs. NOD; 2-way ANOVA.
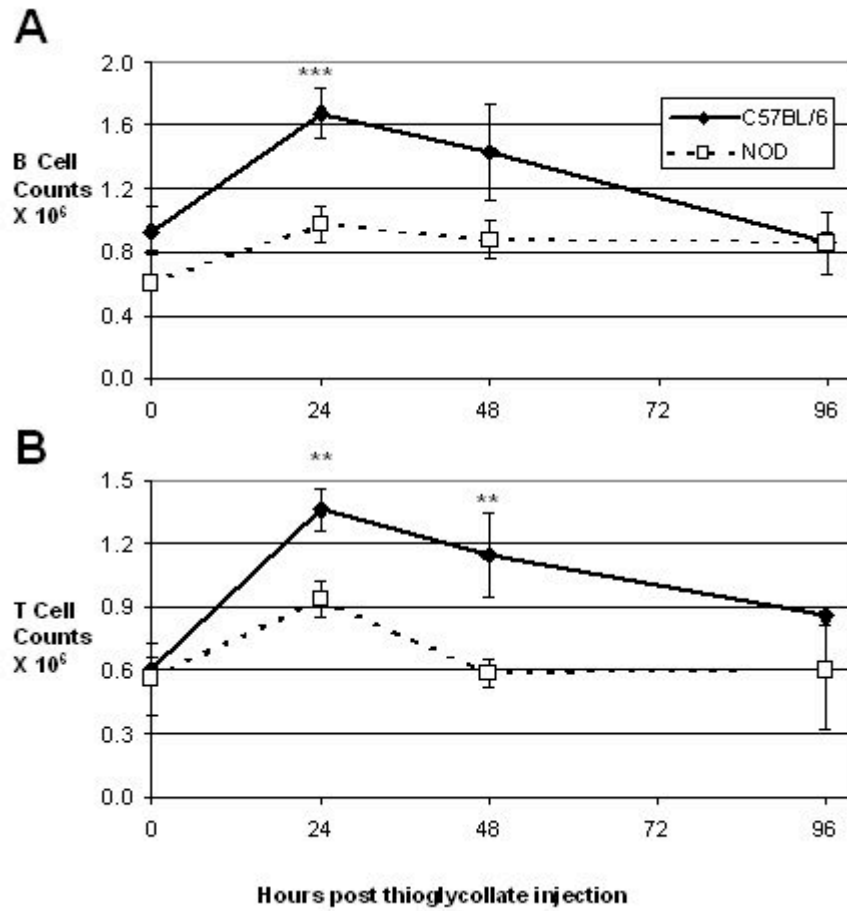
Figure 7- 2   NOD mice recruit fewer lymphocytes during thioglycollate peritonitis
Peritonitis was induced with an ip injection of 1ml 3% TG. Peritoneal cells were recovered by lavage, immunolabeled and then analysed by flow cytometry. 8 mice were used for the 24-hour time point, 5 mice per strain for all other time points. C57BL/6 mice in solid lines, NOD in dashed lines. NOD mice exhibited a defect in the recruitment of B lymphocytes (A) and T lymphocytes (B) to the peritoneum compared to C57BL/6 controls. *** $p < 0.001$, ** $p < 0.01$; C57BL/6 vs. NOD; 2-way ANOVA.

7.2.2 Defective recruitment of leukocytes by NOD mice is apparent by 4 hours

Having demonstrated a similar pattern of leukocyte recruitment in NOD mice over the course of 96 hours to that published by Paul Potter (Potter et al., 2003) , it was decided to investigate the first 24 hours in greater detail. Jean-Francois Cailhier (Cailhier et al., 2005)demonstrated that events early occurring within the first 4 hours of TG peritonitis set the pattern of PMN recruitment with MIP-2 (CXCL2) production by resident peritoneal Mφ being critical.

Twenty female NOD mice aged 8 to 12 weeks were selected together with age and sex matched C57BL/6 controls. Due to changes in the project license peritonitis was initiated with 0.5ml of TG 10% w/v injected ip instead of 1ml 3% w/v. Mice were sacrificed at zero (naïve), 1, 4, 8 and 24 hours (4 per group) and samples were collected, prepared and stained for flow cytometry as previously described. Defective recruitment of leukocytes by NOD mice was evident by 4 hours and was more marked at 24 hours (figure 7.3). Reassuringly, despite using female mice and 0.5ml of 10% TG, the number of leukocytes recruited to the peritoneum at 24 hours was similar to the previous experiment with male mice and 1ml of 3% TG (see figure 7.4).

As detailed in chapter 2, resident PMφ were F4/80^{HI} / CD11b^{HI} and quite distinct from infiltrating monocyte/Mφ which were F4/80^{MED} / CD11b^{MED}. Within the first hour following TG administration there were clear differences in the peritoneal Mφ populations of NOD mice compared to C57BL/6 mice (figure 7.5). NOD mice retained their mature PMφ, whilst they largely disappeared in the C57BL/6 strain in a manner reminiscent of the MDR (Tomazic et al., 1977). Conversely, recruitment of infiltrating monocytes/Mφ was much brisker in C57BL/6 mice. As a result of these differences, the total numbers of Mφ varied little between the 2 strains of mice until the 4 hour time point by which time the reduced Mφ infiltration resulted in reduced numbers being evident in NOD mice (figure 7.5). PMN recruitment was comparable between NOD and control mice for the first 4 hours of TG peritonitis. No further increase in PMN infiltration was evident in NOD mice whilst PMN numbers continued to climb in C57BL/6 mice and peaked at 24 hours (figure 7.6).
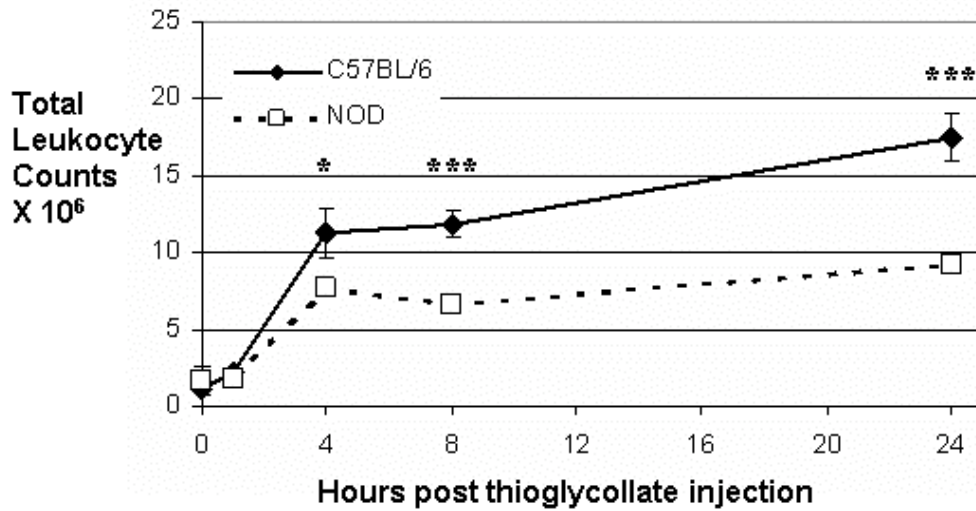
Figure 7- 3   Analysis of leukocyte numbers during TG peritonitis
Peritonitis was induced with an ip injection of 0.5ml 10% TG. Peritoneal cells were recovered by lavage, stained and analysed by flow cytometry. 4 mice were used per time point. C57BL/6 mice in solid lines, NOD in dashed lines. The marked defect in the recruitment of leukocytes exhibited by NOD mice was evident by 4 hours. *** $p < 0.001$, * $p < 0.05$; C57BL/6 vs. NOD; 2-way ANOVA.
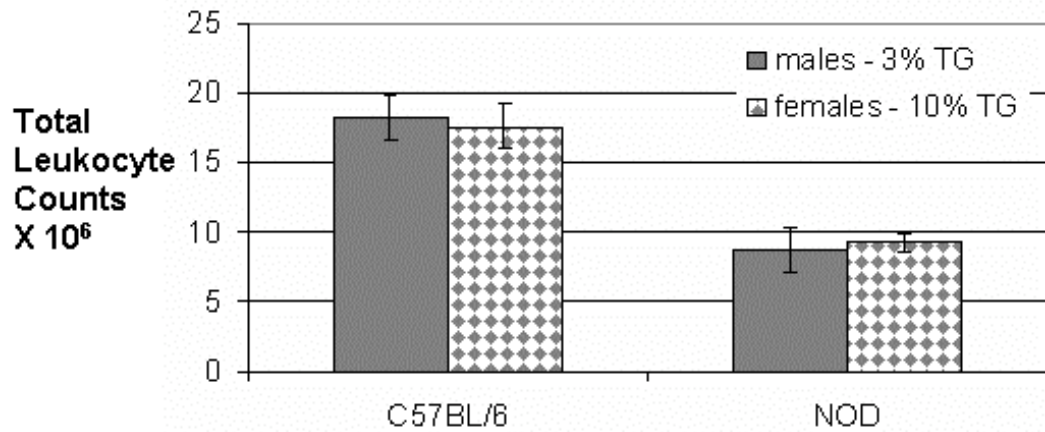
Figure 7- 4   Comparable leukocyte infiltration at 24 hours in male administered 1ml of 3% TG and female mice administered 0.5ml of 10% TG
Peritonitis was induced with an ip injection of either 1ml of 3% TG (males) or 0.5ml of 10% TG (females). Mice were sacrificed 24 hours later, peritoneal cells were recovered by lavage, stained and then analysed by flow cytometry. Male mice are in solid bars, female mice in chequered bars. Total leukocyte numbers recovered at this time point were strikingly similar between males and females of each strain.
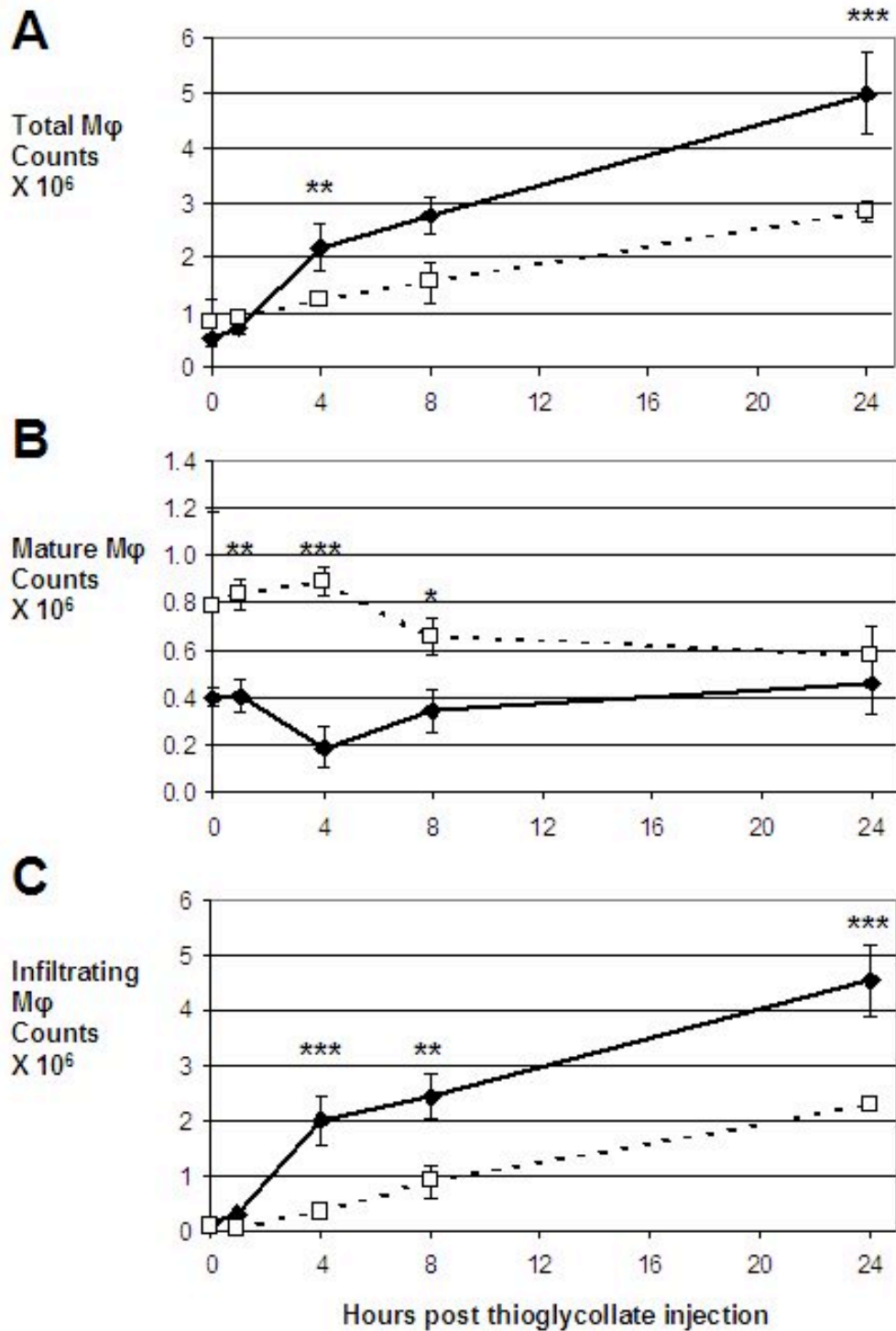
Figure 7- 5   Analysis of infiltrating monocytes/macrophages and mature macrophages during the first 24 hours of TG peritonitis.
Peritonitis was induced with an ip injection of 0.5ml 10% TG. Peritoneal cells were recovered by lavage, immunolabeled and then analysed by flow cytometry. 4 mice were used per time point. Mature PMφ (F4/80^{HI} / CD11b^{HI}) and infiltrating monocytes/Mφ (F4/80^{MED} / CD11b^{MED}) were gated as illustrated in figure 2.22. C57BL/6 mice in solid lines, NOD in dashed lines. NOD mice exhibited a marked defect in the total recruitment of PMφ by 4 hours (A). Unlike C57BL/6 mice, the numbers of mature PMφ in NOD mice did not appear to fall following the injection of TG (B) and the low total Mφ count was primarily attributable to fewer F4/80^{MED} infiltrating monocytes/macrophages (C). *** $p < 0.001$, ** $p < 0.01$, * $p < 0.05$; C57BL/6 vs. NOD; 2-way ANOVA

225
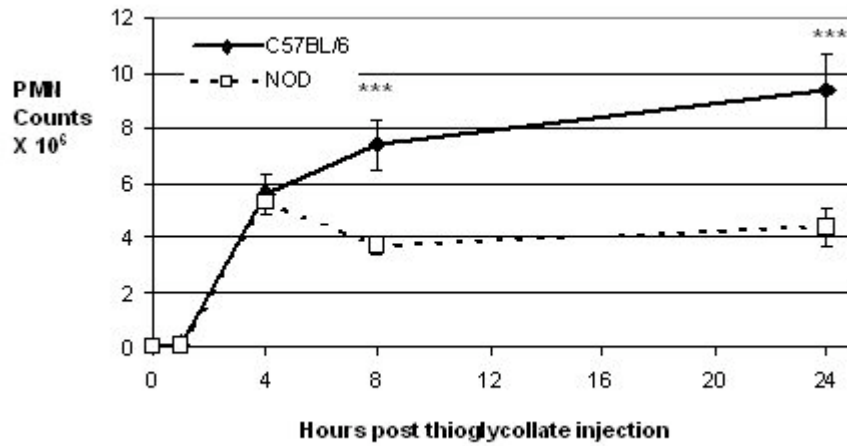
Figure 7- 6   Analysis of PMN recruitment during TG peritonitis
Peritonitis was induced with an ip injection of 0.5ml 10% TG. Peritoneal cells were recovered by lavage, immunolabeled and then analysed by flow cytometry. 4 mice were used per time point. C57BL/6 mice in solid lines, NOD in dashed lines. NOD recruitment of PMN was comparable to C57BL/6 mice until the 4-hour time point; thereafter PMN numbers failed to increase in NOD mice, but continued to rise in C57BL/6 mice. *** $p < 0.001$; C57BL/6 vs. NOD; 2-way ANOVA

7.2.3 NOD and C57BL/6 mice exhibit comparable levels of chemokines and cytokines

In vitro work examining chemokine and cytokine production in response to LPS and TG indicated that NOD BMDMφ were pro-inflammatory whilst PMφ were hypo-responsive compared to C57BL/6 controls. Since reduced secretion of key chemokines or cytokines *in vivo* represented a potential mechanism for the defective leukocyte recruitment in TG peritonitis, the levels of MIP-2, KC, MCP-1, TNFα, IL10 and IFNγ were analysed by specific ELISA in cell free aliquots of lavage fluid stored at -80^oC until analysis.

The levels of MIP-2 were comparable with both NOD and C57BL/6 mice mounting a robust peak at 1 hour that returned to baseline by 4 hours (figure 7.7A). The levels of KC in NOD mice peaked at 4 hours but levels were not statistically significant differences to those in C57BL/6 mice (figure 7.7B). Levels of the important CC chemokine MCP-1 were comparable between the 2 strains (figure 7.7C). Consistent with the *in vitro* studies of BMDMφ, NOD mice exhibited a trend to produce a more pro-inflammatory milieu with more TNFα and less IL-10 production but the differences did not reach statistical significance (figure 7.7D and E). Neither strain produced significant levels of IFNγ, consistent with this being a Mφ dependent model of inflammation (figure 7.7F).

Even though the list of chemokines and cytokines examined was not exhaustive, the explanation for the diminished leukocyte recruitment evident in NOD mice was unlikely to lie in the peritoneal levels of these mediators Rather than continued chemokine and cytokine analysis, it was decided to address whether the defective leukocyte recruitment could be localised to the same idd locus as the phagocytic defect (see chapter 5).

7.2.4 Defective recruitment of leukocytes did not localise to idd18

Bouma et al suggested that impaired leukocyte migration towards inflamed sites might underlie the defective cell recruitment evident in NOD mice (Bouma et al., 2005). Evidence presented in chapter 5 suggested that the *in vivo* phagocytic defect localised to idd18, and by inference to *vav3*, might involve a gene that plays a role in cytoskeletal rearrangement. Clearly such a gene could also be responsible for impaired migratory responses and hence defective leukocyte recruitment. To test this

hypothesis TG peritonitis was initiated in the same congenic NOD strains used to localise the *in vivo* phagocytic defect to idd18. In these studies R323 has idd3/10/18 replaced, R20 has just idd3/10 replaced, R905 has idd9 replaced and 1591 has idd3/5 replaced (see table 5.1 for more details).

The experiment was conducted in 2 stages with each stage comprising 4 NOD mice, 4 C57BL/6 control mice and 4 mice from 2 of the congenic strains. All mice were male and aged 6 to 8 weeks. Peritonitis was initiated by an ip injection of 0.5ml 10% TG and mice were sacrificed 24 hours later by cervical dislocation and peritoneal cells recovered by lavage using ice-cold PBS. Aliquots of lavage fluid from each mouse were stained and analysed by flow cytometry as above. Data from the 2 experiments were combined (resulting in n = 8 for NOD and C57BL/6 mice and n = 4 for all congenic strains) and analysed together.

At the 24 hour time point, C57BL/6 mice exhibited significantly increased numbers of total leukocytes, Mφ and PMN than either the NOD mice or any of the NOD congenic strains. No differences were evident between the NOD mice and any of the congenic strains with respect to numbers of leukocytes recruited (see figure 7.8). Clearly the defective recruitment does not correct by replacing NOD genes in any of the idd loci 3, 5, 9, 10 or 18 and certainly did not correct by replacing the NOD *vav3* gene with a copy of the C57BL/6 *Vav3* gene. The next question examined was whether defective leukocyte recruitment in NOD mice was restricted to peritonitis or also present in other Mφ dependent models of inflammation such as carrageenan (CG) pleurisy.
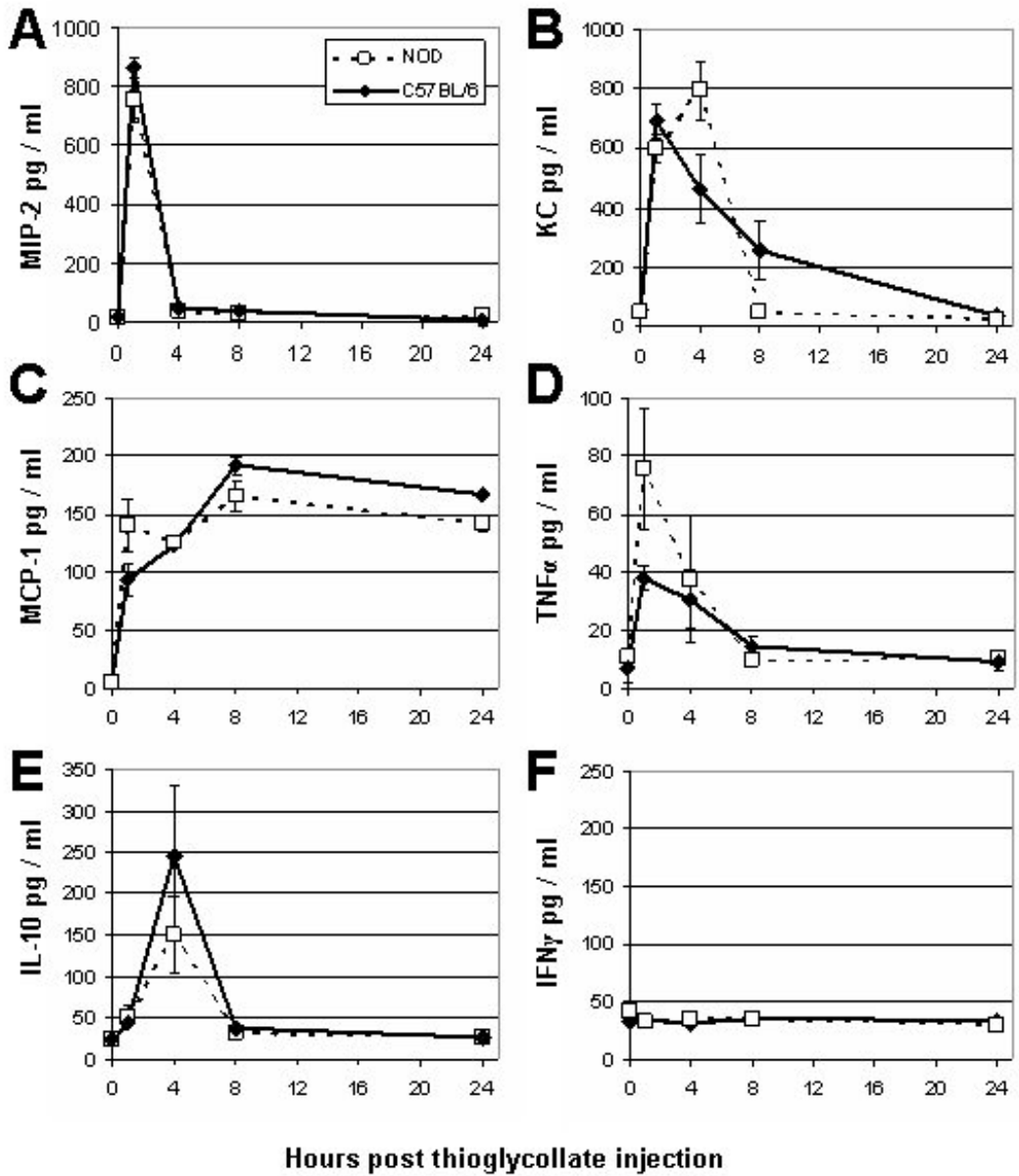
Figure 7- 7   Analysis of chemokine and cytokine levels during TG peritonitis
Peritonitis was induced with an ip injection of 0.5ml 10% TG. Peritoneal lavage was performed a various time points to 24 hours. Samples were centrifuged and supernatants decanted for analysis. 4 mice were used per time point. C57BL/6 mice in solid lines, NOD in dashed lines. No differences were seen between NOD and control mice in the concentrations of any chemokines or cytokines investigated.

229
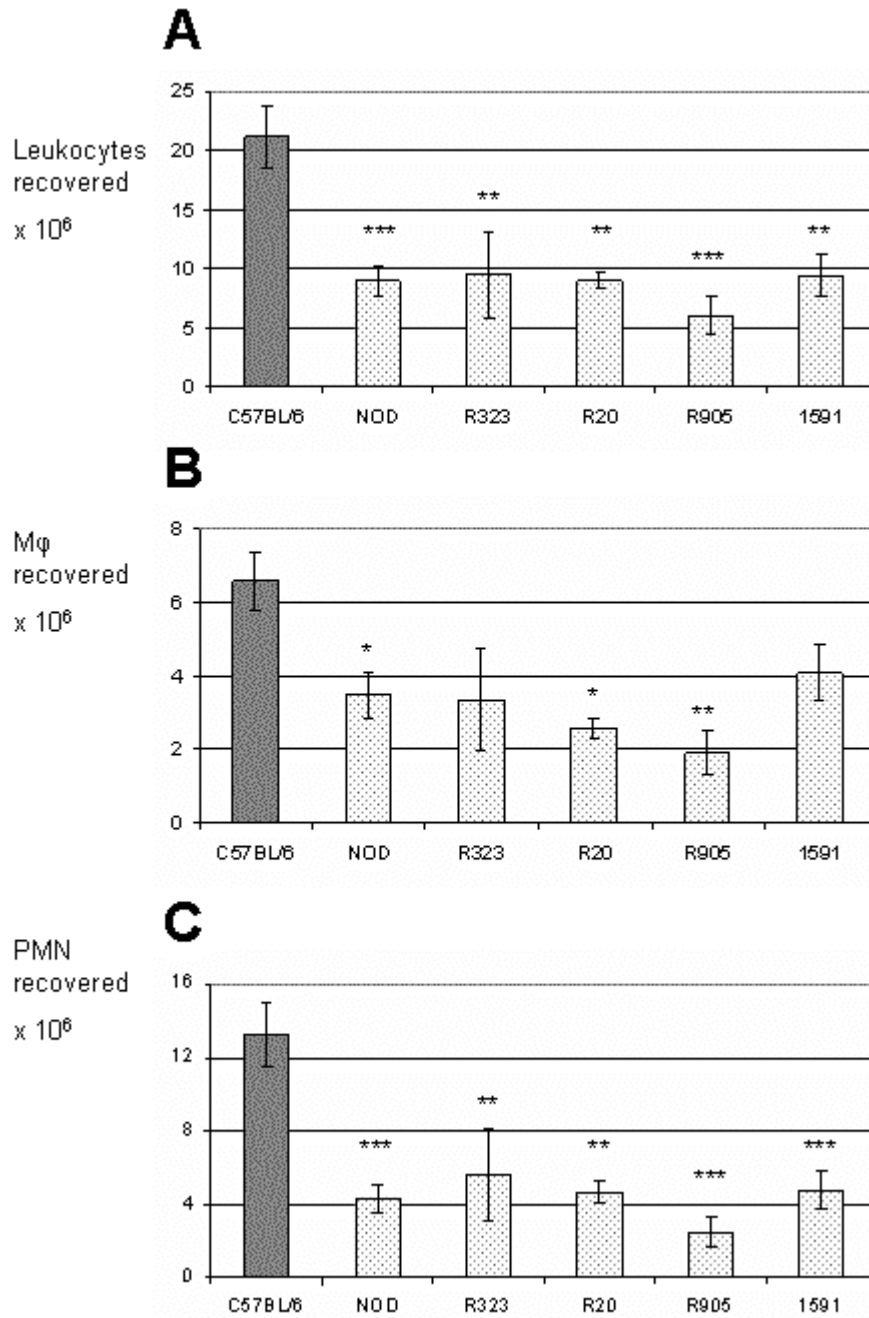
Figure 7- 8   Analysis of leukocyte numbers 24 hours after the initiation of TG peritonitis in C57BL/6, NOD and 4 congenic strains of NOD mice
Peritonitis was initiated by i.p injection of 0.5ml 10% TG, the mice were sacrificed 24 hours later and peritoneal cells recovered by lavage, immunolabeled and analysed by flow cytometry. Total leukocyte counts in graph (A), Mφ counts in graph (B) and PMN counts in graph (C). *** $p < 0.001$, ** $p < 0.01$, * $p < 0.05$; NOD or congenic vs. C57BL/6; ANOVA.

7.3 CARRAGEENAN PLEURISY

Having corroborated defective leukocyte recruitment in one Mφ dependent model of inflammation it was decided to examine the inflammatory response of NOD mice using a different experimental model in a different system in order to determine whether a similar response was seen. CG pleurisy was selected over more 'physiologically relevant' models of inflammation such as bacterial or LPS induced pleurisy because, like TG peritonitis, it is a reproducible model of sterile inflammation characterised by brisk leukocyte recruitment and has previously been demonstrated to be dependent upon resident Mφ function (Cailhier et al., 2005). It was hypothesised that once again NOD mice would exhibit impaired recruitment of leukocytes to the site of inflammation.

7.3.1 Male NOD mice exhibit reduced leukocyte recruitment during CG pleurisy

24 male NOD mice, aged 8 to 12 weeks, together with age and sex matched C57BL/6 controls were divided between 4 time points: zero (naïve), 24, 48 and 72 hours. CG pleurisy was initiated as previously described. In brief, all mice were anaesthetised and 0.1ml 1% CG injected intrapleurally (i.pl.). Mice were sacrificed by exsanguination under general anaesthesia and pleural lavage performed with 1ml 3.88% sodium citrate. The recovered pleural lavage was accurately weighed to gauge volume and aliquots were then transferred to chilled FACS tubes, immunolabeled and analysed as previously described in chapter 2.9.2. The remaining lavage fluid and blood samples were centrifuged to remove cells and the supernatants and serum samples were decanted and frozen at $-80^{o}C$ pending analysis.

Since smaller volumes are used for pleural compared to peritoneal lavage (1ml vs. 5ml) it is possible to use the volume of retrieved lavage fluid to directly gauge the volume of inflammatory exudate. The volumes of inflammatory exudate produced by NOD and C57BL/6 mice during CG pleurisy were similar at all time points examined (figure 7.9). Similar to TG peritonitis, NOD mice again recruited fewer total leukocytes over the time course (figure 7.10A) although the cell numbers at 24 hours were comparable. A striking reduction in recruited Mφ numbers was evident in NOD mice compared to controls (figure 7.10B), despite initially having significantly higher resident PLMφ numbers (0.73 ± 0.09 x 10^6 vs. 0.27 ± 0.03 x 10^6; NOD vs. C57BL/6; $p < 0.001$ by student's t test of individual time point although not

significant in context of the whole experimental time course and 2 way ANOVA). In contrast to TG peritonitis, the peak numbers of PMN at 24 hours were similar. Interestingly, C57BL/6 mice exhibited rapid clearance of significant numbers of PMN at 48 hours whereas NOD mice had a significantly increased PMN infiltrate at this time point (figure 7.10C). It is tempting to argue that the increased numbers of PMN present at 48 hours resulted from the combination of fewer Mφ to remove senescent apoptotic PMNs and an impaired AC phagocytic capacity of Mφ in NOD mice. Unfortunately, no free AC, necessary to prove defective clearance, were identified during examination of cytospins of the lavage fluid of either strain.

Nikolic et al argued that bone-marrow precursors from NOD mice exhibit defective DC maturation *in vitro* (with maturation skewed towards Mφ generation (Nikolic et al., 2005) and the numbers of pleural CD11c^{HI} cells was thus measured in both strains. Fewer pleural DC were identified in NOD mice. Although this result is consistent with diminished maturation of NOD myeloid precursors into DC, the ratio of DC to Mφ in the 2 strains was remarkably similar at all time points (figure 7.11), suggesting that the *in vitro* phenomenon was probably not relevant to this model of inflammation *in vivo*.

7.3.2 Female NOD mice exhibit reduced recruitment of Mφ and PMN 24 hours after initiation of CG pleurisy

As shown earlier, male and female NOD mice exhibited remarkably similar levels of leukocyte recruitment during TG peritonitis at the 24 hour time point although the dose of TG was different. It was hypothesised that the defective recruitment of leukocytes to CG pleurisy would also be independent of gender. CG pleurisy was initiated in 6 female NOD mice aged 6 weeks and 6 age and sex matched C57BL/6 controls. Samples were collected and analysed for leukocytes as described previously. Somewhat surprisingly, in addition to the reduced numbers of total leukocytes and Mφ as seen previously with NOD mice, fewer PMN were also recovered (see figure 7.12). Further work, clarifying the phenotype is required.

7.3.3 NOD mice produce significantly less MCP-1 during CG pleurisy

Following the removal of aliquots for analysis of cell kinetics, lavage samples from the original experiment (using male mice) were spun down and supernatants decanted for analysis. The collection of serum from mice at each time point also enabled the analysis of chemokines and cytokines within the circulation enabling the gradient of chemokine, from serum to exudate to be calculated as this gradient, rather than absolute levels, drives leukocyte recruitment. A range of chemokines and cytokines were examined: KC and MIP-2 by ELISA whilst MCP-1, TNFα, IL-6, IL-10 and IFNγ were analysed by CBA.

Whilst NOD mice exhibited a significantly lower peak of MCP-1 within the pleural lavage fluid and the serum (figure 7.13), suggesting a possible mechanism for the markedly defective recruitment of Mφ seen in this model of inflammation. However, the gradient of MCP-1 from exudate to serum was strikingly similar between the 2 strains (5.8 ± 1.4 vs. 6.5 ± 0.40; NOD vs. C57BL/6; p = ns, student's t test).

It was previously noted with TG peritonitis and from the work of Jean-Francois Cailhier (Cailhier et al., 2005) that most chemokines and cytokines peaked early, within 4 hours with levels falling to baseline by 24 hours (figure 7.7). It was therefore not surprising to find no significant levels of most of these chemokines and cytokines within either the exudate or the serum at the 24 hour time point or later (see 24 hour data displayed in table 7.1; other time points not shown). One notable exception was KC (figure 7.14): NOD mice exhibited significantly higher levels in pleural exudates, lower levels in the serum and as a consequence a much greater gradient of KC from exudate to serum (3.2 ± 0.8 vs. 0.6 ± 0.1; NOD vs. C57BL/6; p < 0.05, student's t test). This is interesting and rather unexpected, since peak PMN recruitment at 24 hours was similar between the 2 strains. There are a number of potential explanations for this anomaly. It could be explained by defective migratory ability of NOD PMN in response to chemokines or a reduced responsiveness of NOD PMN to KC. However, an alternative explanation may be that KC levels at 24 hours are less critical than at earlier time points: Jean-Frncois Cailhier (Cailhier et al., 2006) found that KC levels peaked at 3 hours in CG pleurisy.

In order to obtain a more complete picture of the cytokine and chemokine kinetics, it would be critical to examine levels at earlier time points in CG pleurisy. However, bearing in mind that the chemokine and cytokine responses *in vivo* during TG

peritonitis did not give a clear mechanism for the diminished recruitment of leukocytes, additional mechanisms may be involved during CG pleurisy. The numbers of circulating leukocytes were determined and experiments were undertaken to determine whether NOD mice are capable of mounting a vigorous inflammatory response in a less Mφ dependent model of inflammation.
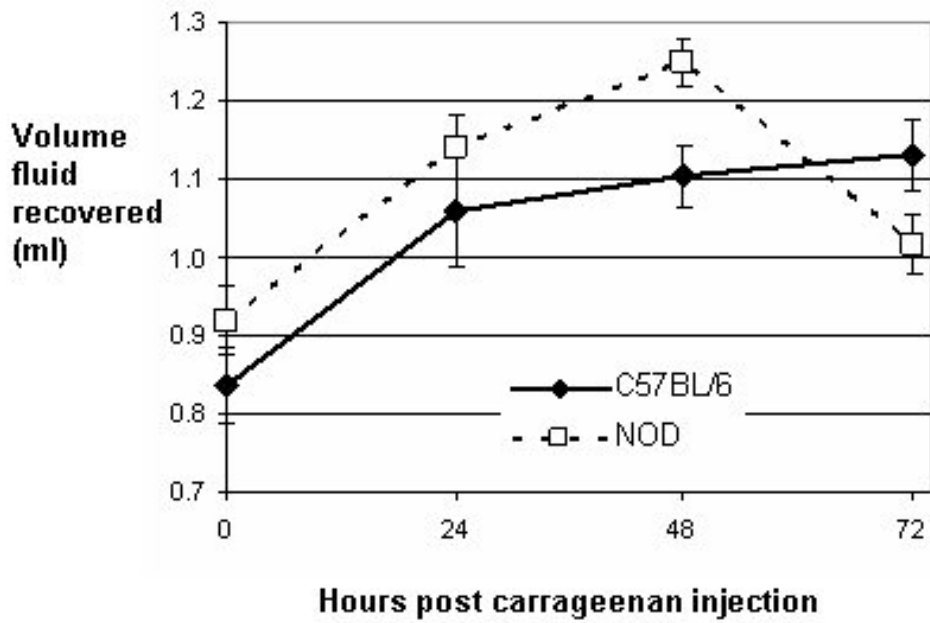
Figure 7- 9   Analysis of volumes of recovered pleural lavage fluid
Pleurisy was induced with an intra-pleural injection of 0.1ml 1% CG. Pleural lavage was performed with 1ml 3.88% sodium citrate. Volumes of fluid recovered were accurately weighed to measure of the volume present. 6 mice were used per time point; C57BL/6 mice in solid lines, NOD in dashed. There were no significant differences in the volumes of fluid recovered at any time point examined; C57BL/6 vs. NOD; 2-way ANOVA
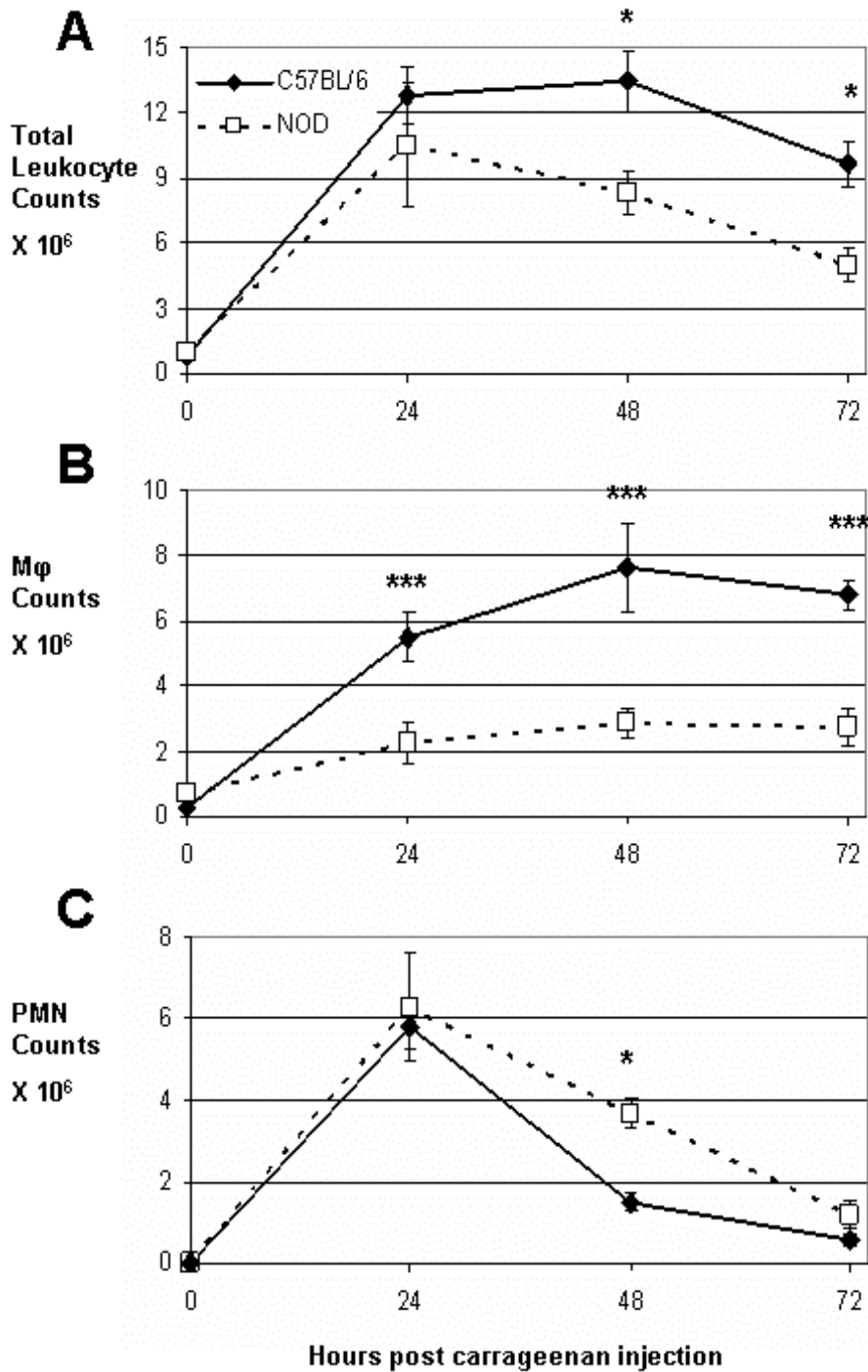
Figure 7- 10   Analysis of leukocyte numbers in CG pleurisy
Pleurisy was induced with an intra-pleural injection of 0.1ml 1% CG. Pleural cells were recovered by lavage, immunolabeled and analysed by flow cytometry. 6 mice were used per time point; C57BL/6 mice in solid lines, NOD in dashed. NOD recruitment of leukocytes was reduced compared to C57BL/6 controls (A), with a striking failure to recruit Mφ (B). In contrast to TG peritonitis, PMN recruitment was similar in both strains, although PMN clearance was less rapid in NOD mice (C). *** $p < 0.001$, * $p < 0.05$; C57BL/6 vs. NOD; 2-way ANOVA

236
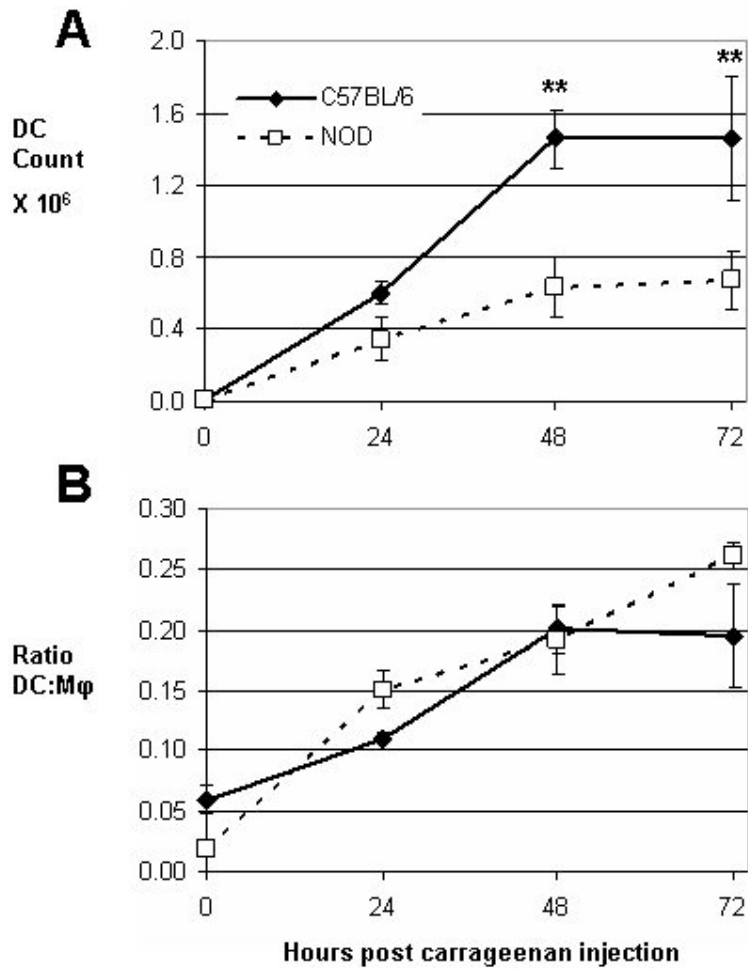
Figure 7- 11   Analysis of DC numbers and comparison to Mφ numbers in CG pleurisy

Pleurisy was induced with an intra-pleural injection of 0.1ml 1% CG. Pleural cells were recovered by lavage, immunolabeled for CD11c and then analysed by flow cytometry. 6 mice were used per time point; C57BL/6 mice in solid lines, NOD in dashed lines. Numbers of DC within the inflammatory milieu were diminished in NOD mice compared to C57BL/6 controls (A). However the reduction in DC numbers was proportional to Mφ numbers, with a similar DC:Mφ ratio as control mice at all time points examined (B). ** $p < 0.01$; C57BL/6 vs. NOD; 2-way ANOVA
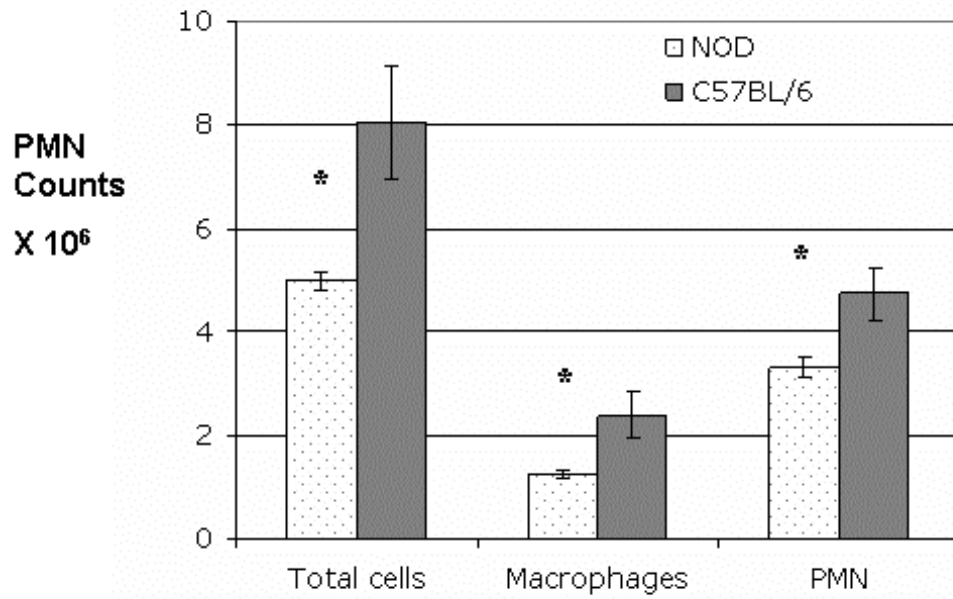
Figure 7- 12   Analysis of leukocyte numbers in CG pleurisy in female mice at 24 hours
Pleurisy was induced with an intra-pleural injection of 0.1ml 1% CG. 24 hours later pleural cells were recovered by lavage, immunolabeled and analysed by flow cytometry. 6 mice per strain were used; C57BL/6 mice in solid bars, NOD in polka dots. NOD mice exhibited reduced recruitment of total leukocytes, Mφ and PMN. * $p < 0.05$; C57BL/6 vs. NOD; Student's t test
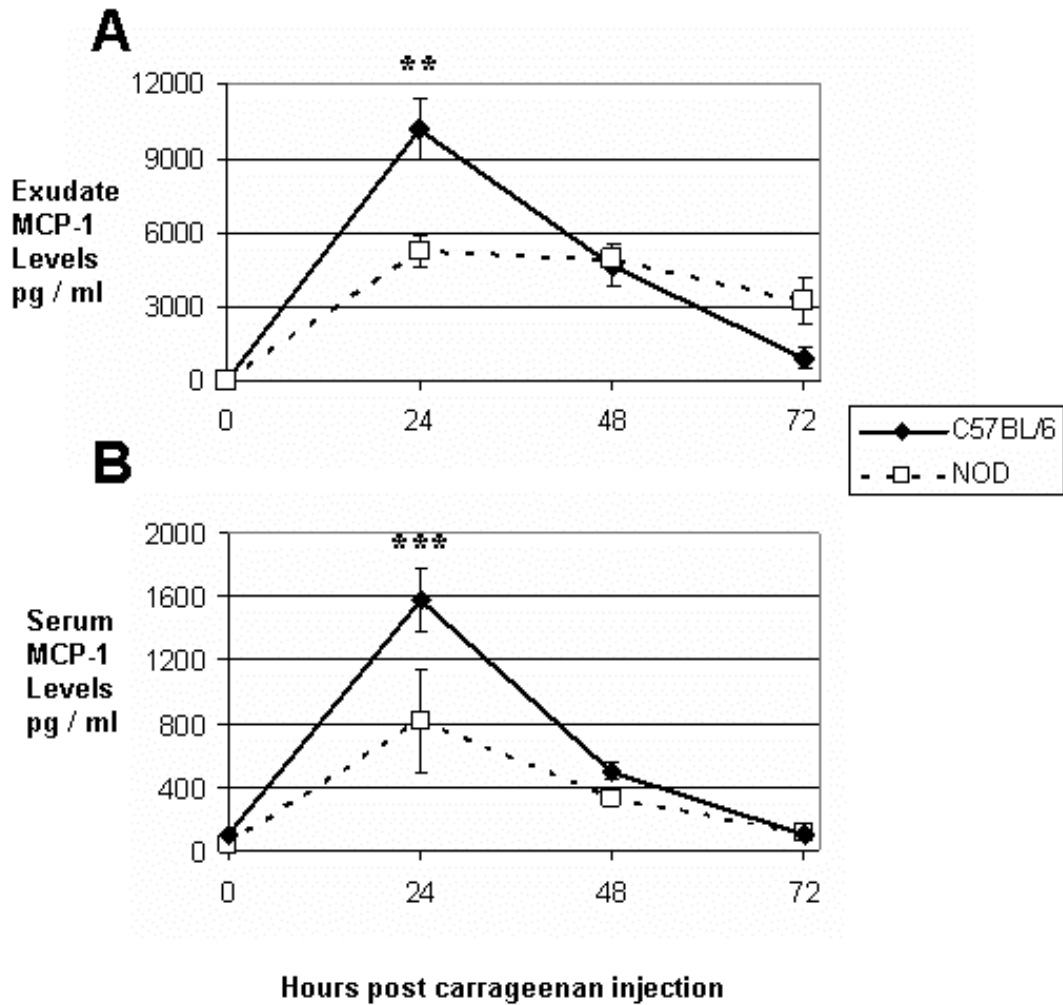
Figure 7- 13   Analysis of MCP-1 levels during CG pleurisy
Pleurisy was induced with an intra-pleural injection of 0.1ml 1% CG. The mice were sacrificed by exsanguination under general anaesthesia, blood was harvested, spun down and the serum decanted for analysis. Pleural inflammatory exudate was recovered by pleural lavage, cells removed by centrifugation and supernatants decanted for analysis. MCP-1 levels within the serum and exudate samples were measured by CBA. 6 mice were used per time point; C57BL/6 mice in solid lines, NOD in dashed lines. Peak MCP-1 levels in both the exudate (A) and serum (B) were significantly lower in the NOD mice. *** $p < 0.001$, ** $p < 0.01$; C57BL/6 vs. NOD; 2-way ANOVA.

239
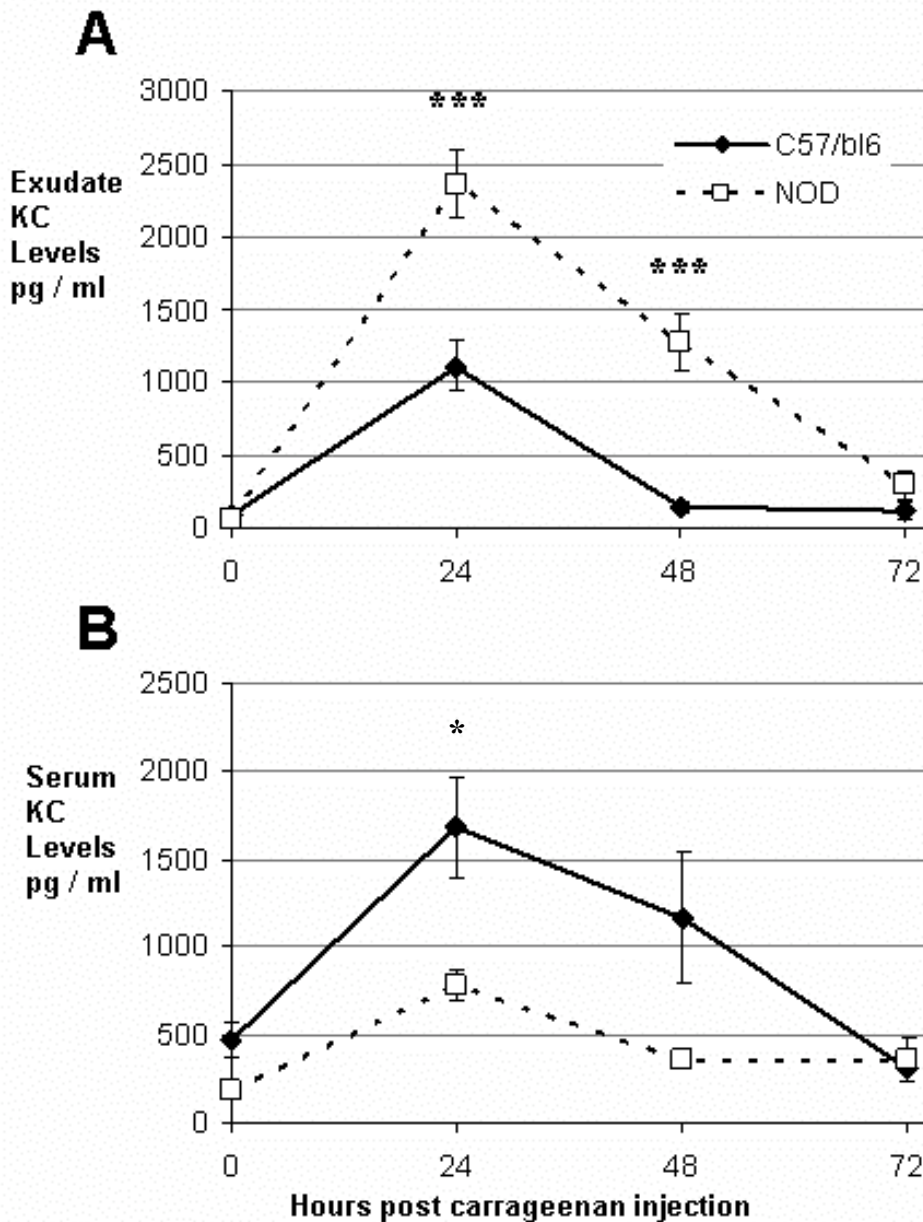
Figure 7- 14   Analysis of KC levels during CG pleurisy
Pleurisy was induced with an intra-pleural injection of 0.1ml 1% CG. The mice were sacrificed by exsanguination under general anaesthesia, blood was harvested, spun down and the serum decanted for analysis. Pleural inflammatory exudate was recovered by pleural lavage, cells removed by centrifugation and supernatants decanted for analysis. KC levels within the serum and exudate samples were measured by ELISA. 6 mice were used per time point; C57BL/6 mice in solid lines, NOD in dashed lines. KC levels in the exudate (A) appear higher in the NOD mice whereas KC levels in the serum (B) appeared higher in the C57BL/6 strain significantly lower in the NOD mice. *** $p < 0.001$, * $p < 0.05$; C57BL/6 vs. NOD; 2-way ANOVA

24 hour	NOD mice		C57BL/6 mice	
time point	pg/ml	(sem)	pg/ml	(sem)
Exudate				
MIP-2	41	(10.5)	28	(7.0)
TNF α	54	(11.7)	42	(4.0)
IL-10	82	(9.3)	130	(22.8)
IFN γ	20	(3.3)	22	(6.7)
Serum				
MIP-2	32	(8.1)	66	(8.1)
TNF α	20	(0.6)	29	(2.6)
IL-10	30	(17.3)	31	(6.6)
IFN γ	8	(0.5)	14	(2.0)

Table 7- 1   Analysis of cytokine and chemokine levels 24 hours after initiation of CG pleurisy
Pleurisy was induced with an i.pl injection of 0.1ml 1% CG. The mice were sacrificed by exsanguination under general anaesthesia, blood was harvested, spun down and the serum decanted for analysis. Pleural inflammatory exudate was recovered by pleural lavage, cells removed by centrifugation and supernatants decanted for analysis. The levels of chemokines and cytokines within the serum and exudates were measured by either ELISA or CBA. 6 mice were used per time point. No significant differences are evident between NOD and C57BL/6 mice 2-way ANOVA.

7.4 CIRCULATING LEUKOCYTES

7.4.1 Circulating leukocyte numbers are comparable between NOD and C57BL/6 mice

Clearly any inflammatory response will be influenced by the numbers of circulating leukocytes. It was thus necessary to determine whether the differences in the inflammatory responses between NOD and C57BL/6 mice merely reflected lower circulating leukocyte levels.

Blood was obtained by a tail bleed from 6 female NOD mice aged 8 to10 weeks, together with 4 aged and sex matched C57BL/6 controls and analysed by flow cytometry as described in chapter 2. No difference in the total numbers of circulating monocytes was evident between the strains although there was a trend for lower levels in NOD mice. NOD mice, however, were noted to have a reduced population of circulating GR-1^{HI} monocytes (figure 7.15A). Importantly, no differences were seen in the numbers of circulating PMN between strains (figure 7.16).

Geismann et al (Geissmann et al., 2003) described 2 distinct populations of monocytes that can be differentiated by the level of expression of GR-1. GR-1^{HI} monocytes home to sites of inflammation whilst GR-1^{LO} monocytes differentiate into resident Mφ populations. One possible explanation for the lower circulating numbers of GR-1^{HI} monocytes of NOD mice could be that these 'pro-inflammatory' monocytes are sequestered within areas of pancreatic inflammation (insulitis) thereby lowering circulating numbers. The difference in the levels of GR-1^{LO} monocytes between NOD and C57BL/6 mice may also be a sufficient explanation for the reduced levels of Mφ recruited to the inflamed peritoneum and pleural cavity in NOD mice.

Young male NOD mice are much less likely to have significant insulitis. Circulating leukocyte numbers were therefore determined in 6 male NOD mice aged 5 weeks together with age and sex matched C57BL/6 controls. In this case, the NOD mice had significantly reduced levels of total circulating monocytes combined with significantly fewer numbers of GR-1^{HI} monocytes in their peripheral blood. No significant differences were observed in the number of circulating GR-1^{LO} monocytes (figure 7.15B) or PMN (figure 7.16).
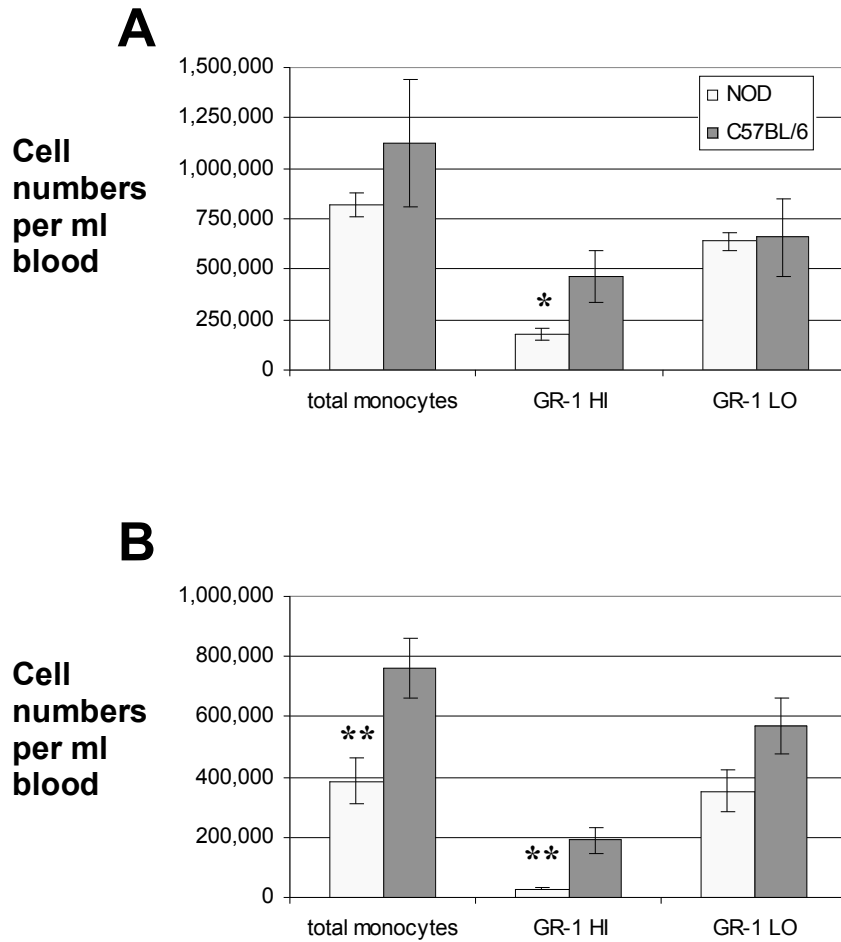
Figure 7- 15   Analysis of circulating monocytes numbers
Peripheral blood was obtained by tail bleeds and immunolabeled prior to red cell lysis. Leukocyte numbers were analysed by flow cytometry. Graph (A) shows data from 8 to 10 week old female mice; 6 NOD mice and 4 matched C57BL/6 mice. Graph (B) shows data from 5 week old male mice; 6 mice per group; C57BL/6 in solid bars, NOD mice in polka dot. ** $p < 0.01$, * p , 0.05; NOD vs. C57BL/6; Student's t test.
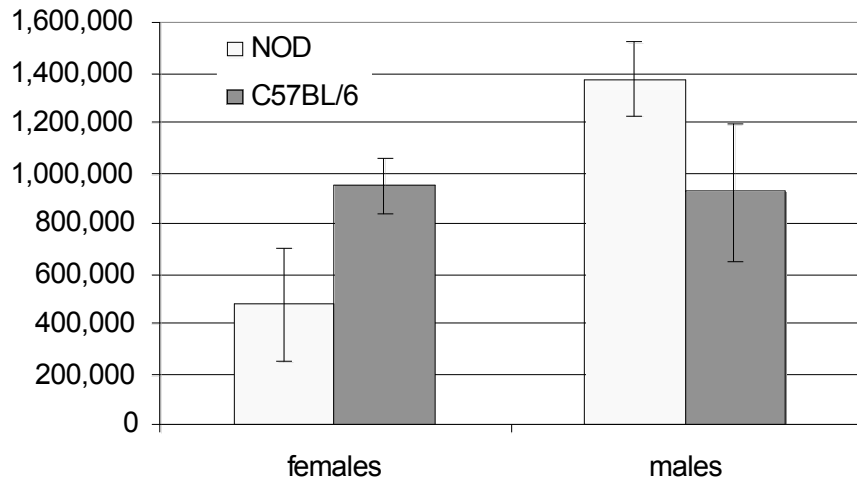
Figure 7- 16   Analysis of circulating PMN numbers per ml of whole blood
Peripheral blood was harvested by tail bleed and stained prior to red cell lysis. PMN numbers were analysed by flow cytometry. No significant differences were seen in the circulating numbers of PMN in 2 different experiments. The first experiment used female mice aged from 8 to 10 weeks old; 6 NOD mice and 4 matched C57BL/6 mice. The second experiment used 5 week old male mice, 6 mice per group. C57BL/6 mice in solid bars, NOD mice in polka dot. Data analysed by student's t test.

7.5 DELAYED-TYPE HYPERSENSITIVITY MODEL OF PLEURISY

It was demonstrated that NOD mice exhibited diminished leukocyte recruitment in TG peritonitis and CG pleurisy. Markedly reduced Mφ recruitment was characteristic of both models of inflammation in the NOD mouse compared to C57BL/6 mice. Although reduced PMN recruitment was clearly part of the phenotype of NOD TG peritonitis, it is a little less clear whether the same holds true for CG pleurisy as similar peak PMN infiltration as control mice was evident on one occasion (figure 7.10C) and slightly reduced numbers were evident at the same time point on a second occasion (figure 7.12). Diminished levels of MCP-1 were found in NOD mice during CG pleurisy in both serum and pleural exudate but no differences in MCP-1 levels were identified in the peritoneal lavage fluid during TG peritonitis. Similarly no other consistent defects in chemokine or cytokine production were identified *in vivo*.

CG and TG were used as inflammatory stimuli principally because resident Mφ within the pleural and peritoneal cavities respectively are critical to the subsequent inflammation(Cailhier et al., 2005; Cailhier et al., 2006). If reduced pro-inflammatory Mφ function (as evident *in vitro*) and not defective leukocyte migration nor reduced numbers of circulating GR-1^{HI} monocytes were to underlie the defective leukocyte recruitment, then it would be reasonable to hypothesise that NOD mice would mount a vigorous inflammatory response in a model of inflammation that was less dependent on resident Mφ function. Pleurisy can be initiated as part of a delayed hypersensitivity reaction in which CD4^{+} T cells rather than resident Mφ are critical. The model of DTH pleurisy was therefore employed to test this hypothesis.

7.5.1 NOD mice exhibit a vigorous inflammatory response during DTH pleurisy

24 male NOD mice aged 6 to 10 weeks, together with age and sex matched C57BL/6 controls, were divided into 4 groups to give similar time points to the CG pleurisy model. Three mice were allocated to the zero time point and 7 mice to each of the 24, 48 and 72 hour time points. DTH pleurisy was initiated as previously described. In brief, all mice were injected intradermally at the base of the tail with 0.1ml 1% methylated bovine serum albumin (meth' BSA) in Complete Freud's Adjuvant (CFA) on day -12. Mice allocated to the zero time point group were sacrificed on day zero whilst all remaining mice were injected with 0.1ml meth' BSA i.pl and

sacrificed 24, 48 or 72 hours later as appropriate. Mice were sacrificed by exsanguination under general anaesthesia. Pleural inflammatory cells and serum was harvested and analysed in a similar fashion to CG pleurisy above.

Both strains of mice produced a vigorous inflammatory response to the i.pl injection of meth' BSA. NOD mice, however, produced a much greater volume of inflammatory exudate (figure 7.17) and recruited greater numbers of leukocytes (figure 7.18A). NOD mice appeared slow to initially recruit Mφ, but the numbers of Mφ recruited by NOD mice exceeded those of the C57BL/6 controls by the 72 hour time point (figure 7.18B). Similarly PMN recruitment by NOD mice exceeded that of control C57BL/6 mice (figure 7.18C).

Thus, depending on the stimulus, NOD can generate a vigorous immune response. This is perhaps not surprising in a mouse strain that develops autoimmunity with the resultant destruction of pancreatic Beta cells.

Hours post meth'BSA injection
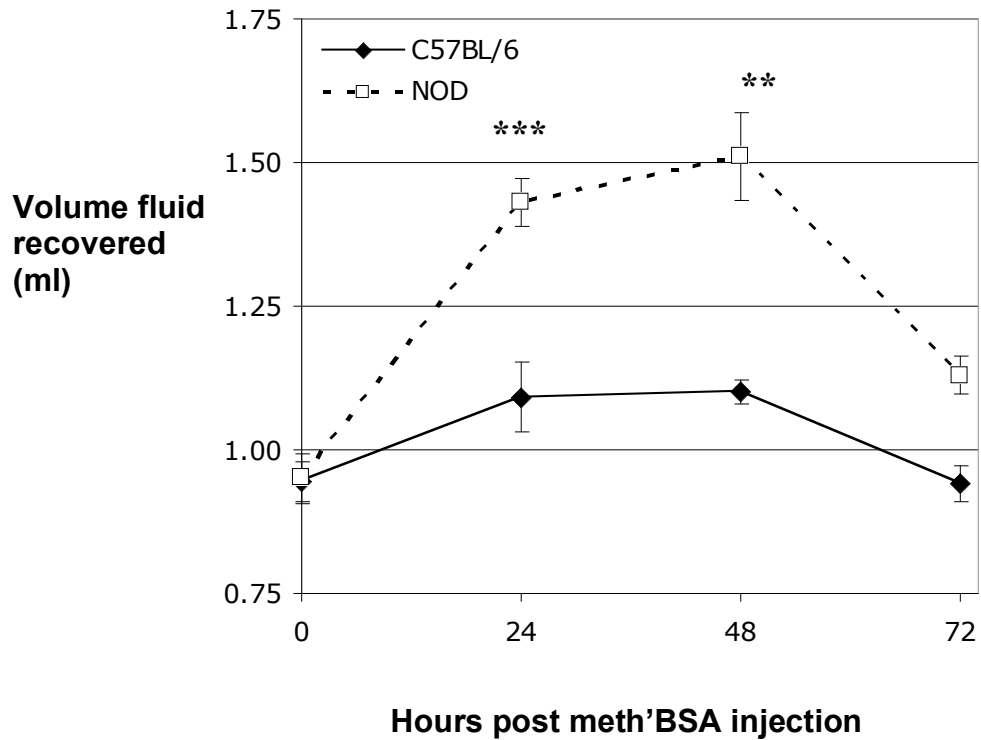
Figure 7- 17   Analysis of pleural lavage volumes during DTH pleurisy
Pleurisy was induced with an intra-pleural injection of 0.1ml methylated BSA 12 days after sensitisation. Pleural lavage was performed with 1ml 3.88% sodium citrate. Volumes of fluid recovered were accurately weighed to measure the volume. There were 3 mice per group at the zero time point with 7 mice per group for all subsequent time points: C57BL/6 mice in solid lines, NOD mice in dashed lines. NOD mice produced significantly more inflammatory exudate; *** $p < 0.001$, ** $p < 0.01$; C57BL/6 vs. NOD; 2 way ANOVA
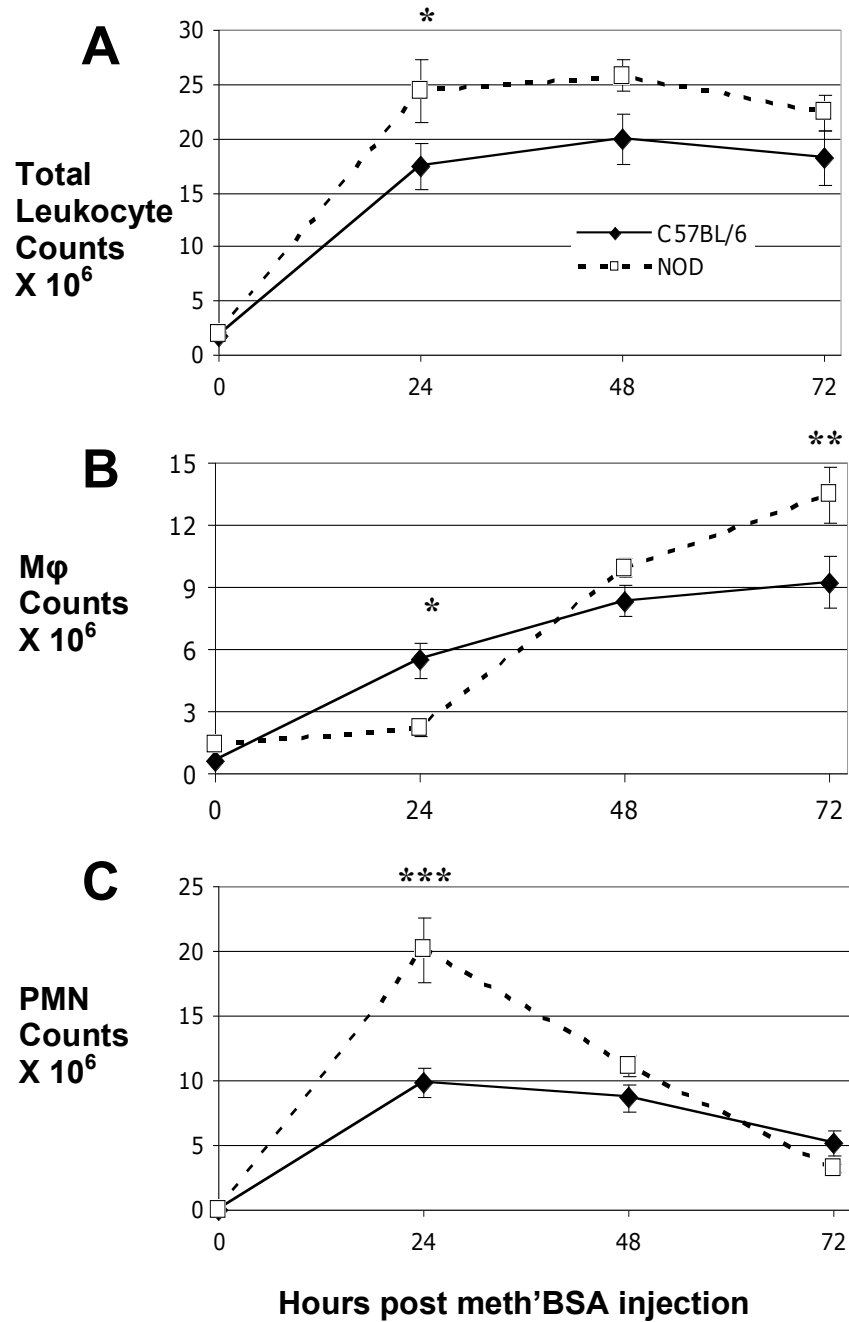
Figure 7- 18   Analysis of leukocyte recruitment during DTH pleurisy
Pleurisy was induced with an intra-pleural injection of 0.1ml methylated BSA 12 days after sensitisation. Pleural cells were recovered by lavage, immunolabeled and analysed by flow cytometry. There were 3 mice per group at the zero time point with 7 mice per group for all subsequent time points; C57BL/6 mice in solid lines, NOD mice in dashed lines. NOD mice recruited significantly more leukocytes including both PMN and Mφ. *** $p < 0.001$, ** $p < 0.01$, * $p < 0.05$; C57BL/6 vs. NOD; 2 way ANOVA

7.6 SUMMARY

In this chapter it has been shown:

In Mφ dependent models of inflammation, NOD mice have a grossly impaired ability to mount an inflammatory response with reduced total leukocyte numbers as well as Mφ and PMN infiltration in TG peritonitis and CG pleurisy. Lymphocyte recruitment was also less in the NOD mouse during TG peritonitis.

The pattern of monocyte recruitment, as well as absolute numbers, was abnormal. NOD mice exhibited a diminished reduction in mature Mφ numbers and grossly impaired influx of inflammatory monocyte/Mφ.

The ratio of DC to Mφ during CG pleurisy was unaffected suggesting that the defective maturation of NOD DC *in vitro* was not relevant *in vivo.*

No gross abnormality was identified in the production of chemokines or cytokines during TG peritonitis, although reduced levels of MCP-1 were identified during CG pleurisy.

Circulating levels of GR-1^{HI} monocytes were reduced in the NOD mice. Since previous work suggests that these monocytes become inflammatory Mφ the reduced numbers of GR-1^{HI} monocytes could explain, at least in part, the diminished Mφ recruitment.

The defective inflammatory phenotype in TG peritonitis is independent of idd18, suggesting no involvement of the *vav3* gene putatively linked to impaired AC phagocytosis in NOD Mφ.

In DTH pleurisy, an immunological T cell driven and less Mφ dependent model of inflammation, NOD mice are capable of mounting a very vigorous inflammatory response with robust leukocyte infiltration.

Chapter 8. Discussion

8.1 MACROPHAGES FROM NOD MICE EXHIBIT DEFECTIVE PHAGOCYTOSIS

An *in vitro* phagocytic defect in Mφ derived from NOD mice was first described by O'Brien and colleagues (O'Brien et al., 2002) with further work providing evidence of defective AC phagocytosis *in vivo* (O'Brien et al., 2006). Their seminal studies, however, restricted the phagocytic defect to AC, as the phagocytic clearance of polystyrene beads was comparable between Mφ derived from NOD and control strains. Defective AC phagocytosis was more pronounced in female mice and a diminution of the defect was observed as NOD mice aged (O'Brien et al., 2002)(O'Brien et al, 2002).

O'Brien's group had previously described the wave of apoptosis evident within the pancreas during the neo-natal period in various strains of mice as the pancreas is re-modelled for adult life. Increased numbers of free AC were observed in pancreas of NOD mice compared to control strains (Trudeau et al., 2000). As discussed in chapter 1.5.2, there is compelling circumstantial evidence linking defective clearance of AC to later development of systemic autoimmune diseases such as SLE. O'Brien and colleagues argued that the defective clearance of apoptotic beta cells within this very narrow time frame in the neonatal period contributed to organ-specific autoimmunity, resulting in the development of diabetes in female NOD mice (O'Brien et al., 2002).

8.1.1 NOD mice exhibit a phagocytic defect for apoptotic cells and latex beads but not IgG opsonised pneumococci *in vitro*

This study demonstrated (chapter 3) that the phagocytic defect evident in NOD Mφ *in vitro* is far more pervasive than originally suggested by O'Brien and colleagues. Whilst PMφ from young female NOD mice clearly exhibited defective clearance of AC, the defective clearance of latex beads was equally evident (chapter 3.2.1). Furthermore, in additional studies we clearly demonstrated that the defect was evident in PMφ and BMDMφ from older NOD mice (chapter 3.2.3).

O'Brien and colleagues in their original paper had noted NOD-derived PMφ exhibited almost normal phagocytic clearance of apoptotic thymocytes opsonised with monoclonal anti-murine anti-CD3 Ig G antibodies (O'Brien et al., 2002). Likewise we found the *in vitro* clearance of pneumococci opsonised with IgG was

comparable between NOD and C57BL/6 derived Mφ (chapter 3.2.2). The phagocytic defect therefore does not apply to all particles, at least *in vitro*.

8.1.2 NOD mice exhibit a phagocytic defect for apoptotic cells and latex beads *in vivo*

As discussed in chapter 4, the assays employed by O'Brien and her colleagues to assess phagocytic clearance of AC *in vivo* (O'Brien et al., 2006) were potentially flawed. Counting and comparing free AC numbers within thymuses of NOD and C57BL/6 mice takes no account of the previously published observations that NOD thymocytes are resistant to undergoing apoptosis; a phenotype of NOD mice linked to idd 6 (Bergman et al., 2003). Equally, measuring AC phagocytosis by performing cytospins of PMφ at various time points after an injection of AC into the peritoneal cavity fails to appreciate the dynamic nature of peritoneal cell kinetics and the fact that PMφ localise to the greater omentum or exit the peritoneal cavity following the phagocytosis of AC and are therefore not retrievable by peritoneal lavage (Simon Watson, PhD thesis, University of Edinburgh).

We elected to utilize the *in vivo* phagocytosis assay employed by Phillip Taylor and colleagues (Taylor et al., 2000) and adapted by Simon Watson (PhD thesis, University of Edinburgh). We concentrated on the number of free AC recovered by peritoneal lavage (counted by flow cytometry) at various time points after the injection of a known number of AC and made no attempt to assess cytospins. The numbers of PMφ available to phagocytose AC were also counted at each time point. This assay made the assumption that loss of free AC was a surrogate marker for phagocytic clearance by PMφ.

This assay demonstrated that NOD and C57BL/6 mice appeared to clear AC with equal efficiency from the peritoneal cavity, but NOD mice had considerably more PMφ *in situ* than C57BL/6 mice to ingest the administered AC (figure 4.1). Mathematically modelling of the data was undertaken by Professor Jonathan Sherrat (chapter 4.2.3) and a clear phagocytic defect was unmasked. Interestingly mathematical modelling was able to extract additional information from the experimental data. For example NOD PMφ would take approximately 30 minutes to clear an AC compared to 15 minutes for C57BL/6 PMφ, at the time point when there was 2 million free AC within the peritoneum. Moreover the rate limiting step for the

NOD PMφ appeared to be the ingestion and not the locating and binding of the AC, whereas the opposite was true for C57BL/6 PMφ. Phagocytosis of latex beads by NOD PMφ was also reduced *in vivo* (chapter 4.2.4), confirming the *in vitro* studies.

8.1.3 The mechanism underlying the phagocytic defect appears consistent with dysfunction of the *Vav3* gene

Although phagocytic defects in NOD Mφ have been identified and published as discussed above, the underlying mechanism has remained elusive. Following confirmation of the previously published work of O'Brien and colleagues, that NOD Mφ exhibited defective clearance of AC and having extended these findings to other particles as discussed above, we set about to dissect the underlying mechanism.

Initial attempts concentrated on looking for differences between NOD and C57BL/6 mice in the quantity of mRNA present in comparable Mφ populations for certain receptors known to be involved in phagocytic clearance of AC (table 1.4). The quantity of mRNA present was used as a surrogate marker for receptor production. BMDMφ and PMφ from each strain were assessed for a range of receptors and the mRNA for each quantified by real time PCR. No consistent differences emerged between the two strains for both Mφ populations assessed (figures 5.1 and 5.2). Surface expression of some of these receptors was assessed by flow cytometry and compared across the 2 strains. Unfortunately attempts were limited by the avidity with which murine antibodies for these receptors bound to PMφ (chapter 5.2.2). However, as with the mRNA studies above, no clear, pattern emerged.

These early studies were always 'fishing expeditions' dependent on the availability of PCR probes and monoclonal antibodies. As additional data accumulated from the *in vitro* phagocytosis assays it became clear the defect was more profound than merely affecting the clearance of AC. The mechanism underlying defective phagocytosis of a wider range of particles could easily lie within intracellular pathways as well as surface receptors.

The experimental strategy was therefore changed and rather than continue with assessing surface receptors or mRNA, it was decided to use NOD congenic strains. As discussed in chapter 1.2.2, NOD congenic strains are essentially NOD mice with small genetic areas (idd loci) replaced with genetic material from non-autoimmune prone strains, usually C57BL/6 mice. As a consequence of switching these small

chromosomal segments, NOD congenic mice are protected from developing diabetes. Since clearance of AC cells by Mφ *in vivo* is perhaps more physiologically relevant than *in vitro* data, it was decided to use the peritoneal *in vivo* assay to compare NOD, C57BL/6 and various NOD congenic strains of mice. Linda Wicker at the Cambridge Medical Research Institute (CMRI), an international authority on the genetics of NOD mice, was consulted and a range of congenic strains made available for this purpose.

NOD mice bred at the CMRI are from the Taconic colony established by Merck in the United States of America. NOD mice at the animal facility, Little France, Edinburgh were purchased from Charles River, France. The two strains appear subtly different in that those from France had consistently higher numbers of resident PMφ then C57BL/6 mice but cleared similar numbers of AC whilst Taconic NOD mice had similar numbers of PMφ to control mice and cleared fewer AC. These two NOD colonies separated from the original Japanese colony with about 30 back-cross generations between them and subtle genetic differences presumably explain this difference.

The *in vivo* phagocytosis of AC of several NOD congenic strains was compared to NOD and C57BL/6 mice. In this manner idd 3, 5, 9, 10 and 18 were assessed for the gene or genes underlying defective phagocytosis of AC. The results were quite unequivocal (chapter 5.2.3). NOD mice with C57BL/6 genes covering idd 3/10/18 phagocytosed AC just as rapidly as C57BL/6 mice, whilst NOD mice with a combination of C57BL/6 or C57BL/10 genes covering idd 3/10, idd 3/5 or idd 9, cleared AC at rates comparable with NOD mice. By implication therefore the NOD genes responsible for defective phagocytosis lie within this region on chromosome 3. Scrutiny of the gene within idd 18 indicates that *Vav3* is the only candidate gene that may explain defective phagocytosis (Maier and Wicker, 2005).

Furthermore the fact that the phagocytic defect localised to a diabetes susceptibility locus is further circumstantial evidence linking defective phagocytosis to autoimmunity, although not necessarily organ specific. It is possible that the phenotype contributes to the autoimmune-permissive genetic background of NOD mice rather than autoimmune diabetes *per se*.

As a GEF, *Vav3* is an interesting candidate gene. It was discussed in chapter 1.4.2 how GEFs, including those of the *Vav* family, were recruited to nascent phagosomes following ligation of FcR and CR. Interestingly, however, phagocytosis following FcR or CR ligation appears to use subtly different intracellular pathways to activate actin polymerisation to achieve phagocytosis (Hall et al., 2006). Although GEF were necessary to affect actin polymerisation for both pathways, *Vav* appeared to be unnecessary for FcR mediated phagocytosis of particles opsonised with IgG. This sits very comfortably indeed with our data that showed no phagocytic defect *in vitro* for pneumococci opsonised with IgG (chapter 3.2.2). There are however a couple of points that require further consideration and explanation.

There are 3 isoforms of *Vav* within the murine genome; *Vav1* is confined to haematopoietic cells whereas *Vav2* and *Vav3* are more ubiquitous. Amy Hall and colleagues found that *in vitro* both *Vav1* and *Vav3* had to be knocked out before a phagocytic defect could be elicited (Hall et al., 2006). However, *in vitro* work using BMDMφ, does not always predict *in vitro*, let alone *in vivo* findings with resident PMφ, as clearly demonstrated by further work in this study (chapters 6 and 7). Alternatively, additional unknown factors related specifically to NOD Mφ may function in such a way to make the loss of *Vav3* more critical.

Menna Clatworthy and colleagues in Cambridge demonstrated that Mφ from autoimmune prone strains of mice, including NOD mice, express 50% less FcγR2b on their cell surface (Clatworthy and Smith, 2004). FcγR2b is an inhibitory FcR, and cross ligation with an activating FcγR results in inhibition of phagocytosis. Loss of FcγR2b is therefore associated with increased phagocytosis. As predicted, in their experiments C57BL/6 Mφ derived from FcγR2b KO mice exhibited a marked increase in phagocytosis of opsonised pneumococci compared to wild-type Mφ (Clatworthy and Smith, 2004). Ken Smith's group in Cambridge have clearly demonstrated how the activity of FcγR2b may control the effective balance between phagocytic clearance of bacterial or malarial parasites on the one hand and autoimmune diseases such as SLE on the other in both mice and humans (Clatworthy and Smith, 2004; Clatworthy et al., 2007; Floto et al., 2005). From this data, NOD Mφ would be expected to exhibit increased phagocytosis of IgG opsonised particles such as pneumococci compared to C57BL/6 mice rather than comparable phagocytosis. Once again however, these were *in vitro* experiments and not *in vivo*.

Furthermore, they were between FcγR2b KO and wild-type (C57BL/6) PMφ and there may be additional factors pertaining to NOD PMφ in particular, that explain the effects we observed.

8.1.4 Further work

Additional work is required to prove the link between the phagocytic defect observed in NOD-derived Mφ and idd 18. As discussed above, the data currently available link idd 18 to the defect by exclusion: the defect was rescued by C57BL/6 genes across idd 3/10/18 but not by control genes across idd 3/10. It is just possible the observed phagocytic defect results from multiple genes, some of which may lie in (or be influenced by) idd 3 or idd 10 plus idd 18. Further *in vivo* phagocytosis experiments are planned comparing NOD and C57BL/6 mice with two additional NOD congenic strains that replace idd 18 and idd 10 individually. If the phagocytosis of AC and beads is rescued within the idd 18 NOD congenic strain, whilst it is still evident in the idd 10 NOD congenic strain, defective phagocytosis would have been conclusively tied to the genes with idd 18 on murine chromosome 3.

If the link between defective phagocytosis and idd 18 is proven by the strategy described above, additional steps could be taken to specifically link the defect in NOD Mφ to *Vav3*.

- The definitive experiment would be to rescue the defect by expressing C57BL/6-derived *Vav3* within NOD Mφ. This could potentially be achieved using viral vectors containing C57BL/6-derived *Vav3* to transfect NOD Mφ.

- Alternatively small interfering RNA (siRNA) technology could be employed to knock down *Vav3* in C57BL/6 mice *in vitro* or *in vivo*, with the hypothesis that a similar phagocytic defect as seen with NOD mice would then emerge.

- Western blots could be used to quantitatively measure the expression of *Vav3* within NOD Mφ compared to C57BL/6.

- Over-expression of constituitively active Rac within NOD Mφ should rescue the phagocytic defect if due to defective *Vav* genes (Hall et al., 2006).

8.2 BONE MARROW DERIVED MACROPHAGES AND RESIDENT MACROPHAGES FROM NOD MICE EXHIBIT DIVERGENT PHENOTYPES *IN VITRO*

Having examined the phagocytic defect present within NOD-derived Mφ, it was felt important to assess another key aspect of Mφ function: the ability to orchestrate inflammation. The literature appears divided as to whether Mφ from NOD mice are hyper-inflammatory (Sen et al., 2003; Stoffels et al., 2004) or hypo-inflammatory (Fan et al., 2004) in their cytokine and chemokine responses to inflammatory stimuli *in vitro*.

This study addressed the question by comparing different Mφ populations from NOD and C57BL/6 mice to different pro-inflammatory stimuli. BMDMφ were compared to resident PMφ and resident PLMφ with the different Mφ populations being obtained from the same mice whenever possible. Different time points were assessed (1, 4 and 24 hours) and quiescent chemokine and cytokine responses were measured and compared to stimulation with LPS, TG and CG. The latter two substances were selected as they were to be used for subsequent *in vivo* models of peritonitis and pleurisy respectively. A mixture of pro-inflammatory (TNFα and IFNγ) and anti-inflammatory (IL-10) cytokines were measured together with IL-6, apparently having both pro- and anti-inflammatory properties. MCP-1, an important CC chemokine together with KC and MIP-2, key CXC chemokines, were also assessed. In this manner it was hoped to get a reasonably 'full' picture of how Mφ from the two strains of mice might differ in their response to stimuli.

Our data suggested BMDMφ from NOD mice were much more pro-inflammatory than their C57BL/6 counterparts to all three stimuli assessed (figures 6.2 and 6.3 for responses to LPS; figures 6.4 and 6.5 for responses to CG; figures 6.6 and 6.7 for responses to TG). Levels of pro-inflammatory cytokines and chemokines were higher from NOD mice whilst the levels of the important anti-inflammatory cytokine IL-10 were reduced. As expected, no significant IFNγ was detected as it is predominantly released by T cells

Rather surprisingly however, the data implied resident Mφ populations from the same NOD mice were hypo-responsive to inflammatory stimuli. Although the data for resident PLMφ and PMφ were not as consistent as that seen with BMDMφ across

the time courses, the patterns nevertheless appeared consistent enough (see figures 6.8 through to 6.11 for PLMφ and figures 6.12 through to 6.17 for PMφ). It could be hypothesised that since the resident Mφ were *ex vivo* they had possibly a less uniform exposure to stimuli during maturation than BMDMφ all maturing in the same Teflon pot.

The almost diametrically opposed phenotypes observed between the NOD BMDMφ and resident Mφ may go some way to explain differences in the published literature, particularly as some groups (Fan et al., 2004) worked predominantly with peritoneal Mφ (albeit TG elicited) whilst others used splenic Mφ and BMDMφ (Sen et al., 2003).

The data from this series of experiments also firmly underlines the difficulty of extrapolating data from one Mφ subset to another. BMDMφ are frequently chosen to represent 'generic Mφ' because of the relative ease in obtaining large numbers of them. Our data would argue that whilst useful information can be obtained from BMDMφ, it must be remembered they are always a model for *in vivo* Mφ populations and will not necessarily behave in an identical fashion.

8.2.1 Further work

It was mentioned in chapter 5 that BMDMφ from NOD mice contained significantly more mRNA for CD14 than BMDMφ from C57BL/6 mice (figure 5.1), however no significant differences in CD14 mRNA levels were identified between PMφ from the two strains (figure 5.2). Interestingly, reduced surface expression of CD14 was perhaps apparent on the surface of NOD PMφ (figure 5.3). CD14 functions in conjunction with TLR4 as a receptor for LPS. Although the above data does not offer an explanation for defective phagocytosis apparent in both BMDMφ and PMφ, it does have the potential to explain a heightened pro-inflammatory response to LPS observed by BMDMφ but not PMφ.

Further work quantifying CD14 mRNA in resident PLMφ and likewise quantifying surface expression of CD14 by both BMDMφ and PLMφ may be helpful. If the pattern proves consistent, additional experiments with CD14 blocking antibodies would help to clarify the role CD14 may play in the divergent phenotypes observed between BMDMφ and resident Mφ from NOD mice.

Alternatively, relative activity of the NFκB pathways in these population could be assessed and compared to C57BL/6 Mφ.

8.3 NOD MICE EXHIBIT DEFECTIVE RECRUITMENT OF LEUKOCYTES IN MACROPHAGE-DEPENDENT MODELS OF INFLAMMATION

Having probed the cytokine and chemokines responses of NOD and C57BL/6 Mφ to LPS, CG and TG *in vitro*, it was felt important to try and examine the function of NOD-derived Mφ *in vivo*. TG peritonitis and CG pleurisy were selected as *in vivo* models of inflammation to assess Mφ function because the inflammatory response in both these models was dependent upon the resident Mφ population (Cailhier et al., 2005; Cailhier et al., 2006). In the absence of the resident Mφ the subsequent inflammatory response was extremely muted.

The hypothesis suggested by the *in vitro* data was that since these models were reliant on PMφ function, reduced acute inflammation would be evident in NOD mice. To contrast with these models, the inflammatory response in a model of inflammation considered less dependent on resident Mφ function, DTH pleurisy, was also assessed.

8.3.1 NOD mice recruit fewer leukocytes to TG peritonitis

Paul Potter and colleagues from the Hammersmith Hospital originally published that SLE-prone strains of mice had abnormal inflammatory responses to TG (Potter et al., 2003). Hanli Fan then published several similarities between Mφ from NOD and Lupus-prone strains of mice with TG elicited PMφ from these strains of mice apparently sharing a hypo-responsive cytokine phenotypes (Fan et al., 2004)and abnormal Rho activity (Fan et al., 2006) in the presence of AC or the lipid component of FBS. Gerben Bouma and colleagues subsequently published that NOD mice had an impaired ability to recruit leukocytes to TG peritonitis (Bouma et al., 2005).

Experiments in this study corroborated the findings of Gerben Bouma and colleagues and demonstrated impaired recruitment of leukocytes in response to TG peritonitis. Our data was subtly different insofar as the recruitment deficit we observed was not as dramatic. Bouma et al. noted that Mφ and PMN numbers in NOD mice approached 30% and 15% respectively of those achieved by C57BL/6 control mice

at 24 hours, we recorded values nearer 50% for both leukocyte types (see figure 7.1). Interestingly the cell kinetics we noted bore a striking similarity to those described by Paul Potter and colleagues (Potter et al., 2003). It is quite possible these differences may reflect differences in NOD colonies as described earlier.

Since the earlier work of Jean-Francois Cailhier within our group had emphasised the fundamental importance of resident PMφ in the initiation of TG peritonitis (Cailhier et al., 2005), it was decided to examine the cell kinetics of TG peritonitis in the first 24 hours following TG injection in much greater detail.

Blood borne monocytes, from which tissue Mφ are derived, have a low CD11b and F4/80 expression as assessed by flow cytometry (see figure 2.27B) compared to resident PMφ (see figure 2.22). It therefore seems reasonable to assume Mφ within the peritoneum that have CD11b and F4/80 expression profiles closer to monocytes are likely to represent recently infiltrated inflammatory monocytes / Mφ. On the basis of this assumption an interesting pattern emerged regarding Mφ subtypes within the peritoneum in the first 24 hours after TG injection. C57BL/6 mice promptly 'lost' the mature Mφ phenotype from the peritoneum in a reaction reminiscent of the macrophage disappearance reaction (Melnicoff et al., 1989) and a rapid influx of infiltrating monocytes / Mφ was evident. In contrast, NOD mice retained the mature Mφ within the inflammatory cell infiltrate and had a much slower recruitment of additional monocytes / Mφ (figure 7.5).

In contrast to Mφ recruitment, which was clearly different between the two strains from a very early stage, PMN recruitment in TG peritonitis appears more complicated. Recruitment of PMN up to 4 hours was comparable between NOD and C57BL/6 mice. C57BL/6 mice continued to increase PMN numbers until they appeared to peak at 24 hours whilst, in contrast, NOD mice failed to increase peritoneal PMN numbers beyond the 4 hour time point (figure 7.6).

Thus the data clearly indicated that, as hypothesised and consistent with previously published work, leukocyte recruitment in NOD mice was severely impaired in a Mφ-dependent model of inflammation,

8.3.2 NOD mice recruit fewer leukocytes to CG pleurisy

As mentioned above, CG pleurisy is another well-characterised model of *in vivo* inflammation proven to be dependent on the function of the resident Mφ population (Cailhier et al., 2006). As hypothesised the recruitment of leukocytes by NOD mice was also diminished in this model of inflammation (figure 7.10A). A subtle difference, however, was evident from TG peritonitis. Although monocyte / Mφ recruitment was impaired, PMN recruitment by male mice was remarkably similar (figure 7.10 B and C). This pattern however was not consistent and CG pleurisy within female NOD mice exhibited reduced recruitment of both Mφ and PMN (figure 7.12).

8.3.3 NOD mice exhibit a vigorous inflammatory response to DTH pleurisy

DTH pleurisy is initiated by pleural antigen presenting cells processing antigen, to which the mice had previously been sensitized, and presenting it to $CD4^+$ T cells. These $CD4^+$ cells then release a T_h1 profile of chemokines and cytokines to initiate the inflammatory response. Although monocytes / Mφ are recruited and certainly are involved in the inflammatory response, the inflammation is predominantly considered to be less Mφ dependent.

Using this model of inflammation, injecting methylated bovine serum albumin into the pleural cavity twelve days after sensitization in the presence of complete Freud's adjuvant, we found that the inflammatory response in NOD mice exceeded that observed in the C57BL/6 mice, with increased exudate formation and increased numbers of both monocytes / Mφ and PMN recruited (figures 7.17 and 7.18).

These observations were important, clearly demonstrating that under certain circumstances NOD mice are capable of mounting a robust and exaggerated inflammatory response.

8.4 POTENTIAL MECHANISMS FOR IMPAIRED LEUKOCYTE RECRUITMENT IN TG PERITONITIS AND CG PLEURISY

The inflammatory responses observed in TG peritonitis and CG pleurisy were therefore entirely consistent with the original hypothesis that predicted a diminished inflammatory response in would be observed in NOD mice as a consequence of hypo-responsive resident Mφ populations. The inflammatory response to DTH pleurisy was also consistent with the hypothesis that NOD mice would be expected to mount robust inflammatory responses in models of inflammation less dependent on resident Mφ function.

The next step was to try and isolate if possible which precise aspect of NOD resident Mφ function underpinned the defective recruitment of inflammatory leukocytes, and to assess other potential explanations for the observations made during TG peritonitis, CG pleurisy and DTH pleurisy.

8.4.1 Chemokine and cytokine levels

As mentioned earlier, production of the important CXC chemokine MIP-2 by resident Mφ had been shown to be critical to subsequent PMN recruitment in these inflammatory models (Cailhier et al., 2005; Cailhier et al., 2006). Reduced production of MIP-2 by NOD Mφ was predicted by the *in vitro* data and therefore the first hypothesis to explain the subsequent failure to recruit sufficient PMN in TG peritonitis. It was therefore somewhat surprising to observe extremely similar levels of MIP-2 measured in the peritoneal lavage fluid from the two strains of mice (figure 7.7A). Similarly, no differences were in MIP-2 levels were identified in pleural exudates from NOD or C57BL/6 mice, although key time points have not yet been assessed (table 7.1).

Could differences in the other chemokines measured explain the reduced inflammatory cell infiltrate? Although a few minor differences were identified in pleural chemokine levels between NOD and C57BL/6 mice, as discussed in chapter 7.3.3, they are unlikely to be physiologically important. For example, although KC levels in NOD mice were significantly higher at 24 hours than those observed in C57BL/6 mice, this observation must be treated with caution since KC levels peak much earlier at 3 hours and we do not yet have the data pertinent to this time point. Levels of the powerful CC chemokine MCP-1 were low in the pleural exudates from NOD mice and represent a tempting explanation for reduced monocyte / Mφ

recruitment. However serum levels were similarly low and the exudates-serum gradients, down which infiltrating monocytes would travel, were strikingly similar (figure 7.13). No differences were identified in peritoneal levels of KC or MCP-1 (figure 7.7B and figure 7.7C).

It should be noted however, that the NOD mice had approximately twice as many resident PMφ or PLMφ *in situ* and also retained them for longer within the serosal cavity (at least as far the peritoneum was concerned) to produce the chemokines and cytokines measured. It could be argued therefore that the similar levels of chemokines and cytokines observed *in vivo* were compatible with the differences identified in chemokine production by resident PMφ *in vitro*.

Milky spots on the greater omentum are the major site of influx (or efflux) of leukocytes from the peritoneal cavity (Cranshaw and Leak, 1990). Similar sites are known to occur within pleural cavities (Pereira Ade et al., 1994). If the milky spots in NOD and C57BL/6 mice are comprised of similar Mφ numbers, then it could be argued NOD mice might produce less MIP-2 where it 'really matters', that is to say in the milky spots themselves. However, normal recruitment rates of PMN in the first few hours of TG peritonitis are entirely consistent with similar levels of MIP-2 signal and suggest an alternative explanation beyond chemokine or cytokine production was the cause of the diminished ability of NOD Mφ to mount a robust response to TG peritonitis.

8.4.1.1 *Further work*

Experiments assessing chemokine and cytokine levels in pleural exudates at early time points (1 and 3 hours) following CG pleurisy are planned.

8.4.2 Migratory capabilities of NOD leukocytes

Could impaired migratory capacity of NOD leukocytes explain the diminished leukocyte recruitment observed in TG peritonitis and CG pleurisy? Again it is difficult to argue that a general impairment of migratory ability underlies the recruitment defect if PMN numbers (and therefore rate of PMN migration) are similar between the two strains for the first few hours of TG peritonitis and indeed increased during DTH pleurisy.

Nonetheless, Gerben Bouma and colleagues argued day four TG elicited PMφ from NOD mice demonstrated impaired movement towards MCP-1 in a Boyden chamber *in vitro* (Bouma et al., 2005). However some caution is warranted in the interpretation as both their own data and our data would suggest the inflammatory processes that had recruited and 'programmed' these PMφ were very different between the two strains of mice.

On the other hand, since our data suggested the phagocytic defect observed in NOD mice localised to *Vav3*, a GEF known to be involved in actin polymerisation, cytoskeletal rearrangement and therefore potentially migration, it was considered clearly important to examine whether the impaired recruitment of leukocytes localised to the same gene. As shown by figure 7.8, replacing the NOD *Vav3* gene for C57BL/6 made no difference to the inflammatory response or leukocyte recruitment.

8.4.2.1 *Further work*

The migratory abilities of both resident Mφ (PMφ and PLMφ) and BMDMφ to MCP-1 should be assessed *in vitro* in a Boyden chamber should be assessed, avoiding TG elicited PMφ. Unfortunately it is extremely difficult to obtain sufficient numbers of *ex vivo* PMN for these experiments and TG elicited PMN are best avoided for the same reasons as argued above.

Conducting in vivo migration tests by injecting chemokines directly into peritoneal cavities of NOD and C57BL/6 mice can give data that is difficult to interpret. These experiments, as conducted by Bouma et al. do not just assess leukocyte migration but are also affected by circulating numbers and the inflammatory response engendered by the chemokine itself.

8.4.3 Circulating numbers of NOD leukocytes

Could circulating leukocyte numbers explain the defective recruitment of leukocytes? In a seminal paper Geismann and colleagues (Geissmann et al., 2003) (Geismann et al, 2003) demonstrated two subsets of circulating monocytes, distinguished by their expression of GR-1. GR-1^{HI} monocytes were rapidly recruited into inflamed tissue whereas GR-1^{LO} monocytes remained in the circulation longer and matured into resident tissue Mφ. Our data, in accordance with that of Bouma and colleagues, demonstrated reduced numbers of circulating GR-1^{HI} monocytes in naïve

NOD mice (figure 7.15). This therefore does raise an intriguing explanation for reduced monocyte recruitment and is consistent with the initially slower Mφ recruitment seen in DTH pleurisy (figure 7.18).

Circulating PMN numbers were not significantly different between the two groups of mice. It is thought a large reservoir of PMN capable of rapid mobilization to sites of inflammation is held within the bone marrow by the chemokine SDF-1 (Martin et al., 2003). Although there are no data published regarding whether the size of this 'reservoir' varies between different strains of mice, the presence of a smaller reservoir within the bone marrow of NOD mice could explain the initial normal PMN response we observed in response to TG peritonitis followed by the subsequent failure to increase numbers. It is difficult to reconcile this explanation to the increased inflammatory response seen in DTH, unless the sensitisation procedure itself stimulated NOD mice to somehow increase this pool of PMN within the bone marrow.

8.4.3.1 *Further work*

Assessment of PMN numbers within the bone marrow is not as easy as it initially sounds. It should be possible to harvest femurs and promptly flush the contents into FACS tubes. A single cell suspension could be obtained, washed, stained for GR-1 and analysed by flow cytometry. Naïve mice from different strains could be compared along with mice following an inflammatory stimulus such as TG peritonitis. Lower resting numbers PMN in the bone marrow of NOD mice followed by depletion would support the hypothesis that the diminished PMN recruitment witnessed is merely a reflection of reduced 'PMN reserve'. The main difficulties would be to (a) ensure all PMN from each femur were flushed and counted and (b) take into account variations in femur size. Normalising the data to a control stromal cell is has the potential to correct for both these sources of error. It would also be informative to assess the circulating numbers of leukocytes in the two strains of mice following sensitisation with complete Freud's adjuvant.

8.4.4 Complement component C5a

As discussed in chapter 1.6.4, C5a is a powerful chemotactic agent, principally for PMN but also for monocytes. C5a also up-regulates endothelial adhesion molecules. Several strains of inbred mice, including FVB, DBA, NZB and NOD are known to

be completely deficient in C5 due to a two base "TA" deletion near the 5' end of the gene (Jackson Laboratories data sheets). Could C5a deficiency underlie the impaired recruitment of leukocytes? Although TG peritonitis is thought to be independent of complement (White et al., 2002) and CG pleurisy is thought to be more reliant on complement, in reality inflammation *in vivo* is unlikely to be so clear-cut. As described in chapter 1, the complement system plays an integral part of the whole inflammatory process, triggered by surfaces of pathogens, antibodies and AC.

Olga Stein and colleagues examined TG peritonitis in a range of strains of mice and noted reduced recruitment in four of them: 129/sv, FVB, NZB and A/J (Stein et al., 2006). Strikingly, two of these strains (FVB and NZB) are C5 deficient as mentioned above, making C5 deficiency an attractive mechanism for the underlying defective recruitment of leukocytes in these models.

Bouma and colleagues tried to address this very issue by demonstrating the defect persisted even when C5a alone was used as the inflammatory stimulus in either peritonitis or an air-pouch model of inflammation. The problem with this approach is that it does not get around the fact that an inflammatory response initiated by C5a would be expected to generate further C5a production in C5 sufficient mice and hence enhanced leukocyte recruitment. Therefore although similar levels of C5a were used to initiate the inflammation, subsequent C5a deficiency may still underlie the poor inflammatory response in NOD mice. A similar argument could be used to explain why other chemokines and cytokines used in isolation elicited a diminished inflammatory response in NOD mice.

DTH pleurisy offers some evidence C5a deficiency is not the root cause of the reduced inflammatory response in NOD mice to TG peritonitis and CG pleurisy. Although, as stated earlier, this model is primarily an immunologically driven response, driven by T_h1 $CD4^+$ cells, it is most unlikely that complement activation would not take place in the ensuing inflammation with apoptotic PMN and local tissue damage etc. However, in this setting at least, C5a deficiency does not appear to dampen the immune response and it is quite possible other small complement components such as C3a and C4a (that have similar but weaker actions to C5a) fulfil the functions of C5a in these mice.

8.4.5 Further work

Additional work is requires to prove the hypothesis that the observed hypo-inflammatory responses seen in NOD mice with TG peritonitis and CG pleurisy are indeed due to the hypo-responsive phenotypes of the PMφ and PLMφ respectively.

One interesting way would be to use Mφ depletion models. Richard Lang's group generated transgenic mice expressing human diphtheria toxin receptor under the CD11b promoter in FVB mice (CD11b-DTR), it has been convincingly demonstrated that PMφ ablation results following intraperitoneal injection of toxin (Cailhier et al, 2005). By depleting resident PMφ as above, followed by adoptive transfer of either NOD or C57BL/6 PMφ into the depleted FVB mice immediately prior to initiating CG pleurisy (or TG peritonitis), it should be possible to test the hypothesis directly. Two main assumptions are made in this experiment, (a) NOD and C57BL/6 MHC genes would be equally pro-inflammatory in FVB mice and (b) that within a 24 hour time frame Mφ from both strains of mice would not be rejected. Controls would be required but the experiment would be testing the pro-inflammatory capacity of NOD and C57BL/6 Mφ in comparable *in vivo* environments.

8.5 SUMMARY

The first aim of this thesis was to confirm or refute the phagocytic defect observed in Mφ derived from NOD mice. As discussed above, a phagocytic defect in NOD mice was confirmed both *in vitro* and *in vivo*. The extent of the phagocytic defect was extended beyond that originally published (O'Brien et al, 2002) to include AC, latex beads and un-opsonized pneumococci. Pneumococci opsonized with IgG were phagocytosed *in vitro* without apparent difficulty. Work with NOD congenic strains has identified a prime candidate gene underlying this defect, namely *Vav3*, a Guanidine Exchange Factor. Published work has implicated Vav3 in the down-stream signalling events following phagocytosis via CR but not FcR. Because the phagocytic defect appears to localise to a diabetes susceptibility locus this offers additional circumstantial evidence linking defective phagocytosis to autoimmunity.

The second aim of the thesis was to probe the apparent contradictory nature of the inflammatory phenotype of NOD-derived Mφ, both *in vitro* and *in vivo*. Intriguingly, the phenotypes of BMDMφ and resident PMφ or PLMφ *in vitro* appeared diametrically opposed. BMDMφ were hyper-responsive to inflammatory stimuli whilst the resident Mφ were hypo-responsive. Trying to assess how these phenotypes may influence inflammation *in vivo* is much more complicated. Although, as predicted, hypo-inflammatory responses were witnessed in two Mφ-dependent models of inflammation (TG peritonitis and CG pleurisy), the expected explanation of decreased chemokine production was not evident. *In vivo* models are by their very nature much more complicated and the migratory abilities of leukocytes, circulating numbers and inherent differences in other factors such as the anaphalactin C5a could all play a contributory role. More work, as outlined above, is required to answer these questions more fully.

REFERENCES

Acha-Orbea, H., and McDevitt, H. O. (1987). The first external domain of the nonobese diabetic mouse class II I-A beta chain is unique. Proc Natl Acad Sci U S A *84*, 2435-2439.

Ackerman, N., Tomolonis, A., Miram, L., Kheifets, J., Martinez, S., and Carter, A. (1980). Three day pleural inflammation: a new model to detect drug effects on macrophage accumulation. J Pharmacol Exp Ther *215*, 588-595.

Akakura, S., Singh, S., Spataro, M., Akakura, R., Kim, J. I., Albert, M. L., and Birge, R. B. (2004). The opsonin MFG-E8 is a ligand for the alphavbeta5 integrin and triggers DOCK180-dependent Rac1 activation for the phagocytosis of apoptotic cells. Exp Cell Res *292*, 403-416.

Aliberti, J., Viola, J. P., Vieira-de-Abreu, A., Bozza, P. T., Sher, A., and Scharfstein, J. (2003). Cutting edge: bradykinin induces IL-12 production by dendritic cells: a danger signal that drives Th1 polarization. J Immunol *170*, 5349-5353.

Alleva, D. G., Pavlovich, R. P., Grant, C., Kaser, S. B., and Beller, D. I. (2000). Aberrant macrophage cytokine production is a conserved feature among autoimmune-prone mouse strains: elevated interleukin (IL)-12 and an imbalance in tumor necrosis factor-alpha and IL-10 define a unique cytokine profile in macrophages from young nonobese diabetic mice. Diabetes *49*, 1106-1115.

Amos, A. F., McCarty, D. J., and Zimmet, P. (1997). The rising global burden of diabetes and its complications: estimates and projections to the year 2010. Diabet Med *14 Suppl 5*, S1-85.

Anderson, C. F., and Mosser, D. M. (2002). A novel phenotype for an activated macrophage: the type 2 activated macrophage. J Leukoc Biol *72*, 101-106.

Anderson, M. S., and Bluestone, J. A. (2005). The NOD mouse: a model of immune dysregulation. Annu Rev Immunol *23*, 447-485.

Andre, I., Gonzalez, A., Wang, B., Katz, J., Benoist, C., and Mathis, D. (1996). Checkpoints in the progression of autoimmune disease: lessons from diabetes models. Proc Natl Acad Sci U S A *93*, 2260-2263.

References

Atkinson, M. A., and Leiter, E. H. (1999). The NOD mouse model of type 1 diabetes: as good as it gets? Nat Med *5*, 601-604.

Bach, J. F. (2005). Infections and autoimmune diseases. J Autoimmun *25 Suppl*, 74-80.

Balasubramanian, K., Chandra, J., and Schroit, A. J. (1997). Immune clearance of phosphatidylserine-expressing cells by phagocytes. The role of beta2-glycoprotein I in macrophage recognition. J Biol Chem *272*, 31113-31117.

Baron, E. J., and Proctor, R. A. (1982). Elicitation of peritoneal polymorphonuclear neutrophils from mice. J Immunol Methods *49*, 305-313.

Baumgarth, N., Herman, O. C., Jager, G. C., Brown, L. E., Herzenberg, L. A., and Chen, J. (2000). B-1 and B-2 cell-derived immunoglobulin M antibodies are nonredundant components of the protective response to influenza virus infection. J Exp Med *192*, 271-280.

Baxter, A. G., Koulmanda, M., and Mandel, T. E. (1991). High and low diabetes incidence nonobese diabetic (NOD) mice: origins and characterisation. Autoimmunity *9*, 61-67.

Belge, K., Dayyani, F., Horelt, A., Siedlar, M., Frankenberger, M., Frankenberger, B., Espevik, T., Ziegler-Heitbrock L. (2002). The proinflammatory CD14+CD16+DR++ monocytes are a major source of TNF. J Immunol *168*, 3536–3542.

Bergman, M. L., Duarte, N., Campino, S., Lundholm, M., Motta, V., Lejon, K., Penha-Goncalves, C., and Holmberg, D. (2003). Diabetes protection and restoration of thymocyte apoptosis in NOD Idd6 congenic strains. Diabetes *52*, 1677-1682.

Birkhofer, A., Rehbock, J., and Fricke, H. (1996). T lymphocytes from the normal human peritoneum contain high frequencies of Th2-type CD8+ T cells. Eur J Immunol *26*, 957-960.

Boes, M., Schmidt, T., Linkemann, K., Beaudette, B. C., Marshak-Rothstein, A., and Chen, J. (2000). Accelerated development of IgG autoantibodies and autoimmune disease in the absence of secreted IgM. Proc Natl Acad Sci U S A *97*, 1184-1189.

Border, W. A., and Noble, N. A. (1994). Transforming growth factor beta in tissue fibrosis. N Engl J Med *331*, 1286-1292.

Bose, J., Gruber, A. D., Helming, L., Schiebe, S., Wegener, I., Hafner, M., Beales, M., Kontgen, F., and Lengeling, A. (2004). The phosphatidylserine receptor has essential functions during embryogenesis but not in apoptotic cell removal. J Biol *3*, 15.

Botto, M., Dell'Agnola, C., Bygrave, A. E., Thompson, E. M., Cook, H. T., Petry, F., Loos, M., Pandolfi, P. P., and Walport, M. J. (1998). Homozygous C1q deficiency causes glomerulonephritis associated with multiple apoptotic bodies. Nat Genet *19*, 56-59.

Botto, M., and Walport, M. J. (2002). C1q, autoimmunity and apoptosis. Immunobiology *205*, 395-406.

Bouma, G., Nikolic, T., Coppens, J. M., van Helden-Meeuwsen, C. G., Leenen, P. J., Drexhage, H. A., Sozzani, S., and Versnel, M. A. (2005). NOD mice have a severely impaired ability to recruit leukocytes into sites of inflammation. Eur J Immunol *35*, 225-235.

Brode, S., Raine, T., Zaccone, P., and Cooke, A. (2006). Cyclophosphamide-induced type-1 diabetes in the NOD mouse is associated with a reduction of CD4+CD25+Foxp3+ regulatory T cells. J Immunol *177*, 6603-6612.

Brodnicki, T. C., McClive, P., Couper, S., and Morahan, G. (2000). Localization of Idd11 using NOD congenic mouse strains: elimination of Slc9a1 as a candidate gene. Immunogenetics *51*, 37-41.

Brodnicki, T. C., Quirk, F., and Morahan, G. (2003). A susceptibility allele from a non-diabetes-prone mouse strain accelerates diabetes in NOD congenic mice. Diabetes *52*, 218-222.

Brown, S., Heinisch, I., Ross, E., Shaw, K., Buckley, C. D., and Savill, J. (2002). Apoptosis disables CD31-mediated cell detachment from phagocytes promoting binding and engulfment. Nature *418*, 200-203.

References

Brown, S. B., and Savill, J. (1999). Phagocytosis triggers macrophage release of Fas ligand and induces apoptosis of bystander leukocytes. J Immunol *162*, 480-485.

Cailhier, J. F., Partolina, M., Vuthoori, S., Wu, S., Ko, K., Watson, S., Savill, J., Hughes, J., and Lang, R. A. (2005). Conditional macrophage ablation demonstrates that resident macrophages initiate acute peritoneal inflammation. J Immunol *174*, 2336-2342.

Cailhier, J. F., Sawatzky, D. A., Kipari, T., Houlberg, K., Walbaum, D., Watson, S., Lang, R. A., Clay, S., Kluth, D., Savill, J., and Hughes, J. (2006). Resident pleural macrophages are key orchestrators of neutrophil recruitment in pleural inflammation. Am J Respir Crit Care Med *173*, 540-547.

Calderon, B., Suri, A., and Unanue, E. R. (2006). In CD4+ T-cell-induced diabetes, macrophages are the final effector cells that mediate islet beta-cell killing: studies from an acute model. Am J Pathol *169*, 2137-2147.

Carnaud, C., Gombert, J., Donnars, O., Garchon, H., and Herbelin, A. (2001). Protection against diabetes and improved NK/NKT cell performance in NOD.NK1.1 mice congenic at the NK complex. J Immunol *166*, 2404-2411.

Casciola-Rosen, L. A., Anhalt, G., and Rosen, A. (1994). Autoantigens targeted in systemic lupus erythematosus are clustered in two populations of surface structures on apoptotic keratinocytes. J Exp Med *179*, 1317-1330.

Castellano, F., Chavrier, P., and Caron, E. (2001). Actin dynamics during phagocytosis. Semin Immunol *13*, 347-355.

Chavakis, T., Bierhaus, A., Al-Fakhri, N., Schneider, D., Witte, S., Linn, T., Nagashima, M., Morser, J., Arnold, B., Preissner, K. T., and Nawroth, P. P. (2003). The pattern recognition receptor (RAGE) is a counterreceptor for leukocyte integrins: a novel pathway for inflammatory cell recruitment. J Exp Med *198*, 1507-1515.

Chen, M. C., Proost, P., Gysemans, C., Mathieu, C., and Eizirik, D. L. (2001). Monocyte chemoattractant protein-1 is expressed in pancreatic islets from prediabetic NOD mice and in interleukin-1 beta-exposed human and rat islet cells. Diabetologia *44*, 325-332.

Clatworthy, M. R., and Smith, K. G. (2004). FcgammaRIIb balances efficient pathogen clearance and the cytokine-mediated consequences of sepsis. J Exp Med *199*, 717-723.

Clatworthy, M. R., Willcocks, L., Urban, B., Langhorne, J., Williams, T. N., Peshu, N., Watkins, N. A., Floto, R. A., and Smith, K. G. (2007). Systemic lupus erythematosus-associated defects in the inhibitory receptor FcgammaRIIb reduce susceptibility to malaria. Proc Natl Acad Sci U S A *104*, 7169-7174.

Clynes, R., Maizes, J. S., Guinamard, R., Ono, M., Takai, T., and Ravetch, J. V. (1999). Modulation of immune complex-induced inflammation in vivo by the coordinate expression of activation and inhibitory Fc receptors. J Exp Med *189*, 179-185.

Cougoule, C., Hoshino, S., Dart, A., Lim, J., and Caron, E. (2006). Dissociation of recruitment and activation of the small G-protein Rac during Fcgamma receptor-mediated phagocytosis. J Biol Chem *281*, 8756-8764.

Cranshaw, M. L., and Leak, L. V. (1990). Milky spots of the omentum: a source of peritoneal cells in the normal and stimulated animal. Arch Histol Cytol *53 Suppl*, 165-177.

Cuzzocrea, S., McDonald, M. C., Filipe, H. M., Costantino, G., Mazzon, E., Santagati, S., Caputi, A. P., and Thiemermann, C. (2000). Effects of tempol, a membrane-permeable radical scavenger, in a rodent model of carrageenan-induced pleurisy. Eur J Pharmacol *390*, 209-222.

Cuzzocrea, S., Pisano, B., Dugo, L., Ianaro, A., Maffia, P., Patel, N. S., Di Paola, R., Ialenti, A., Genovese, T., Chatterjee, P. K.*, et al.* (2004). Rosiglitazone, a ligand of the peroxisome proliferator-activated receptor-gamma, reduces acute inflammation. Eur J Pharmacol *483*, 79-93.

Cuzzocrea, S., Sautebin, L., De Sarro, G., Costantino, G., Rombola, L., Mazzon, E., Ialenti, A., De Sarro, A., Ciliberto, G., Di Rosa, M.*, et al.* (1999). Role of IL-6 in the pleurisy and lung injury caused by carrageenan. J Immunol *163*, 5094-5104.

References

Dahlen, E., Dawe, K., Ohlsson, L., and Hedlund, G. (1998). Dendritic cells and macrophages are the first and major producers of TNF-alpha in pancreatic islets in the nonobese diabetic mouse. J Immunol *160*, 3585-3593.

Devitt, A., Moffatt, O. D., Raykundalia, C., Capra, J. D., Simmons, D. L., and Gregory, C. D. (1998). Human CD14 mediates recognition and phagocytosis of apoptotic cells. Nature *392*, 505-509.

DoH (2001). National Service Framework for Diabetes: Standards, D. o. Health, ed.

DoH (2002). Current and Future Research on Diabetes: A Review for the Department of Health and the Medical Research Council.

DoH (2007). Making Every Young Person with Diabetes Matter.

Duffield, J. S. (2003). The inflammatory macrophage: a story of Jekyll and Hyde. Clin Sci (Lond) *104*, 27-38.

Duffield, J. S., Forbes, S. J., Constandinou, C. M., Clay, S., Partolina, M., Vuthoori, S., Wu, S., Lang, R., and Iredale, J. P. (2005). Selective depletion of macrophages reveals distinct, opposing roles during liver injury and repair. J Clin Invest *115*, 56-65.

Eaves, I. A., Wicker, L. S., Ghandour, G., Lyons, P. A., Peterson, L. B., Todd, J. A., and Glynne, R. J. (2002). Combining mouse congenic strains and microarray gene expression analyses to study a complex trait: the NOD model of type 1 diabetes. Genome Res *12*, 232-243.

Erwig, L. P. and Henson, P. M. (2007). Immunological consequences of apoptotic cell phagocytosis. Am J Pathol *171*, 2-8.

Erwig, L. P., Kluth, D. C., Walsh, G. M., and Rees, A. J. (1998). Initial cytokine exposure determines function of macrophages and renders them unresponsive to other cytokines. J Immunol *161*, 1983-1988.

Erwig, L. P., McPhilips, K. A., Wynes, M. W., Ivetic, A., Ridley, A. J., Henson, P. M. (2006). Differential regulation of phagosome maturation in macrophages and dendritic cells mediated by Rho GTPases and ezrin–radixin–moesin (ERM) proteins. PNAS *103*, 12825–12830

Esteban, L. M., Tsoutsman, T., Jordan, M. A., Roach, D., Poulton, L. D., Brooks, A., Naidenko, O. V., Sidobre, S., Godfrey, D. I., and Baxter, A. G. (2003). Genetic control of NKT cell numbers maps to major diabetes and lupus loci. J Immunol *171*, 2873-2878.

Eurodiab (2000). Variation and trends in incidence of childhood diabetes in Europe. EURODIAB ACE Study Group. Lancet *355*, 873-876.

Fadok, V. A., Bratton, D. L., Konowal, A., Freed, P. W., Westcott, J. Y., and Henson, P. M. (1998). Macrophages that have ingested apoptotic cells in vitro inhibit proinflammatory cytokine production through autocrine/paracrine mechanisms involving TGF-beta, PGE2, and PAF. J Clin Invest *101*, 890-898.

Fadok, V. A., Bratton, D. L., Rose, D. M., Pearson, A., Ezekewitz, R. A., and Henson, P. M. (2000). A receptor for phosphatidylserine-specific clearance of apoptotic cells. Nature *405*, 85-90.

Fadok, V. A., de Cathelineau, A., Daleke, D. L., Henson, P. M., and Bratton, D. L. (2001). Loss of phospholipid asymmetry and surface exposure of phosphatidylserine is required for phagocytosis of apoptotic cells by macrophages and fibroblasts. J Biol Chem *276*, 1071-1077.

Fadok, V. A., Voelker, D. R., Campbell, P. A., Cohen, J. J., Bratton, D. L., and Henson, P. M. (1992). Exposure of phosphatidylserine on the surface of apoptotic lymphocytes triggers specific recognition and removal by macrophages. J Immunol *148*, 2207-2216.

Fajans, S. S., Bell, G. I., and Polonsky, K. S. (2001). Molecular mechanisms and clinical pathophysiology of maturity-onset diabetes of the young. N Engl J Med *345*, 971-980.

Fan, H., Longacre, A., Meng, F., Patel, V., Hsiao, K., Koh, J. S., and Levine, J. S. (2004). Cytokine dysregulation induced by apoptotic cells is a shared characteristic of macrophages from nonobese diabetic and systemic lupus erythematosus-prone mice. J Immunol *172*, 4834-4843.

Fan, H., Patel, V. A., Longacre, A., and Levine, J. S. (2006). Abnormal regulation of the cytoskeletal regulator Rho typifies macrophages of the major murine models of spontaneous autoimmunity. J Leukoc Biol *79*, 155-165.

Floto, R. A., Clatworthy, M. R., Heilbronn, K. R., Rosner, D. R., MacAry, P. A., Rankin, A., Lehner, P. J., Ouwehand, W. H., Allen, J. M., Watkins, N. A., and Smith, K. G. (2005). Loss of function of a lupus-associated FcgammaRIIb polymorphism through exclusion from lipid rafts. Nat Med *11*, 1056-1058.

Fogg, D. K., Sibon, C., Miled, C., Jung, S., Aucouturier, P., Littman, D. R., Cumano, A., and Geissmann, F. (2006). A clonogenic bone marrow progenitor specific for macrophages and dendritic cells. Science *311*, 83-87.

Gallily, R., Warwick, A., and Bang, F. B. (1964). Effect of Cortisone of Genetic Resistance to Mouse Hepatitis Virus in Vivo and in Vitro. Proc Natl Acad Sci U S A *51*, 1158-1164.

Gardner, S. G., Bingley, P. J., Sawtell, P. A., Weeks, S., and Gale, E. A. (1997). Rising incidence of insulin dependent diabetes in children aged under 5 years in the Oxford region: time trend analysis. The Bart's-Oxford Study Group. Bmj *315*, 713-717.

Geissmann, F., Jung, S., and Littman, D. R. (2003). Blood monocytes consist of two principal subsets with distinct migratory properties. Immunity *19*, 71-82.

Georgiou, H. M., Constantinou, D., and Mandel, T. E. (1995). Prevention of autoimmunity in nonobese diabetic (NOD) mice by neonatal transfer of allogeneic thymic macrophages. Autoimmunity *21*, 89-97.

Geutskens, S. B., Nikolic, T., Dardenne, M., Leenen, P. J., and Savino, W. (2004). Defective up-regulation of CD49d in final maturation of NOD mouse macrophages. Eur J Immunol *34*, 3465-3476.

Gilroy, D. W., Colville-Nash, P. R., Willis, D., Chivers, J., Paul-Clark, M. J., and Willoughby, D. A. (1999). Inducible cyclooxygenase may have anti-inflammatory properties. Nat Med *5*, 698-701.

References

Gilroy, D. W., Newson, J., Sawmynaden, P., Willoughby, D. A., and Croxtall, J. D. (2004). A novel role for phospholipase A2 isoforms in the checkpoint control of acute inflammation. Faseb J *18*, 489-498.

Gordon, S. (2003). Alternative activation of macrophages. Nat Rev Immunol *3*, 23-35.

Hall, A. B., Gakidis, M. A., Glogauer, M., Wilsbacher, J. L., Gao, S., Swat, W., and Brugge, J. S. (2006). Requirements for Vav guanine nucleotide exchange factors and Rho GTPases in FcgammaR- and complement-mediated phagocytosis. Immunity *24*, 305-316.

Hall, R. J., Hollis-Moffatt, J. E., Merriman, M. E., Green, R. A., Baker, D., and Merriman, T. R. (2003). An autoimmune diabetes locus (Idd21) on mouse chromosome 18. Mamm Genome *14*, 335-339.

Hamilton-Williams, E. E., Serreze, D. V., Charlton, B., Johnson, E. A., Marron, M. P., Mullbacher, A., and Slattery, R. M. (2001). Transgenic rescue implicates beta2-microglobulin as a diabetes susceptibility gene in nonobese diabetic (NOD) mice. Proc Natl Acad Sci U S A *98*, 11533-11538.

Hamon, Y., Broccardo, C., Chambenoit, O., Luciani, M. F., Toti, F., Chaslin, S., Freyssinet, J. M., Devaux, P. F., McNeish, J., Marguet, D., and Chimini, G. (2000). ABC1 promotes engulfment of apoptotic cells and transbilayer redistribution of phosphatidylserine. Nat Cell Biol *2*, 399-406.

Harada, M., and Makino, S. (1984). Promotion of spontaneous diabetes in non-obese diabetes-prone mice by cyclophosphamide. Diabetologia *27*, 604-606.

Haskins, K., and Wegmann, D. (1996). Diabetogenic T-cell clones. Diabetes *45*, 1299-1305.

Hayakawa, K., Hardy, R. R., and Herzenberg, L. A. (1985). Progenitors for Ly-1 B cells are distinct from progenitors for other B cells. J Exp Med *161*, 1554-1568.

Hengartner, M. O. (2000). The biochemistry of apoptosis. Nature *407*, 770-776.

Herrmann, M., Voll, R. E., Zoller, O. M., Hagenhofer, M., Ponner, B. B., and Kalden, J. R. (1998). Impaired phagocytosis of apoptotic cell material by monocyte-

derived macrophages from patients with systemic lupus erythematosus. Arthritis Rheum *41*, 1241-1250.

Hu, Y., Nakagawa, Y., Purushotham, K. R., and Humphreys-Beher, M. G. (1992). Functional changes in salivary glands of autoimmune disease-prone NOD mice. Am J Physiol *263*, E607-614.

Huang, F. P., Platt, N., Wykes, M., Major, J. R., Powell, T. J., Jenkins, C. D., and MacPherson, G. G. (2000). A discrete subpopulation of dendritic cells transports apoptotic intestinal epithelial cells to T cell areas of mesenteric lymph nodes. J Exp Med *191*, 435-444.

Hughes, J., Liu, Y., Van Damme, J., and Savill, J. (1997). Human glomerular mesangial cell phagocytosis of apoptotic neutrophils: mediation by a novel CD36-independent vitronectin receptor/thrombospondin recognition mechanism that is uncoupled from chemokine secretion. J Immunol *158*, 4389-4397.

Hummel, K. P., Dickie, M. M., and Coleman, D. L. (1966). Diabetes, a new mutation in the mouse. Science *153*, 1127-1128.

Huynh, M. L., Fadok, V. A., and Henson, P. M. (2002). Phosphatidylserine-dependent ingestion of apoptotic cells promotes TGF-beta1 secretion and the resolution of inflammation. J Clin Invest *109*, 41-50.

Ivakine, E. A., Gulban, O. M., Mortin-Toth, S. M., Wankiewicz, E., Scott, C., Spurrell, D., Canty, A., and Danska, J. S. (2006). Molecular genetic analysis of the Idd4 locus implicates the IFN response in type 1 diabetes susceptibility in nonobese diabetic mice. J Immunol *176*, 2976-2990.

Janeway, Paul Travers, Mark Walport, and Shlomchik, M. J. (2004). Immunobiology: The Immune System in Health and Disease (New York, Garland Science Publishing).

Jansen, A., Homo-Delarche, F., Hooijkaas, H., Leenen, P. J., Dardenne, M., and Drexhage, H. A. (1994). Immunohistochemical characterization of monocytes-macrophages and dendritic cells involved in the initiation of the insulitis and beta-cell destruction in NOD mice. Diabetes *43*, 667-675.

References

Jarpe, A. J., Hickman, M. R., Anderson, J. T., Winter, W. E., and Peck, A. B. (1990). Flow cytometric enumeration of mononuclear cell populations infiltrating the islets of Langerhans in prediabetic NOD mice: development of a model of autoimmune insulitis for type I diabetes. Reg Immunol *3*, 305-317.

Kagan, V. E., Gleiss, B., Tyurina, Y. Y., Tyurin, V. A., Elenstrom-Magnusson, C., Liu, S. X., Serinkan, F. B., Arroyo, A., Chandra, J., Orrenius, S., and Fadeel, B. (2002). A role for oxidative stress in apoptosis: oxidation and externalization of phosphatidylserine is required for macrophage clearance of cells undergoing Fas-mediated apoptosis. J Immunol *169*, 487-499.

Kanduc, D., Mittelman, A., Serpico, R., Sinigaglia, E., Sinha, A. A., Natale, C., Santacroce, R., Di Corcia, M. G., Lucchese, A., Dini, L*., et al.* (2002). Cell death: apoptosis versus necrosis (review). Int J Oncol *21*, 165-170.

Kaplan, G. (1977). Differences in the mode of phagocytosis with Fc and C3 receptors in macrophages. Scand J Immunol *6*, 797-807.

Katsilambros, N., Rahman, Y. A., Hinz, M., Fussganger, R., Schroder, K. E., Straub, K., and Pfeiffer, E. F. (1970). Action of streptozotocin on insulin and glucagon responses of rat islets. Horm Metab Res *2*, 268-270.

Kawamura, T., Seki, S., Takeda, K., Narita, J., Ebe, Y., Naito, M., Hiraide, H., and Abo, T. (1999). Protective effect of NK1.1(+) T cells as well as NK cells against intraperitoneal tumors in mice. Cell Immunol *193*, 219-225.

Kerr, J. F., Harmon, B., and Searle, J. (1974). An electron-microscope study of cell deletion in the anuran tadpole tail during spontaneous metamorphosis with special reference to apoptosis of striated muscle fibers. J Cell Sci *14*, 571-585.

Kikutani, H., and Makino, S. (1992). The murine autoimmune diabetes model: NOD and related strains. Adv Immunol *51*, 285-322.

Kipari, T., Cailhier, J. F., Ferenbach, D., Watson, S., Houlberg, K., Walbaum, D., Clay, S., Savill, J., and Hughes, J. (2006). Nitric oxide is an important mediator of renal tubular epithelial cell death in vitro and in murine experimental hydronephrosis. Am J Pathol *169*, 388-399.

Kissler, S., Stern, P., Takahashi, K., Hunter, K., Peterson, L. B., and Wicker, L. S. (2006). In vivo RNA interference demonstrates a role for Nramp1 in modifying susceptibility to type 1 diabetes. Nat Genet *38*, 479-483.

Klein, A., Pinho, V., Alessandrini, A. L., Shimizu, T., Ishii, S., and Teixeira, M. M. (2002). Platelet-activating factor drives eotaxin production in an allergic pleurisy in mice. Br J Pharmacol *135*, 1213-1218.

Klein, A., Talvani, A., Cara, D. C., Gomes, K. L., Lukacs, N. W., and Teixeira, M. M. (2000). Stem cell factor plays a major role in the recruitment of eosinophils in allergic pleurisy in mice via the production of leukotriene B4. J Immunol *164*, 4271-4276.

Kluth, D. C., Erwig, L.-P., and Rees, A. J. (2004). Multiple facets of macrophages in renal injury. Kidney Int *66*, 542-557.

Koh, J. S., Wang, Z., and Levine, J. S. (2000). Cytokine dysregulation induced by apoptotic cells is a shared characteristic of murine lupus. J Immunol *165*, 4190-4201.

Laichalk, L. L., Danforth, J. M., and Standiford, T. J. (1996). Interleukin-10 inhibits neutrophil phagocytic and bactericidal activity. FEMS Immunol Med Microbiol *15*, 181-187.

Lampeter, E. F., Signore, A., Gale, E. A., and Pozzilli, P. (1989). Lessons from the NOD mouse for the pathogenesis and immunotherapy of human type 1 (insulin-dependent) diabetes mellitus. Diabetologia *32*, 703-708.

Lan, Y. Y., Wang, Z., Raimondi, G., Wu, W., Colvin, B. L., de Creus, A., and Thomson, A. W. (2006). "Alternatively activated" dendritic cells preferentially secrete IL-10, expand Foxp3+CD4+ T cells, and induce long-term organ allograft survival in combination with CTLA4-Ig. J Immunol *177*, 5868-5877.

Lanfrancone, L., Boraschi, D., Ghiara, P., Falini, B., Grignani, F., Peri, G., Mantovani, A., and Pelicci, P. G. (1992). Human peritoneal mesothelial cells produce many cytokines (granulocyte colony-stimulating factor [CSF], granulocyte-monocyte-CSF, macrophage-CSF, interleukin-1 [IL-1], and IL-6) and are activated and stimulated to grow by IL-1. Blood *80*, 2835-2842.

References

Lee, K. U., Amano, K., and Yoon, J. W. (1988). Evidence for initial involvement of macrophage in development of insulitis in NOD mice. Diabetes *37*, 989-991.

Letterio, J. J., and Roberts, A. B. (1998). Regulation of immune responses by TGF-beta. Annu Rev Immunol *16*, 137-161.

Li, F. K., Davenport, A., Robson, R. L., Loetscher, P., Rothlein, R., Williams, J. D., and Topley, N. (1998). Leukocyte migration across human peritoneal mesothelial cells is dependent on directed chemokine secretion and ICAM-1 expression. Kidney Int *54*, 2170-2183.

Li, Y. M., Baviello, G., Vlassara, H., and Mitsuhashi, T. (1997). Glycation products in aged thioglycollate medium enhance the elicitation of peritoneal macrophages. J Immunol Methods *201*, 183-188.

Lieberman, S. M., and DiLorenzo, T. P. (2003). A comprehensive guide to antibody and T-cell responses in type 1 diabetes. Tissue Antigens *62*, 359-377.

Litherland, S. A., Grebe, K. M., Belkin, N. S., Paek, E., Elf, J., Atkinson, M., Morel, L., Clare-Salzler, M. J., and McDuffie, M. (2005). Nonobese diabetic mouse congenic analysis reveals chromosome 11 locus contributing to diabetes susceptibility, macrophage STAT5 dysfunction, and granulocyte-macrophage colony-stimulating factor overproduction. J Immunol *175*, 4561-4565.

Loghmani, F., Mohammed, K. A., Nasreen, N., Van Horn, R. D., Hardwick, J. A., Sanders, K. L., and Antony, V. B. (2002). Inflammatory cytokines mediate C-C (monocyte chemotactic protein 1) and C-X-C (interleukin 8) chemokine expression in human pleural fibroblasts. Inflammation *26*, 73-82.

Lynch, D. M., and Kay, P. H. (1995). Studies on the polymorphism of the fifth component of complement in laboratory mice. Exp Clin Immunogenet *12*, 253-260.

Lyons, P. A., Armitage, N., Lord, C. J., Phillips, M. S., Todd, J. A., Peterson, L. B., and Wicker, L. S. (2001). Mapping by genetic interaction: high-resolution congenic mapping of the type 1 diabetes loci Idd10 and Idd18 in the NOD mouse. Diabetes *50*, 2633-2637.

References

Lyons, P. A., Hancock, W. W., Denny, P., Lord, C. J., Hill, N. J., Armitage, N., Siegmund, T., Todd, J. A., Phillips, M. S., Hess, J. F.*, et al.* (2000). The NOD Idd9 genetic interval influences the pathogenicity of insulitis and contains molecular variants of Cd30, Tnfr2, and Cd137. Immunity *13*, 107-115.

Mahnke, K., Johnson, T. S., Ring, S., and Enk, A. H. (2007). Tolerogenic dendritic cells and regulatory T cells: a two-way relationship. J Dermatol Sci *46*, 159-167.

Maier, L. M., and Wicker, L. S. (2005). Genetic susceptibility to type 1 diabetes. Curr Opin Immunol *17*, 601-608.

Makino, S., Kunimoto, K., Muraoka, Y., Mizushima, Y., Katagiri, K., and Tochino, Y. (1980). Breeding of a non-obese, diabetic strain of mice. Jikken Dobutsu *29*, 1-13.

Many, M. C., Maniratunga, S., and Denef, J. F. (1996). The non-obese diabetic (NOD) mouse: an animal model for autoimmune thyroiditis. Exp Clin Endocrinol Diabetes *104 Suppl 3*, 17-20.

Martin, C., Burdon, P. C., Bridger, G., Gutierrez-Ramos, J. C., Williams, T. J., and Rankin, S. M. (2003). Chemokines acting via CXCR2 and CXCR4 control the release of neutrophils from the bone marrow and their return following senescence. Immunity *19*, 583-593.

McAleer, M. A., Reifsnyder, P., Palmer, S. M., Prochazka, M., Love, J. M., Copeman, J. B., Powell, E. E., Rodrigues, N. R., Prins, J. B., Serreze, D. V., and et al. (1995). Crosses of NOD mice with the related NON strain. A polygenic model for IDDM. Diabetes *44*, 1186-1195.

McKnight, A. J., Macfarlane, A. J., Dri, P., Turley, L., Willis, A. C., and Gordon, S. (1996). Molecular cloning of F4/80, a murine macrophage-restricted cell surface glycoprotein with homology to the G-protein-linked transmembrane 7 hormone receptor family. J Biol Chem *271*, 486-489.

Melnicoff, M. J., Horan, P. K., and Morahan, P. S. (1989). Kinetics of changes in peritoneal cell populations following acute inflammation. Cell Immunol *118*, 178-191.

References

Mevorach, D., Mascarenhas, J. O., Gershov, D., and Elkon, K. B. (1998). Complement-dependent clearance of apoptotic cells by human macrophages. J Exp Med *188*, 2313-2320.

Miyazaki, A., Hanafusa, T., Yamada, K., Miyagawa, J., Fujino-Kurihara, H., Nakajima, H., Nonaka, K., and Tarui, S. (1985). Predominance of T lymphocytes in pancreatic islets and spleen of pre-diabetic non-obese diabetic (NOD) mice: a longitudinal study. Clin Exp Immunol *60*, 622-630.

Mocharla, R., Mocharla, H., and Hodes, M. E. (1987). A novel, sensitive fluorometric staining technique for the detection of DNA in RNA preparations. Nucleic Acids Res *15*, 10589.

Morin, J., Boitard, C., Vallois, D., Avner, P., and Rogner, U. C. (2006). Mapping of the murine type 1 diabetes locus Idd20 by genetic interaction. Mamm Genome *17*, 1105-1112.

Mosser, D. M. (2003). The many faces of macrophage activation. J Leukoc Biol *73*, 209-212.

Murai, N., Nagai, K., Fujisawa, H., Hatanaka, K., Kawamura, M., and Harada, Y. (2003). Concurrent evolution and resolution in an acute inflammatory model of rat carrageenin-induced pleurisy. J Leukoc Biol *73*, 456-463.

Mutsaers, S. E. (2004). The mesothelial cell. Int J Biochem Cell Biol *36*, 9-16.

Nakhooda, A. F., Like, A. A., Chappel, C. I., Wei, C. N., and Marliss, E. B. (1978). The spontaneously diabetic Wistar rat (the "BB" rat). Studies prior to and during development of the overt syndrome. Diabetologia *14*, 199-207.

Nelson, D. S., and Boyden, S. V. (1963). The loss of macrophages from peritoneal exudates following the injection of antigens into guinea-pigs with delayed-type hypersensitivity. Immunology *6*, 264-275.

Nikolic, T., Geutskens, S. B., van Rooijen, N., Drexhage, H. A., and Leenen, P. J. (2005). Dendritic cells and macrophages are essential for the retention of lymphocytes in (peri)-insulitis of the nonobese diabetic mouse: a phagocyte depletion study. Lab Invest *85*, 487-501.

References

O'Brien, B. A., Geng, X., Orteu, C. H., Huang, Y., Ghoreishi, M., Zhang, Y., Bush, J. A., Li, G., Finegood, D. T., and Dutz, J. P. (2006). A deficiency in the in vivo clearance of apoptotic cells is a feature of the NOD mouse. J Autoimmun *26*, 104-115.

O'Brien, B. A., Huang, Y., Geng, X., Dutz, J. P., and Finegood, D. T. (2002). Phagocytosis of apoptotic cells by macrophages from NOD mice is reduced. Diabetes *51*, 2481-2488.

O'Reilly, L. A., Hutchings, P. R., Crocker, P. R., Simpson, E., Lund, T., Kioussis, D., Takei, F., Baird, J., and Cooke, A. (1991). Characterization of pancreatic islet cell infiltrates in NOD mice: effect of cell transfer and transgene expression. Eur J Immunol *21*, 1171-1180.

O'Shea, J. J., Ma, A., and Lipsky, P. (2002). Cytokines and autoimmunity. Nat Rev Immunol *2*, 37-45.

Ogden, C. A., deCathelineau, A., Hoffmann, P. R., Bratton, D., Ghebrehiwet, B., Fadok, V. A., and Henson, P. M. (2001). C1q and mannose binding lectin engagement of cell surface calreticulin and CD91 initiates macropinocytosis and uptake of apoptotic cells. J Exp Med *194*, 781-795.

Oka, K., Sawamura, T., Kikuta, K., Itokawa, S., Kume, N., Kita, T., and Masaki, T. (1998). Lectin-like oxidized low-density lipoprotein receptor 1 mediates phagocytosis of aged/apoptotic cells in endothelial cells. Proc Natl Acad Sci U S A *95*, 9535-9540.

Penha-Goncalves, C., Moule, C., Smink, L. J., Howson, J., Gregory, S., Rogers, J., Lyons, P. A., Suttie, J. J., Lord, C. J., Peterson, L. B.*, et al.* (2003). Identification of a structurally distinct CD101 molecule encoded in the 950-kb Idd10 region of NOD mice. Diabetes *52*, 1551-1556.

Pereira Ade, D., Aguas, A. P., Oliveira, M. J., Cabral, J. M., and Grande, N. R. (1994). Experimental modulation of the reactivity of pleural milky spots (Kampmeier's foci) by Freund's adjuvants, betamethasone and mycobacterial infection. J Anat *185 (Pt 3)*, 471-479.

References

Pinho, V., Oliveira, S. H., Souza, D. G., Vasconcelos, D., Alessandri, A. L., Lukacs, N. W., and Teixeira, M. M. (2003). The role of CCL22 (MDC) for the recruitment of eosinophils during allergic pleurisy in mice. J Leukoc Biol *73*, 356-362.

Platt, N., Suzuki, H., Kodama, T., and Gordon, S. (2000). Apoptotic thymocyte clearance in scavenger receptor class A-deficient mice is apparently normal. J Immunol *164*, 4861-4867.

Platt, N., Suzuki, H., Kurihara, Y., Kodama, T., and Gordon, S. (1996). Role for the class A macrophage scavenger receptor in the phagocytosis of apoptotic thymocytes in vitro. Proc Natl Acad Sci U S A *93*, 12456-12460.

Podolin, P. L., Wilusz, M. B., Cubbon, R. M., Pajvani, U., Lord, C. J., Todd, J. A., Peterson, L. B., Wicker, L. S., and Lyons, P. A. (2000). Differential glycosylation of interleukin 2, the molecular basis for the NOD Idd3 type 1 diabetes gene? Cytokine *12*, 477-482.

Poligone, B., Weaver, D. J., Jr., Sen, P., Baldwin, A. S., Jr., and Tisch, R. (2002). Elevated NF-kappaB activation in nonobese diabetic mouse dendritic cells results in enhanced APC function. J Immunol *168*, 188-196.

Pomerleau, D. P., Bagley, R. J., Serreze, D. V., Mathews, C. E., and Leiter, E. H. (2005). Major histocompatibility complex-linked diabetes susceptibility in NOD/Lt mice: subcongenic analysis localizes a component of Idd16 at the H2-D end of the diabetogenic H2(g7) complex. Diabetes *54*, 1603-1606.

Potter, P. K., Cortes-Hernandez, J., Quartier, P., Botto, M., and Walport, M. J. (2003). Lupus-prone mice have an abnormal response to thioglycolate and an impaired clearance of apoptotic cells. J Immunol *170*, 3223-3232.

Qureshi, R., and Jakschik, B. A. (1988). The role of mast cells in thioglycollate-induced inflammation. J Immunol *141*, 2090-2096.

Ramalingam, T., Rajan, B., Lee, J., and Rajan, T. V. (2003). Kinetics of cellular responses to intraperitoneal Brugia pahangi infections in normal and immunodeficient mice. Infect Immun *71*, 4361-4367.

References

Reddy, S., Liu, W., and Elliott, R. B. (1993). Distribution of pancreatic macrophages preceding and during early insulitis in young NOD mice. Pancreas *8*, 602-608.

Reddy, S., Yip, S., Karanam, M., Poole, C. A., and Ross, J. M. (1999). An immunohistochemical study of macrophage influx and the co-localization of inducible nitric oxide synthase in the pancreas of non-obese diabetic (NOD) mice during disease acceleration with cyclophosphamide. Histochem J *31*, 303-314.

Ren, Y., and Savill, J. (1998). Apoptosis: the importance of being eaten. Cell Death Differ *5*, 563-568.

Rich, T., Allen, R. L., and Wyllie, A. H. (2000). Defying death after DNA damage. Nature *407*, 777-783.

Rivero, V. E., Cailleau, C., Depiante-Depaoli, M., Riera, C. M., and Carnaud, C. (1998). Non-obese diabetic (NOD) mice are genetically susceptible to experimental autoimmune prostatitis (EAP). J Autoimmun *11*, 603-610.

Robson, M. G., Cook, H. T., Botto, M., Taylor, P. R., Busso, N., Salvi, R., Pusey, C. D., Walport, M. J., Davies, K. A. (2001). Accelerated nephrotoxic nephritis is exacerbated in C1q-deficient mice. J Immunol *166*, 6820-6828.

Rolf, J., Motta, V., Duarte, N., Lundholm, M., Berntman, E., Bergman, M. L., Sorokin, L., Cardell, S. L., and Holmberg, D. (2005). The enlarged population of marginal zone/CD1d(high) B lymphocytes in nonobese diabetic mice maps to diabetes susceptibility region Idd11. J Immunol *174*, 4821-4827.

Romano, M., Sironi, M., Toniatti, C., Polentarutti, N., Fruscella, P., Ghezzi, P., Faggioni, R., Luini, W., van Hinsbergh, V., Sozzani, S.*, et al.* (1997). Role of IL-6 and its soluble receptor in induction of chemokines and leukocyte recruitment. Immunity *6*, 315-325.

Rosen, A., and Casciola-Rosen, L. (1999). Autoantigens as substrates for apoptotic proteases: implications for the pathogenesis of systemic autoimmune disease. Cell Death Differ *6*, 6-12.

References

Rothe, H., Jenkins, N. A., Copeland, N. G., and Kolb, H. (1997). Active stage of autoimmune diabetes is associated with the expression of a novel cytokine, IGIF, which is located near Idd2. J Clin Invest *99*, 469-474.

Salomon, B., Rhee, L., Bour-Jordan, H., Hsin, H., Montag, A., Soliven, B., Arcella, J., Girvin, A. M., Padilla, J., Miller, S. D., and Bluestone, J. A. (2001). Development of spontaneous autoimmune peripheral polyneuropathy in B7-2-deficient NOD mice. J Exp Med *194*, 677-684.

Sampaio, A. L., Rae, G. A., and Henriques, M. M. (2000). Role of endothelins on lymphocyte accumulation in allergic pleurisy. J Leukoc Biol *67*, 189-195.

Savill, J. (1997). Recognition and phagocytosis of cells undergoing apoptosis. Br Med Bull *53*, 491-508.

Savill, J., Dransfield, I., Gregory, C., and Haslett, C. (2002). A blast from the past: clearance of apoptotic cells regulates immune responses. Nat Rev Immunol *2*, 965-975.

Savill, J., Hogg, N., Ren, Y., and Haslett, C. (1992). Thrombospondin cooperates with CD36 and the vitronectin receptor in macrophage recognition of neutrophils undergoing apoptosis. J Clin Invest *90*, 1513-1522.

Savill, J. S., Wyllie, A. H., Henson, J. E., Walport, M. J., Henson, P. M., and Haslett, C. (1989). Macrophage phagocytosis of aging neutrophils in inflammation. Programmed cell death in the neutrophil leads to its recognition by macrophages. J Clin Invest *83*, 865-875.

Sean Eardley, K., and Cockwell, P. (2005). Macrophages and progressive tubulointerstitial disease. Kidney Int *68*, 437-455.

Segal, A. W. (2005). How neutrophils kill microbes. Annu Rev Immunol *23*, 197-223.

Sen, P., Bhattacharyya, S., Wallet, M., Wong, C. P., Poligone, B., Sen, M., Baldwin, A. S., Jr., and Tisch, R. (2003). NF-kappa B hyperactivation has differential effects on the APC function of nonobese diabetic mouse macrophages. J Immunol *170*, 1770-1780.

References

Silveira, P. A., and Baxter, A. G. (2001). The NOD mouse as a model of SLE. Autoimmunity *34*, 53-64.

Simpson, P. B., Mistry, M. S., Maki, R. A., Yang, W., Schwarz, D. A., Johnson, E. B., Lio, F. M., and Alleva, D. G. (2003). Cuttine edge: diabetes-associated quantitative trait locus, Idd4, is responsible for the IL-12p40 overexpression defect in nonobese diabetic (NOD) mice. J Immunol *171*, 3333-3337.

Skeen, M. J., Freeman, M. M., and Ziegler, H. K. (2004). Changes in peritoneal myeloid populations and their proinflammatory cytokine expression during infection with Listeria monocytogenes are altered in the absence of gamma/delta T cells. J Leukoc Biol *76*, 104-115.

Standiford, T. J., Strieter, R. M., Greenberger, M. J., and Kunkel, S. L. (1996). Expression and regulation of chemokines in acute bacterial pneumonia. Biol Signals *5*, 203-208.

Stein, O., Dabach, Y., Ben-Naim, M., Halperin, G., and Stein, Y. (2006). Lower macrophage recruitment and atherosclerosis resistance in FVB mice. Atherosclerosis *189*, 336-341.

Stern, J., Johnson, P. R., Greenwood, M. R., Zucker, L. M., and Hirsch, J. (1972). Insulin resistance and pancreatic insulin release in the genetically obese Zucker rat. Proc Soc Exp Biol Med *139*, 66-69.

Stoffels, K., Overbergh, L., Giulietti, A., Kasran, A., Bouillon, R., Gysemans, C., and Mathieu, C. (2004). NOD macrophages produce high levels of inflammatory cytokines upon encounter of apoptotic or necrotic cells. J Autoimmun *23*, 9-15.

Stuart, L. M., and Ezekowitz, R., A., (2008). Phagocytosis and comparative innate immunity: learning from the fly. Nat Rev Immunol *8*, 131-141.

Stuart, L. M., Lucas, M., Simpson, C., Lamb, J., Savill, J., and Lacy-Hulbert, A. (2002). Inhibitory effects of apoptotic cell ingestion upon endotoxin-driven myeloid dendritic cell maturation. J Immunol *168*, 1627-1635.

Szczepanik, M., Akahira-Azuma, M., Bryniarski, K., Tsuji, R. F., Kawikova, I., Ptak, W., Kiener, C., Campos, R. A., and Askenase, P. W. (2003). B-1 B cells mediate

required early T cell recruitment to elicit protein-induced delayed-type hypersensitivity. J Immunol *171*, 6225-6235.

Taylor, P. R., Carugati, A., Fadok, V. A., Cook, H. T., Andrews, M., Carroll, M. C., Savill, J. S., Henson, P. M., Botto, M., and Walport, M. J. (2000). A hierarchical role for classical pathway complement proteins in the clearance of apoptotic cells in vivo. J Exp Med *192*, 359-366.

Tian, J., Zekzer, D., Lu, Y., Dang, H., and Kaufman, D. L. (2006). B cells are crucial for determinant spreading of T cell autoimmunity among beta cell antigens in diabetes-prone nonobese diabetic mice. J Immunol *176*, 2654-2661.

Tilg, H., Dinarello, C. A., and Mier, J. W. (1997). IL-6 and APPs: anti-inflammatory and immunosuppressive mediators. Immunol Today *18*, 428-432.

Tomazic, V., Bigazzi, P. E., and Rose, N. R. (1977). The macrophage disappearance reaction (mdr) as an in vivo test of delayed hypersensitivity in mice. Immunol Commun *6*, 49-62.

Topley, N., Jorres, A., Luttmann, W., Petersen, M. M., Lang, M. J., Thierauch, K. H., Muller, C., Coles, G. A., Davies, M., and Williams, J. D. (1993). Human peritoneal mesothelial cells synthesize interleukin-6: induction by IL-1 beta and TNF alpha. Kidney Int *43*, 226-233.

Trudeau, J. D., Dutz, J. P., Arany, E., Hill, D. J., Fieldus, W. E., and Finegood, D. T. (2000). Neonatal beta-cell apoptosis: a trigger for autoimmune diabetes? Diabetes *49*, 1-7.

Vallois, D., Grimm, C. H., Avner, P., Boitard, C., and Rogner, U. C. (2007). The type 1 diabetes locus Idd6 controls TLR1 expression. J Immunol *179*, 3896-3903.

Vella A, Cooper JD, Lowe CE, Walker N, Nutland S, Widmer B (2005). Localization of a type 1 diabetes locus in the IL2RA/CD25 region by use of tag single-nucleotide polymorphisms. Am J Hum Genet 76, 773-779.

Vijayakrishnan, L., Slavik, J. M., Illes, Z., Greenwald, R. J., Rainbow, D., Greve, B., Peterson, L. B., Hafler, D. A., Freeman, G. J., Sharpe, A. H*., et al.* (2004). An

autoimmune disease-associated CTLA-4 splice variant lacking the B7 binding domain signals negatively in T cells. Immunity *20*, 563-575.

Voll, R. E., Herrmann, M., Roth, E. A., Stach, C., Kalden, J. R., and Girkontaite, I. (1997). Immunosuppressive effects of apoptotic cells. Nature *390,* 350-351.

Wang, J., Yoshida, T., Nakaki, F., Hiai, H., Okazaki, T., and Honjo, T. (2005). Establishment of NOD-Pdcd1-/- mice as an efficient animal model of type I diabetes. Proc Natl Acad Sci U S A *102,* 11823-11828.

White, P., Liebhaber, S. A., and Cooke, N. E. (2002). 129X1/SvJ mouse strain has a novel defect in inflammatory cell recruitment. J Immunol *168*, 869-874.

WHO (2006). Definition and Diagnosis of Diabetes Mellitus and Intermediate Hyperglycemia, W. H. O. I. D. Federation, ed. (Geneva, WHO).

Wicker, L. S., Chamberlain, G., Hunter, K., Rainbow, D., Howlett, S., Tiffen, P., Clark, J., Gonzalez-Munoz, A., Cumiskey, A. M., Rosa, R. L.*, et al.* (2004). Fine mapping, gene content, comparative sequencing, and expression analyses support Ctla4 and Nramp1 as candidates for Idd5.1 and Idd5.2 in the nonobese diabetic mouse. J Immunol *173*, 164-173.

Wicker, L. S., Clark, J., Fraser, H. I., Garner, V. E., Gonzalez-Munoz, A., Healy, B., Howlett, S., Hunter, K., Rainbow, D., Rosa, R. L.*, et al.* (2005). Type 1 diabetes genes and pathways shared by humans and NOD mice. J Autoimmun *25 Suppl*, 29-33.

Wicker, L. S., Miller, B. J., and Mullen, Y. (1986). Transfer of autoimmune diabetes mellitus with splenocytes from nonobese diabetic (NOD) mice. Diabetes *35*, 855-860.

Wicker, L. S., Todd, J. A., and Peterson, L. B. (1995). Genetic control of autoimmune diabetes in the NOD mouse. Annu Rev Immunol *13*, 179-200.

Wild, S., Roglic, G., Green, A., Sicree, R., and King, H. (2004). Global prevalence of diabetes: estimates for the year 2000 and projections for 2030. Diabetes Care *27*, 1047-1053.

References

Wilson, H. M., Stewart, K. N., Brown, P. A., Anegon, I., Chettibi, S., Rees, A. J., and Kluth, D. C. (2002). Bone-marrow-derived macrophages genetically modified to produce IL-10 reduce injury in experimental glomerulonephritis. Mol Ther *6*, 710-717.

Wilson, S. B., and Delovitch, T. L. (2003). Janus-like role of regulatory iNKT cells in autoimmune disease and tumour immunity. Nat Rev Immunol *3*, 211-222.

Witowski, J., Thiel, A., Dechend, R., Dunkel, K., Fouquet, N., Bender, T. O., Langrehr, J. M., Gahl, G. M., Frei, U., and Jorres, A. (2001). Synthesis of C-X-C and C-C chemokines by human peritoneal fibroblasts: induction by macrophage-derived cytokines. Am J Pathol *158*, 1441-1450.

Wong, F. S., Visintin, I., Wen, L., Flavell, R. A., and Janeway, C. A., Jr. (1996). CD8 T cell clones from young nonobese diabetic (NOD) islets can transfer rapid onset of diabetes in NOD mice in the absence of CD4 cells. J Exp Med *183*, 67-76.

Wyllie, A. H., Kerr, J. F., and Currie, A. R. (1980). Cell death: the significance of apoptosis. Int Rev Cytol *68*, 251-306.

Xing, Z., Gauldie, J., Cox, G., Baumann, H., Jordana, M., Lei, X. F., and Achong, M. K. (1998). IL-6 is an antiinflammatory cytokine required for controlling local or systemic acute inflammatory responses. J Clin Invest *101*, 311-320.

Yao, V., McCauley, R., Cooper, D., Platell, C., and Hall, J. C. (2004). Peritoneal mesothelial cells produce cytokines in a murine model of peritonitis. Surg Infect (Larchmt) *5*, 229-236.

Zachariadis, O., Cassidy, J. P., Brady, J., and Mahon, B. P. (2006). {gamma}{delta} T Cells Regulate the Early Inflammatory Response to Bordetella pertussis Infection in the Murine Respiratory Tract. Infect Immun *74*, 1837-1845.

Zigler-Heitbrock, L. (2007). The CD14+ CD16+ blood monocytes: their role in infection and inflammation. J Leukoc Biol *81*, 584-592.